Chromosome Congression by CENP-E and CENP-Q Dependent Pathways

James M. Bancroft

A *thesis* submitted for the degree of Doctor of Philosophy

in Medical Sciences

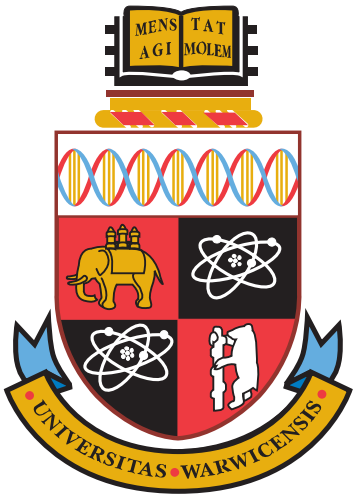

University of Warwick, Warwick Medical School

December 2013

Declaration and inclusion of material from a prior thesis

This thesis is submitted to the University of Warwick in support of my application for the degree of Doctor of Philosophy. It has been composed by myself and has not been submitted in any previous application for any degree. The Materials and Methods chapter of this thesis (chapter 2) is based on the methods section I produced for my M.Phil. to PhD upgrade report (2011), but has been extensively modified and supplemented.

December 2013

Acknowledgements

Undertaking a PhD is without a doubt the greatest endeavour I have ever embarked upon. The last three years have been the best, worst, hardest, most stressful and sleep depriving of my life. I have had times when I have questioned my vocation and others when the highs of science have convinced me that I never want to do anything else. I will look back fondly upon my time at the University of Warwick and I would like to take this opportunity to thank the people who have helped me over the last 3 years…

To Andrew McAinsh, for being my supervisor, my source of knowledge and guidance. For scientific discussions at all hours of the day and for nurturing my strengths and helping me address my weaknesses. For seeing the potential in a microscope sales representative and helping him to become a scientist. Your help and support over the last 3 years has made my achievements possible.

To Rachel Hampshire, my fiancée and partner of over 8 years for giving me the confidence to embark upon a PhD. For your understanding when I have spent late nights or all night in the lab and for being the reason I look forward to getting home. For feeding me, spell checking, helpful discussions and for financial support. Without you I would not have made it to the end. Hopefully we can have our lives back soon!

To my parents Martin and Susan and brother John, your love and support has been a source of great strength to me.

To Rob Cross for helpful discussions and detailed proof reading and feedback which has made the writing process a little less painful.

To my colleagues in the McAinsh lab. To Chris Smith for help with the necessary evil that is MatLab, for proof reading and for scientific discussion. Our jokes have helped keep me going. To Elina Vladimirou, you have been a good friend to me as well as a source of much support and knowledge within the lab. I appreciate the your honest feedback, your help with presentations and your help with mathematical analysis and statistics. To Catarina Samora for help with learning laboratory and analysis techniques and for discussions about all things CENP-Q related. Your work has helped me to take informed steps forward. To Sophie Glinton for being a great lab technician, running partner and true friend. To Edward Harry for the modifications you made to our existing kinetochore tracking software. To Hauke Drechsler for proof reading my results. The rest of the McAinsh lab, Muriel Erent, Virginia Silio and Phil Auckland.

To my friends in the Straube lab, Ben Fitton and Ulrike Theisen for help with making graphs and cloning respectively as well as great company.

To the other people within Warwick Medical School who have helped and supported me during my PhD, you are too numerous to name but your contributions will not be forgotten.

Inclusion of published work

As Appendix 1 I attach a copy of a paper entitled “Step-Wise Assembly, Maturation and Dynamic Behavior of the Human CENP-P/O/R/Q/U Kinetochore Sub-Complex” by Eskat et al., 2011. I include this paper as I generated the data for, and composed, Figure 7. For this contribution I am named on the paper.

Summary

The timely and efficient movement of chromosomes to the spindle equator during mitosis is a prerequisite for accurate chromosome segregation. Recent work has shown that the majority of chromosomes are able to congress and biorientate almost instantaneously after nuclear envelope breakdown due to their position relative to the forming spindle. However, other mechanisms are required to facilitate the congression of chromosomes, which do not congress in this initial wave. Congression of these remaining chromosomes is mediated by multiple mechanisms including: (1) Kinetochore sliding along the microtubule lattice using the Kinesin-7 CENP-E, and (2) kinetochores biorientating near the pole and congressing through microtubule depolymerisation-coupled movement. Here, we show that the constitutive centromere associated network (CCAN) subunit CENP-Q is required for both mechanisms. CENP-Q is required to recruit CENP-E to kinetochores thus explaining the absence of lateral sliding in CENP-Q depleted cells. Because depletion or inhibition of the CENP-E motor does not affect depolymerisation-coupled pulling, we identify a CENP-E recruitment-independent role for CENP-Q in chromosome congression. Following congression we find that biorientated kinetochore movements require both CENP-Q and CENP-E dependent mechanisms. This suggests that as biorientated kinetochores congress they switch into a mode that requires CENP-E motor activity.

Abbreviations

a-MT	Astral-microtubule
ATP	Adenosine-5'-triphosphate
ADP	Adenosine-5'-diphosphate
BSA	Bovine serum albumin
C. elegans	*Caenorhabditis elegans*, nematode worm
D. melanogaster	*Drosophila melanogaster*, fruit fly
Da	Dalton
DAPI	4,6- diamidino-2-phenylindole
ddH_2O	Double-distilled water
DNA	*Escherichia coli*
eGFP	Enhanced green fluorescent protein
EGTA	Ethylene glycol tetraacetic acid
EM	Electron microscopy
g	Gram
hr(s)	Hour(s)
in vitro	Latin, 'within the glass'; in a test tube
in vivo	Latin, 'within the living'; in the living organism
ip-MT	Inter-polar microtubules
KT	Kinetochore
K-fibre	Kinetochore-fibre
K-MT	Kinetochore-microtubule
LB	Lysogeny broth
MSD	Mean squared displacement
MAP	Microtubule associated protein
ml	Millilitre
µl	Microlitre
µm	Micrometre

MT	Microtubule
min	Minute
NA	Numerical aperture
NEB	Nuclear envelope breakdown
nm	Nanometre
nK-MT	Non-kinetochore microtubule
OD	Optical density
PBS	Phosphate buffered saline
pH	Negative logarithm of the hydrogen ion concentration in solution
SD	Standard deviation
SDS	Sodium dodecyl sulfate
SDS-PAGE	SDS polyacrylamide gel electrophoresis
sec	Second
SOC	Super optimal broth with catabolite repression

Index of tables and illustrated materials

Figures

Tables

Table of contents

CHAPTER 1: Introduction

1.1 Overview of mitosis

Mitosis is the process by which a cell segregates its replicated chromosomes into daughter cells during cell division, thereby ensuring accurate transmission of its genetic material. In animal cells mitosis is perhaps the most overt stage within the cell cycle: during G2 there is a commitment checkpoint to mitosis, which leads to a dramatic remodelling of the cytoskeleton (see schematic in Figure 1.1a). The interphase microtubule (MT) network is largely depolymerised and the two duplicated centrosomes (which will go on to form the spindle poles) nucleate two MT asters; large radial arrays of dynamic MTs. During this period, known as prophase, chromatin is condensed, forming the compact mitotic chromosomes, each chromosome formed from a pair of sister chromatids. The asters then move apart along the surface of the nucleus after which the nuclear envelope breaks down, this marks the end of prophase and the beginning of prometaphase. With the nuclear envelope gone, microtubules from the two asters begin to form the mitotic spindle.

The mitotic spindle is built from not only microtubules, but also hundreds of other interacting proteins (reviewed in Gadde & Heald, 2004; Walczak & Heald, 2008). Together these proteins drive the self-assembly of a bipolar cage-like structure (see prometaphase in Figure 1.1a), that in human cells has approximate dimensions 10 x 10 x 10 μm. A subset of microtubules from each pole overlap in the centre (inter-polar microtubules; ip-MTs), stabilising the structure, whilst astral microtubules (a-MTs) contact the cell cortex and control spindle location within the cell (reviewed in Meunier & Vernos, 2012). Free spindle microtubule plus-ends also begin making attachments to chromosomes via interaction with kinetochores; multi-protein, microtubule-binding complexes that assemble on the centromere of each sister chromatid, forming a pair of sister kinetochores. The “search and capture”, of kinetochores by microtubules is only possible because of the intrinsic dynamic instability property of microtubules, which causes cycles of growth and shrinkage and

Figure 1.1

a

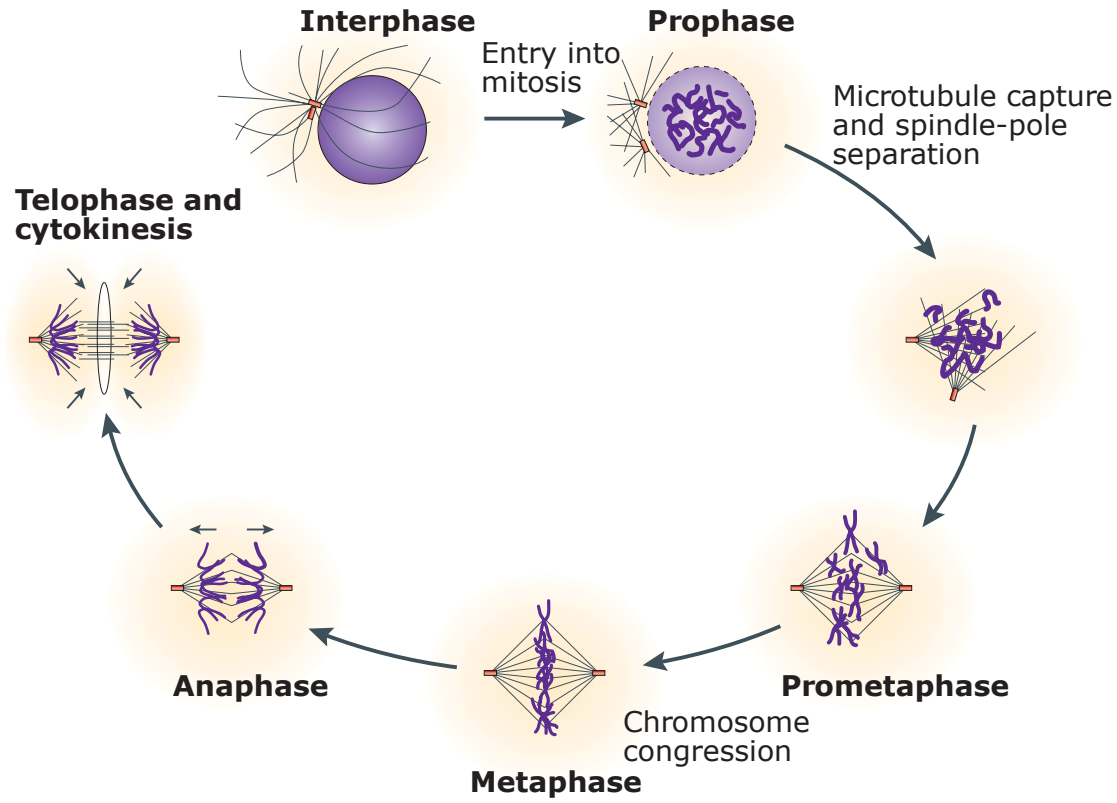

Figure 1.1 (a) The stages of mitosis. As cells enter mitosis they condense their chromatin (purple) forming dense mitotic chromosomes composed of two sister chromatids joined at the centromere. The nuclear envelope breaks down and the two spindle poles separate as the mitotic spindle forms (prophase). Chromosomes then begin capturing spindle microtubules (prometaphase). Microtubule capture is mediated by the kinetochore; a large macromolecular assembly at the centromere of each sister chromatid. Chromosomes align to the spindle equator (metaphase). After a period of time aligned at the spindle equator chromosomes split into their two constituent sister chormatids, and one sister chromatid is pulled towards each pole (anaphase). The cell then begins to constrict at the spindle equator (telophase) and eventually separates to form the two new daughter cells (cytokinesis). Black lines in the figure represent microtubules and orange rectangles represent spindle poles. Figure is adapted from Jackson et al., 2007.

thereby allows microtubules to search the volume within a cell efficiently (Kirschner & Mitchison, 1986).

Once spindle microtubules are captured by kinetochores they are termed kinetochore-microtubules (K-MTs). Microtubule-attached kinetochores move towards the spindle equator through a process known as chromosome congression. The timescale of this process in human cells is ~15-20 min. Cells with all chromosomes aligned are defined as being in metaphase (see metaphase in Figure 1.1a). The aligned chromosomes are said to form a metaphase plate (Bajer, 1958). The mechanisms underlying chromosome congression have been the focus of much research (Kops et al., 2010; Walczak et al., 2010) and will be discussed in section 1.4. In order to achieve alignment at the spindle equator the majority of chromosomes become biorientated (although other pathways to alignment exist, see section 1.4). Biorientation is the process by which the kinetochore on each sister chromatid form attachments with K-MTs emanating from opposite spindle poles. The biorientated state is the only state compatible with the correct disjunction of sister chromatids in anaphase. Moreover, it is the tension across sister-kinetochore pairs generated by this biorientated state that is monitored by the spindle assembly checkpoint (SAC), a mechanism that prevents cells from progressing further in mitosis until all kinetochores are correctly attached to the mitotic spindle (Kops et al., 2005; Sczaniecka & Hardwick, 2008).

Cells maintain chromosomes at the spindle equator (metaphase plate) for a period of time before anaphase onset, during which, chromosomes oscillate back and forth about the metaphase plate (Pereria & Maiato, 2012; Lewis, 1939; Hughes & Swann, 1949). Upon deactivation of the SAC, the cohesin ring complex, which holds the sister chromatids together, is cleaved and sister chromatids are separated, a process known as anaphase (see anaphase in Figure 1.1a) (Hardwick & Shah, 2010). These initial anaphase chromosome movements are powered by the concerted depolymerisation of the K-MTs (anaphase A), whilst the spindle midzone elongates (anaphase B), which has the effect of increasing the distance between the two spindle poles (Brust-Mascher & Scholey, 2011; Vazquez-Novelle et al., 2010). The net result of the anaphase process is that one

copy of each sister chromatid is moved towards each spindle pole. Mistakes in this process causes aneuploidy, i.e. the loss or gain of whole chromosomes, this state is associated with ~80% of solid human tumours (Sheltzer & Amon, 2011). Indeed, many cancer cells are chromosomally unstable, often exhibiting cromosomes that lag behind the two groups of chromatids during anaphase (Weaver et al., 2007), indicating the importance of understanding how high fidelity chromosome segregation is mediated.

1.2 Kinetochores

1.2.1 Ultrastructure of the kinetochore

Kinetochores are mega-dalton sized multi protein complexes that assemble on the centromere of each sister chromatid forming an attachment site for spindle microtubules. Electron microscopy studies have shown that human kinetochores appear as a ~500 nm diameter disk organised into a "three stacked plate" structure (Brinkley & Stubblefield, 1966; Jokelainen, 1967). The inner plate is ~50 nm thick and forms a physical link to the underlying centromeric chromatin. The middle plate is electron lucent, and connects the electron dense inner and outer plates. Further studies have, however, suggested that the electron lucent middle layer may in fact be an artefact of fixation (McEwen et al., 1998). The outer plate is also ~50 nm deep and is the location at which the plus-ends of spindle microtubules terminate (McEwen et al, 1998). More recent studies employing high pressure freezing EM techniques, to better preserve sub-cellular structures, provide evidence that the kinetochore has a more open morphology (Dong et al., 2007). In the absence of microtubules a fibrous corona can be visualised extending from the outer plate into the cytoplasm, however the association of microtubules with the kinetochore appears to reduces this corona (Cassimeris et al., 1990; Rieder et al., 1982). This corona contains microtubule-binding proteins, as well as proteins involved in the SAC (reviewed in Cleveland et al., 2003). Interestingly, work in the late 1990s provided evidence that this fibrous corona and the outer plate may be a continuous structure (McEwen et al., 1998). High-resolution electron tomography has allowed visualisation of other interesting structures within the kinetochore; recent work has revealed fibril structures, which

connect microtubules with kinetochores (McIntosh et al., 2008). These fibrils appear to bind directly to protofilaments, which bend away from the microtubule axis. These protofilaments have a ram's horn like structure and are associated with depolymerisation. Thus, fibrils contacting these protofilaments may be important in coupling depolymerisation to kinetochore force generation (McIntosh et al., 2008).

The *S. cerevisiae* kinetochore is simplified in that it binds only a single microtubule compared to the 20-30 of its human counterpart (reviewed in Westermann et al., 2007). Recently our understanding of kinetochore ultrastructure was advanced by the impressive biochemical feat of purifying the *S. cerevisiae* kinetochore (Gonen et al., 2012). These kinetochores were able to bind MTs and could be imaged using electron microscopy and electron tomography (Gonen et al., 2012). This work revealed that the *S. cerevisiae* kinetochore is approximately 126 nm in length, and is formed from a large central hub from which approximately 8 globular domains extend. When visualised in the presence of microtubules several kinetochores could be seen to possess a ring-like structure encircling the microtubule (Gonen et al., 2012). A major challenge is to understand how the protein components of kinetochores relate to these nanometre scale structural features.

1.2.2 Centromeric chromatin

The inner kinetochore (plate) engages the centromeric DNA, which in humans, consists primarily of tandemly repeated AT-rich arrays of a 171-base pair (bp) α-satellite sequence (reviewed in Cheeseman & Desai, 2008). Within this repeat sequence there is an additional 17-bp motif called the CENP-B box23 sequence, which allows stable binding of the inner centromere CENP-B protein (Masumoto et al., 1989). Centromeric chromatin is found at a single locus on each sister chromatid, and therefore human chromosomes are defined as being mono-centric. A key feature of centromeric chromatin is the presence of nucleosomes containing the histone H3 varient Centromere Associated Protein-A (CENP-A). These nucleosomes are formed from an octomer containing two heterotetramers consisting of histone proteins, which bind DNA via a histone fold

domain and organise DNA by supercoiling it around the structure of the nucleosome. Canonical nucleosomes consist of two copies of four histone proteins; H2A, H2B, H3 and H4. However, centromeric nucleosomes replace histone H3 with CENP-A. Like histone H3, CENP-A interacts with DNA by its histone fold domain and forms a heterotetramer with histone H4 that binds to two H2A-H2B dimers (Blower et al., 2002; reviewed in Cheeseman & Desai, 2008). It has been suggested that CENP-N (see section 1.2.3.3 below) may act to guide the integration of newly expressed pre-nucleosomal CENP-A protein into centromeric nucleosomes. However this seems unlikely as the affinity of CENP-N is much higher for nucleosomal CENP-A (i.e. DNA bound) than non-nucleosomal CENP-A. Additionally, CENP-N is not present in the HJURP complex, which is known to chaperone CENP-A to the centromere after translation (reviewed in Sekulic & Black 2009). It is therefore most likely that the requirement of CENP-A loading into the centromere upon CENP-N is an indirect one, mediated by additional factors recruited directly or indirectly by CENP-N (Carroll et al., 2009). When integrated into centromeric chromatin CENP-A protein acts as an epigenetic marker in the establishment of the centromere (Black et al., 2007), i.e. the DNA sequence of the centromere does not determine the locus of CENP-A incorporation. CENP-A then provides a structural platform for the assembly of other kinetochore proteins (see section 1.2.3 and Figure 1.2).

High resolution structural work has shown that it is likely that the divergence of CENP-A from canonical histone H3 results in important structural features at CENP-A containing nucleosomes required for establishment of the centromere and kinetochore (Sekulic et al., 2010). Within CENP-A containing nucleosomes the CENP-A–CENP-A interaction is rotated relative to the H3–H3 interaction. The residues responsible for this CENP-A–CENP-A rotation are required for efficient incorporation into centromeric chromatin. Additionally, the charge on the protruding L1 loop of CENP-A is reversed compared to that of histone H3 L1 loop, providing a potential site to generate differential substrate specificity to histone H3 (Sekulic et al., 2010). Despite these unique features, localisation of the CENP-A protein alone is not sufficient to drive kinetochore assembly in human

cells (Gascoigne et al., 2011), suggesting that in metazoans kinetochore establishment is likely to require multiple cues.

1.2.3 Constitutive centromere associated network (CCAN)

The presence of CENP-A containing nucleosomes at centromeres acts as a key marker for assembly of the Constitutive Centromere Associated Network (CCAN). The CCAN is a network of 16 kinetochore proteins that is composed of several loosely associated sub-complexes (Okada et al., 2006; Foltz et al., 2006; see model in Figure 1.2). The CCAN was named based on the idea that the complex was constitutively bound to centromeres throughout the cell cycle, and although subsequent studies have shown that this may not be the case for all CCAN proteins, it is true that the majority of CCAN proteins can be found bound at the centromere during all cell cycle stages (Foltz et al., 2006; Okada et al., 2006).

1.2.3.1 Discovery of CCAN

The initial 6 members (CENP-M, CENP-N and CENP-T, CENP-U/CENP-50/PBIP1, CENP-C and CENP-H) of the human CCAN complex were identified by their affinity purification with CENP-A nucleosomes (Foltz et al., 2006). These proteins were initially designated as the nucleosome-associated complex (NAC). Of these proteins CENP-C, CENP-H and CENP-I had previously been identified as kinetochore proteins (Fukagawa et al., 2001; Nishihashi et al., 2002; Liu et al., 2003). By affinity purification of the NAC proteins a further 8 proteins were identified (CENP-I, CENP-K, CENP-L, CENP-O, CENP-P, CENP-Q, CENP-R and CENP-S) and named the CENP-A distal proteins (CAD (Foltz et al., 2006)). However, other studies have shown that division of the CCAN proteins into NAC or CAD is somewhat artificial as these divisions do not reflect function or biochemical organisation.

Evidence for the breakdown of the NAC/CAD designation comes from the identification of overlapping sets of proteins. In the same issue of Nature Cell Biology that the Foltz study was

Figure 1.2

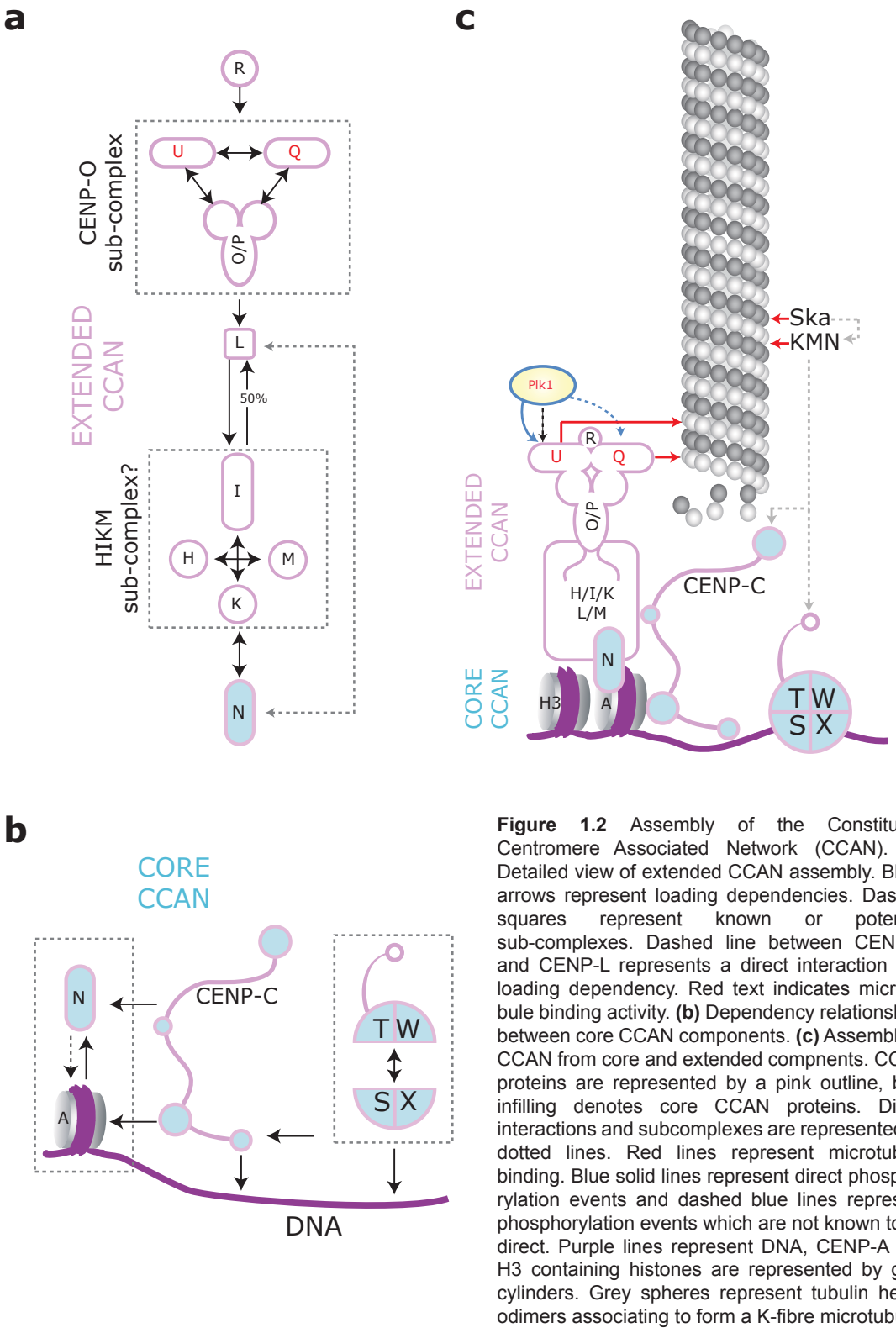

Figure 1.2 Assembly of the Constitutive Centromere Associated Network (CCAN). **(a)** Detailed view of extended CCAN assembly. Black arrows represent loading dependencies. Dashed squares represent known or potential sub-complexes. Dashed line between CENP-N and CENP-L represents a direct interaction and loading dependency. Red text indicates microtubule binding activity. **(b)** Dependency relationships between core CCAN components. **(c)** Assembly of CCAN from core and extended compnents. CCAN proteins are represented by a pink outline, blue infilling denotes core CCAN proteins. Direct interactions and subcomplexes are represented by dotted lines. Red lines represent microtubule binding. Blue solid lines represent direct phosphorylation events and dashed blue lines represent phosphorylation events which are not known to be direct. Purple lines represent DNA, CENP-A and H3 containing histones are represented by grey cylinders. Grey spheres represent tubulin heterodimers associating to form a K-fibre microtubule.

published, a similar study by Okada and colleagues was also published. This study identified 9 of the CCAN proteins that were also identified by Foltz (Okada et al., 2006; Foltz et al., 2006). Okada and colleagues called their set of CCAN proteins the CENP-H/I complex. The Okada study divided these proteins into 3 groups based on dependency experiments, knockout (KO) phenotypes and viability in chicken DT40 cells. These groups were the CENP-H, I, K, L group, the CENP-O, P, Q, U(50) group and CENP-M alone (Okada et al., 2006). Also in 2006 a third study, which isolated centromere complexes from interphase HeLa cell nuclei in their native state, identified CENP-C, CENP-H, CENP-I and CENP-U as part of the interphase centromere complex (ICEN) along with around 40 other non-CCAN proteins (Izuta et al., 2006). Subsequent studies have identified a further two CCAN proteins; CENP-W and CENP-X. CENP-W identification was aided by its association with the previously identified CENP-T protein (Hori et al., 2008a). Later, work in chicken DT40 cells and human cells identified CENP-X by its association with CENP-S (Amano et al., 2009). Interestingly both CENP-S and CENP-X have been previously identified as Fanconia Anemia M (FANCM) associated proteins (where they were designated MHF1 and MHF2). This suggests the possibility of a dual role for these proteins (Yan et al., 2010; Singh et al., 2010). Thus the list of identified human CCAN proteins is currently as follows; CENP-C, H, I, K, L, M, N, O, P, Q, R, S, T, U, W and X (reviewed in McAinsh & Meraldi, 2011).

1.2.3.2 Evolutionary conservation of the CCAN

The human CCAN subunits have clear orthologues in all mammals, birds and most metazoans but identification of potential orthologues in flies and worms has not been possible. This is surprising, as orthologues have been identified in much more distantly related organisms (see *S. pombe* and *S. cerevisiae* below). The exception is CENP-C, which can be clearly detected in *D. melanogaster* and *C. elegans* and even in plants (*A. thaliana*). This may reflect a crucial and conserved role of CENP-C in anchoring kinetochores to chromatin (Carroll et al., 2010; Ando et al., 2002; Hori et al., 2008a; Obuse et al., 2004; see section 1.2.3.3 below for detail). One possible reason for the reduction of the *C. elegans* complement of CCAN proteins to only CENP-C may be the inherent structural differences between the *C. elegans* and human centromere. Humans, like the majority of

eukaryotes are monocentric, i.e. they have a single centromere and kinetochore per sister chromatid, whereas *C. elegans* are holocentric; having diffuse centromeric regions and kinetochores along the length of each sister chromatid. This considerable structural difference could explain the divergence of the *C. elegans* complement of CCAN proteins from that of humans. However, *D. melanogaster* does have monocentric centromeres and therefore one may initially discount the loss of CCAN proteins as a result of divergence driven by holocentricity. Recent studies suggest that the earliest common ancestor of all insects may have been holocentric and monocentricity may have arisen later (Melters et al., 2012). Indeed, holocentricity is relatively common within insects, being found in mayflies (order Ephemeroptera), earwigs (order Dermaptera), butterflies and moths (order Lepidoptera) and dragonflies (order Odonata) to name but a few. Thus the CCAN proteins may have been lost from the *D. melanogaster* holocentric ancestor, explaining their absence (Melters et al., 2012). The CCAN is, however, well conserved in fungi. By combining the evidence from multiple studies, orthologues of all CCAN proteins (except for CENP-R) can be found in *S. pombe* and *S. cerevisiae* (Meraldi et al., 2006; Schleiffer et al., 2012; Perpelescu & Fukagawa, 2011; McAinsh & Meraldi, 2011). Given this conservation it is perhaps not surprising that a number of human CCAN proteins, such as CENP-O/CENP-N, were in fact identified as a result of their sequence similarity to their yeast counterparts (Meraldi et al., 2006). Work on the yeast orthologues has provided additional key insight into the CCAN. Most notable are the crystal structures of the budding yeast Ctf19p/Mcm21p (human CENP-P/CENP-O) and Iml3p/Chl4p (CENP-M/CENP-N) dimers (Schmitzberger & Harrison, 2012; Hinshaw & Harrison, 2013). With the exception of *AME1* (CENP-U) and *OKP1* (CENP-Q) all budding yeast CCAN genes are non-essential, but are required for high-fidelity chromosome segregation (Burns et al., 1994; Pot et al., 2005). Interestingly, the budding yeast Ctf19 complex consisting of Ctf19, Okp1, Mcm21 and Ame1 (CENP-P/U/O/Q in humans) are important for cohesin loading to centromeres (Fernius & Marston, 2009).

1.2.3.3 "Core" CCAN assembly

Several CCAN proteins are able to bind to centromeric DNA or directly to CENP-A nucleosomes: these proteins are known as the "core CCAN" (reviewed in Westhorpe & Straight, 2013; see Figure 1.2b and blue proteins in Figure 1.2c). One such core CCAN protein is CENP-C, which binds to DNA, but in order to do so it must first bind to nucleosomes. Whether these nucleosomes are CENP-A-containing or canonical H3-containing, remains the subject of much debate. One study has provided evidence that the interaction is a direct one, requiring the extreme C-terminus of CENP-A (Carroll et al., 2010). Conversely, other studies suggest that CENP-C is more likely to bind histones containing canonical histone H3 (Ando et al., 2002; Hori et al., 2008a; Obuse et al., 2004). Super-resolution imaging by kinetochore-speckle high resolution co-localization (K-SHREC), which allows measurement of the average separation between the centroids of two different frourescently labelled kinetochore proteins (with an accuracy of less than 5 nm), has revealed that CENP-C is the most proximal CCAN protein to CENP-A (Wan et al., 2009). However, this does not offer confirmation of a direct interaction. After binding to nucleosomes, CENP-C can then bind to DNA, but does not bind in a sequence-specific manner. CENP-C loading to the centromere is also dependent upon the CENP-K protein (Kwon et al., 2007) and CENP-N protein (Carroll et al., 2009; see Figure 1.2b). CENP-N, like CENP-C, has also been shown to bind to CENP-A, an interaction that is required for CENP-N kinetochore targeting (Carroll et al., 2009). However, CENP-N does not possess DNA binding activity, although biochemical evidence suggests that CENP-N exhibits increased affinity for CENP-A nucleosomes bound to DNA over naked nucleosomes (Carroll et al., 2010). *In vitro* CENP-N binding of CENP-A is not competitive with CENP-C binding of CENP-A, suggesting that the two proteins target different regions of the CENP-A protein (Carroll et al., 2010). Interestingly, the CENP-N dependency on CENP-A for loading is also semi-reciprocal, as depletion of CENP-N results in a reduced integration of newly synthesised CENP-A into centromeric chromatin (discussed above in centromeric chromatin).

CENP-T and CENP-W also bind to DNA and this interaction is mediated via a histone fold domain like that of CENP-A. The short CENP-W protein (<100 amino acids) is formed solely from a histone

fold domain (Hori et al., 2008a), whilst CENP-T has a histone fold domain in its C-terminal region and a long unstructured N-terminal tail (Hori et al., 2008a; Suzuki et al., 2011). Furthermore, it is now known that CENP-T and W actually form a complex, which co-assembles with the CENP-S-X complex; both CENP-S and CENP-X also possess histone fold DNA binding domains. The result is the formation of a stable CENP-T/W/S/X heterotetramer (Nishino et al., 2012; see Figure 1.2b). A high-resolution structural study has shown that this heterotetramer forms a structure similar to histone H3 containing nucleosomes, and is able to bind to and supercoil DNA (Nishino et al., 2012). Thus, CENP-T/W/S/X complexes are proposed to form a nucleosome or nucleosome-like structure, providing another platform for kinetochore assembly. This complex preferentially binds to the linker DNA between nucleosomes and by binding the CENP-T/W/S/X complex causes this DNA to become positively super-coiled, unlike CENP-A or H3 containing nucleosomes which negatively super-coil DNA (Takeuchi et al., 2013).

1.2.3.4 Assembly of the extended CCAN

A key challenge is to understand how the remaining CCAN subunits assemble to the three core CCAN components: CENP-C, CENP-N and CENP-S/T/W/X. Our understanding is limited because the only physical interaction reported in humans is between CENP-L and CENP-N (Carroll et al., 2009; see Figure 1.2a). Consistently, depletion of CENP-N does unbind CENP-L from kinetochores. Experiments in *S. pombe* show that CENP-L (Fta1) can also bind directly to CENP-C (Mis6; Tanaka et al., 2009). If preserved in humans this would represent a further potential stabilising interaction within the CCAN (Carroll et al., 2009). Dependency style experiments using protein depletions/knock-outs and immunofluorescence in human and DT40 cells have allowed us to build an outline map of how the CCAN assembles (see schematic in Figure 1.2 for details). Depletion of CENP-N unbinds CENP-H/I/K/M/O/P/Q/U/R – a set of proteins termed the “extended CCAN” (Westhorpe and Straight, 2013; see Figure 1.2a). CENP-N is also required for the recruitment of CENP-C to kinetochores, but does not affect CENP-T/W (Foltz et al., 2006). CENP-C is required for the loading of CENP-H/I/K, but unlike CENP-N, is also necessary for CENP-T to bind kinetochores (Carroll et al., 2010). The depletion of CENP-T has the greatest effect on protein

loading, causing all non-histone CENP proteins to be displaced from the kinetochore (summarised in Perpelescu & Fukagawa, 2011).

Assembly of the extended CCAN can be separated into two steps; the CENP-H/I/K/L/M proteins require each other for kinetochore-binding and are necessary for assembly of the CENP-O/P/Q/U/R, but not vice versa (see Figure 1.2a). Of these proteins CENP-O/P/Q/U require each other for kinetochore-binding, but do not require CENP-R. However, the CENP-R protein does require the presence of CENP-O/P/Q/U for kinetochore binding (Hori et al., 2008b). This suggests a simple linear hierarchy: CENP-H/I/K/L/M > CENP-O/P/Q/U > CENP-R (see Figure 1.2a). Indeed, CENP-O/P/Q/U have been shown to form a stable protein complex with recombinant proteins, with a 1:1:1:1 stoichiometry (Hori et al., 2008b), this complex can also bind CENP-R. Work from yeast also shows that the *Saccharomyces cerevisiae* orthologues of CENP-P/O (Ctf19/Mcm21) also interact via RWD domain, and the crystal structure of this heterodimer has recently been solved (Schmitzberger & Harrison, 2012). In contrast the biochemical organisation of the CENP-H/I/K/M proteins is unknown, although dependency experiments support the idea that these proteins also form an interdependent complex (Foltz et al., 2006). Within the CENP-O/P/Q/U/R sub-complex, it is known that CENP-U and CENP-Q interact directly by the C-terminal region of CENP-U (residues 200–418) and the predicted coiled-coil region of CENP-Q (Kang et al., 2011). The CENP-Q coiled coil region has been shown to be important for the formation of CENP-Q oligomers (Kang et al., 2011). Disruption of the predicted CENP-Q coiled-coil domain by mutating the conserved leucine residue 179 to a proline, breaks the interaction (Kang et al., 2011). This would be consistent with the finding that CENP-Q is able to form stable homo-octomers *in vitro* (Amaro et al., 2010).

In partnership with our collaborators we have also been able to gain further insight into the assembly of the CENP-O/P/Q/U/R sub-complex (Eskat et al., 2012). Fluorescent three-hybrid (F3H) assays and fluorescence resonance energy transfer (FRET) indicated that the subunits exist in a tightly packed arrangement that involves multifold protein-protein interactions. Our data also

indicated that the CENP-O/P/Q/U/R complex assembles on kinetochores in S-phase (Eskat et al., 2012). These proteins did not assemble into sub-complexes in the cytoplasm before kinetochore binding but instead assembeled at the kinetochore as individual monomers of CENP-O, P, Q or U and pre-formed CENP-O-P dimers. This work also found that the binding of CENP-O/P/Q/U/R complex to the kinetochore is mediated by the CENP-N binding protein CENP-L, as well as CENP-K (Eskat et al., 2012). Once assembled at the kinetochore these proteins have an extremely low turnover rate, exchanging very slowly with the nucleoplasmic pool of CENP-O/P/Q/U/R proteins. Experiments measuring fluorescence recovery after photo-bleaching clearly illustrate this slow turn over, as the time for half fluorescence signal recovery was extremely high. In G1 the slowest recovery was that of CENP-R (t½ 125 ± 15 min) and the fastest recovery was that of CENP-Q (t½ 57 ± 10 min). Interestingly it was also found that at the end of S-phase, CENP-Q and CENP-U undergo oligomerisation, one possibility being that this change in stoichiometry represents a pre-mitotic priming step required for the complex to become active (Eskat et al., 2012).

1.2.3.5 Role of CCAN in assembly of the kinetochore

In addition to recruitment of other CCAN subunits, many CCAN proteins are also involved in assembly of additional kinetochore components. One example is the recruitment of the mitotic kinase polo like kinase 1 (Plk1) by CENP-U. Plk1 is a key serine/threonine kinase required for regulation of diverse roles throughout mitosis such as mitotic entry, centrosome maturation and separation and chromosome congression (van Vugt & Medema, 2005; Sumara et al., 2004; Lenart et al., 2007; Hanisch et al., 2006b). Plk1 phosphorylates CENP-U at T78, creating a site that can bind the polo box domain of Plk1 and tether the kinase to the kinetochore (Park et al., 2011; Kang et al., 2011; see Figure 1.2c). Thus, depletion of CENP-U causes decreased levels (~50%) of kinetochore bound Plk1. The binding of Plk1 to CENP-U also results in the phosphorylation of CENP-Q (see Figure 1.2c), however the residues at which CENP-Q is phosphorylated remain unreported (Kang et al., 2011). These phosphorylation events have been suggested to delocalise CENP-U and CENP-Q from kinetochores at metaphase and inhibition or depletion of Plk1 causes increased kinetochore-bound levels of CENP-Q and CENP-U (Kang et al., 2011). Within the core

CCAN, CENP-C facilitates recruitment of the checkpoint protein Mad2 and the Mis12 complex, a component of the microtubule-binding KMN network (Kwon et al., 2007). It is now known that the dependency of the Mis12 complex upon CENP-C is due to a direct interaction between the two (Screpanti et al., 2011). Moreover, targeting CENP-C to artificial chromosomal loci is sufficient to drive ectopic recruitment of the Mis12 complex, KNL1/Spc105 and Ndc80/Hec1 (Przewloka et al., 2011). Furthermore artificial CENP-C targeting in DT40 cells gives rise to kinetochores functional in chromosome segregation, able to bind microtubules and maintain normal SAC signalling (Hori et al., 2013; Gascoigne et al., 2011). In human cells ectopic expression of CENP-C or CENP-T results in the recruitment of a number of kinetochore proteins, however the expression of both proteins is required to drive the formation of functional kinetochores (Hori et al., 2013; Gascoigne et al., 2011). The N-terminal region of CENP-T forms a direct interaction with the Ndc80 complex subunits Spc24/25 via their RWD domains (Nishino et al., 2013; see Figure 1.2c). Thus CENP-T represents a second physical linkage between the core CCAN and the microtubule-binding KMN network (Nishino et al., 2013). In *S. cerevisiae* the binding of the CENP-T orthologue (Cnn1) to Spc24 and Spc25 has been shown to compete with the Mis12 complex (Bock et al., 2012), suggesting a role in regulating the interactions between the KMN. Additionally, an interaction between Ndc80/Hec1 and CENP-H has been reported, and although the relevance of this two-hybrid result is unclear, it may represent another direct CCAN-KMN interaction (Mikami et al., 2005).

1.2.3.6 Function of CCAN

In addition to the roles discussed above in kinetochore protein recruitment and CENP-A loading, it is now thought that CCAN itself is important in promoting chromosome alignment to the spindle equator. Indeed, depletion of any CCAN protein disrupts chromosome congression (Foltz et al., 2006; Okada et al., 2006; McClelland et al., 2007; Hori et al., 2008a; Amaro et al., 2010). It is unlikely that these congression defects are a result of the indirect, partial loss of the KMN from kinetochores because kinetochores are clearly still able to establish end-on biorientated attachments to K-MTs and form a metaphase plate (McClelland et al., 2007; Mchedlishvili et al.,

2012; Amaro et al., 2010; Foltz et al., 2006). CCAN depletions cause an increase in the width of the metaphase plate and the presence of a small number of unaligned chromosomes (Foltz et al., 2006; Okada et al., 2006; McClelland et al., 2007; Amaro et al., 2010). Interestingly, depletion of CENP-O and CENP-L also results in the accumulation of monopolar spindles due to slow spindle assembly when centrosomes are not fully separated at nuclear envelope breakdown (see below; Toso et al., 2009; McClelland et al., 2007; Mchedlishvili et al., 2012).

How CCAN regulates congression is unknown. It is known that K-MT dynamics are important for chromosome movement. CENP-H depletion disrupts K-MT dynamics, leading to an increased rate of K-MT plus-end turnover (Amaro et al., 2010). Depletion of CENP-H also disrupts poleward K-MT flux and increases spindle MT acetylation, suggesting that the K-fibre lattice is hyper-stable. Consistent with this, K-MTs in CENP-H depleted cells have increased resistance to cold induced depolymerisation (Amaro et al., 2010). The CCAN may therefore contribute to congression by controlling K-MT dynamics.

Consistently, other CCAN depletions also affect K-MT dynamics: CENP-L depletion causes increased K-MT plus-end turnover and non-homogeneous poleward microtubule flux. In contrast to CENP-H depletion, K-MTs in CENP-L depleted cells are less cold stable (Mchedlishvili et al., 2012). This can explain the monopolar phenotype observed in CENP-L depleted cells as it has previously been shown that kinetochores drive prometaphase centrosome separation by controlling poleward K-MT flux. Addition of tubulin hetrodimers at K-MTs plus-ends imparts a pushing force, which powers centrosome separation (Toso et al., 2009). Thus, CENP-L depletion results in a 5-6 min delay in spindle pole separation which causes severe chromosome segregation defects due to the formation of syntelic and merotelic kinetochore–microtubule attachments (McClelland et al., 2007; Mchedlishvili et al., 2012). However, this is only the case in cells that have not separated their spindle poles prior to nuclear envelope breakdown (Mchedlishvili et al., 2012). In CENP-O depleted cells, where CENP-L remains bound, the failure to separate centrosomes results from a decrease in the stability of K-fibres, which are therefore less efficient in imparting centrosome

pushing forces (Toso et al., 2009; McClelland et al., 2007). It remains unknown by which mechanisms the CCAN controls K-MT dynamics. Two possible candidates are CENP-Q and CENP-U (see CCAN proteins labelled in red in see Figure 1.2a, c), both of which interact with MTs *in vitro* (Amaro et al., 2010; Hua et al., 2011). Of these two proteins CENP-Q is perhaps the most likely candidate as recent work in our lab has shown that CENP-Q is able to modulate MT dynamics *in vitro* and depletion of the protein reduces K-MT plus-end turnover *in vivo* (Samora C.P., PhD thesis, 2012). However, other CCAN recruited factors may alternatively be responsible for regulating K-MT dynamics.

1.2.4 The core kinetochore-microtubule interface

In order for microtubule dynamics to power chromosome movements they must first be stably bound to the kinetochore in an end-on orientation, *i.e.* the plus-end of the microtubule terminating at the kinetochore. On a basic level this would seem to be a relatively simple interaction, however, when one considers that microtubules are dynamic polymers constantly undergoing growth and catastrophe events, the extra level of complication becomes apparent. It is essential that the kinetochore is able to maintain end-on attachments with both growing and shrinking microtubules. It is now known that the majority of the force required for chromosome movement is generated at the poleward (P) moving kinetochore, with net microtubule shrinkage within the K-fibre effectively pulling the P kinetochore pair (Dumont et al., 2012; Khodjakov & Rieder, 1996). On mono-orientated kinetochores a stable interaction therefore ensures efficient poleward transport and, at amphitelic attached sister-kinetochores pairs (where each sister is attached to opposite spindle poles), powers biorientated alignment to, and maintenance at, the spindle equator (see section 1.4 for more details). The proteins and protein complexes involved in the maintenance of these attachments are discussed below and are shown in Figure 1.3.

1.2.4.1 The KMN network

The KMN complex is the key microtubule binding protein network within the kinetochore. In vertebrates this protein network consists of the Knl1 (kinetochore null lethal; also known as Blinkin) protein and its binding partner Zwint, the four subunit Mis12 complex (Mis12, Nnf1, Nsl1, Dsn1) and the four subunit Ndc80 complex (Hec1/Ndc80, Nuf2R, Spc24, Spc25) (Cheeseman et al., 2006; Cheeseman et al., 2004; DeLuca et al., 2006; Kops et al., 2005). The entire KMN network of proteins represents a dynamic feature of the kinetochore, assembling in prophase and disassembling in telophase (reviewed in Santaguida & Musacchio, 2009; Gascoigne & Cheeseman, 2013). The Ndc80 complex is the major microtubule binding protein complex within the KMN (Cheeseman et al., 2006) and is a 57nm long heterotetramer consisting of a Hec1-Nuf2 and a Spc24-Spc25 dimer (Figure 1.3). The dimers are held together by coiled-coil domains located at the N-termini of Spc24 and Spc25 and the C-termini of the Ndc80 and Nuf2 (Ciferri et al., 2008; Wei et al., 2007). In humans the Ndc80 complex is anchored to the kinetochore by the Spc24 and Spc25 subunits, which interact directly with the C-terminal region of the Mis12 complex subunit Nsl1 (Petrovic et al., 2010), and also CENP-T (Gascoigne et al., 2011; Figure 1.3).

The key microtubule binding subunit within the complex is the Hec1/Ndc80 protein (Cheeseman et al., 2006). Hec1 mediates its interaction with microtubules by a calponin homology (CH) domain within the N-terminal region of Hec1 and by a positively-charged region spanning ~80 amino acids within Hec1 located at the extreme N-terminus; the combined action of these two domains gives rise to a microtubule binding dissociation constant of 0.5 μM (Wei et al., 2007; Ciferri et al., 2008; Guimaraes et al., 2008; Cheeseman et al., 2006). The combined action of both domains is required to create normal stable kinetochore-microtubule attachments and pulling forces and thus facilitate timely mitotic progression (Sundin et al., 2011; Tooley et al., 2011; Deluca et al., 2005). The positively charged amino-terminus of Hec1 binds to tubulin monomers within microtubules at their negatively charged C-terminal tails or “E-hooks” (Alushin et al., 2010; Ciferri et al., 2008; Tooley et al., 2011). Within the Hec1 CH domain there is a region known as the Hec1 “toe”. This region recognises a site between two tubulin monomers (at both inter and intra-dimer interfaces). This

Figure 1.3

a

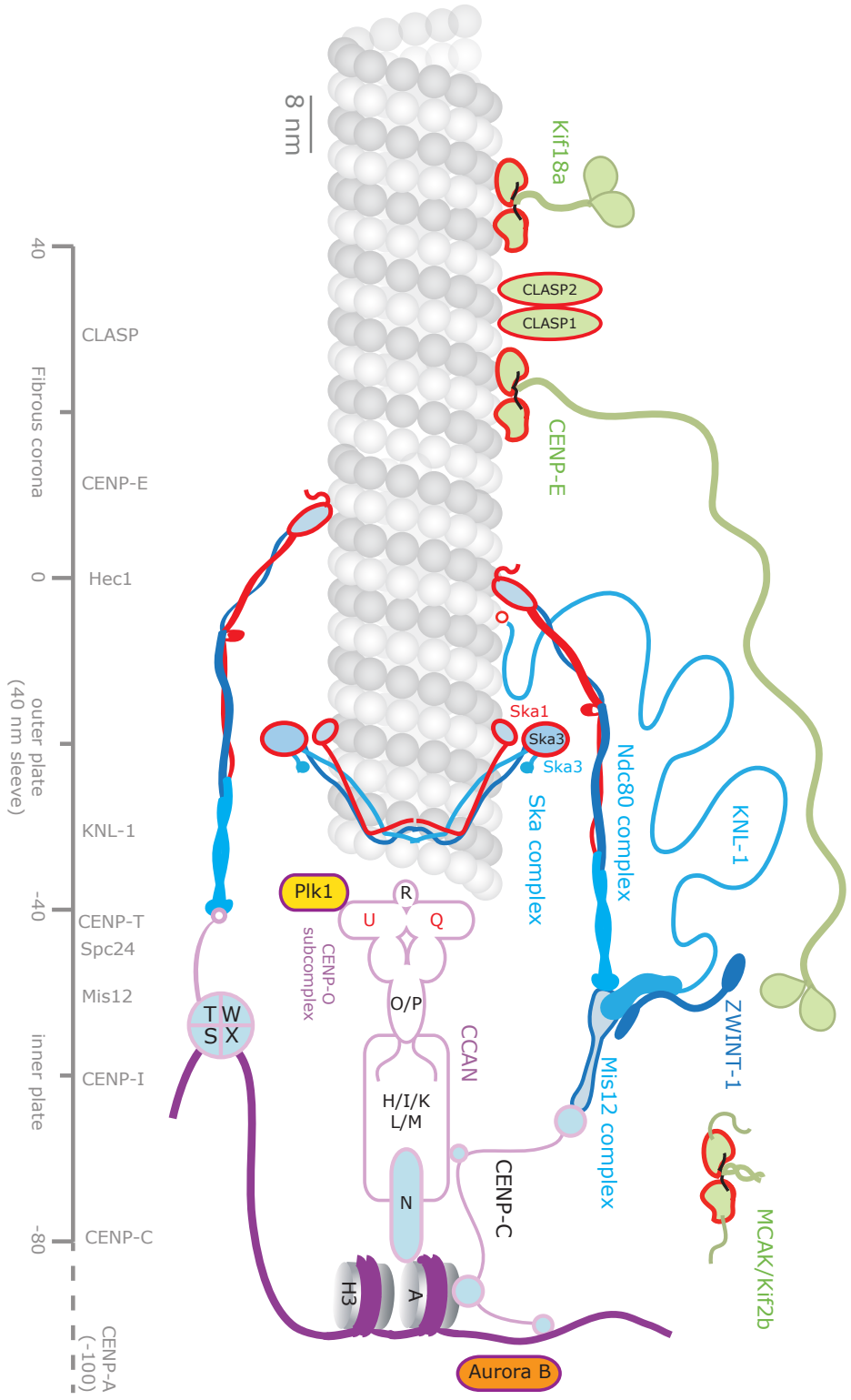

Figure 1.3 Schematic of the human kinetochore showing key kinetochore proteins that form the microtubule-attachment site. These factors can be classified as CCAN (pink), KMN and Ska complexes (blue) and kinetochore-associated kinesins motors (green). Red outlines indicate microtubule interacting proteins. Kinases are shown as ovals with purple outlines. The grey scale bar shown on the left represents subpixel position of individual proteins within the kinetochore relative to Hec1. (adapted from Wan et al., 2009). DNA is represented by dark purple lines. Figure is adapted from original illustration by Andrew McAinsh.

"toe-print" changes shape when microtubules begin to curve at depolymerising microtubule ends, and as the "toe" has a higher affinity for the straight microtubules Hec1 has a higher affinity for the MT lattice rather than depolymerising ends (Alushin et al., 2010). It is believed that this property of the Hec1 protein gives rise to a biased diffusion, allowing the Ndc80 complex to remain attached to depolymerising MTs (Alushin et al., 2010). Like Hec1, the Nuf2 protein also contains a CH domain, however, unlike Hec1 this CH domain does not contribute significantly to the generation of stable kinetochore-microtubule attachments (Sundin et al., 2011). Mutations in this region nonetheless show that the Nuf2 CH domain is important in creating normal microtubule dependent kinetochore force and promoting timely chromosome congression (Sundin et al., 2011).

The Ndc80 complex is also a key effector of the error correction machinery, which ensures that incorrect microtubule-kinetochore attachments (such as syntelic attachments) are destabilised (reviewed in Varma & Salmon, 2012). The key protein in initiating error correction is the kinase Aurora B (Figure 1.3). It is known that Aurora B phosphorylates several targets within the Ndc80 complex and elsewhere in the KMN, causing incorrect microtubule attachments to be released by reducing the microtubule binding activity of the complex (Welburn et al., 2010; Cheeseman et al., 2006; Chan et al., 2012; reviewed in Varma & Salmon, 2012). The Hec1 protein is a prime example of an Aurora B error correction target, Hec1 contains nine Aurora B kinase phosphorylation sites localised in its microtubule-binding domain. Phosphorylation of these sites reduces the affinity of Hec1 for microtubules as phosphorylation disrupts the positive charge required for electrostatic binding to microtubules (Cheeseman et al., 2006; Santaguida & Musacchio, 2009; Welburn et al., 2010). Phosphorylation of Hec1 allows removal of erroneous microtubule attachments so that kinetochores can reattempt biorientation (Cheeseman et al., 2006; Cimini et al., 2006; DeLuca et al., 2006; Sandall et al., 2006; Welburn et al., 2010). Hec1 is also phosphorylated by the Nek2 protein kinase at serine 165, which promotes the recruitment of the spindle assembly checkpoint (SAC) proteins Mad1 and Mad2 (Wei et al., 2011; Chen et al., 2002). Whether this is a direct binding is unknown, although there is a reported yeast two-hybrid interaction between Mad1 and Hec1 (Guimaraes et al., 2008; Martin-Lluesma et al., 2002; Miller et al., 2008; Wei et al., 2011).

The Ndc80 complex further contributes to SAC signalling through the Aurora B phosphorylation-dependent recruitment of the checkpoint kinase MPS1/TTK (Vigneron et al., 2004; Hewitt et al., 2010; Santaguida et al., 2010; Maciejowski et al., 2010).

KNL1 is a 2316 amino acid long molecule, which contains a microtubule binding sequence at the extreme amino-terminus, a kinetochore-targeting domain at the C-terminus and a series of repeat sequence motifs in between (reviewed in Varma & Salmon, 2012; Figure 1.3). It has been shown that in *C. elegans* KNL1 is dispensable for generating stable kinetochore microtubule attachments but is required for SAC activity (Espeut et al., 2012). In contrast depleting KNL1 from human mitotic cells disrupts the formation of stable K-MTs, and upon progression to anaphase these cells often exhibit sister chromosome missegregation (Cheeseman et al., 2008; Kiyomitsu et al., 2007; Schittenhelm et al., 2009). Both human and *C. elegans* KNL1 exhibit low affinity microtubule binding *in vitro* (Cheeseman et al., 2006; Welburn et al., 2010; Espeut et al., 2012). Additional *in vitro* assays have shown that the microtubule affinity of Hec1 is increased by the presence of KNL1 (Cheeseman et al., 2006). Interestingly, microtubule binding by KNL1 and the Ndc80 complex is also further increased by the addition of other KMN components, suggesting that the KMN complex binds microtubules synergistically (Cheeseman et al., 2006). One possibility is that this synergy is required to allow the components of the KMN to bind to microtubules with sufficient affinity to generate a physiologically functional microtubule binding interface.

KNL1 is also an Aurora B phosphorylation target, and phosphorylation of these sites also disrupts MT binding activity (Welburn et al., 2010; Espeut et al., 2012). Recent work has shown that KNL1 is important in the recruitment of protein phosphatase 1 (PP1), which acts antagonistically to Aurora B, dephosphorylating KMN components thus allowing the KMN network to stably bind microtubules (Liu et al., 2010). It has also been proposed that KNL1 is involved in the recruitment of several key SAC proteins to the kinetochore including BUB1 and BUBR1 (Kiyomitsu et al., 2007). Recent work has shown that in budding yeast, the recruitment of BUB1, BUBR1 is dependent upon Spc105 phosphorylation by the SAC kinase MPS1 (London et al., 2012; Shepperd

et al., 2012; Yamagishi et al., 2012; Krenn et al., 2012). Given these multiple roles and interactions it is thought that KNL1 may act as a sensor for discerning correct kinetochore-microtubule attachment and influencing subsequent SAC deactivation (Espeut et al., 2012).

The 277 amino acid long protein Zwint-1 (ZW10 interacting protein-1) consists of at least two coiled-coil domains and is know to bind tightly to the C-terminus of KNL1 (Petrovic et al., 2010) forming a KNL1-Zwint-1 complex (Figure 1.3). Zwint-1 also interacts with RZZ complex, which is composed of Rod, ZW10 and Zwilch (Starr et al., 2000; Kops et al., 2005; reviewed in Varma & Salmon, 2012). RZZ is required for the recruitment of Mad1-Mad2 and Spindly, which in turn recruits Dynein-dynactin to kinetochores (Buffin et al., 2005; Kops et al., 2005; Griffis et al., 2007; Chan et al., 2009). This set of protein-protein interactions are involved in both the activation and silencing of the SAC (Karess, 2005; Gassmann et al., 2010). Like many other KMN proteins Zwint-1 has also been shown to be an Aurora B phosphorylation target and it is thought that this phosphorylation is required for the recruitment of the RZZ complex (Kasuboski et al., 2011). There is also evidence that Zwint binds to the Hec1 subunit of the NDC80 sub-complex (Lin et al., 2006) and to Mis12 (Obuse et al., 2004), thus providing a possible link between KMN sub-complexes.

Unlike the Ndc80 complex and KNL1, the Mis12 complex does not possess microtubule binding activity, although its presence does increase the MT binding activity of the Ndc80 complex and KNL1 (Cheeseman et al., 2006). Instead, the function of the Mis12 complex is a largely structural one, acting as the “keystone” of KMN assembly (Cheeseman & Desai, 2008). Negative stain electron microscopy shows the Mis12 complex to be a 22 nm long rod structure, with the four proteins that form the complex (Nnf1, Mis12, Dsn1, Nsl1) being visible as 4 consecutive domains within the rod (Petrovic et al., 2010). The main function of the Mis12 complex is to form a structural platform for the loading of the major KMN microtubule binding components; the Ndc80 complex and the KNL1 protein (Petrovic et al., 2010). The C-terminal region of Nsl1 binds the C-terminal domains of Spc24 and Spc25 tethering the Ndc80 complex, and to the C-terminus of KNL1 (Petrovic et al., 2010). The Mis12 complex itself is bound to the kinetochore through a direct

interaction with CENP-C (Figure 1.3). However it is currently unknown which Mis12 subunit(s) mediate this interaction in vertebrate cells (Screpanti et al., 2011). In *D. melanogaster*, which lack the Dsn1 subunit of the Mis12 complex, it has been shown that there is a direct interaction between CENP-C and the Nnf1 subunit of the Mis12 complex (Przewloka et al., 2011). Depletions of Nnf1/Mis12/Dsn1/Nsl1 result in perturbation of chromosome biorientation, faithful chromosome alignment and segregation as well as a failure to form stable K-fibres (Kline et al., 2006; Venkei et al., 2011; reviewed in Varma & Salmon, 2012). These depletion phenotypes are not as severe as depletion of the Ndc80 complex, consistent with the dual loading of this complex to kinetochores by Mis12 and CENP-T. The Mis12 complex may also be controlled by phosphorylation as the Dsn1 protein is a confirmed target of Aurora B kinase (Welburn et al., 2010).

1.2.4.2 The Ska complex

The Ska complex, consisting of Ska1, Ska2 and Ska3/Rama1 has also been identified as a major microtubule-binding complex localising to the kinetochore and K-fibres (Hanisch et al., 2006a; Gaitanos et al., 2009; Welburn et al., 2009; Daum et al., 2009; Raaijmakers et al., 2009). High-resolution structural work has shown that 2 copies of each of the 3 subunits associate to form a W-shape (Figure 1.3), which is approximately 35 nm wide (Jeyaprakash et al., 2012). The resulting complex has 4 microtubule binding sites, one from each of the 2 copies of Ska1 and Ska3. These sites are located at the two ends of the W-shape and interact electrostatically with microtubules (Jeyaprakash et al., 2012). It is thought that the W-conformation of the Ska complex may aid in binding to the curved sides of microtubules. *In vitro* studies with the human Ska proteins have shown that binding of the Ska complex to microtubules is cooperative (Welburn et al., 2009). Furthermore, the Ska complex can form oligomers, which are able to bind to the plus-ends of depolymerising MT ends along both straight and curved MT protofilaments and move processively with the depolymerising ends (Welburn et al., 2009; Schmidt et al., 2012). This distinguishes the Ska complex from the Ndc80 complex, which is only able to bind efficiently to the straight microtubule lattice (Alushin et al., 2010; Welburn et al., 2009).

The binding of the Ska complex to the kinetochore requires the presence of the Ndc80 complex (Hanisch et al., 2006a), with which it binds via the loop domain of Ndc80/Hec1 (Zhang et al., 2012). *In vitro* assays have shown that this interaction allows the Ndc80 complex to efficiently track microtubule plus-ends, a property that is required for the kinetochore to maintain end-on attachments to K-MTs (Schmidt et al., 2012) and facilitate force generation following MT catastrophe events. Recent work shows that in addition to interactions with the Ndc80 complex, the Ska complex also interacts with the Mis12 complex and KNL1, yeast 2-hybrid experiments have provided evidence for interactions between Hec1-Ska1, Mis12-Ska2 (also confirmed by pull-down assays) and Spc24-Ska3 (Chan et al., 2012). Robust binding of Ska to the kinetochore requires all three of these KMN members (Chan et al., 2012). Like the KMN, the Ska complex is also a target of Aurora B, with Ska1 and Ska3 being phosphorylated by the kinase. These phosphorylation events break the interaction between the Ska complex and the KMN, preventing the recruitment of the Ska complex to the kinetochore, which in turn inhibits its role in stabilising kinetochore-microtubule plus-end binding (Chan et al., 2012). As may be expected from a protein complex that contributes to kinetochore-microtubule plus-end binding, depletion of Ska proteins results in destabilised K-fibres, perturbed chromosome congression and cell death (Gaitanos et al., 2009). However, these depletions only result in a small reduction in KMN kinetochore-binding (Gaitanos et al., 2009).

1.3 Kinetochore-bound MAPs & molecular motors

In addition to the KMN-Ska complexes discussed above, a number of other proteins bind microtubules and regulate their dynamics when kinetochore-bound. These include members of the kinesin superfamily of molecular motors and cytoplasmic dynein, all of which can generate force by “walking” along the microtubule lattice powered by the hydrolysis of ATP. This force generation can be linked to the movement of chromosomes (through stepping along the lattice or influencing microtubule dynamics), but also the delivery and removal of cargos from the kinetochore. Discussed below is a subset of these proteins that are most relevant to this study.

1.3.1 Microtubule associated proteins (MAPs)

The EB protein family of MAPs (consisting of EB1, EB2 and EB3) are known to track the plus-ends of growing microtubules, an association which has been shown both in living cells (Stepanova et al., 2003), and in *in vitro* reconstitution assays (Bieling et al., 2007). They are thus the founding members of the set of MAPs known as plus-tip interacting proteins (+TIPs). Biochemical studies show that EB1 increases the net growth rate and rescue frequency of dynamic microtubules *in vitro* as well as reducing depolymerisation rate (Manna et al., 2008; Lopus et al., 2012; Vitre et al., 2008). However, it is also known that EB proteins are important in targeting other proteins to the plus-ends of microtubules, a role which has been demonstrated *in vitro* with CLIP-170 (Lopus et al., 2012), and $p150^{Glued}$ CAP-Gly domain (Manna et al., 2008). In both of these examples adding EB1 plus the additional component greatly increased the effect of EB1 on growth rate, rescue frequency and catastrophe suppression. However, the microtubule depolymerase MCAK must also bind to EB1 to reach its site of action at the plus-ends of microtubules (Honnappa et al., 2009). It has been shown that EB proteins localise to the kinetochore in a microtubule dependent manner, being enriched on the trail kinetochore (Tirnauer et al., 2002). Consistent with a role in mitosis, depletion of EB1 in HeLa cells affects the movement and orientation and position of the metaphase plate but does not affect kinetochore attachment to K-fibres (Draviam et al., 2006). However, the most striking aspect of depletion is a large increase in anaphase errors such as DNA bridges and lagging chromosomes (Draviam et al., 2006). The same defects also resulted from the depletion of the adenomatous polyposis coli protein (APC), which is recruited to the kinetochore/K-fibre plus tip by EB1 suggesting that the effect of EB1 depletion on mitosis may be an indirect one (Draviam et al., 2006).

It has been known for almost two decades that the APC protein binds to EB1 (Su et al., 1995), and it is now also known that this interaction is required for the targeting of APC to microtubule plus-ends (Draviam et al., 2006). APC increases microtubule growth rate and stability, and reduces

catastrophe frequency (reviewed in Rusan & Peifer, 2008; Bahmanyar et al., 2009). During mitosis the APC protein localises to kinetochores in a microtubule dependent manner (Fodde et al., 2001), as well as other key mitotic sites such as the centrosome and cell cortex (reviewed in Bahmanyar et al., 2009). Consistent with a role in mitosis the APC protein was discovered as a result of it often being mutated in isolated colonic cancer cells (Kinzler et al., 1996). Subsequent studies have shown that depletion of APC or mutations that disrupt its interaction with EB1 result in chromosomal instability (Fodde et al., 2001). Live cell imaging has revealed that APC depletions and mutations result in incorrect spindle positioning, disrupted metaphase alignment, chromosome segregation errors and failure to maintain normal SAC signalling (reviewed in Rusan & Peifer, 2008; Bahmanyar et al., 2009). Given the role of APC in promoting MT growth it is thought that these defects caused by its depletion may result from disrupted K-fibre MT dynamics (Su et al., 2009; Dikovskaya et al., 2007).

Like APC, the CAP-Gly protein CLIP-170 is also an EB1 interactor, and this interaction is indispensible in facilitating CLIP-170 microtubule plus-end tracking (Komarova et al., 2005). *In vitro* assays have shown that CLIP-170 alone is able to bind to microtubules *in vitro*, but does not show plus-end specificity (Diamantopoulos et al., 1999). It is known that CLIP-170 has a stabilising effect on microtubule dynamics, increasing growth rate and decreasing catastrophe frequency *in vitro* (Lopus et al., 2012). Interestingly this effect is synergistically increased by the presence of EB1, with a mixture of EB1 and CLIP-170 together being effective at concentrations much lower than either protein in isolation (Lopus et al., 2012). Although CLIP-170 is present throughout the cell cycle it has been shown to associate with kinetochores during mitosis but is displaced in metaphase (Dujardin et al., 1998; Tanenbaum et al., 2006). Interestingly it is thought that at least part of the kinetochore bound population of CLIP-170 is delivered by the dynein/dynactin complex (Tanenbaum et al., 2006). CLIP-170 has also been shown to bind non-microtubule bound kinetochores, leading to the suggestion that the protein aids in the initial formation of stable kinetochore-microtubule attachment (Dujardin et al., 1998). Depletion of CLIP-170 results in perturbed chromosome congression (Dujardin et al., 1998; Tanenbaum et al., 2006). Consistent

with a role in modulation of microtubule dynamics and its localisation to the kinetochore, depletion of CLIP-170 results in the perturbation of normal metaphase alignment and the destabilisation of kinetochore-microtubule binding (Dujardin et al., 1998; Tanenbaum et al., 2006). Work on the role of *S. pombe* CLIP-170 homologue Tip1 in mitosis has shown that the protein is important in poleward transport of chromosomes (Goldstone et al., 2010).

CLASP proteins are also microtubule-binding proteins capable of plus-end tracking and were initially identified by their interaction with CLIP-170/CLIP-115 (Akhmanova et al., 2001; see Figure 1.3). However, the *D. melanogaster* homologue Orbit/Mast had previously been identified (Lemos et al., 2000; Inoue et al., 2000). CLASPs localise to the plus-ends of growing microtubules, displaying a comet like distribution similar to the EB family proteins (Akhmanova et al., 2001). Interestingly CLASP1 and CLASP2 have also been shown to interact with actin filaments and thus may function to integrate the actin and microtubule cytoskeletons (Tsvetkov et al., 2007). CLASP proteins bind to microtubules via a conserved TOG-domain, *in vitro* and *in vivo* work has shown that these proteins promote microtubule polymerisation and reduce catastrophe events (Al-Bassam et al., 2010; reviewed in Al-Bassam & Chang, 2011). A recent study by our laboratory has demonstrated that CLASP1 and MAP4 proteins work together to ensure correct positioning of the mitotic spindle (Samora et al., 2011). During mitosis CLASP proteins are enriched at the plus-ends of growing spindle microtubules and form a component of the outer corona of the kinetochore in metaphase and prometaphase (Maiato et al., 2003a; Maffini et al., 2009). However, during anaphase CLASP1 re-localises to the central spindle and spindle poles, and accumulates in the midbody in telophase (Maffini et al., 2009). Initial work showed that inhibition of CLASP1 by microinjecting cells with anti-CLASP1 antibodies disrupted normal K-fibre dynamics as the growth and shrinkage events that give rise to kinetochore oscillation were no longer observed (Maiato et al., 2003a). This initial work also showed that K-fibres were shorter in the absence of CLASP1 activity. Furthermore, the absence of CLASP1 activity also greatly increased monopolar spindle formation, and in spindles that did achieve bipolarity, chromosome congression to the spindle equator was perturbed (Maiato et al., 2003a; Maiato et al., 2003b). Similar effects are seen in *D.*

melanogaster cells depleted of the CLASP homologue MAST/Orbit (Maiato et al., 2005), where it was demonstrated that MAST/Orbit was required to incorporate tubulin dimers into the spindle to drive K-fibre flux. Recent work in human cells has also demonstrated the requirement of CLASPs to drive poleward MT flux in human cells. The depletion of CLASPs also decreased K-MT plus-end turnover (Maffini et al., 2009). It is now known that the loading of CLASP1 and CLASP2 to the kinetochore is facilitated by the kinesin 7 CENP-E, independent of its motor activity (Maffini et al., 2009).

1.3.2 Molecular motors

Molecular motors are a group of proteins able to use the energy from nucleotide hydrolysis in order to do physical work. Two classes of molecular motor are kinesins and dynein, both of which use ATP hydrolysis to power walking movements along microtubule tracks, with dynein walking towards microtubule minus ends and kinesin generally (but not always) walking towards microtubule plus-ends (reviewed in Vogel, 2005; von Delius & Leigh, 2011). In addition to walking, some of these molecules are also able to influence the dynamics of the microtubules themselves (Wu et al., 2006). The microtubule-interacting motor proteins most relevant to this study are discussed below (shown in Figure 1.3).

1.3.2.1 CENP-E

Centromere protein E (CENP-E) belongs to the kinesin-7 family and is a slow, but processive, plus-end directed motor protein (Kim et al., 2008). The human CENP-E protein is 2663 amino acids in length, consisting of an N-terminal motor domain, an extensive flexible coiled-coil region, a kinetochore binding domain, a further short coiled-coil domain and a C-terminal microtubule-binding domain (Wood et al., 1997; Gudimchuk et al., 2013; Kim et al., 2008; Figure 1.3). CENP-E is a dimeric kinesin, the two CENP-E monomers dimerising by the coiled-coil region of the molecule. *In vitro* assays have also shown that CENP-E has a stabilising effect on dynamic microtubules, greatly increasing plus-end elongation (Sardar et al., 2010). As the addition of tubulin subunits is tightly coupled to ATP turnover this activity must require the motor domain of CENP-E.

In line with this result *in vivo* work has shown that depletion of CENP-E results in reduced spindle length and reduced K-fibre poleward flux as well as chromosome congression defects (Maffini et al., 2009). However, this study also showed that K-fibre plus-end turnover was reduced in CENP-E depleted cells. More recent *in vitro* work has shown that unlike many kinesins, which detach upon reaching microtubule tips, full length human CENP-E remains attached to microtubules, switching from lateral attachment to tip tracking (Gudimchuk et al., 2013). This tip tracking activity requires the combined activity of both the CENP-E motor domain and the additional microtubule-binding domain in the C-terminal tail of the molecule. In this tip-tracking mode CENP-E is able to remain attached to both depolymerising and polymerising microtubules. Previous studies using truncated CENP-E did not see this behaviour as these truncations lack the C-terminal microtubule-binding domain (Gudimchuk et al., 2013; Kim et al., 2008).

CENP-E is bound to kinetochores during mitosis and it is thought that the ability of CENP-E to track depolymerising microtubules may represent an additional mechanism by which kinetochores can maintain attachment with depolymerising MTs (Gudimchuk et al., 2013). Recent work has shown that, in addition to CENP-E's role in mono-orientated chromosome congression (see section 1.4 below), the protein may function to maintain stable kinetochore-microtubule attachments (Gudimchuk et al., 2013; Kim et al., 2008). Indeed, work within the Grishchuk laboratory has shown that allosteric inhibition of the CENP-E motor domain with the small molecule inhibitor GSK923295 results in a number of chromosomes falling away from the metaphase plate (Gudimchuk et al., 2013). This inhibitor binds to loop-5 of CENP-E and prevents the kinesin from releasing inorganic phosphate (Pi) produced by ATP hydrolysis, this in turn results in the motor becoming rigor bound to microtubules (Wood et al., 2010). The loss of chromosomes from the metaphase plate in the presence of the inhibitor seems to suggest a subset of chromosomes require active CENP-E to maintain kinetochore-microtubule attachment, however it is also possible that these chromosomes, although aligned, have not yet become biorientated and therefore remain dependent upon CENP-E. It has also been demonstrated that inhibition of CENP-E disrupted the ability of kinetochores to

track K-fibres depolymerised by nocodazole treatment, thus providing further evidence that CENP-E may help kinetochores track depolymerising microtubules (Gudimchuk et al., 2013).

It has also been proposed that the long coiled-coil of CENP-E may allow the protein to aid in the initial capture of microtubules by kinetochores as the length and flexibility of the molecule (~230 nm) would allow it to efficiently seek out microtubules over a relatively large area (Kim et al., 2008). In support of this idea studies have shown that CENP-E is enriched on unattached kinetochores (Hoffman et al., 2001) suggesting a possible role in attachment generation.

1.3.2.2 Klf18a

The mitotic kinesin Kif18a (Klp67A in *D. melanogaster*; KipB in *A. nidulans*, Kip3p in *S. cerevisiae* and klp5/6 in *S. pombe*) is a member of the kinesin-8 family and has also been shown to be a slow processive plus-end directed motor protein (Mayr et al., 2007). In addition to its N-terminal motor domain, Kif18A also contains a MT-binding domain within its C-terminus. This domain provides a second site to tether Kif18a to the microtubule lattice increasing its processivity by preventing detachment. *In vitro* studies have shown that this C-terminal MT-binding domain allows Kif18a to accumulate at microtubule plus-ends (Stumpff et al., 2011). The expression of Kif18a is highest during M phase, and during mitosis Kif18a is enriched at kinetochores but is also visible on K-fibres (Mayr et al., 2007; Weaver et al., 2011). Unlike CENP-E, there is evidence that Kif18a may act as a microtubule depolymerase *in vitro* (Stumpff et al., 2011; Mayr et al., 2007). The same being true of the yeast othologue Kip3, which has been shown to control spindle length by microtubule depolymerisation (Varga et al., 2009). Interestingly, it is thought that Kif18a depolymerises longer microtubules at a higher rate than short ones, however it is unknown by what mechanism Kif18a biases its depolymerisation activity based on microtubule length (Mayr et al., 2007). Consistent with this activity and its localisation to kinetochores it has been shown that depletion of Kif18a results in increased spindle length (Mayr et al., 2007; Weaver et al., 2011). The most conspicuous effect of Kif18a depletion is perturbed chromosome congression with cells often being unable to form a metaphase plate, this failure to congress results in a large accumulation of mitotic cells

(Mayr et al., 2007; Huang et al., 2009; Mayr et al., 2011; Stumpff & Wordeman, 2007). Other studies have suggested that rather than being an active depolymerase Kif18a may act to suppress microtubule plus-end polymerisation (Du et al., 2010; Stumpff et al., 2012). Consistent with this idea it has been shown that Kif18a acts to suppress kinetochore movements in late metaphase (Stumpff et al., 2008), and its depletion results in increased K-MT plus-end turnover (Manning et al., 2010). Depletion of the protein increases the speed of kinetochore movement (Jaqaman et al., 2010). Interestingly it has been shown that the presence of Kif18a at the kinetochore may be required for the efficient kinetochore loading of CENP-E (Huang et al., 2009). CENP-E and Kif18a co-immunoprecipitate in mitotic cells, suggesting that they are in the same complex and it is therefore possible that this dependency reflects a direct or indirect physical interaction (Huang et al., 2009).

1.3.2.3 MCAK

Unlike Kif18a and CENP-E the protein MCAK (mitotic centromere-associated kinesin) is a non-motile kinesin-13 family protein that is associated with the inner kinetochore/centromere during mitosis (Wordeman & Mitchison, 1995; see Figure 1.3). MCAK possesses an N-terminal coiled-coil domain important for dimerisation and a motor-like domain that is located towards the middle of the molecule (Hertzer et al., 2006). Although MCAK is non-motile its motor-like domain is still able to hydrolyse ATP, but rather than using this hydrolysis to drive movement the molecule uses it to drive microtubule depolymerisation (Hertzer et al., 2006; Hunter et al., 2003; reviewed in Moores & Milligan, 2006). This depolymerisation activity occurs at microtubule ends and it has been shown that MCAK ATPase activity is specifically stimulated by association of the molecule with microtubule plus-ends (Hunter et al., 2003). The depolymerisation activity of MCAK has been demonstrated to use approximately 5 ATP molecules for each tubulin heterodimer removed from a microtubule (Hunter et al., 2003). To enable efficient localisation to its site of action at microtubule plus ends in the absence of motor activity, MCAK contains an SxIP motif, which allows it to bind to EB1. The plus-tip tracking activity of EB1 then ensures accurate delivery of MCAK to microtubule plus-ends (Honnappa et al., 2009). In accordance with the loading of MCAK to the

kinetochore/centromere during mitosis and its depolymerising activity recent work has shown that MCAK functions to reduce mitotic spindle length (Domnitz et al., 2012). This work also showed that due to its depolymerisation activity, MCAK antagonises the separation of centrosomes and the rate of bipolar spindle formation. However, this delay has been shown to promote the formation of robust attachments between K-fibres and kinetochores, as MCAK-depleted cells maintain high levels of kinetochore-bound Mad2, even after biorientation has occurred (Domnitz et al., 2012). In line with this, other studies have shown that depletion of MCAK can increase the frequency of lagging chromosomes during mitosis (Maney et al., 1998; Huang et al., 2007; Ganguly et al., 2011; Kline-Smith et al., 2004). One possibility is that the presence of MCAK causes tension generated by depolymerisation of K-MTs, and this tension is required to stabilise kinetochore-microtubule attachments to ensure faithful chromosome segregation. It has been shown that MCAK is under phosphorylative control by Aurora B, and that this phosphorylation negatively regulates MCAK depolymerisation activity by inducing conformational changes, which reduce its association with microtubules (Ems-McClung et al., 2103; Knowlton et al., 2006; Andrews et al., 2004). As Aurora B phosphorylation is known to be important for removing inappropriate attachments, it is possible that MCAK activity must first be reduced in order to facilitate detachment. Logically a reduction in this activity would reduce K-MT depolymerisation, therefore reducing inter-kinetochore tension, resulting in further Aurora B driven attachment destabalisation.

1.3.2.4 Dynein

Dynein differs from kinesins as it is a multi-subunit minus-end directed motor. Dynein is known to be required for many cellular transport activities requiring minus-end directed transport along microtubules, including organelle transport and retrograde axonal transport (reviewed in Holzbaur & Vallee, 1994). In order to facilitate its many roles, dynein binds to a range of adaptor proteins that gives rise to its differing cellular localisations and functions. Perhaps the best characterised of these adaptor proteins is the plus-tip protein $p150^{Glued}$ (Vaughan & Vallee, 1994). The $p150^{Glued}$ protein contains a CAP-Gly domain that interacts with the EEY/F motif at the C-terminus of α-

tubulin, the end-binding protein EB1 or CLIP-170, and by binding to $p150^{Glued}$ the minus-end directed motor dynein is able to localise to the plus-ends of microtubules (Ligon et al., 2006).

As cells enter mitosis, dynein releases its interphase adaptor proteins and cargos allowing localisation to multiple mitotic loci including the spindle poles, the cell cortex and the kinetochore (reviewed in Bader & Vaughan, 2010). Consistent with localisation at the pole and cortex, dynein has been implicated in spindle positioning (O'Connell & Wang, 2000; Samora et al., 2011; Kiyomitsu & Cheeseman, 2013). Dynein at the kinetochore has been implicated in several specific mitotic roles including chromosome movement to the pole by dynein motor activity (discussed below in section 1.4; Yang et al., 2007; Li et al., 2007). Dynein has also been implicated in helping to generate stable kinetochore-microtubule attachments (Hoffman et al., 2001; Yang et al., 2007). Displacement of dynein from the kinetochore by expression of competitive dynein tail fragments or depletion of the dynein heavy chain results in the generation of cold labile K-fibres (Varma et al., 2008). The same study also provided evidence that dynein may be important in the maintenance of kinetochore orientation relative to the K-fibre (Varma et al., 2008). It has been proposed that due to the minus-end directed motor activity of dynein the protein may function to physically strip checkpoint proteins, including BUBR1 and Mad2, from the kinetochore upon the establishment of stable kinetochore-microtubule attachments, removing itself in the process (Hoffman et al., 2001; Varma et al., 2008; Howell et al., 2001; Wojcik et al., 2001). This stripping mechanism has also been proposed for the removal of CENP-E upon biorientation (Hoffman et al., 2001). Consistent with this stripping mechanism it has been shown that the Zest White 10 (Zw10) protein is required for kinetochore localisation of dynein. Zw10 forms part of the Rod, Zw10 and Zwilch complex, which is also required for kinetochore localisation and subsequent removal of the checkpoint proteins Mad1 and Mad2 (reviewed in Karess, 2005). RNA interference screens have also identified that the protein Spindly is required for kinetochore localisation of dynein in both *D. melanogaster* and human cells (Griffis et al., 2007; Gassmann et al., 2010). This initial work showed that Spindly is enriched on unattached kinetochores and that the protein is required for SAC silencing as depletion of the protein causes cells to arrest in metaphase with elevated

kinetochore-bound levels of Mad2 and Rod/Zw10/Zwilch (RZZ) (Griffis et al., 2007). Spindly depletion also causes reduced inter-KT tension, unstable KT fibres, chromosome misalignment, spindle rotation and an extensive prometaphase delay (Chan et al., 2009). It is now thought that Spindly plays a dynein independent role in kinetochore congression, as Spindly mutants that abrogate dynein localisation do not result in the chromosome congression defects like those seen in Spindly depletion. However, these mutants do result in prolonged checkpoint signalling suggesting that dynein mediated removal of Spindly from the kinetochore is required for timely checkpoint silencing (Gassmann et al., 2010).

1.4 Mechanisms of chromosome congression

In humans, chromosome congression is a 15-20 min long process by which chromosomes move themselves to the midpoint between the spindle poles during mitosis thus forming the metaphase plate (Kops et al., 2010; Walczak et al., 2010). Given the importance of chromosome congression in ensuring mitotic fidelity it is perhaps unsurprising that several congression pathways exist, these pathways are discussed below (see Figure 1.4).

1.4.1 Instantaneous congression

During mitosis in human cells and mouse oocytes the majority of chromosomes become biorientated rapidly after nuclear envelope breakdown (Kitajima et al., 2011; Magidson et al., 2011). This rapid biorientation mechanism is dependent upon the geometry of the chromosomes in early prometaphase, when they are arranged in a ring-like (toroidal) conformation. The generation of this toroid structure requires the polar ejection force (Rieder et al., 1986), which is primarily generated by the chromokinesin KID (Kinesin-10) (Tokai et al., 1996; Brouhard & Hunt, 2005; Yajima et al., 2003), but also the pushing effect of polymerising spindle microtubules. Shortly after nuclear envelope breakdown, the chromatin is arranged as a disc within the cell, but as the spindle poles separate and the spindle forms, KID uses the microtubule architecture to eject chromosome arms from the centre of the newly formed spindle (Magidson et al., 2011; Tokai et al., 1996). This

results in the formation of a toroid of chromosomes with a central chromosome free region of ~4 μm and an outer diameter of 7 μm (Magidson et al., 2011). The majority of chromosomes within the toroid have their kinetochores located towards the centre of the structure, proximal to the chromatin free region from which KID has displaced chromosome arms, thus preventing these arms from blocking the kinetochore-microtubule binding sites. However, it has been shown that in mouse oocytes, KID is dispensable for the formation of this toroid (Kitajima et al., 2011). Regardless of how this geometry is reached, it is clear that toroid formation allows kinetochores to rapidly bind microtubules during the process of search and capture (Magidson et al., 2011). Search and capture is the process by which spindle microtubules initially search out kinetochores, the microtubules undergo continuous growth and catastrophe events leading to cytoplasmic probing and eventual contact of kinetochores which then bind the microtubules (Kirschner & Mitchison, 1986).

Search and capture can be modelled *in silico* (Paul et al., 2009), a recent study simulated search and capture on a toroidal arrangement of chromosomes versus random distributions. This simulation showed that search and capture is likely to be much more efficient when chromosomes are arranged as a toroid (Magidson et al., 2011). The simulation also showed that within 3 min, ~70% of kinetochores would be contacted by microtubules in a toroid conformation, whereas only ~30% were predicted to be contacted within 3 min in a random distribution. The simulation predicted that the toroid distribution would result in ~60% of chromosomes being stably attached within 3 min, and would reduce the time taken to attach all chromosomes by 6-8 min (Magidson et al., 2011). To test whether the predictions of the model were correct, Magidson and colleagues depleted KID to disrupt toroid formation and found that, in agreement with the model, mitotic timing increased by ~6 min compared to control depleted cells (Magidson et al., 2011). However, there is also evidence that in Xenopus the polar ejection force generated by Xkid may be actively involved in congression to the metaphase plate (Antonio et al., 2000; Funabiki & Murray, 2000), although this is not the case in humans (Levesque & Compton, 2001).

Figure 1.4

a

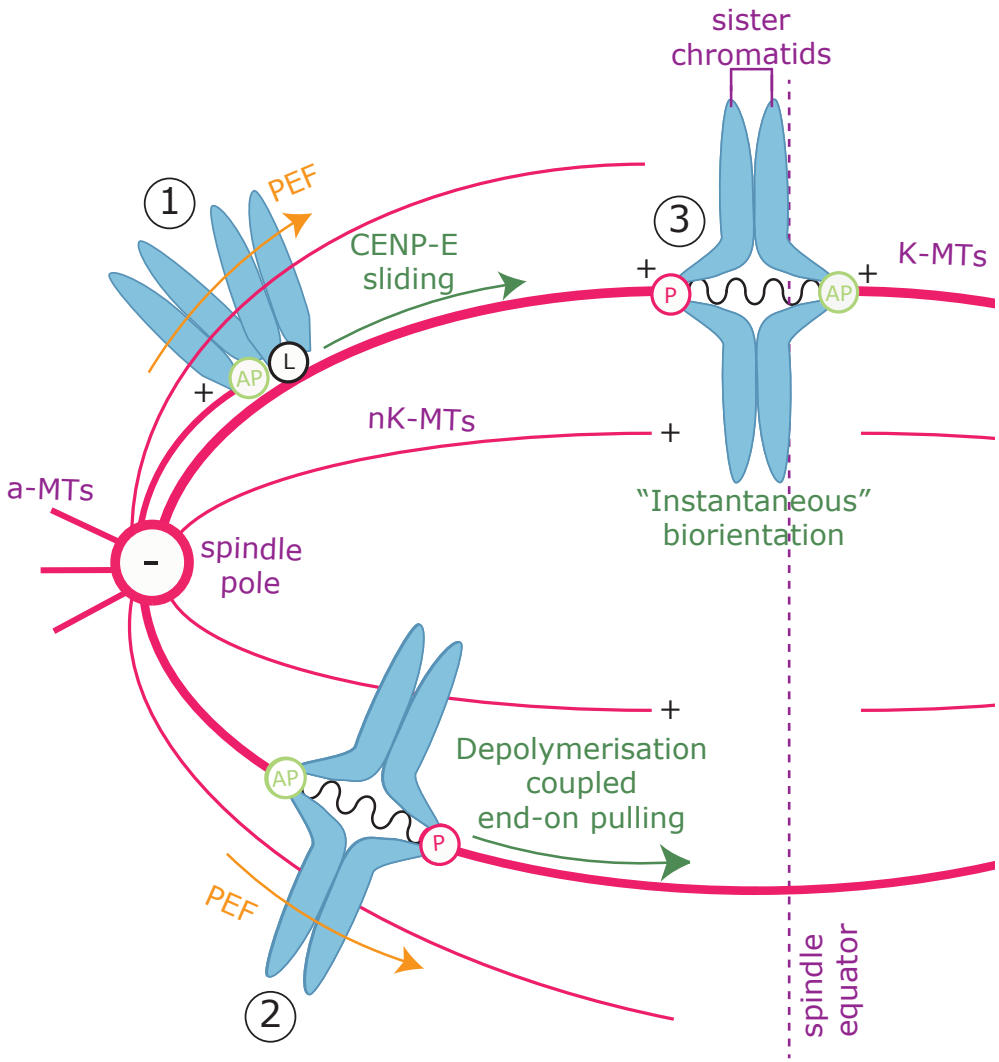

Figure 1.4 (a) Multiple mechanisms of chromosome congression. **Chromosome 1** has formed a monotelic end on attachment and is attached laterally to an adjacent K-fibre by the other sister kinetochore. The chromosome is congressing to cellular equator through the action of CENP-E on the laterally attached sister. As CENP-E motors walk towards the plus end of the adjacent K-fibre the chromosome is "towed" to the metaphase plate (Kapoor et al 2006). **Chromosome 2** is biorientated but unaligned, and is congressing through depolymerisation coupled pulling at the poleward (P) sister. **Chromosome 3** has been captured in the initial wave of biorientation due to its position close to the cellular equator. This chromosome oscillates back and forth about the metaphase plate, and is maintained at the plate as oscillations result in equal displacements to both sides of the plate. Green arrows represent the direction of kinetochore generated force, orange arrow represents force from polar ejection force on chromosome arms.

By following this “instentanious” pathway the majority of chromosomes appear to be able to rapidly congress to the metaphase plate because the toroid of chromatin is positioned at the cellular equator shortly after initiation of nuclear envelope breakdown and biorientation follows rapidly (Magidson et al., 2011; see Chromosome 3 in Figure 1.4). After biorientation the chromosome positions at the cellular equator are honed and maintained by depolymerisation-coupled pulling (see section 1.4.3 below). Although chromosomes biorientate almost instantaneously due to the geometries discussed above, evidence from studies in mouse oocytes suggests that almost 90% of chromosomes undergo at least one round of Aurora B kinase dependent error correction (Kitajima et al., 2011). It is also known that not all chromosomes are able to congress by the “instantaneous” pathway and for this reason additional mechanisms of chromosome congression and biorientation are required.

1.4.2 Lateral sliding

It is well established that the kinesin-7 CENP-E is important for normal chromosome congression. Multiple studies have shown that deletion, depletion or inhibition of CENP-E results in a sub-population of chromosomes that remain trapped proximal to the spindle pole, though the majority of chromosomes are able to congress to form a metaphase plate (Schaar et al., 1997; Kapoor et al., 2006; Gudimchuk et al., 2013; Putkey et al., 2002; Weaver et al., 2003; Wood et al., 2010). These polar chromosomes represent a population of chromosomes that have failed to biorientate at the spindle equator (as described in section 1.4.1). These chromosomes may have been in close proximity to the pole after nuclear envelope breakdown or may have been transported to the pole by kinetochore-bound dynein or mono-orientated depolymerisation-coupled pulling (described in section 1.4.3) after failing to biorientate at the equator (Skibbens et al., 1993). Chromosomes are able to mono-orientate (one kinetochore end-on attached, the other unattached) at the spindle pole but require CENP-E for congression to the metaphase plate before becoming bi-orientated (Kapoor et al., 2006). CENP-E facilitates the congression of these chromosomes to the metaphase plate by a mechanism known as lateral sliding (see Chromosome 1 in Figure 1.4). Upon congression, these

mono-orientated chromosomes are then much more likely to be able to biorientate due to the high number of microtubules emanating from the opposite pole (Kapoor et al., 2006).

A population of kinetochore bound CENP-E molecules powers lateral sliding and unsurprisingly CENP-E is enriched on unaligned/non-biorientated chromosomes (Hoffman et al., 2001; Kapoor et al., 2006). The motors on the unattached kinetochore of a mono-orientated kinetochore pair bind laterally to an adjacent K-fibre, along which the motors then slide towards the metaphase plate. CENP-E motors power this sliding by hydrolysing ATP to take 8 nm steps along the microtubule lattice (Yardimci et al., 2008). Single molecule studies have shown that CENP-E is a highly processive kinesin due to a C-terminal MT binding domain, which complements its motor domain and prevents MT detachment (Gudimchuk et al., 2013; Musinipally et al., 2013). It is likely that this processive property is important in maintaining continuous lateral sliding, although in its normal physiological role CENP-E functions as a group of motor proteins rather than as a single molecule.

Recent work has shown that the CENP-E mediated congression activity is under phosphorylative control by the Aurora A&B kinases (Kim et al., 2010). At kinetochores around the spindle poles CENP-E is phosphorylated by Aurora A at the T422 residue. This has the effect of reducing the affinity of CENP-E for single microtubules but not for bundles (Kim et al., 2010). This means that CENP-E is more likely to move in a processive manner along bundles of MTs (i.e. K-fibres), rather than single MTs (i.e. astral microtubules). Thus Aurora A phosphorylation is proposed to be the mechanism by which mitotic cells ensure that the net effect of CENP-E activity is transport of monorientated chromosomes towards the cellular equator rather than towards the cellular cortex (Kim et al., 2010). As chromosomes move towards the equator, phosphorylation of CENP-E residue T422 by Aurora A located at the pole is reduced, this allows the T422 residue to be dephosphorylated by the action of Protein Phosphatase 1 (PP1). Dephosphorylation of the T422 residue of CENP-E was shown to be required for mono-orientated kinetochores to become biorientated after having congressed to the metaphase plate by lateral sliding (Kim et al., 2010), however why this residue must be dephosphorylated remains unknown. The Grishchuk laboratory

have recently published findings suggesting that even after alignment to the metaphase plate a sub-population of chromosomes may remain dependent upon CENP-E to maintain alignment (Gudimchuk et al., 2013). This study showed that inhibition of CENP-E motor activity by treatment with the small molecule CENP-E inhibitor GSK923295 results in a small number of chromosomes "dropping out" of metaphase alignment. This result could reflect a role for CENP-E in maintaining end-on attachments, but it could equally reflect a subpopulation of chromosomes that are still laterally attached to microtubules.

1.4.3 Depolymerisation-coupled pulling

Chromosomes may also biorientate whilst unaligned (i.e. before reaching the spindle equator). These biorientation events may take place as chromosomes approach the spindle equator by lateral sliding (see section 1.4.2 above) or at the spindle pole. Kinetochores may localise to the pole in early prometaphase or may be transported to the spindle pole by dynein motors. Alternatively mono-orientated kinetochores may be dragged to the spindle pole by depolymerisation-coupled pulling of the attached sister. Depolymerisation-coupled pulling is powered by the shrinking of K-fibre microtubules and has also been termed "Pacman" (Cassimeris et al., 1987); kinetochores remain attached to these microtubules as they shrink and this powers poleward transport. Evidence for this process was provided by *in vitro* experiments which showed that isolated chromosomes could be pulled along a glass slide powered only by a shrinking microtubule to which the kinetochore remained attached (Koshland et al., 1988). This ability to remain attached to shrinking microtubules represents perhaps the most remarkable ability of kinetochores and is a feat akin to climbing a burning rope. Some early *in vivo* evidence of microtubule dynamics powering chromosome movements was shown in experiments by Mitchison and Salmon, using cells labelled with photoactivatable tubulin. These experiments showed that the rate of chromosome poleward movement was greater than that of photoactivated tubulin poleward flux, this lead to the conclusion that it was K-MT dynamics at the plus-end of K-fibres that powered chromosome movements (Mitchison & Salmon, 1992). Subsequently work on *D. melanogaster*

demonstrated that kinesin proteins were important for controlling microtubule depolymerisation to power chromosome movement (Rogers et al., 2004).

After reaching the spindle pole, chromosomes oscillate back and forth in a mono-orientated state. If the unattached sister is able to bind microtubules emanating from the opposite pole these mono-orientated pairs can switch to a biorientated state, after which chromosomes continue to undergo oscillations (Skibbens et al., 1993). These oscillations allow chromosomes to align to the metaphase plate because they make longer duration movements towards the spindle equator (Skibbens et al., 1993; Chromosome 2 Figure 1.4). Once aligned to the metaphase plate, oscillations maintain metaphase alignment as movements to each side of the plate average out at a net zero displacement (Jaqaman et al., 2010; Skibbens et al., 1993). Laser ablation studies suggested that the site of force generation powering biorientated movement is the poleward (P) moving kinetochore (Khodjakov & Rieder, 1996). This has been confirmed by recent work showing that the P kinetochore is compressed relative to the AP kinetochore due to the pulling forces it experiences from the shrinking K-fibre (Dumont et al., 2012).

In order for kinetochore movement to be powered by depolymerisation-coupled pulling the process must involve proteins that (1) mediate end-on microtubule-kinetochore attachments, (2) maintain attachment to depolymerising microtubules and (3) ensure the K-fibre remains in a net depolymerising state through control of K-MT dynamics. The Ndc80 and Ska complexes can directly bind microtubules (with low affinity) *in vitro*, with the Ska complex (but not Ndc80) able to autonomously track depolymerising microtubule plus-ends (Schmidt et al., 2012). Extensive depletion of either complex causes a severe failure in chromosome congression and the inability to form a metaphase plate (Daum et al., 2009; Gaitanos et al., 2009). Thus, the Ndc80 and Ska complexes are proposed to form the end-on attachment sites within the kinetochore. However, little is known about the mechanisms by which K-fibre microtubule dynamics are modulated to control the process of depolymerisation-coupled pulling.

Kinetochore oscillations can be measured by automated tracking software that is able to follow the movement of kinetochores tagged with eGFP-CENP-A from 3-dimensional time-lapse movies (Jaqaman et al., 2010). These tracking experiments confirm that stabilisation of the K-fibre microtubules with taxol abolishes oscillations, whereas depletion of the microtubule depolymerases MCAK and Kif18a have little effect on the period of the oscillations although they do affect the speed of kinetochore movement (Jaqaman et al., 2010). In contrast depletion of the CCAN subunits CENP-H and CENP-L completely abolish regular oscillatory motion and disrupt K-fibre microtubule dynamics (Amaro et al., 2010; Mchedlishvili et al., 2012). The CCAN therefore represents a prime candidate for the regulation of K-fibre microtubule dynamics to control the process of depolymerisation-coupled pulling and chromosome congression. How CCAN mediates this activity is unknown, one possibility being that one of the multiple proteins or complexes recruited by the CCAN is required to control the MT dynamics required for depolymerisation-coupled pulling. Another possibility is that the K-fibre MT dynamics required for normal depolymerisation-coupled pulling are controlled directly by CCAN. Two prime candidates are the CENP-U and CENP-Q subunits of the CENP-O sub-complex as both of these proteins have been shown to be able to bind microtubules *in vitro* (Amaro et al., 2010; Hua et al., 2011).

1.5 Aims of thesis

It is known that K-MT dynamics are crucial for controlling kinetochore movement by depolymerisation-coupled end-on pulling as well as facilitating the oscillation of kinetochores positioned at the metaphase plate. Recent work within our laboratory has shown that CENP-Q is able to modulate MT dynamics *in vitro* and *in vivo.* It has been demonstrated that depletion of the protein abolishes K-MT plus-end turnover *in vivo* (Samora C.P., PhD thesis, 2012). *In vitro* work has shown that purified CENP-Q protein is able to bind taxol-stabilised microtubules (Amaro et al., 2010), and in dynamic microtubule assays is able to increase the frequency microtubules switch between catastrophe and rescue events whilst slowing the rate of tubulin heterodimer addition and loss. Interestingly, total internal reflection microscopy (TIRF) work also demonstrated that the

protein is able to track depolymerising microtubules (Samora C.P., PhD thesis, 2012). We therefore predict that CENP-Q will be important in controlling chromosome congression and aligned kinetochore/chromosome dynamics.

The primary aim of this study is to uncover the role played by the CENP-Q protein in controlling chromosome congression movements. We will examine the function of the protein during chromosome congression and at aligned kinetochores. We will also assess the effects of losing CENP-Q on the protein composition of the kinetochore and strive to understand effects of any resulting change in kinetochore composition. To achieve these aims I will use a combination of immunoblotting, siRNA mediated protein depletion and rescue experiments, fixed cell immunofluorescence imaging, live cell imaging and high temporal-spatial resolution tracking of aligned kinetochores.

CHAPTER 2: Materials and Methods

2.1 Cell biology

2.1.1 Tissue culture & cell lines

All cell lines used (see Table 1) were grown in Dulbecco's modified Eagle's medium (DMEM) (Life technologies) with 10% foetal calf serum (FCS; Sigma), 100 µg ml^{-1} streptomycin and 100 U/ml penicillin (Invitrogen) and kept in a humidified incubator at 37°C with 5% CO_2. For maintenance, cell lines were grown to ~90% confluency, washed twice with PBS then incubated with 1 ml of 0.05% trypsin (Invitrogen) for 4 min at 37°C. Cells were split 1 in 10 into fresh pre-warmed DMEM. Modified Eagle's medium (MEM) (Gibco) was used during siRNA treatments with 10% FCS, 100 µg ml^{-1} streptomycin and 100 U/ml penicillin. Opti-MEM (Gibco) was used when preparing siRNA and had no serum or antibiotics added. Opti-MEM was replaced 1 month after opening to avoid acidification. Cell lines were replaced with fresh liquid nitrogen stored stocks after 10-15 passages and were checked for mycoplasma contamination on a bi-monthly basis using MycoSensor PCR assay kit (Agilent).

Table 1 – Cell Lines used in this study				
Cell Line Name	**Initial Cell Line Used**	**Tagged Proteins**	**Selective Agent Used For Maintenance**	**Origin**
MC001	HeLa-E1	None	None	McAinsh et al., 2006 (original from Sorger lab)
MC015	HeLa-E1	mRFP-αTubulin-Puro eGFP-Histone2B	None	Toso et al, 2009
MC025	HeLa-K-FRT	RFP-Histone2B	None	Meraldi Lab
MC042*	MC025	mCherry-αTubulin-Puro RFP-Histone2B	0.4 μg ml^{-1} Puromycin	Meraldi Lab
MC051	HeLa-K	mCherry-CENP-A	0.3 μg ml^{-1} Puromycin	McAinsh Lab – made by Muriel Erent
MC060	HeLa-K	eGFP-CENP-A / eGFP-Centrin1	0.3 μg ml^{-1} Puromycin 300 μg ml^{-1} G418	Meraldi Lab – made by Nunu Mchedlishvili
MC069	mCherry-CENP-A MC051	eGFP-CENP-Q / mCherry-CENP-A	0.3 μg ml^{-1} Puromycin 300 μg ml^{-1} G418	This thesis
*Histone marker only present in sub-population of cells.				

2.1.2 Cryopreservation of cells

Cells were seeded in a 75 cm^2 (Nunc) tissue culture flask and grown to ~90% confluency. Cells were trypsinised and re-suspended in 10 ml of cold DMEM. These cells were spun in a 15 ml falcon tube at 1200 g for 5 min in a centrifuge precooled to 4 ºC. This tube was transferred to ice and the supernatant was removed and 10 ml of ice cold freezing medium was then added to cells (DMEM fortified with 10 % DMSO and 13 % FCS). Cells were re-suspended in this medium and 1 ml of the medium was distributed into each of 10 cryo tubes that had been precooled on ice. These tubes were placed in a Mr. Frosty freezing container (Thermo Scientific) precooled to 4ºC and placed into a -80ºC freezer overnight. These tubes were moved into liquid nitrogen storage taking care not to warm them during transfer.

2.1.3 siRNA mediated protein depletion

Small interfering (si)RNA oligonucleotides were employed to facilitate protein depletion. siRNAs were delivered into cells using Oligofectamine (Invitrogen) using the following methodology: HeLa cells were seeded from a 75 cm^2 (Nunc) tissue culture flask grown to ~90% confluency; cells were trypsinised and re-suspended in 10 ml of pre-warmed DMEM. The volume of cells seeded was varied depending on vessel size and duration of siRNA, for a 48 hr experiment 90 μl of cells were seeded into 1.5 ml DMEM for a 3.5 cm well or fluoro dish and 360 μl of cells were seeded into 6 ml of DMEM for a 10 cm dish. For 72 hr long RNAi experiments 60 μl of cells were seeded into 1.5 ml DMEM for a 3.5cm well or fluoro dish and 120 μl of cells were seeded into 6 ml of DMEM for a 10 cm dish. Cells were grown for 24 hr, after which the medium was changed to the same volume of pre-warmed modified Eagle's medium (MEM) (Gibco). The siRNA (Table 3) and other components were prepared in a tissue culture hood as in Table 2 adding Opi-MEM first. The siRNA was prepared in 1.5ml Eppendorf tubes or 15ml tubes (Falcon) for multiple parallel experiments in 10cm dishes where larger volumes are required.

Table 2 – siRNA transfection component volumes

Vessel Size	**Single wells of a 6 well plate (6x3.5mm) or 3.5mm Fluoro Dish**	**10cm Diameter Dish**
	Tube 1	
Opti-MEM	150 μl	600 μl
siRNA Oligo (20 μM stock)*	4.5 μl	18 μl
	Tube 2	
Opti-MEM	36 μl	144 μl
Oligofectamine	9 μl	36 μl
* Final concentration of siRNA used was 53 nM (Elbashir et al., 2001).		

After addition to tubes, all components were mixed by pipetting up and down and incubated for 5 min at room temperature. The contents of tube two was added to tube one and pipetted up and down to mix, after which the siRNA mixture was incubated at room temperature for 25 min. The siRNA solution was added to cells in a drop-wise manner adding 200 μl to 3.5 mm fluoro dish or 1

well of a 6 well plate and 800 µl to a 10cm dish, dishes were then agitated to evenly disperse the siRNA. After treatment cells were incubated with the siRNA for 24 hr, after which the medium was changed back to pre-warmed DMEM for the remaining treatment time. After all siRNA treatments were grown on for a total of 48 hr (24 hr in MEM + 24 hr in DMEM), except for *CENP-P* siRNA, which lasted 72 hr (24 hr in MEM + 48 hr in DMEM) and CENP-E partial depletion which was 20 hr (in MEM, changed to DMEM before imaging). For double siRNA experiments full siRNA preparations were made separately and then added to cells by adding the full volume to the cells sequentially. In all experiments where double siRNA treatments were used, single siRNA conditions within the same experiment were complemented with *control* siRNA to ensure the final volumes added were equivalent.

2.1.4 siRNA rescue experiments

For rescue experiments cells were first treated with siRNA as described in section 2.1.3. For CENP-Q rescues the medium was changed from MEM with siRNA after 12 hr (rather than the standard 24) and replaced with warmed DMEM. Cells were allowed to recover for 30 min in an incubator before transfecting them with the siRNA protected rescue vector or control vector as described in section 2.1.5. After 48 hr incubation cells were treated with MG132 for 90 min to prevent anaphase onset (see table 4). Fixation and staining was then conducted as described in 2.2.3.

Table 3 – siRNA oligonucleotide sequences				
siRNA Name	siRNA Sequence (5'-3')	Target mRNA	Source	Reference
Control siRNA	GGACCUGGAGGUCUGCUGU	None	Ambion	Samora et al., 2011
CENP-Q-1 siRNA	GGUCUGGCAUUACUACAGGAAGAAA	CENP-Q	Invitrogen Stealth	This study
CENP-Q-2 siRNA	CAGAGUUAAUGACUGGGAAUAUUCA	CENP-Q	Invitrogen Stealth	This study
CENP-P-2 siRNA	GAACCCTGGTAGGACTGCTTGGAAT	CENP-P	Invitrogen Stealth	This study
CENP-E siRNA	ACUCUUACUGCUCUCCAGUTT[1]	CENP-E	Ambion	Meraldi et al., 2004
CENP-H siRNA	CAGAGAGGAUAAAGAUCAUACGACA	CENP-H	Invitrogen Stealth	Amaro et al., 2010
CENP-O siRNA	ATATGAGTCTGGTCTCCTA	CENP-O	Ambion	McAinsh et al., 2006
Kif18a siRNA	CCAACAACAGUGCCAUAAATT	Kif18a	Ambion	Stumpff et al., 2008

2.1.5 Transient transfections

The transfection of plasmids into all HeLa cell lines was carried out using FuGene6 (Roche). For 3.5 mm fluoro dishes and individual wells of 6 x 3.5 mm well plates 1 µg of DNA was used along with 4 µl of FuGene, the total volume was brought to 100 µl by the addition of Opti-MEM. In each case the required amount of Opti-MEM was added to a 1.5 ml Eppendorf tube followed by 4 µl of FuGene directly into the Opti-MEM, this was vortexed briefly and incubated for 5 min at room temperature. After incubation 1 µg of plasmid DNA was added in H_2O and the tube was vortexed briefly to mix and incubated for a further 25 min. The 100 µl total plasmid transfection mixture was added to cells in a drip wise manner followed by gentle rocking of the vessel to disperse evenly. For 10 cm diameter tissue culture dishes the components of the transfection mixture (including plasmid) were multiplied 4 times.

[1] A second set of experiments was conducted using an siRNA oligo that lacked the terminal dTdT overhang. Results using this oligo were identical to those shown in the results chapters of this thesis.

2.1.6 Generation of stable cell lines

To generate a stable cell line expressing CENP-Q-eGFP (MC069) the MC051 (HeLa K - mCherry-CENP-A) cell line was used as a starting point. These cells were seeded into 2 x 3.5 mm wells of a 6 well plate and grown until ~35% confluent. These cells were transfected with CENP-Q-eGFP (pMC308) as described above (section 2.1.5). After 48 hr, transfected cells were treated with 500 µl of trypsin for 3 min and resuspended in 1.5 ml of warmed DMEM (total volume to 2 ml). During this time 4 x 15 cm dishes were prepared, two containing 0.3 µg ml^{-1} puromycin and 300 µg ml^{-1} of geneticin (G418) and two containing 0.3 µg ml^{-1} puromycin and 500 µg ml^{-1} of geneticin (G418). 200 µl of cells were transferred to one plate and 1800 µl to the other plate (*i.e.* 10% and 90%) and agitated by hand to disperse cells evenly. Cells were grown for 3 to 4 weeks, changing to fresh medium every 3 days until single colonies were clearly visible by eye. At this point the plates were gently washed with 20 ml of PBS and colonies were picked. Note that that only colonies that were clearly separated from neighbouring colonies were picked to ensure a monoclonal population. To pick colonies, cloning discs that had been presoaked in trypsin were placed over the colony using fine forceps and the plate returned to the 37ºC incubator for 5 min. Discs were next removed from the dish and transferred to single wells from a 24 well plate containing the appropriates selective medium. Plates were incubated at 37ºC for further 2 weeks, trypsinysed, resuspended in 1 ml and transferred to single wells in a 6 well dish. At the same time, 40µl of cells were seeded into 8 well LabTek microscope slides for visual screening by microscopy. Each cell line was screened for the presence of the CENP-Q-eGFP construct, using mCherry-CENP-A as a kinetochore reference. Those cells positive for eGFP at kinetochores were expanded and stocks frozen down in liquid nitrogen (see section 2.1.2). The positive clone with the closest CENP-Q-eGFP expression level to endogenous CENP-Q expression level (MC069) was chosen using western blotting to compare protein levels.

2.1.7 Drug treatments

All drugs were made to working concentration by diluting in DMEM that had been pre-warmed to 37 ºC. To ensure homogeneity of drugs the tubes were mixed by vortex mixer for 30 sec after

addition. Where the dilution required was greater than 1 µl in 25,000 microliters a serial dilution was conducted to avoid pipetting volumes less than 1 µl. Drugs were added to cells by aspirating away existing medium and pipetting on the new medium laced with the required drugs. The details of the drugs used, including concentration used and treatment time, can be found in table 4 below.

Table 4 – Drugs

Drug Name	Working Concentration	Treatment Period	Purpose	Supplier
Nocodazole	1µg ml^{-1}	14 hr	To depolymerise microtubules	Tocris
Taxol	10 µM	60 min	To stabilise microtubules	Sigma
GSK 923295	300 & 25 nM	14 hr & 1hr	To inhibit CENP-E motor activity	Medchemexpress
MG132	1 µg ml^{-1}	90 min	To inhibit the proteasome, preventing anaphase onset and protein degradation	Tocris
Monastrol	100 µM	90 min	Inhibition of Eg5 – inducing monopolar spindles	Sigma

2.2 Imaging, analysis & sample preparation

2.2.1 Live cell imaging

Fluorescence time-lapse imaging of H2B-GFP/mRFP-α-tubulin cells was carried out on a Personal Deltavision microscope (Applied Precision, LLC) using a 40 x NA 1.3 objective, an GFP (excitation 475/28, emission 525/50) and mCherry (excitation 575/25, emission 632/60) filter set with a Quad-mCherry dichroic mirror (reflection bands 381-401, 464-492, 561-590, 625-644, transmission bands 409-456, 500-553, 598-617, 652-700) (Chroma), Xenon light source and a CoolSNAP HQ2 camera (Roper Scientific). Image stacks (7 x 2 µm z-sections) were collected every 3 min for a total time of 10 h. These conditions were also used to image mitotic progression in CENP-Q-eGFP/mCherry-CENP-A cells (MC069) and mCherry-CENP-A cells (MC051), but without using the GFP channel. The GFP channel was not used as the signal was too weak to facilitate overnight image without considerable photo-toxic effects. However, the presence of CENP-Q-eGFP was confirmed before the start of the experiment. Maximum intensity projections of the acquired time series were then generated using SoftWorks (Applied Precision, LLC). For initial experiments

confirming the expression and localisation of CENP-Q-eGFP and eGFP-CENP-P relative to mCherry-CENP-A or mRFP-α-tubulin the same conditions were used as for H2B-GFP/mRFP-α-tubulin, with the exception of a 100 x NA 1.4 plan apochromatic objective and a reduced total imaging time of ~15 min. Kinetochore tracking movies and fate movies of eGFP-CENP-A/eGFP-Centrin1 cells were carried out on a Personal Deltavision microscope (Applied Precision, LLC) using a 100 x NA 1.4 plan apochromatic objective, a GFP (excitation 475/28, emission 525/50) filter set with a Quad-mCherry dichroic mirror (reflection bands 381-401, 464-492, 561-590, 625-644, transmission bands 409-456, 500-553, 598-617, 652-700) (Chroma), Xenon light source and a CoolSNAP HQ2 camera (Roper Scientific). Image stacks (30 x 0.5 μm z-sections) were collected every 7.5 sec for a total time of 5 min total., The total experiment length was increased to 10 min for tracking unaligned chromosomes in unperturbed cells. These images were deconvolved using SoftWorks (Applied Precision, LLC); 8 iterations of ratio mode deconvolution with medium noise filtering.

2.2.2 Kinetochore tracking

Automatic kinetochore detection and tracking and data analysis was performed as previously described (Jaqaman et al., 2010), with the exception of the metaphase plate fitting step, which was modified by Edward Harry (McAinsh lab). This step was modified due to the high number of unaligned chromosomes present in CENP-Q depleted cells. The original plate fitting strategy would very often fail when there were multiple unaligned kinetochores, even though a metaphase plate structure was clearly visible. This was because the average nearest-neighbour distribution was similar for inliers as it was within each cluster of unaligned spots, therefore presenting no outliers to exclude. A more robust method of metaphase plate finding and fitting was therefore implemented. In each frame: (1) A graph was created between all spots with a cut-off distance of two microns. This creates a cluster of sub-graphs in which the metaphase plate structure (sometimes plus a few outliers) was one sub-graph. (2) Sub-graphs were identified by flood-filling the graph. Each flood-fill was continued until no more new nodes were being filled. If any unfilled nodes remained a new flood-fill was started on an empty node. All the nodes filled in each flood were taken to belong to a

new, separate sub-graph. (3) The original plate fitting algorithm (Jaqaman et al., 2010) was used on the sub-graph with the highest number of nodes (the metaphase plate structure is normally the sub-graph with the highest number of nodes). Spots not in the sub-graph were taken as outliers automatically. (4) If a plate was not successfully fitted the process was repeated on the next largest sub-graph until a correct plate fit was generated. (5) All spots in each frame were reclassified as inlier (aligned) or outlier (unaligned) based on their distance away from the fitted plate (> 2.5 SD) for outliers as previously described (Jaqaman et al., 2010). This plate fit modified version of the tracking code was used for all conditions.

2.2.3 Immunofluorescence sample preparation

Cover slips with adherent HeLa cells were placed into 3.5 cm 6 well plates, those already grown in 6 well plates were aspirated to remove DMEM. Taking care to ensure cells didn't dry out 2 ml of pre-extraction buffer was added to each cover slip containing well for 1 min. Pre-extraction buffer contains the following: 20 mM PIPES pH 6.8 containing 10 mM EGTA, 1 mM $MgCl_2$, 0.2% Triton X-100. After 1 min the well was aspirated and PTEMF buffer was added to fixed cells. PTMEF buffer contains the following: 20 mM PIPES pH 6.8 containing 10 mM EGTA, 1 mM $MgCl_2$, 0.2% Triton X-100 and 4% formaldehyde. After 10 min the PTEMF buffer was aspirated out of each well and replaced with 2 ml of PBS and incubated for 10 min to wash, this step was repeated twice more. Following the wash, 2 ml of PBS with 3% bovine serum albumin (BSA) was added to each well to prevent non-specific antibody binding and incubated for 30 min. Cover slips were then removed from wells and excess liquid was removed by drying the edge on tissue paper. Cover slips were then placed on a parafilm covered glass tile and primary antibodies were added in 250 µl of PBS with 3% BSA. Primary antibodies (see Table 6) were incubated with cells for 1 hr covering with a plastic container to reduce evaporation. The cover slips were then aspirated to remove the primary antibodies and washed for 10 min with 300 µl PBS, this wash process was then repeated two more times. Secondary fluorescent antibodies (see Table 6) along with DAPI stain (diluted 1 in 2000) were added to cover slips in 250 µl PBS with 3% BSA for 30 min covering with a plastic container

to reduce evaporation and foil to reduce photo bleaching. After 30 min secondary antibodies were aspirated off of cover slips and replaced with 300 μl of PBS and incubated for 10 min to wash, this was step was repeated twice more. The cover slips were then placed face down on an 11 μl dot of Vectashield mountant (Vector Laboratories) and sealed with clear nail varnish (Superdrug). Slides were then visualised via fluorescence microscopy.

2.2.4 Imaging immunofluorescence experiments

Fixed cell imaging was conducted on a Deltavision Core microscope (Applied Precision, LCC) with an Olympus main body and objectives. Epi-fluorescent illumination was provided by a xenon light source with fibre-optic light guide with a DAPI-FITC-Rhod/TR-CY5 filter set. Images were captured on a CoolSNAP HQ2 camera (Roper) using 0.2 μm z-steps (between 10 and 18 μm total) using a 100X oil NA 1.4 objective. Exposure times were varied depending on fluorescence staining intensity but were fixed within each experiment to allow direct comparison. These images stacks were deconvolved using SoftWorx (Applied Precision, LLC); 8 iterations of ratio mode deconvolution with medium noise filtering. Intensity quantifications at the kinetochore taken from deconvolved image stacks were also carried out in SoftWorx. The average intensity was taken at the maximal intensity plane for the kinetochore within a 5x5 pixel box along with adjacent background. The intensity of the channel being measured was corrected by background subtraction and was calculated as a ratio against CENP-A as an internal control.

2.2.5 Kinetochore-monopole distance measurements

For analysis of distances from kinetochores to spindle poles the Volocity 3D image analysis software package (PerkinElmer) was used. The centre of mass of the monopolar spindle was determined in 3D using the anti-γ-tubulin signal., Kinetochores (stained with anti-CENP-A) were identified by the built in Velocity spot detection algorithm, this detection was confined to the chromatin region (DAPI signal). The distance from every kinetochore to the spindle monopole centre of mass was measured in 3D; this was repeated for a minimum of 8 cells per experiment.

Cumulative distribution frequencies (CDF) were calculated using MATLAB, the average of these CDFs was plotted for each condition, standard deviation was also calculated and is shown as a shaded area.

2.2.6 CENP-Q kinetochore positioning

To visualise the positioning of CENP-Q within the kinetochore relative to CENP-A and Hec1, we first had to correct for chromatic aberrations within the optical path. To achieve this, cells were stained with a mouse anti-CENP-A monoclonal antibody followed by a mix of 3 secondary anti-mouse antibodies with fluorophores emitting at 488, 594 and 647 nm. The triple tagged CENP-A cells were imaged in all 3 channels with high axial sampling (50-nm) and the x,y,z shifts in each channel were measured relative to the 488 nm channel in Huygens Professional (X11). Cells transiently transfected with eGFP-CENP-Q were fixed and stained with antibodies against CENP-A and Hec1. These cells were imaged as above, except that z sampling was every 100 nm. The resulting image stacks were then corrected for chromatic aberration using the earlier measured deviation. After correction, intensity line profiles were taken through kinetochore pairs using the open source ImageJ analysis package to identify peaks for each protein.

2.3 Molecular biology

2.3.1 PCR

PCR reactions mixes were prepared on ice in thin walled PCR tubes. The total reaction volume used for each was 100 µl with 250ng sample DNA. Forward and reverse primers (see Table 4) were used at 10 µM each added in 2 µl H_2O. 20µl Phusion polymerase (Finzymes) buffer and 0.8µl of 100mM dNTPs were added followed by H_2O to make the reaction volume up to 99 µl total., Finally 1µl Phusion polymerase (Finzymes) was added and mixed by gently pipetting up and down. These PCR reactions were then placed in a PCR cycler (Biometra T3000) with heated lid, having preheated the reaction block to 98°C for an initial 5 min denaturation. After denaturation, the temperature was cycled 20 times between 95°C for 45 sec to denature, 55°C for 45 sec to anneal

and 72°C for 2 min to allow extension (Phusion extension rate = 15-30 s/kb). After cycling the temperature was held at 4°C until the PCR products could be removed. PCR products were then analyzed by gel electrophoresis to determine yield and required purification. If additional bands were present in the PCR product, the entire product was run on agrose gel by electrophoresis and the desired band was excised and purified by gel extraction column (Qiagen). If PCR products were specific the reaction product was simply purified by PCR purification column (Qiagen). PCR primers used for insert amplification in this study are shown below in Table 4.

Table 5 – PCR primers

Primer Name	Primer Code	Primer Sequence (5'-3')	Primer Restriction Site	Source
CENP-Q FW For pECFP-N1	MC246	ggatcgaattcatgtctggtaaagcaaatgc	EcoRI	Invitrogen
CENP-Q RV For pECFP-N1	MC248	ggatcggatccggagatgcatccagtttc	BamHI	Invitrogen

2.3.2 Restriction digests

Restriction digests were prepared in 0.5 µl Eppendorf tubes made up to 30 µl total volume with H_2O using 2000 to 3000 ng DNA. To each digestion 1 µl of restriction enzyme 1 and 1 µl of restriction enzyme 2 were added along with 3 µl of the appropriate enzyme buffer, all restriction enzymes were sourced from New England Biolabs. In addition 3 µl of 10 x bovine serum albumin (BSA) (New England Biolabs) were also added when required by enzymes. Digests were then carried out for 2 hr at 37°C in a water bath. When digesting vectors for later ligation with an insert 1 µl of calf intestine phosphotase was (CIP, New England Biolabs) added to the digest after 1.5 hr to remove the 5' phosphate from the vector preventing vector only re-ligation. Digests were then analysed by gel electrophoresis (see section 2.3.4).

2.3.3 DNA ligations

Digested DNA inserts and vectors were ligated together in a 3:1 molar ratio using 50ng of cut vector. To calculate the amount (ng) of insert required when using 50 ng of cut vector, we used the

following formula: ((insert length (bp) x vector length (bp)) x 3) x 50 = ng insert. The ligation reaction mix was made on ice in a PCR tube with 1 µl of T4 DNA ligase buffer and 1 µl T4 DNA ligase (NEB) made to a final volume of 10µl with H_2O. Control ligation reactions were also set up using cut vector and insert alone. Reactions were incubated at 16°C for 10 hr. The ligation reactions were then transformed into XL10 Gold super competent *E. coli* cells (Stratagene) (see transformations). Colonies were picked from agar plates containing appropriate antibiotic. These were amplified by inoculating 2ml of LB medium (10g/l Tryptone, 5g/l yeast extract, 10g/l NaCl, pH7.5), with appropriate antibiotic at 37°C in a shaker incubator overnight. Plasmid DNA was isolated from cultures using a Qiagen mini-prep kit (Qiagen). These plasmids were tested for presence of insert by restriction digest analysis and DNA sequencing (Warwick Life Sciences; see section 2.3.8). Plasmids with correct sequence were isolated using either a midi prep kit (Invtrogen) for HeLa transfections or mini prep kit (Qiagen) for use in further molecular biology.

2.3.4 Gel electrophoresis

For agarose gel electrophoresis a 1% agarose (Invitrogen) gel was made in 1x TAE buffer (10 mM Tris-Cl pH 7.5 and 1mM EDTA pH 8.0) by heating. To visualize DNA 6 µl of Safeview (Vectashield) UV DNA marker was added per 100 µl of agarose gel. Gels were poured in the Run-one system (Embitech) and, when solidified, the comb was removed and the gel covered with 1 x TAE buffer. DNA samples were then mixed with loading dye (NEB) at a 1:6 ratio. To mark molecular weights 1 µl of 1 kb DNA ladder (NEB) was run on each gel. Gels were run at 200 V until the loading dye migrated 75% of the way along the gel. Gels were then visualized under long wavelength ultraviolet (UV) light in a bench top UV transilluminator (BioDoc-It Imaging systems). For purification of DNA, bands were cut out of the gel and purified using quick spin gel extraction column kit (Qiagen) as per the manufacturers instructions. DNA was eluted in 30 µl of H_2O for further manipulations.

2.3.5 Site directed mutagenesis

Site directed mutagenesis was carried out using a Quick Change kit as per the manufacturers guidelines (Stratagene) with the following modification: all transformations carried out using XL10

Gold super competent bacteria (Stratagene) because this resulted in a higher transformation frequency. The primers used for site directed mutagenesis can be found in Table 6.

Table 6 – Primers for site-directed mutagenesis

Primer Name	Primer Code	Primer Sequence (5'-3')	Primer Purpose	Source
CENP-Q siRNA Protection FW	MC297	GACAAAGCTAATGAAGAAG GCCTAGCGTTGCTCCAAGA GGAAATAGATAAAATGGTAG AG	The silent mutagenesis of CENP-Q cDNA to protect it from CENP-Q1 siRNA	Invitrogen
CENP-Q siRNA Protection RV	MC298	CTCTACCATTTTATCTATTTC CTCTTGGAGCAACGCTAGG CCTTCTTCATTAGCTTTGTC	The silent mutagenesis of CENP-Q cDNA to protect it from CENP-Q1 siRNA	Invitrogen
CENP-Q Leu179Pro FW	MC295	ATGACTGGGAATATTCAGA GCCCAAAGAACAAAATTCA GATTCTG	The mutagenesis of CENP-Q cDNA to create a translational mutation L179P	Invitrogen
CENP-Q Leu179Pro RV	MC296	CAGAATCTGAATTTTGTTCT TTGGGCTCTGAATATTCCCA GTCAT	The mutagenesis of CENP-Q cDNA to create a translational mutation L179P	Invitrogen
CENP-Q – S50A S51A FW	MC357	AATAAAAATCATCTGAAAGA TCTGGCTGCTGAAGGACAA ACAAAGCACACTA	The mutagenesis of CENP-Q cDNA to create the translational mutations S50A S51A	Invitrogen
CENP-Q – S50A S51A RV	MC358	TAGTGTGCTTTGTTTGTCCT TCAGCAGCCAGATCTTTCA GATGATTTTTATT	The mutagenesis of CENP-Q cDNA to create the translational mutations S50A S51A	Invitrogen
CENP-Q – S248A S249A FW	MC365	CTCTTCTAAAGGACTTGGAT ATTCTTCATAATGCAGCACA GATGAAGAGCATG	The mutagenesis of CENP-Q cDNA to create the translational mutations S248A S249A	Invitrogen
CENP-Q – S248A S249A RV	MC366	CATGCTCTTCATCTGTGCTG CATTATGAAGAATATCCAAG TCCTTTAGAAGAG	The mutagenesis of CENP-Q cDNA to create the translational mutations S248A S249A	Invitrogen
CENP-Q – S50D S51D FW	MC359	AGTGAAAAAAAATAAAAATC ATCTGAAAGATCTGGATGAT GAAGGACAAACAAAGCACA CTAACCTAAAACAC	The mutagenesis of CENP-Q cDNA to create the translational mutations S50D S51D	Invitrogen
CENP-Q – S50D S51D RV	MC360	GTGTTTTAGGTTAGTGTGCT TTGTTTGTCCTTCATCATCC AGATCTTTCAGATGATTTTT ATTTTTTTTCACT	The mutagenesis of CENP-Q cDNA to create the translational mutations S50D S51D	Invitrogen
CENP-Q – S248D S249D FW	MC367	CAAACCAGAATGCTCTTCTA AAGGACTTGGATATTCTTCA TAATGACGACCAGATGAAG AGCATGTCAACCTt	The mutagenesis of CENP-Q cDNA to create the translational mutations S248D S249D	Invitrogen
CENP-Q – S248D S249D RV	MC368	AAGGTTGACATGCTCTTCAT CTGGTCGTCATTATGAAGAA TATCCAAGTCCTTTAGAAGA GCATTCTGGTTTG	The mutagenesis of CENP-Q cDNA to create the translational mutations S248D S249D	Invitrogen

2.3.6 Bacterial transformations

All transformations in this study were carried out in XL-10 Gold super competent bacteria cells. Prior to beginning transformations a water bath was preheated to 42°C and the required number of Falcon 2059 tubes placed on ice. XL-10 Gold super competent bacteria cell aliquots were thawed on ice and 8 µl of β-mecapthaethanol added to each 200 µl aliquot. 75 µl of cells were then added to each Falcon 2059 tube and incubated on ice for 10 min. DNA ligation products or plasmids were added to the 2059 tube(s) and incubated on ice for 30 min swirling every 5 min. After incubation on ice the competent cells with DNA were heat pulsed at 42°C in a water bath for 30 sec followed by recovery on ice for 2 min. After recovery, 1 ml of SOC medium (2% w/v tryptone, 0.5% w/v yeast extract, 10mM NaCl, 2.5mM KCl, 10mM $MgCl_2$ in ddH_2O; pH 7), warmed to 42°C was added to each 2059 tube and the tubes placed in a shaker incubator at 37°C for 1 hr. The bacteria were then transferred into 1.5 ml eppendorf tubes and spun for 5 mins at 13,000 rpm. The supernatant was removed except for ~100 µl into which the pellet was re-suspend. Bacterial suspension were plated on appropriate selective media and incubated over night at 37ºC.

2.3.7 DNA concentration quantification

DNA concentration was determined using both NanoDrop spectrophotometer (Thermo) assays, which calculate DNA concentration by absorbance at 260 nm assays and also by using diagnostic gels comparing DNA sample to a known amount of ladder as reference.

2.3.8 DNA sequencing

To confirm the presence of the desired mutation after site directed mutagenesis and ensure the fidelity of DNA sequences following PCR-based cloning, plasmids were sent for DNA sequencing. The primers used for sequencing were MC261 and MC262 for CENP-P, primers MC246 and MC248 for CENP-Q. Sequencing reactions were carried out by the University of Warwick Sequencing Service, using 400 ng of plasmid and 0.5 pM of primer in 10 µl of H_2O.

2.3.9 Vector construction

Details of the molecular biology protocols used in this thesis are described above in detail (section 2.3.1-2.3.8). Here the stepwise application of the methods used to generate the vectors required for this thesis is described. To generate a human CENP-Q-eGFP expression vector, the CENP-Q coding sequence was amplified by PCR (using primers MC246 and MC248) and purified by PCR purification column. The product was then ligated into pEGFP-N1 (pMC004; empty vector; Clontech) after digestion with BamHI and EcoRI. Correct insertion was confirmed by digestion and sequencing (with primers MC246 and MC248) and the resulting plasmid was designated pMC276. The pMC276 plasmid was then mutated using a quickchange site-directed mutagenesis kit (Stratagene), and primers MC297 and MC298, to render the transgene resistant to the CENP-Q siRNA oligonucleotide. Correct silent mutation was confirmed by sequencing (using primers MC246 and MC248) and was designated pMC308. To generate a human eGFP-CENP-P expression vector, the CENP-P coding sequence was amplified by PCR (using primers MC261 and MC262) and purified by PCR purification column. The purified product was ligated into pEGFP-C1 (pMC005; empty vector; Clontech) after digestion with EcoRI and XmaI. Correct insertion was confirmed by digestion and sequencing (using primers MC261 and MC262) and the resulting plasmid was designated pMC297. The pMC297 plasmid was mutated using a quickchange site-directed mutagenesis kit (Stratagene), and primers MC293 and MC294, to render the transgene resistant to the *CENP-P* siRNA oligonucleotide. Correct silent mutation was confirmed by sequencing (using primers MC261 and MC262) and was designated pMC301.

Table 7 - Plasmids						
Plasmid Name	**Plasmid Code**	**Backbone /origin**	**Selection**	**Insert**	**Plasmid Purpose**	**Source**
CENP-Q-eGFP	pMC276	pEGFP-N1	Kan^R	CENP-Q	Expression of CENP-Q-eGFP	A. McAinsh
CENP-Q-eGFP siRNA Protected	pMC308	pMC276	Kan^R	*CENP-Q* siRNA protected	Expression of siRNA protected CENP-Q-eGFP	J. Bancroft
CENP-Q-L179P-eGFP	pMC309	pMC308	Kan^R	CENP-Q-L179P-siRNA protected	Expression of CENP-Q-L179P-eGFP- siRNA protected	J. Bancroft
eGFP-N1	pMC004	NA	Kan^R	None	Cloning vector and control transfection	Clontech
eGFP-C1	pMC005	NA	Kan^R	None	Cloning vector and control transfection	Clontech
CENP-Q- S50A S51A S248A S249A	pMC355	pMC308	Kan^R	CENP-Q-Δ4 x S-A	Expression of CENP-Q-S50A S51A S248A S249A-eGFP - siRNA protected	J. Bancroft
CENP-Q- S50D S51D S248D S249D	pMC356	pMC308	Kan^R	CENP-Q-Δ4 x S-D	Expression of CENP-Q-S50D S51D S248D S249D-eGFP - siRNA protected	J. Bancroft

2.4 Biochemistry

2.4.1 Crude cellular protein extracts

Plates or wells containing cells were aspirated to remove DMEM and washed twice with PBS (2 ml for 3.5 cm wells and 10 ml for 10 cm tissue culture dishes). Cells were detached with trypsin (0.5 ml for 3.5 cm wells and 1.5 ml for 10 cm diameter dishes). Ice cold DMEM was used to re-suspend cells, 2 wells can be pooled at this stage by carrying over re-suspension from one well to the next. The suspended cells were added to 15ml falcon tube and spun in a cooled centrifuge at 4°C and 1200 RPM for 5 min. The supernatant was removed and the pellet washed with 1 ml of ice cold PBS followed by re-centrifuging for 5 min at 4°C and 1200 RPM to re-pellet any suspended cells. Remove supernatant and flash freeze cells in liquid nitrogen. On the day of running the protein gel the pellets were thawed on ice and re-suspended in 3 volumes of ice cold PBS. This suspension was diluted 2 in 3 with Nu-Page loading and reducing reagents (Invitrogen) (Nu-Page made from 50% loading buffer and 50% reducing reagent) and heated 80°C for 10 min. After heating the

samples were rested on ice for 5 min and then sonicated for 10 min at 4°C. For loading the extracts onto gels see western blotting.

2.4.2 Liquid nitrogen cellular protein extracts

Plates or wells containing cells were aspirated to remove DMEM and washed twice with PBS (2 ml for 3.5 cm wells and 10 ml for 10 cm tissue culture dishes). Cells were detached with trypsin (0.5 ml for 3.5 cm wells and 1.5 ml for 10 cm diameter dishes). Ice cold DMEM was used to resuspend cells, 2 wells can be pooled at this stage by carrying over resuspension from one well to the next. The suspended cells were added to 15ml falcon tube and spun in a cooled centrifuge at 4°C and 1200 RPM for 5 min. The supernatant was removed and the pellet washed with 1ml of ice cold PBS followed by recentrifuging for 5 min at 4°C and 1200 RPM to re-pellet any suspended cells. Remove supernatant and flash freeze cells in liquid nitrogen. The extracts were thawed on ice and re-suspended in 1.5 pellet volumes of H100 buffer, this buffer contained 50mM HEPES pH 7.9, 1 mM EDTA, 100 mM KCl, 10% glycerol, 1 mM $MgCl_2$ and on the day of use a protease inhibitor tablet (Roche) was dissolved per 50 ml of the buffer. The cell suspensions in the H100 buffer were then added rapidly to a liquid nitrogen cooled pestle containing liquid nitrogen. The suspension forms droplets that were ground with a mortar until all liquid nitrogen had evaporated at which point the residue was scraped away and placed into a 1.5 ml Eppendorf tube with a pinhole in the lid. The tube was spun at 14,000 rpm at 4°C in a cooled centrifuge for 30 min. The supernatant (the protein extracts) was removed and its absorbance at 260 nm was measured to calculate the concentration of protein present. Extracts then brought to a final concentration of ~20 µg in 7 µl, to which 3 µl of Nu-Page buffer (50% loading buffer and 50% reducing reagent; Invitrogen) was added. The samples (final concentration ~20 µg in 10 µl) were heated at 90°C for 10 min. After heating the samples were rested on ice for 5 min before loading on gels. For loading the extracts onto gels see western blotting. For the *CENP-Q* siRNA rescue western blot the pellet was also run, re-suspending in 3 x pellet volume of H100 buffer. From these pellet suspensions 7 µl was mixed with 3 µl Nu-Page buffer as above.

2.4.3 Western blotting

All gels used in this thesis were pre-casted 12 % (Invitrogen), using MOPS running buffer (Invitrogen). Gels were removed from packet, the comb and tape were removed and the gel was rinsed with H_2O. Gels were secured into the gel tank, a blank plate was used if running a single gel. Running buffers were prepared by adding 50ml of running buffer and 750 ml of H_2O. The gel tank was filled with running buffer, starting with smaller central section. To provide a protein reference ladder a 5 µl sample of pre-stained protein marker (BioRad) was loaded into the first well of the gel after which samples were then loaded. When using liquid nitrogen extracts containing a known amount of protein 10 µl of cell extract containing approximately 20 µg of protein were loaded into each well of a 10 well gel. When using crude cellular protein extracts ~10 µl of extract was also used, however when uneven loading resulted, fresh gels were loaded and the amount of extract loaded was used to compensate.

Gels were run gel at 200 V for 50 min with MOPS buffer and 35 min with MES buffer. While the gel was running semi-dry transfer blotting paper and nitrocellulose membrane was prepared. Four blotting pads were soaked in transfer buffer along with required number of 6x8cm nitrocellulose membranes. The transfer buffer was made in 2 L measures containing 5.8g glycine, 11.6g Tris, 0.74g SDS, 400 ml methanol made to 2 L with H_2O and stored at 4°C. The power supply to the tank was disconnected and gel removed. Gels were removed from cases and laid flat on nitrocellulose membranes, sandwiched between two blotting pads (BioRad) on each side. This assembly was placed into a semi-dry transfer machine (BioRad) and run at 20 V for 1 hr. To confirm transfer from the gel to the membrane and approximate even loading, the membrane was stained with Ponceau Red by covering the membrane for 2 min and gently washing with H_2O to remove excess. If the transfer was successful protein bands were marked in red.

The membrane was blocked by soaking in 5% milk powder (Sigma) in PBS containing 0.1% Tween 20 (Sigma) (PBS-T) for 1 hr in a Petri dish on a rocking stand. The milk PBS-T used for blocking was then discarded and replaced with the primary antibody (see Table 6) suspended in 5% milk

powder in PBS-T and incubated on a rocker overnight at 4°C. The following day milk PBS-T was removed and the membrane was washed for 3 x 20 min in PBS-T. The appropriate secondary antibody conjugated to horseradish peroxidase (GE Healthcare) (see Table 6) was added at a 1 in 10,000 dilution in 5% milk PBS-T, for 1 hr at room temperature on a rocking stand. The membrane was then washed 3 times for 10 min with PBS-T. To detect bands FEMTO View (Thermo) detection reagent was dripped over to cover the membrane. The membrane was then wrapped in a thin plastic film and taped into position within a film exposure cassette. This cassette was then taken to a dark room and super sensitive chemi-luminescene detection film (Kodak) was exposed (exposure time was varied depending on signal intensity) to detect luminescence corresponding to protein bands. Development of the film then revealed bands.

2.4.4 Antibodies

The antibodies used in this thesis and specific details are listed below.

Table 8 – Antibodies used in this study

Antibody Name	Species Raised In	Antibody Target	Dilution For Immuno Fluorescence	Dilution For Western Blot	Source
Primary Antibodies					
Anti-CENP-Q	Rabbit Polyclonal	CENP-Q	1/200	1/500	Rockford
Anti-CENP-P1	Rabbit Polyclonal	CENP-P	1/200	1/500	McAinsh lab; Pepceuticals as serum
Anti-CENP-A	Mouse Monoclonal	CENP-A	1/500	1/4000	Abcam
Human CREST anti-sera	Human Polyclonal	Various kinetochore proteins	1/500	NA	Antibodies Incorporated
Anti-α-tubulin	Mouse Monoclonal	α-Tubulin	1/1000	1/10,000	Sigma
Anti-γ-tubulin	Rabbit Polyclonal	γ-Tubulin	1/250	NA	Sigma
Anti-CENP-E	Rabbit Polyclonal	CENP-E	1/1500	1/1000	Gift from P. Meraldi
Anti-Plk1	Mouse Monoclonal	Plk1	1/250	NA	Santa Cruz Biotechnology
Anti-Hec1	Mouse Monoclonal	Hec1/Ndc80	1/1000	NA	Abcam
Anti-Ska3	Rabbit Polyclonal	Ska3/RAMA1	1/250	NA	Gift from A. Santamaria
Anti-CENP-O	Rabbit Polyclonal	CENP-O / Mcm21R	1/500	NA	Pepceuticals as serum
Western Blot Secondary Antibodies					
Donkey Anti-Mouse Horseradish Peroxidase Conjugate	Donkey	Mouse IgG	NA	1/10,000	GE Healthcare
Donkey Anti-Rabbit Horseradish Peroxidase Conjugate	Donkey	Rabbit IgG	NA	1/10,000	GE Healthcare
Immuno Fluorescence Secondary Antibodies					
Goat Anti-Mouse-with fluorphore (454, 594 or 647) Highly cross absorbed	Goat	Mouse IgG	1:500	NA	Invitrogen
Goat Anti-Rabbit-with fluorphore (454, 594 or 647) Highly cross absorbed	Goat	Rabbit IgG	1:500	NA	Invitrogen
Goat Anti-Human-with fluorphore (454, 594 or 647) Highly cross absorbed	Goat	Human IgG	1:500	NA	Invitrogen

CHAPTER 3: Chromosome Congression is Promoted by CENP-Q and CENP-E Dependent Pathways

3.1 Introduction

The congression of all chromosomes to the metaphase plate during mitosis is crucial to ensure their accurate disjunction during anaphase. Three key chromosome congression pathways have been identified: (1) sister kinetochores can undergo (almost) instantaneous biorientation at the spindle equator shortly after nuclear envelope breakdown (Magidson et al., 2011), (2) laterally-attached kinetochores can slide along pre-existing K-fibres from near the spindle pole to the metaphase plate driven by the plus-end directed kinesin-7 CENP-E (Kapoor et al., 2006; Kim et al., 2010) and (3) sister kinetochores that biorientate near the pole can move to the metaphase plate by depolymerisation-coupled pulling (Koshland et al., 1988; Coue et al., 1991; Mitchison & Salmon, 1992; see chapter 1 for a thorough description of these three congression pathways). The molecules and mechanisms required for depolymerisation-coupled pulling are poorly understood and how this process is coordinated with CENP-E dependent lateral sliding is unknown. Logically, depolymerisation-coupled pulling must require factors that can: (1) mediate end-on attachment to K-MTs, (2) maintain kinetochore attachment to both polymerising and depolymerising K-MTs and, (3) precisely regulate K-MT dynamics to ensure that K-MTs remain in the correct depolymerising or polymerising state. The four subunit Ndc80 complex directly binds to the microtubule lattice *in vitro* and is well established as being a core part of the kinetochore-microtubule interface (Cheeseman et al., 2006; Cheeseman et al., 2004; DeLuca et al., 2006; Kops et al., 2005). More recently, the three subunit Ska complex has emerged as being essential for microtubule-kinetochore attachment (Hanisch et al., 2006a; Gaitanos et al., 2009; Jeyaprakash et al., 2012; Schmidt et al., 2012). This complex is also able to autonomously track depolymerising microtubule plus-ends *in vitro* (Schmidt et al., 2012), thus fulfilling the requirements for a factor that could ensure continual attachment of a

kinetochore to a depolymerising K-MT. However, the proteins that directly modulate K-MT dynamics to facilitate the generation of force remain unknown. It is unclear whether these proteins can be functionally separated from those that maintain attachment to the K-MTs. Recent work has shown that disruption of the constitutive centromere associated network (CCAN) causes defects in chromosome congression and in the normal control of K-MT plus-end turnover and poleward MT flux (Amaro et al., 2010; Mchedlishvili et al., 2012). Because depletion of these CCAN proteins does not affect the binding of the Ska or Ndc80 complexes (McClelland et al., 2007; Amaro et al., 2010; Mchedlishvili et al., 2012; for review see: McAinsh & Meraldi, 2011) their deletion allows separation of the effects of microtubule-kinetochore attachment from those of regulated K-MT dynamics. One possibility is that the CCAN is important for controlling depolymerisation-coupled pulling. Biochemical experiments have shown that two CCAN subunits, CENP-Q and CENP-U (CENP-50/PBIP1), can interact directly with taxol-stabilised microtubules (Amaro et al., 2010; Hua et al., 2011), thus raising the possibility that the CCAN complex regulates K-MT dynamics through direct interactions with K-MTs. We therefore set out to investigate the role of CENP-Q during the process of chromosome congression and specifically to test the idea that it is required for depolymerisation-coupled pulling.

3.2 CENP-Q is efficiently depleted by siRNA mediated protein depletion

To investigate the function of human CENP-Q we first depleted the protein in HeLa cells using short interfering RNA (siRNA) oligonucleotides (Elbashir et al., 2001). We conducted immunoblotting with a primary anti-CENP-Q antibody and were able to demonstrate that the total CENP-Q protein levels were reduced by >90% in *CENP-Q* siRNA treated cells (Figure 3.1a, left panel). As a further control we also depleted the CENP-Q protein with a second siRNA oligo (*CENP-Q-2* siRNA, Figure 3.1a, middle panel), we also siRNA depleted the CENP-P protein (Figure 3.1a, right panel), which has previously been shown to form a complex with CENP-Q, CENP-O and CENP-U (Hori et al., 2008b). The second *CENP-Q* siRNA oligo (*CENP-Q-2* siRNA)

Figure 3.1

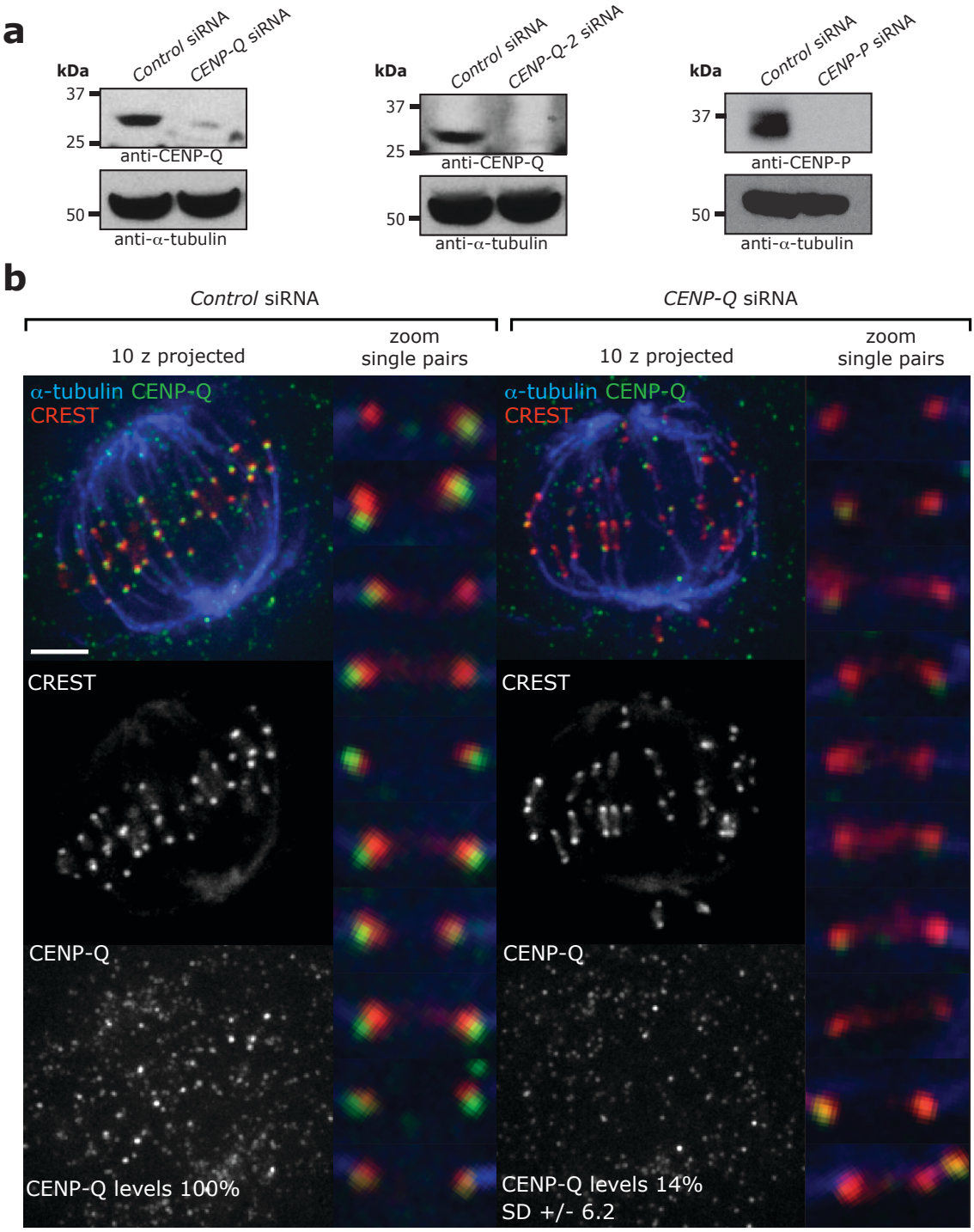

Figure 3.1 siRNA mediated depletion of CENP-Q **(a)** Immunoblots of whole-cell HeLa E1 lysates transfected with control siRNA and either *CENP-Q* siRNA or *CENP-Q-2* siRNA for 48 hours or *CENP-P* siRNA for 72 hours. The *CENP-Q* siRNA blots were then probed with antibodies raised against CENP-Q and α-tubulin or, CENP-P and α-tubulin. *CENP-Q* and *CENP-P* siRNAs depleted CENP-Q and CENP-P by ≥ 90% and α-tubulin blot confirmed equal loading. **(b)** Immunofluorescence microscopy images of metaphase cells and magnified kinetochore pairs in *Control* siRNA and *CENP-Q* siRNA depleted cells stained with CREST (red), CENP-Q (green) and α-tubulin (microtubules, blue) antibodies. The images of metaphase cells correspond to maximum intensity z-projections (10 focal planes at 0.2 μm spacing) and the zoom images of the single kinetochores are from a single focal plane of the stack. Values at the base of the bottom two panels correspond to the relative values of CENP-Q in control and CENP-Q-depleted cells (n=150 kinetochores from 30 cells, from 3 independent experiments). Scale bar = 3 μm.

and the *CENP-P* siRNA oligo also reduced the protein by >90% as detected by immunoblotting (Figure 3.1a). To measure the levels of CENP-Q protein remaining bound at kinetochores in *CENP-Q* siRNA treated cells we used quantitative immunofluorescence. Cells were treated with *CENP-Q* and *control* siRNA. After 48 hrs, these cells were fixed and stained with antibodies against CENP-Q, CREST antibodies (an internal control) and α-tubulin antibodies. Cells were then imaged (Figure 3.1b) and the intensity of the CENP-Q and CREST signal was measured manually. The CENP-Q to CREST signal ratio was taken as measure of CENP-Q kinetochore loading. This showed that treatment with *CENP-Q* siRNA resulted in an 86% (± 6.2) decrease in kinetochore bound CENP-Q compared to cells treated with *control* siRNA (Figure 3.1b).

3.3 The kinetochore localisation of CENP-Q is outside of CENP-A

When examining our immunofluorescence depletion experiments, we noticed that the CENP-Q signal localised outside of the CREST signal within the kinetochore (Figure 3.1b). This suggested that CENP-Q was not localised to the innermost part of the CCAN/kinetochore. Previous work has shown that CENP-Q can bind to microtubules *in vitro* (Amaro et al., 2010) and more recently that CENP-Q is able to modulate MT dynamics *in vitro* and *in vivo* (Samora C.P., PhD Thesis, 2012). Therefore we would expect CENP-Q to localise outside of CENP-A within the kinetochore to enable the protein to interact with the plus-ends of K-MTs. To ascertain if this was the case we conducted immunofluorescence staining against CENP-A as an inner kinetochore marker and Hec1 as an outer kinetochore marker in cells transiently expressing a CENP-Q-eGFP construct. However, to accurately determine the position of CENP-Q relative to these two markers we first needed to correct for any chromatic shift within our imaging system. To achieve this we conducted immunofluorescence using monoclonal anti-CENP-A antibodies and labelling with three fluorescently tagged secondary anti-mouse antibodies, fluorescing at 488, 561 and 647 nm (Figure 3.2a, top row). This provided a reference from which chromatic shift could be measured (see line scan showing chromatic shift in Figure 3.2b, top row). To confirm the measured shift was accurate

Figure 3.2

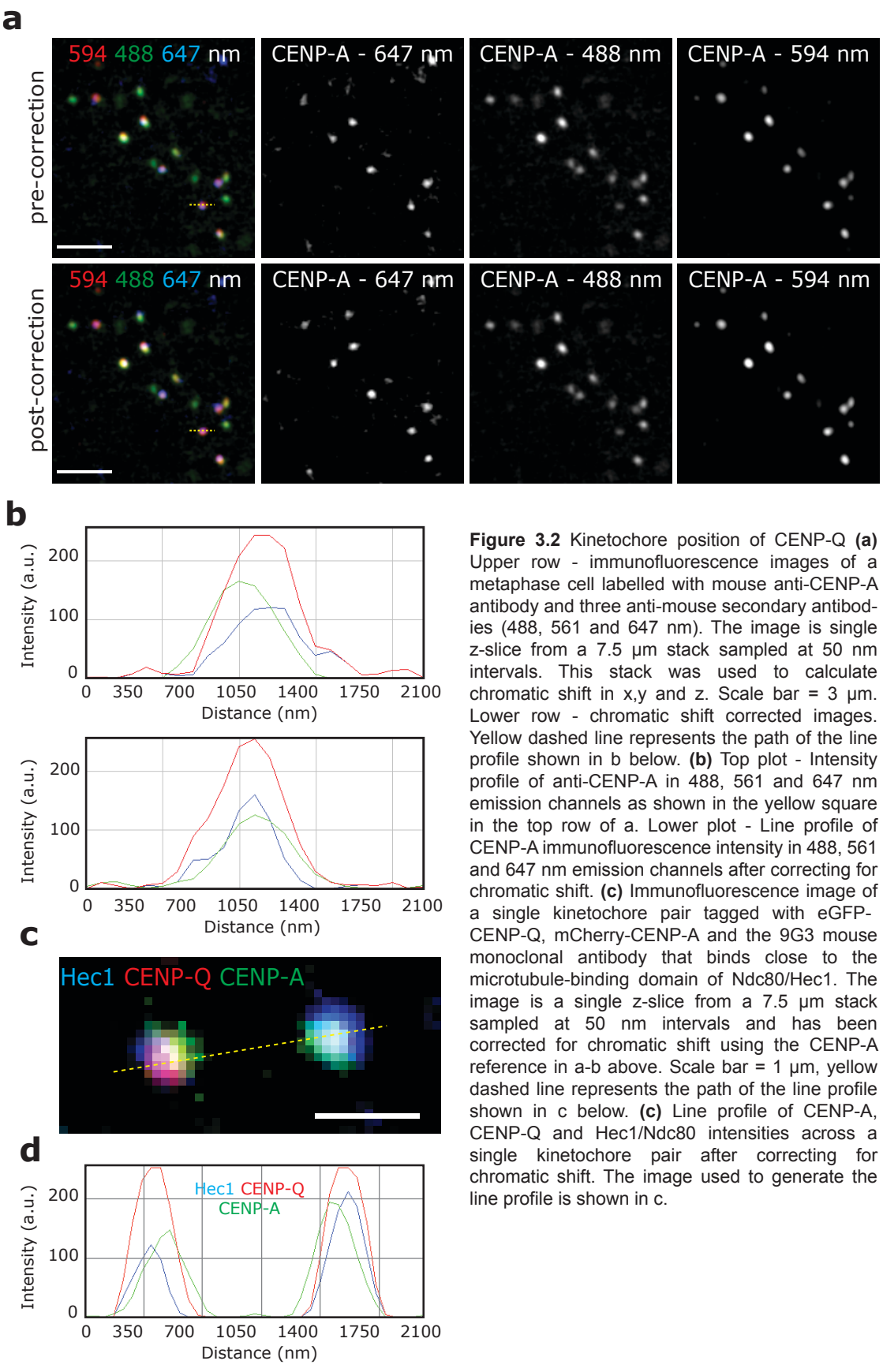

Figure 3.2 Kinetochore position of CENP-Q **(a)** Upper row - immunofluorescence images of a metaphase cell labelled with mouse anti-CENP-A antibody and three anti-mouse secondary antibodies (488, 561 and 647 nm). The image is single z-slice from a 7.5 µm stack sampled at 50 nm intervals. This stack was used to calculate chromatic shift in x,y and z. Scale bar = 3 µm. Lower row - chromatic shift corrected images. Yellow dashed line represents the path of the line profile shown in b below. **(b)** Top plot - Intensity profile of anti-CENP-A in 488, 561 and 647 nm emission channels as shown in the yellow square in the top row of a. Lower plot - Line profile of CENP-A immunofluorescence intensity in 488, 561 and 647 nm emission channels after correcting for chromatic shift. **(c)** Immunofluorescence image of a single kinetochore pair tagged with eGFP-CENP-Q, mCherry-CENP-A and the 9G3 mouse monoclonal antibody that binds close to the microtubule-binding domain of Ndc80/Hec1. The image is a single z-slice from a 7.5 µm stack sampled at 50 nm intervals and has been corrected for chromatic shift using the CENP-A reference in a-b above. Scale bar = 1 µm, yellow dashed line represents the path of the line profile shown in c below. **(c)** Line profile of CENP-A, CENP-Q and Hec1/Ndc80 intensities across a single kinetochore pair after correcting for chromatic shift. The image used to generate the line profile is shown in c.

this was then used to correct the images of triple tagged CENP-A (Figure 3.2a second row and 3.2b lower line profile). This shift correction was then applied to image stacks of fixed cells in which CENP-Q, Hec1 and CENP-A were labelled (corrected image of a kinetochore pair can be seen in Figure 3.2c). Line scans through kinetochore pairs in these corrected cells allowed us to confirm that the CENP-Q did indeed localise outside of the CENP-A signal, but was interior to Hec1 as defined by an antibody targeting the MT binding domain of Hec1 (Figure 3.2d).

3.4 Depletion of CENP-Q results in slow chromosome congression and an accumulation of polar chromosomes

During the above immunofluorescence experiments we observed that depletion of CENP-Q seemed to cause an accumulation of chromosomes around the spindle poles. To investigate this interesting phenotype, we carried out further immunofluorescence on CENP-Q depleted cells, staining with DAPI (to mark chromatin), anti-CENP-A antibodies (to mark kinetochores), γ-tubulin (to mark spindle poles) and α-tubulin (to mark microtubules). Imaging these cells revealed that although the majority of kinetochores were aligned at the metaphase plate, an unaligned subpopulation could be visualised on both sides of the metaphase plate as well as behind the spindle poles (Figure 3.3d). This polar chromosome phenotype is similar to the phenotype observed in the knock-out of CENP-Q in chicken DT40 cells (Hori et al., 2008a).

To further assess this chromosome alignment defect, we collected a series of 3 min time-lapse movies over 12 hrs in HeLa cells stably expressing Histone2B-eGFP/mRFP-α-Tubulin (Figure 3.3a). To analyse the mitotic progression of these cells we took the time of nuclear envelope breakdown (NEB) to be T=0 and determined the timing of last chromosome congression (LCC) relative to this point by manual scoring. In *control* siRNA treated cells we found that 95% of cells had aligned all their chromosomes to the metaphase plate by 24 min from NEB (Figure 3.3b). In contrast, only 10.3% of CENP-Q depleted cells had formed a metaphase plate and aligned all their chromosomes by 24 min (Figure 3.3b). Consistent with our fixed cell experiments, we observed

Figure 3.3

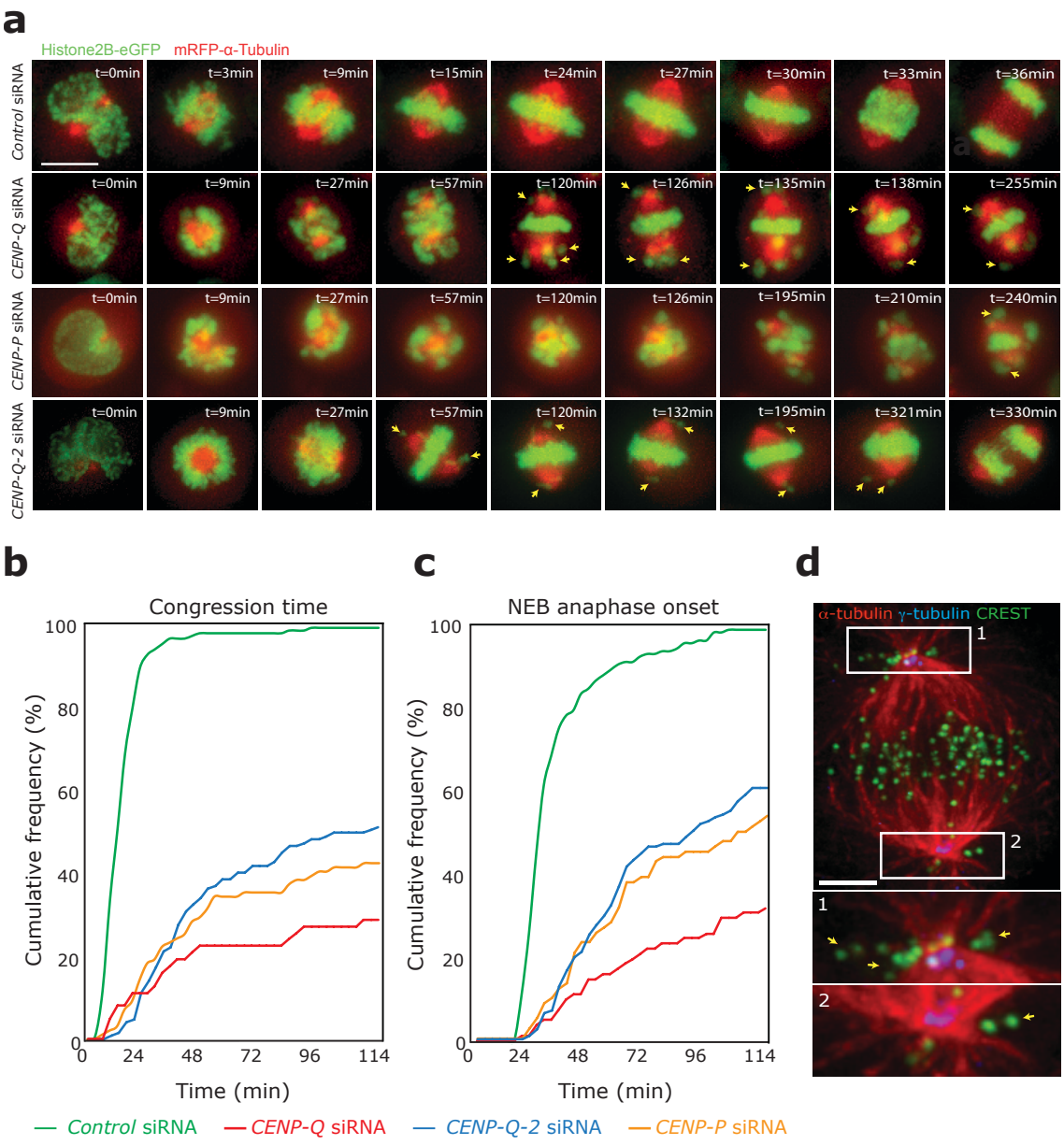

Figure 3.3 Mitotic progression of CENP-Q and CENP-P depleted cells **(a)** Frames from live-cell movies of HeLa E1 cells expressing H2B–eGFP/mRFP–α-tubulin (to mark chromosomes and microtubules respectively) after treatment with *Control* siRNA (top row), *CENP-Q* siRNA cells (second row), *CENP-P* siRNA (third row) and *CENP-Q-2* siRNA (bottom row). Yellow arrows point to unaligned kinetochores. Scale bar indicates 10μm. **(b-c)** Quantification of nuclear envelope breakdown (NEB) to the time when the last chromosome congressed to the metaphase plate (b), and NEB to the time of anaphase onset (c). Data is shown as cumulative frequency plots. Line colours represent the following conditions; *Control* siRNA = green lines, *CENP-Q* siRNA = red lines, *CENP-P* siRNA = orange lines, *CENP-Q-2* siRNA = blue lines. n ≥ 85 cells per condition from a minimum of 3 independent experiments. **(d)** Immunofluorescence microscopy images of a CENP-Q depleted metaphase HeLa E1 cell stained with CREST (kinetochores, green) and α-tubulin (microtubules, red) antibodies. The image is a z-projection (10 focal planes at 0.2 μm spacing). Zoom boxes 1 and 2 are centred on the spindle poles and yellow arrows point to unaligned kinetochores at around the spindle poles. Scale bar = 3 μm.

that a number of chromosomes, where as the majority of cells retained a population of chromosomes trapped around the spindle pole or between the plate and the pole (yellow arrows in Figure 3.3a). We next measured the time from NEB to anaphase onset, again assigning NEB to be T=0 and determined the timing of anaphase by manually scoring the first frame at which chromatin separation in anaphase A could be detected. This analysis revealed that the chromosome congression defects associated with CENP-Q depletion activated the spindle checkpoint, as a prolonged mitotic delay could be observed. Only 26% of CENP-Q depleted cells underwent anaphase within 96 min of NEB, compared to 99% of control cells (Figure 3.3c). Of the cells that underwent anaphase within 114 min, 19% still had uncongressed chromosomes. This suggested that although the checkpoint is active, it is not fully effective. This may be consistent with previous work suggesting that CENP-Q depletion partially perturbs the spindle assembly checkpoint (Matson et al., 2012). We repeated these live cell chromosome congression and anaphase onset experiments with a second *CENP-Q* siRNA oligo (*CENP-Q-2* siRNA) and observed almost identical chromosome congression defects and a similar, albeit slightly shorter delay in chromosome congression and segregation (Figure 3.3a,b,c). Thus CENP-Q is required for accurate and timely congression of chromosomes to the metaphase plate. Depletion of the CENP-P protein, which forms a complex with CENP-Q, CENP-U and CENP-O, caused a similar congression phenotype (Figure 3.3a,b,c).

3.5 Depletion of CENP-Q does not affect the loading of key kinetochore microtubule binding proteins but does prevent Plk1 and CENP-O loading

One possibility is that the depletion of CENP-Q affects the core K-MT binding complexes (the KMN and Ska complexes; Cheeseman et al., 2006, Hanisch et al., 2006a; Gaitanos et al., 2009). To test this we carried out immunofluorescence in control and CENP-Q depleted cells, staining with antibodies against Hec1 (Ndc80 complex, within the KMN) and Ska3/RAMA1 (Ska complex) (Figure 3.4a, b). Hec1 and Ska3 stained cells were co-stained with CREST and anti-CENP-A

Figure 3.4

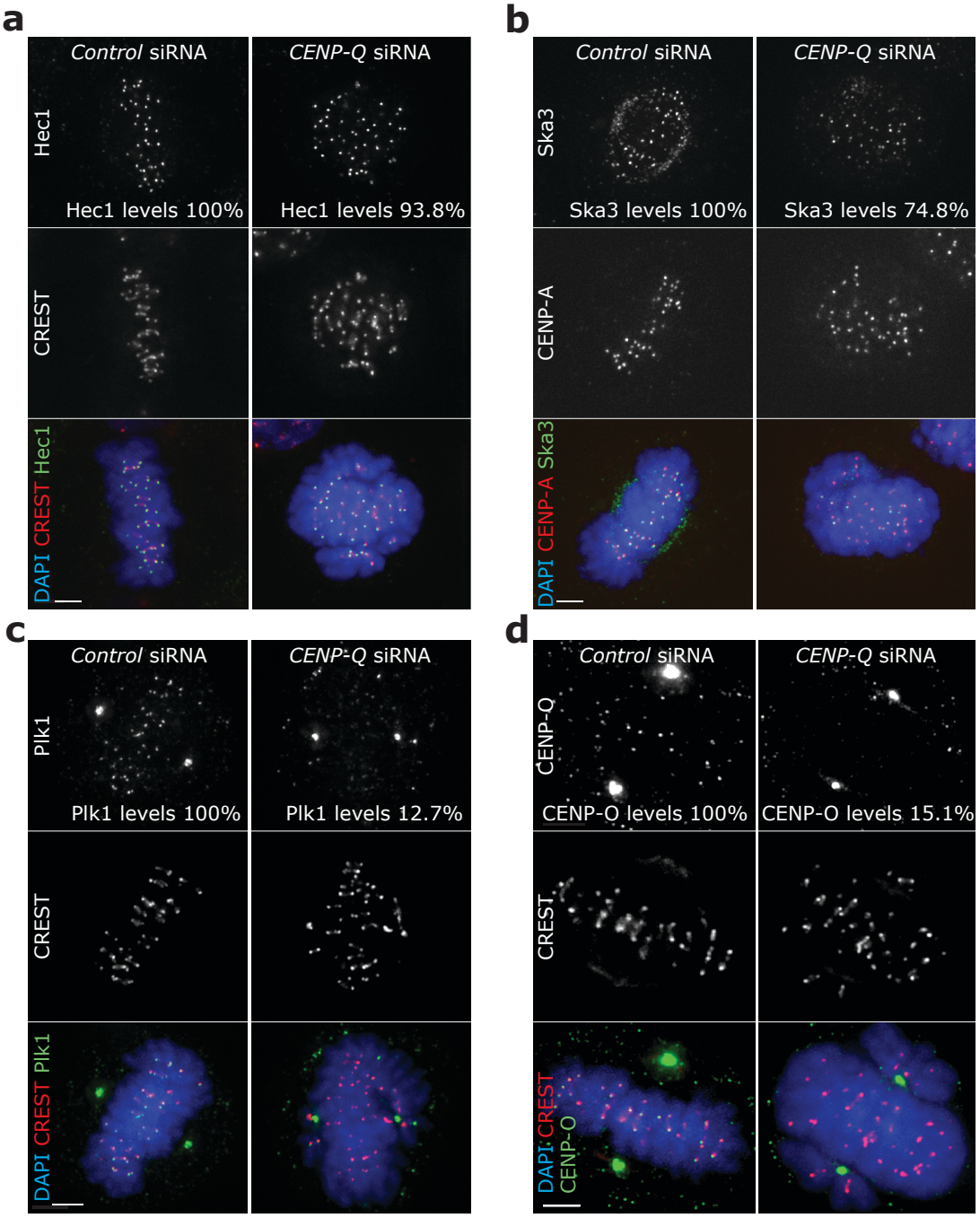

Figure 3.4 CENP-Q protein loading dependencies by IF **(a)** Immunofluorescence images of control and CENP-Q depleted metaphase HeLa E1 cell stained with CREST (kinetochores, red) and Hec1 (green) antibodies and DAPI (DNA, blue). The image is a z-projection (10 focal planes at 0.2µm spacing). Scale bar = 3 µm. Percentage values indicate loading of Hec1 in *Control* siRNA (100%) and *CENP-Q* siRNA (93.8%, SD ± 20.7). For both conditions n=100 kinetochores, 10 cells from 2 independent experiments. **(b)** Immunofluorescence images of control and CENP-Q depleted metaphase HeLa E1 cells stained with CENP-A (kinetochores, red) and Ska3 (green) antibodies and DAPI (DNA, blue). The image is a z-projection (10 focal planes at 0.2µm spacing). Scale bar = 3µm. Percentage values indicate loading of Ska3 in control (100%) and CENP-Q (74.8%). For both conditions n=50 kinetochores, 5 cells from 1 experiment. **(c)** Immunofluorescence images of control and CENP-Q depleted metaphase HeLa E1 cells stained with CREST (kinetochores, red) and Plk1 (green) antibodies and DAPI (DNA, blue). The image is a z-projection (10 focal planes at 0.2µm spacing). Scale bar = 3µm. Percentage values indicate loading of Plk1 in control (100%) and CENP-Q (12.7%, SD ± 4.1), Plk1 levels at the spindle pole are unaffected. For both conditions n=100 kinetochores, 10 cells from 2 independent experiments. **(d)** Immunofluorescence images of control and CENP-Q depleted metaphase HeLa E1 cells stained with CREST (kinetochores, red) and CENP-O (green) antibodies and DAPI (DNA, blue). The image is a z-projection (10 focal planes at 0.2µm spacing). Scale bar = 3µm. Percentage values indicate loading of CENP-O in control (100%) and CENP-Q (15.1%). For both conditions n=50 kinetochores, 5 cells from 1 experiment.

antibodies as an internal control. When compared to control depleted cells the relative levels of kinetochore bound Hec1 were largely unaffected in CENP-Q depleted cells (93.8%, SD ± 20.7 compared to control; Figure 3.4a). Analysis of Ska3 kinetochore loading showed that CENP-Q depletion had only a minor effect on Ska3 levels, which were 74.8 % of those in control depleted cells, representing at most a minor reduction in Ska3 levels (Figure 3.4b). Previous work has shown that reduction of Hec1 or Ska3 by siRNA mediated depletion results in a failure to form a metaphase plate with kinetochore pairs scattered around the spindle (DeLuca et al., 2005; Daum et al., 2009). Given this difference in observed phenotype and the largely unaffected levels of both Hec1 and Ska3, it is clear that the CENP-Q depletion phenotype is not a result of kinetochores being unable to form end-on attachments with K-MTs.

Based on the previously reported co-dependence of CENP-Q and CENP-U for kinetochore loading and the dependence of Plk1 on CENP-U for kinetochore binding (Hori et al., 2008a; Kang et al., 2011; Park et al., 2011), we would expect that depletion of CENP-Q would result in a reduction of Plk1 kinetochore loading. To confirm that this was the case we conducted immunofluorescence on CENP-Q and control depleted cells staining with antibodies against Plk1 and CREST. Quantification revealed a reduction in kinetochore bound Plk1 to just 12.7% (SD ± 4.1, n= 2 independent experiments) of control levels (Figure 3.4c).

Previous work in chicken cells has shown that CENP-O/P/Q/U are interdependent for kinetochore binding (Hori et al., 2008b). We therefore expected to see that levels of CENP-O would decrease at CENP-Q depleted kinetochores. To confirm this we conducted immunofluorescence on CENP-Q and control depleted cells, staining for CENP-O and CENP-A as a reference. Imaging and analysis of these cells revealed that CENP-O levels were reduced by 94.9% in CENP-Q depleted cells (Figure 3.4d). Interestingly, direct depletion of CENP-O leads to an accumulation of monopolar spindles (McClelland et al., 2007), a phenotype not observed in CENP-Q depleted cells, suggesting that the CENP-Q depletion phenotype is the dominant one. These loading relationships are summarised in Figure 3.5.

Figure 3.5

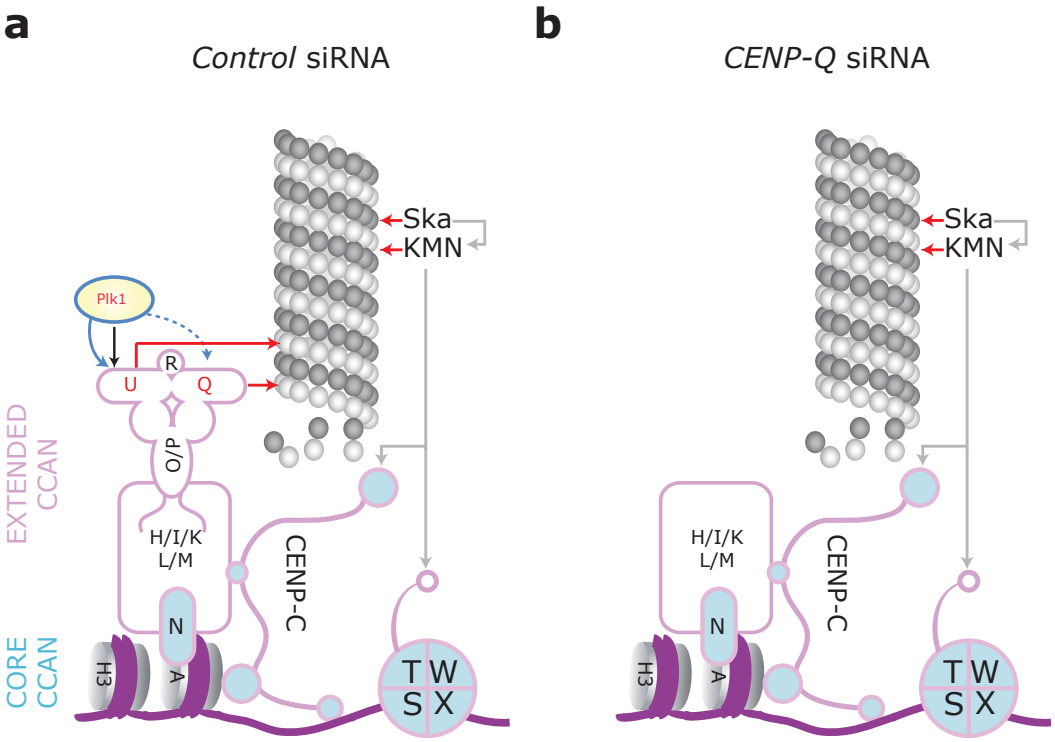

Figure 3.5 (a,b) Kinetochore protein loading depending on CENP-Q. (a) represents kinetochore proteins present in a control depleted cell. (b) represents kinetochore protein loading after the depletion of CENP-Q. The absent proteins are based on the dependencies assessed in Figure 3.4 and known CCAN loading dependencies (See chapter 1 for details). Note the loss of Plk1 and CENP-O whilst the core MT binding complexes (Ndc80 and Ska complexes) remain present. Pink outlines represent CCAN proteins, those with blue infill are core CCAN proteins.Red arrow represnt microtubule binding activity. Grey and black arrows represent direct interactions. Blue arrows represent phosphorylation events.

3.6 The CENP-Q depletion phenotype can be rescued by an siRNA protected CENP-Q-eGFP mammalian expression construct

To confirm the specificity of the *CENP-Q* siRNA treatment we next developed the tools required to conduct *CENP-Q* siRNA rescue experiments. First a CENP-Q-eGFP expression vector was generated, by cloning the CENP-Q cDNA sequence into a mammalian expression vector with a C-terminal eGFP tag and a constitutive cytomegalovirus (CMV) promoter. The resulting plasmid was given the designation pMC273 (see chapter 2 for cloning details). After testing this construct by restriction digest and sequencing we next proceeded to protect the CENP-Q cDNA from *CENP-Q* siRNA recognition. This was achieved by silently mutating 7 bases within the *CENP-Q* siRNA recognition sequence by site directed mutagenesis (Figure 3.6a; see chapter 2 for details). Using DNA sequencing a correctly mutagenised construct was selected; this construct was given the designation pMC308.

To ensure that the silent mutations had not disrupted the ability of the CENP-Q coding sequence to express in human cells, we transiently transfected the construct into HeLa K cells stably expressing mCherry-α-tubulin (see chapter 2). After 48 hrs these cells were imaged in both mCherry and eGFP channels to show microtubules and CENP-Q-eGFP respectively. Imaging revealed that CENP-Q-eGFP expressed and localised to kinetochores at the metaphase plate (Figure 3.6b). We continued to image these cells for 15 min at 3 min intervals and saw that after anaphase onset CENP-Q-eGFP continued to localise to kinetochores and was still clearly visible at telophase (Figure 3.6b). This is in contrast to other studies, which suggest that CENP-Q is lost from the metaphase plate at anaphase onset (Kang et al., 2011). To further test the CENP-Q-eGFP siRNA protected construct we transfected it into HeLa E1 cells containing no fluorescent protein markers. These cells were then fixed and stained with antibodies against CENP-A to mark kinetochores. Upon imaging CENP-Q-eGFP could be visualised at kinetochores as marked by the CENP-A antibody (Figure 3.6c).

Figure 3.6

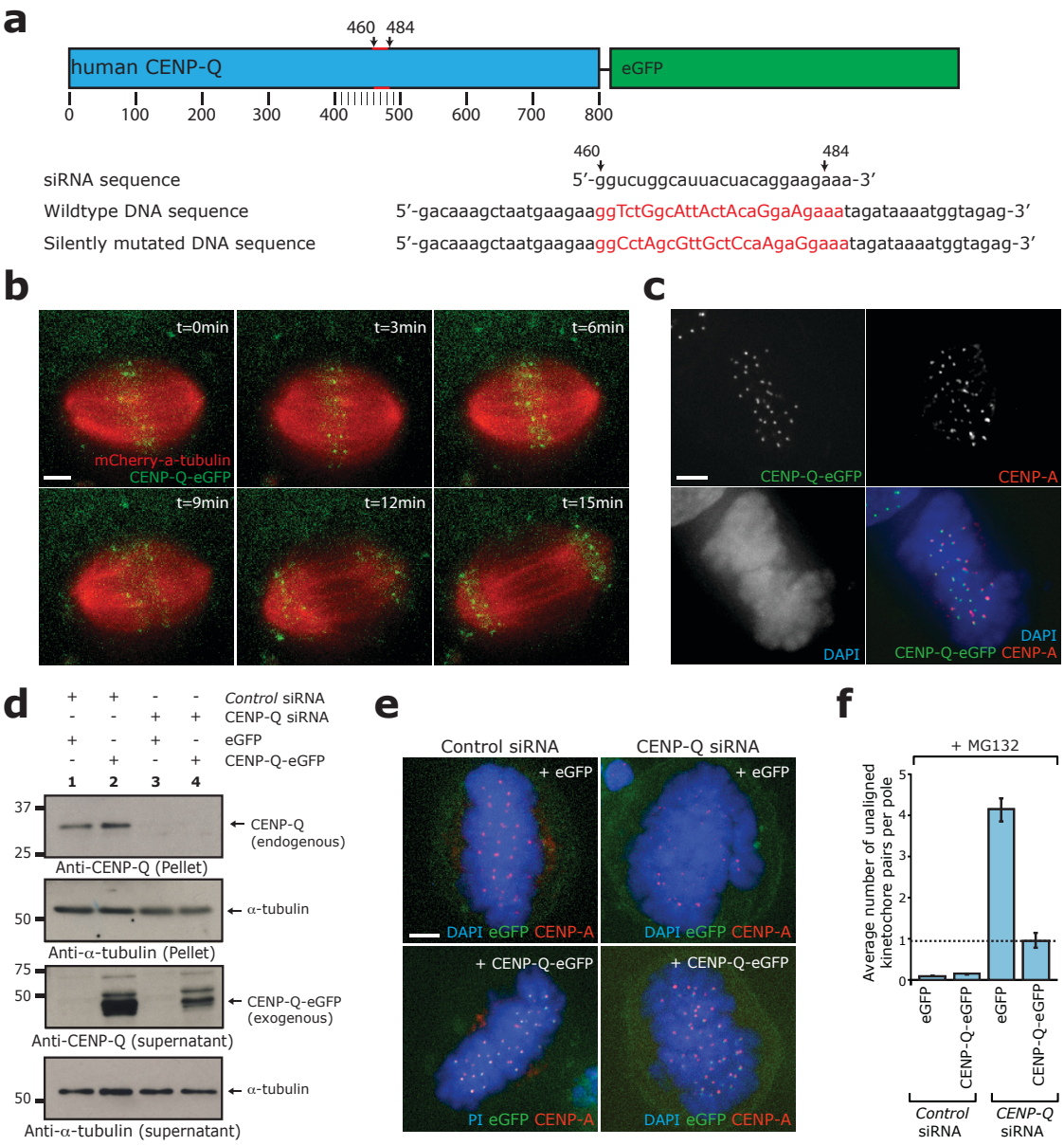

Figure 3.6 CENP-Q siRNA rescue **(a)** Schematic of the CENP-Q-eGFP transgene and nucleotides that were mutated to render the construct resistant to siRNA . The numbers under the schematic represent DNA base pair position within CENP-Q CCD. Numbers above represent the region silently mutated to siRNA protect the construct. **(b)** Frames from live cell imaging of HeLa cells stably expressing mCherry-α-tubulin and transiently expressing siRNA protected CENP-Q-eGFP 48 hours after transfection. Images were acquired every 3 minutes. CENP-Q can be seen localised at kinetochores throughout. Images shown are z-projections, 2 focal planes at 2 µm spacing. Scale bar = 3 µm. **(c)** Immunofluorescence of HeLa cells (z-projections, 10 focal planes at 0.2 µm spacing), 48 hours after transfection with siRNA protected CENP-Q-eGFP. Cells were fixed and stained with DAPI (DNA, blue) and anti-CENP-A antibodies (kinetochores). Scale bar = 3 µm. **(d)** Immunoblots of liquid nitrogen lysates from HeLa cells transfected with Control or CENP-Q siRNA for 12 h and then transfected with a control or siRNA resistant CENP-Q-eGFP construct for 48 h. Blots were probed with antibodies against CENP-Q and α-tubulin. Endogenous CENP-Q and corresponding α-tubulin control are shown in the top two panels. Pellet fraction is shown as nonspecific staining obscured the protein in the supernatant. Transgene and corresponding α-tubulin loading control are shown in the lower two panels. **(e)** Immunofluorescence images (z-projections, 10 focal planes, 0.2 µm spacing) of *CENP-Q* siRNA rescue experiment in HeLa cells. Cells were treated with *CENP-Q* or *Control* siRNA for 14 h and then transfected with an siRNA resistant plasmid expressing CENP-Q-eGFP or control plasmid for a further 48 h. To prevent anaphase MG132 was added at 1µM for 90 min before fixation. Cells were stained with DAPI (DNA, blue) and antibodies against CENP-A (kinetochores, red). Scale bar = 3µm. **(f)** Quantification of average number of unaligned kinetochore pairs per pole in metaphase arrested cells from rescue experiment described above (f). n≥100 poles/50 cells per condition, 2 independent experiments.

We next set out to ascertain whether the silently mutated CENP-Q-eGFP construct pMC308 (from here referred to as CENP-Q-eGFP only) was indeed protected against *CENP-Q* siRNA. To do this we transfected CENP-Q-eGFP and an empty vector (peGFP-N1, pMC004) control into cells, which had been pretreated with *control* or *CENP-Q* siRNA for 12 hrs. Protein extracts were then made from these cells using liquid nitrogen extraction (see chapter 2). These extracts were then used to conduct immunoblotting, the blots being probed with antibodies against CENP-Q, and α-tubulin as a loading control. Detection on photographic film revealed that both lanes corresponding to *control* siRNA contained bands at ~32 kDa when probed with anti-CENP-Q antibodies (Figure 3.6d), corresponding to the endogenous CENP-Q protein. These bands were not present in cells treated with *CENP-Q* siRNA confirming efficient depletion of the endogenous protein (Figure 3.6d). In control-depleted cells transfected with pMC308 a second band at between 50 and 75 kDa was visible, corresponding to the CENP-Q-eGFP transgene. The CENP-Q-eGFP band persisted in *CENP-Q* siRNA treated cells indicating siRNA protection of the construct (Figure 3.6d).

To confirm specificity of the *CENP-Q* siRNA treatment, we tested whether the CENP-Q-eGFP construct was able to rescue the *CENP-Q* siRNA phenotype. To achieve this we conducted fixed cell immunofluorescence on cells treated under the same conditions used in the above immunoblotting assay. After 12 hrs depletion and 48 hrs rescue, cells were treated with the proteosome inhibitor MG132 for 90 min to prevent anaphase onset and thereby rule out differences associated with cell cycle stage. Cells were then fixed and stained with DAPI to mark chromatin and anti-CENP-A antibodies to mark kinetochores. The number of unaligned kinetochore pairs per pole was then manually scored by fluorescence microscopy and representative images were also captured (Figure 3.6e). Depletion of CENP-Q and transfection with empty vector resulted in an average of ~4 unaligned kinetochore pairs per pole. In contrast, transfection with a CENP-Q transgene reduced the number of unaligned kinetochore pairs per pole to ~1 (Figure 3.6f). This demonstrated that the effect of *CENP-Q* siRNA was specific, as reintroduction of the siRNA-protected transgene clearly rescues the phenotype.

3.7 Stable expression of siRNA resistant CENP-Q-eGFP rescues chromosome alignment and mitotic timing in live cells

To study the *CENP-Q* siRNA rescue in live cells in more detail we next undertook the creation of stable cell lines expressing CENP-Q-eGFP by random genomic integration of the CENP-Q-eGFP expression vector. For creation of this cell line we used an existing HeLa K cell line stably expressing mCherry-CENP-A as a kinetochore marker. These cells were transfected with the CENP-Q-eGFP expression vector (pMC308) for 48 hrs, after which cells were maintained in selective medium until single colonies appeared. These colonies were screened for the presence of CENP-Q-eGFP at kinetochores (a positive example can be seen in Figure 3.7a). Colonies with CENP-Q-eGFP present at kinetochores were cultured further and the expressed levels of the transgene were assayed by western blotting with anti-CENP-Q antibodies (see chapter 2). A monoclonal cell line designated MC069 was selected for further experiments, as the levels of the CENP-Q-eGFP protein were most similar to the endogenous CENP-Q protein (Figure 3.7b). The CENP-Q-eGFP expression product was also detectable on immune blots using anti-eGFP antibodies (Figure 3.7b).

To visualise the *CENP-Q* siRNA rescue in live cells, the CENP-Q-eGFP/mCherry-CENP-A (MC069) or the control mCherry-CENP-A cell line (MC051) was treated with either control or *CENP-Q* siRNA for 48 hrs. These cells were then imaged for 12 hrs at 3 min time-lapse intervals using mCherry-CENP-A to visualise kinetochore movements. Resulting movies were then manually analysed, recording the time from nuclear envelope breakdown (NEB) to last chromosome congression (LCC) and the time from NEB to anaphase onset. This mitotic timing data was plotted as cumulative frequency graphs (Figure 3.7c,d). These graphs showed that when treated with *control* siRNA, mitotic progression of the CENP-Q-eGFP (MC069) and control cell (mCherry-CENP-A MC051) lines were almost identical, with >90 % of both cell lines having aligned all chromosomes by 24 min and >96 % having undergone anaphase (Figure 3.7c, d). The similarity between these mitotic timings showed that expression of the CENP-Q-eGFP transgene was not

Figure 3.7

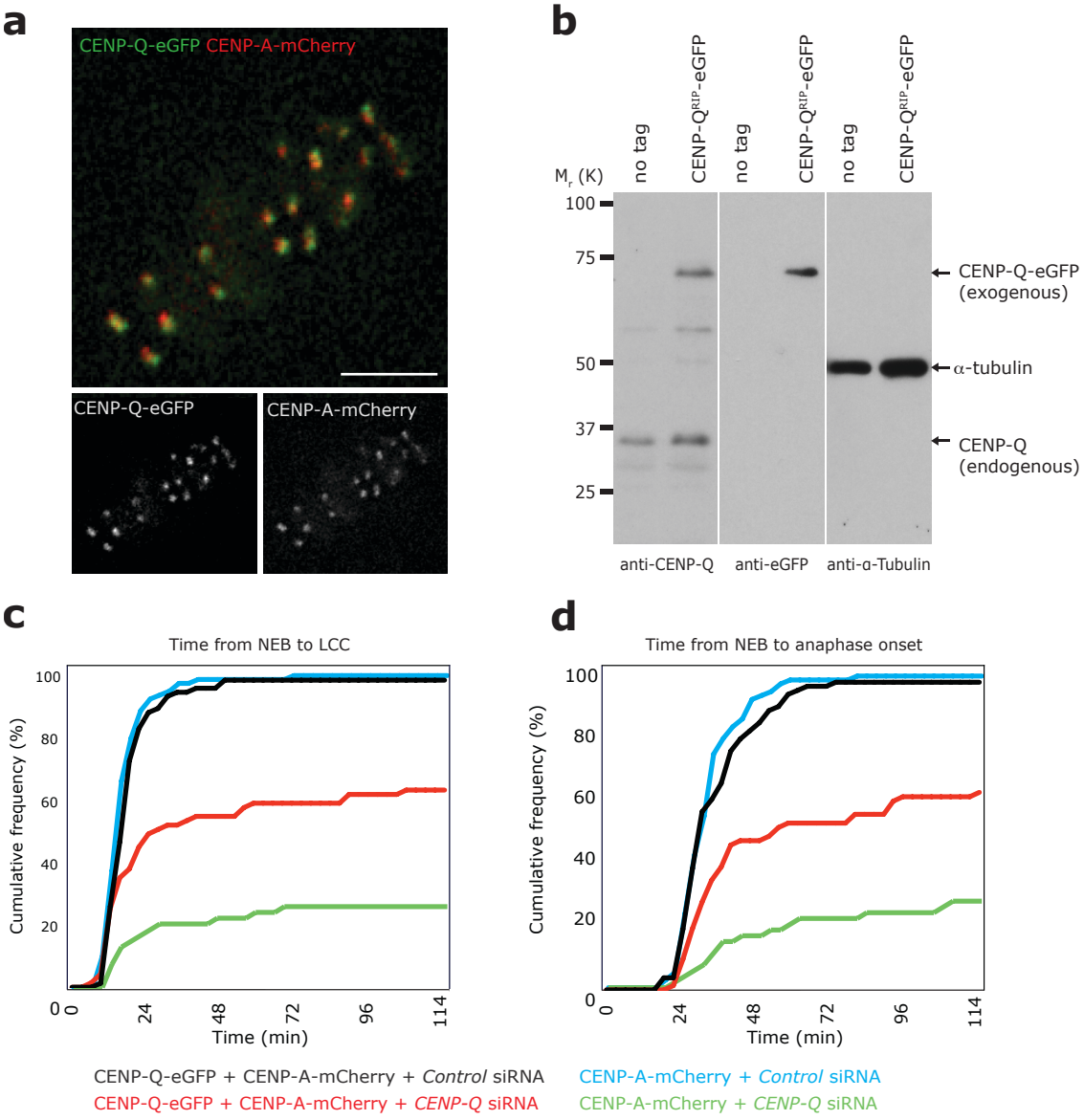

Figure 3.7 CENP-Q siRNA protected cell line analysis **(a)** Single frame from live cell imaging of HeLa cells stably expressing both mCherry-CENP-A and siRNA protected CENP-Q-eGFP (cell line MC069). Image is a z-projection (2 focal planes, 2 µm spacing). Scale bar = 3 µm. Smaller panels on the left show the eGFP and mCherry channels in isolation. **(b)** Immunoblots of lysates from HeLa cells stably expressing both mCherry-CENP-A and siRNA protected CENP-Q-eGFP (cell line MC069, image shown above in a). The blots were probed with antibodies against CENP-Q, eGFP (to visualise eGFP on CENP-Q-eGFP) and α-tubulin. Expression of the CENP-Q-eGFP was similar to endogenous CENP-Q. Approximate equal loading was confirmed by α-tubulin intensity. **(c-d)** Quantification of mitotic timings in cells stably expressing mCherry-CENP-A + siRNA CENP-Q-eGFP (MC069) and cells stably mCherry-CENP-A (MC051) as a control cell line, after treatment with either *Control* or *CENP-Q* siRNA. The time between nuclear envelope breakdown (NEB) to the congression of the last chromosome to the metaphase plate (c), and NEB to the time of anaphase onset (d), were both quantified. Data is shown as cumulative frequency plots. Line colours represent the following conditions; CENP-Q-eGFP + CENP-A-mCherry + *Control* siRNA = black, CENP-Q-eGFP + CENP-A-mCherry + *CENP-Q* siRNA = red, CENP-A-mCherry + *Control* siRNA = blue, CENP-A-mCherry + *CENP-Q* siRNA = green. n ≥ 80 cells per condition from a minimum of 3 independent experiments.

having an adverse effect on mitotic progression. As expected, treatment with *CENP-Q* siRNA resulted in a pronounced mitotic delay in the control mCherry-CENP-A cell line with only 20% of cells having aligned all chromosomes by 24 min and only 20 % having undergone anaphase by 72 min (Figure 3.7c, d). However, when the siRNA protected CENP-Q-eGFP cell line (MC069) was treated with *CENP-Q* siRNA 50% of cells had aligned all chromosomes by 24 min and 53% of cells had progressed to anaphase by 72 min. Thus, stable expression of siRNA protected CENP-Q-eGFP greatly increases both chromosome alignment and progression into anaphase. Although in these cells polar kinetochores were often visible, they were often able to congress. In the control cell line these errant chromosomes remained uncongressed (Figure 3.7c, d).

3.8 CENP-Q is required for kinetochore loading of CENP-E

During our earlier experiments we noted that the CENP-Q depletion phenotype was reminiscent of that reported for the depletion of the kinesin-7 CENP-E (Putkey et al., 2002; Weaver et al., 2003). We therefore proceeded to test whether the CENP-Q and CENP-E depletion phenotypes were phenotypically similar in our established live cell-imaging assay, using cells expressing Histone2B-eGFP/mRFP-α-Tubulin as described above (section 3.3). Cells were treated with *CENP-E*, *CENP-Q* or *control* siRNA and imaged (Figure 3.8a). The phenotype of *CENP-E* siRNA appeared similar to *CENP-Q* siRNA, with cells displaying considerable delay in chromosome congression and anaphase onset with a sub-population of kinetochores remaining around the spindle pole. Interestingly we noted that the unaligned chromosomes around the pole in CENP-E depleted cells seemed more tightly clustered than those in *CENP-Q* siRNA treated cells (Figure 3.8a).

Given the similarity of the CENP-Q and CENP-E depletion phenotypes we investigated whether CENP-Q was required for the loading of CENP-E to kinetochores using immunofluorescence. Cells were treated with *control*, *CENP-Q* or *CENP-E* siRNA and then fixed, staining with antibodies against CENP-E (to measure levels of the kinesin), CREST antisera as a kinetochore reference and anti-α-tubulin antibodies. These cells were then imaged (15 μm at 0.2 μm intervals; Figure

Figure 3.8

a

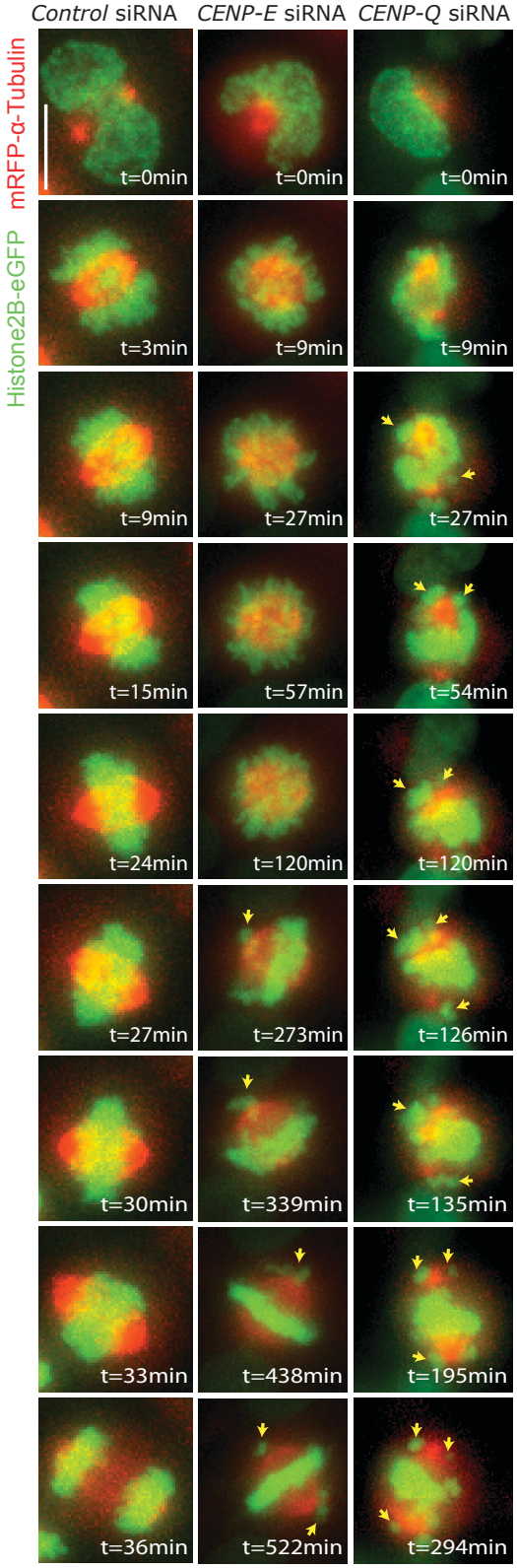

Figure 3.8 CENP-Q vs. CENP-E mitotic progression **(a)** Individual frames from live-cell movies of HeLa E1 cells expressing Histone2B–eGFP (to mark chromosomes) and mRFP–α-tubulin (to mark microtubules) after treatment with *Control* siRNA (left column), *CENP-E* siRNA cells (middle column) or *CENP-Q* siRNA (right column). Yellow arrows point to unaligned (polar) chromosomes. Scale bar = 10μm. Note that both CENP-E and CENP-Q depleted cells arrest in mitosis for a long duration with the majoity of chromosomes aligned at the spindle equator.

3.9a, c), analysis of the resulting images confirmed that treatment with siRNA targeting CENP-E reduced the kinetochore bound CENP-E levels by 95.6% relative to CREST (Figure 3.9a,b). Interestingly depletion of CENP-Q also reduced the levels of CENP-E on kinetochores by 80% (Figure 3.9a, b). These data indicate that CENP-Q is required for normal loading of CENP-E onto kinetochores. To ascertain whether CENP-Q and CENP-E were mutually dependent for kinetochore loading we next carried out the reciprocal experiment treating cells with *control*, *CENP-Q* or *CENP-E* siRNA oligos and staining with antibodies against the CENP-Q protein and CREST antisera. We found, as would be expected, that treatment with *CENP-Q* siRNA reduced the levels of kinetochore bound CENP-Q (82% reduction; Figure 3.9c,d). However, depletion of CENP-E did not affect kinetochore binding by CENP-Q (Figure 3.9c,d). Thus, CENP-E requires CENP-Q for kinetochore binding but not vice versa.

These results raised the question; what is the fate of the CENP-E protein in CENP-Q depleted cells in which CENP-E is no longer kinetochore bound? To address this question we conducted immunoblotting on whole cell liquid nitrogen prepared protein extracts, from control, CENP-Q and CENP-E depleted cells in the presence and absence of the proteasome inhibitor MG132. Blots were generated and probed with antibodies against CENP-E, detection revealed that levels of the kinesin decreased upon treatment with *CENP-Q* siRNA, however, these levels were partially restored upon treatment with MG132 (Figure 3.9e). Treatment with *CENP-E* siRNA to prevent translation of the protein directly resulted in a reduction of CENP-E levels and, as expected, treatment with MG132 was unable to rescue the protein levels. Taken together these results suggest that when CENP-E is unable to bind the kinetochore due to the absence of CENP-Q, the CENP-E protein is degraded by the proteasome.

To further characterise this loading relationship we next set out to determine whether our earlier described *CENP-Q* siRNA rescue assay could restore CENP-E kinetochore binding. As before, cells were treated with c*ontrol* or *CENP-Q* siRNA for 12 hrs and then transfected with the siRNA-protected CENP-Q-eGFP expression vector or a control vector for 48 hrs. After which cells were

Figure 3.9

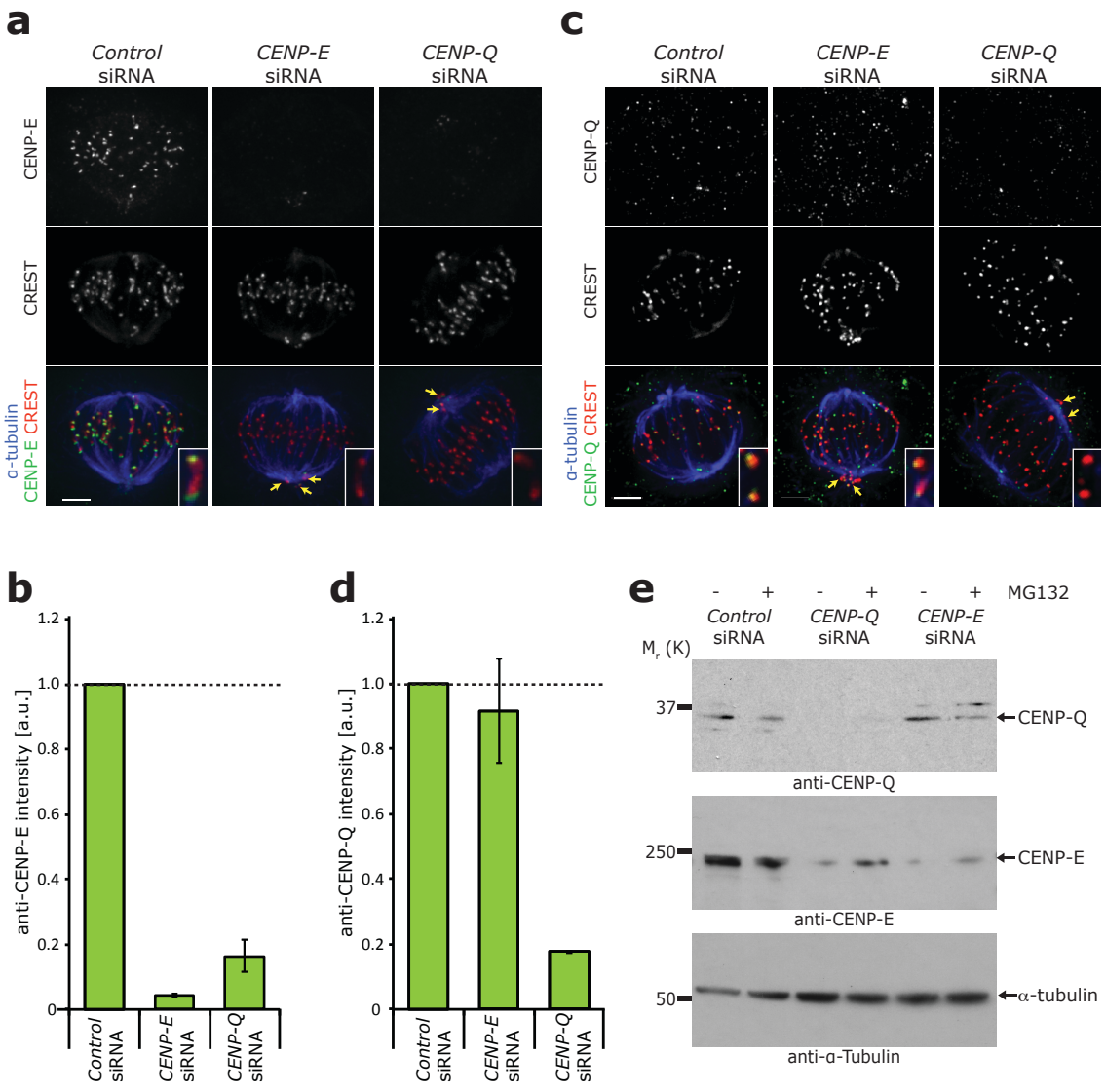

Figure 3.9 CENP-E loading is dependant upon CENP-Q **(a-d)** Immunofluorescence images (z-projection of 10 focal planes at 0.2 µm spacing) of cells are treated with *Control*, *CENP-E* or *CENP-Q* siRNAs and stained with CENP-E (a; green) or CENP-Q (c; green) and CREST (red), α-tubulin (blue) antibodies. Yellow arrows point to unaligned kinetochores. Scale bar = 3µm. Quantification of CENP-E (b) and CENP-Q (d) levels in cells treated with *Control*, *CENP-E* or *CENP-Q* siRNA. n≥150 kinetochores per condition from 3 independent experiments. Dashed line indicates CENP-E or CENP-Q levels in *Control* siRNA cells. Error bar = SD. **(e)** Immunofluorescence of liquid nitrogen extracted HeLa cell lysates, from cells transfected with control, CENP-Q or CENP-E siRNA for 48 h followed by treatment with MG132 or DMSO control for 90 mins. The blot was probed with antibodies against CENP-Q (top panel), CENP-E (middle panel) and α-tubulin (bottom panel).

treated with MG132 for 90 min to prevent mitotic progression and fixed. These cells were stained with anti-CENP-E and anti-CENP-A antibodies and imaged (Figure 3.10a). We first confirmed that the siRNA rescue had restored chromosome alignment (as described above), the kinetochore bound CENP-E levels were measured relative to CENP-A. The CENP-E levels were very similar in *control* siRNA treated cells transfected with the eGFP control plasmid or the siRNA protected CENP-Q-eGFP plasmid (Figure 3.10a,b). *CENP-Q* siRNA treated cells transfected with the control plasmid had very little CENP-E bound at kinetochores (~9 % of *control* siRNA cells transfected with control vector; Figure 3.10a,b). In contrast, cells treated with *CENP-Q* siRNA which had been transfected with the CENP-Q-eGFP siRNA protected construct had over 6 times the level of CENP-E at kinetochores (~62 % of control siRNA + eGFP; Figure 3.10a,b). This assay confirms that CENP-E is specifically dependent upon the presence of CENP-Q for kinetochore loading.

3.9 CENP-E loading may require modulation of microtubule dynamics by CENP-Q

It has been previously shown that CENP-E is enriched on kinetochores from which all microtubules have been removed by nocodazole treatment, and on unattached kinetochores in prometaphase (Hoffman et al., 2001). Given that we had established that CENP-E loading is normally dependent upon the presence of CENP-Q we were curious whether the enrichment of CENP-E on unattached kinetochores would also prove to be CENP-Q dependent. To investigate we treated control and CENP-Q depleted cells with 1 μg ml^{-1} nocodazole overnight to remove microtubules and then fixed these cells, labelling with anti-tubulin antibodies (to confirm microtubules were completely removed), anti-CENP-E antibodies to detect levels of the kinesin and anti-CENP-A as a kinetochore reference (Figure 3.11a). In our control cells we saw similar increases in CENP-E levels to those reported by Hoffman and colleagues in both prometaphase and nocodazole treated cells (Figure 3.11a,b, first and fourth columns of panel a, quantified in b). Surprisingly, we found that treatment of CENP-Q depleted cells with nocodazole allowed CENP-E to bind kinetochores (Figure 3.11a fifth column, quantification in 3.11b). Although the level of CENP-E in CENP-Q

Figure 3.10

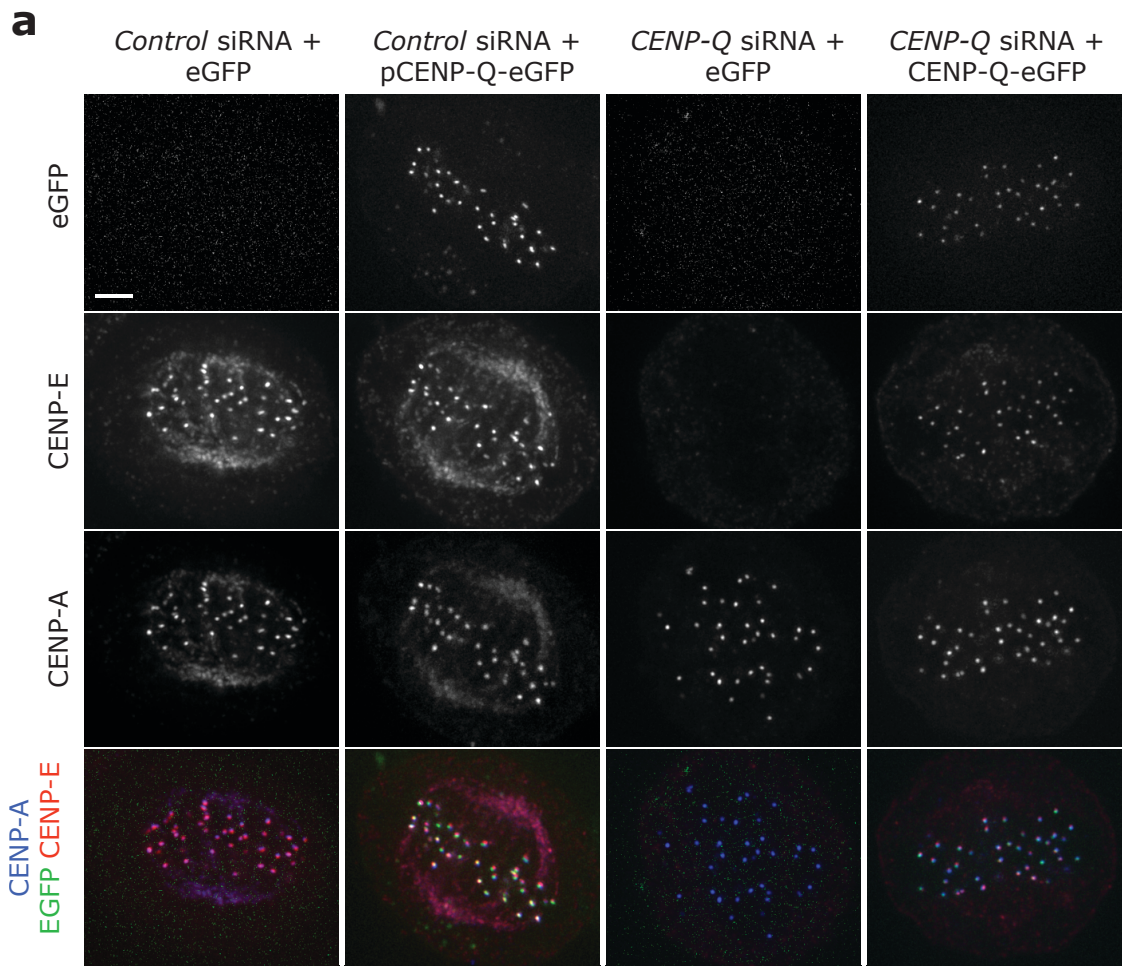

Figure 3.10 CENP-Q siRNA rescue of CENP-E **(a)** Immunofluorescence microscopy images (*z*-projections, 10 focal planes at 0.2 µm spacing) of *CENP-Q* siRNA rescue experiment in HeLa E1 cells. Cells were treated with *CENP-Q* siRNA or *Control* siRNA for 12 h and then transfected with an siRNA resistant CENP-Q-eGFP or eGFP expression plasmid for a further 48 h. To reduce the effect of mitotic stage on alignment, cells were arrested in metaphase with MG132 at a 1 µM final concentration for 90 min followed by fixation. Cell were stained with 4,6-diamidino-2-phenylindole (DAPI; DNA, blue) and probed with antibodies against CENP-A to mark kinetochores (blue) and CENP-E (red). Scale bar = 3µm.**(b)** Quantification of CENP-E levels on kinetochores in a *CENP-Q* siRNA rescue experiment. Cells were treated with *CENP-Q* siRNA or *Control* siRNA for 12 h and then transfected with an siRNA-resistant CENP-Q-eGFP or a control eGFP expression plasmid for a further 48 h. Cells were treated with 1 µM MG132 for 90 min before fixation and staining with DAPI (blue), anti-CENP-A and anti-CENP-E antibodies. Dashed line indicates CENP-Q levels in *Control* siRNA treated cells. Error bar = SD.

Figure 3.11

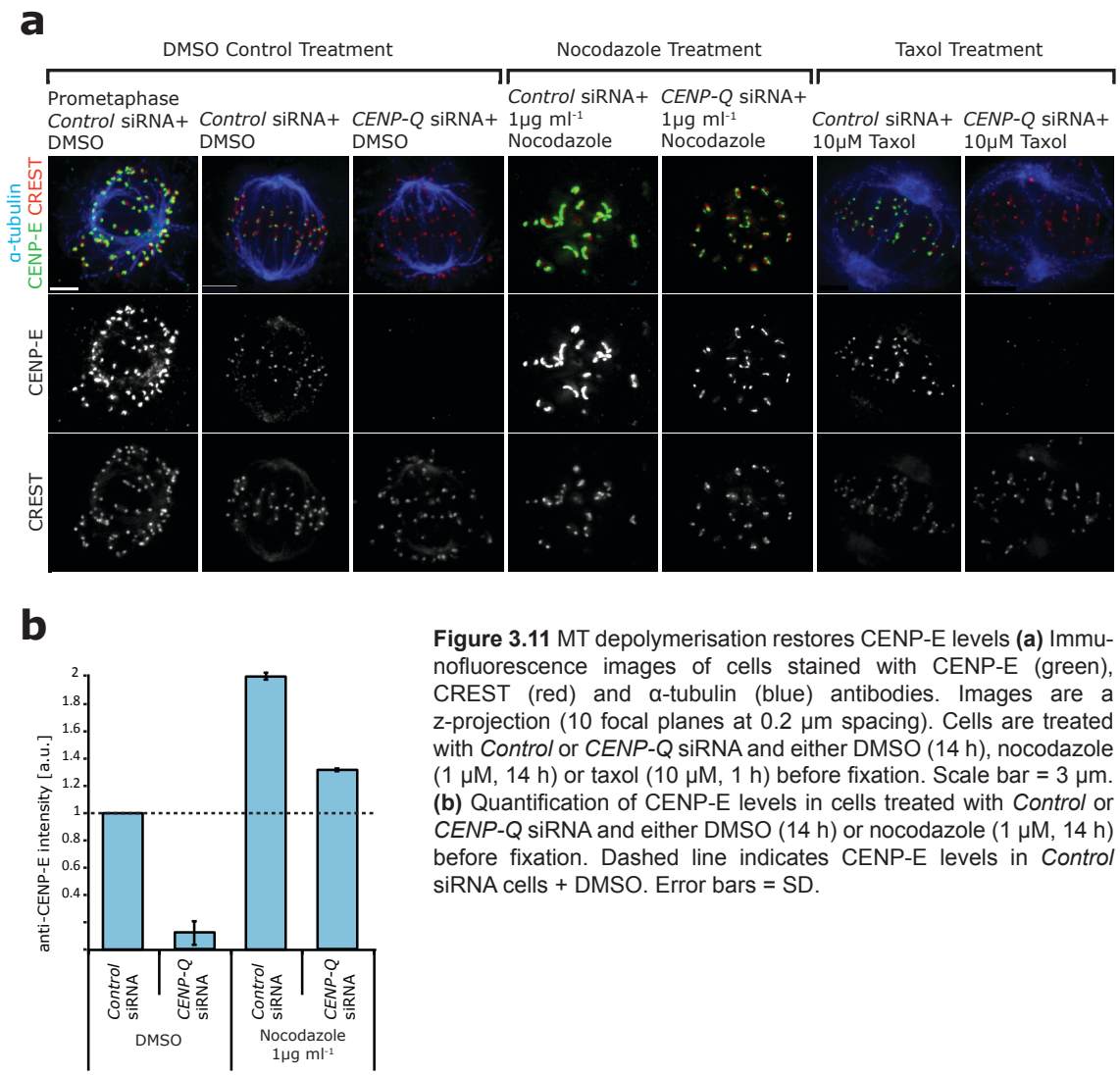

Figure 3.11 MT depolymerisation restores CENP-E levels **(a)** Immunofluorescence images of cells stained with CENP-E (green), CREST (red) and α-tubulin (blue) antibodies. Images are a z-projection (10 focal planes at 0.2 µm spacing). Cells are treated with *Control* or *CENP-Q* siRNA and either DMSO (14 h), nocodazole (1 µM, 14 h) or taxol (10 µM, 1 h) before fixation. Scale bar = 3 µm. **(b)** Quantification of CENP-E levels in cells treated with *Control* or *CENP-Q* siRNA and either DMSO (14 h) or nocodazole (1 µM, 14 h) before fixation. Dashed line indicates CENP-E levels in *Control* siRNA cells + DMSO. Error bars = SD.

depleted cells treated with nocodazole exceeded those in control-depleted cells treated with DMSO, the level of CENP-E at kinetochores did not recover to the level measured in control-depleted cells treated with nocodazole (Figure 3.11b). Thus, CENP-E can bind kinetochores in the absence of CENP-Q, but not to the same extent. In contrast, treatment of CENP-Q depleted cells with 10 μM taxol, which stabilises microtubules, did not rescue CENP-E kinetochore loading (Figure 3.11a, b). We also found that none of these treatments affected the levels of kinetochore bound CENP-Q in control cells and we were unable to restore CENP-Q levels in cells treated with *CENP-Q* siRNA (Figure 3.12a). These data suggest that CENP-Q is required to load CENP-E to kinetochores but that this may be dependant on the status of K-MT as disrupting microtubules with nocodazole allows rebinding of the protein. This finding is in agreement with previous work from our laboratory that has shown CENP-Q depletion slows K-MTs plus-end turnover (Samora C.P., PhD Thesis, 2012). Indeed, *in vitro* TIRF assays demonstrate that although CENP-Q is able to increase the frequency of microtubule catastrophe and rescue events, the speed of these growth and catastrophe events are reduced (Samora C.P., PhD Thesis, 2012). Therefore, one possible explanation for the reduction in CENP-E loading following CENP-Q depletion is that the resulting K-MT state no longer allows CENP-E binding.

In support of this idea, depletion of the CCAN protein CENP-H has previously been shown to have no effect on CENP-E kinetochore binding (Amaro et al., 2010), despite delocalising the CENP-O,-P,-Q,-U sub-complex (Okada et al., 2006). This was surprising, given our earlier observation that CENP-E kinetochore loading is dependent on CENP-Q, which would lead to the expectation that CENP-H depletion would also prevent CENP-E kinetochore loading. However, depletion of CENP-H has the opposite effect on kinetochore microtubule dynamics to CENP-Q depletion, increasing K-MT plus-end turnover (Amaro et al., 2010). We therefore predicted that cells treated a double siRNA against both CENP-Q and CENP-H would still load CENP-E, as the CENP-H phenotype should dominate. We tested this hypothesis by treating cells with siRNA against CENP-Q and a double siRNA treatment against CENP-Q and CENP-H. We then conducted immunofluorescence

Figure 3.12

a

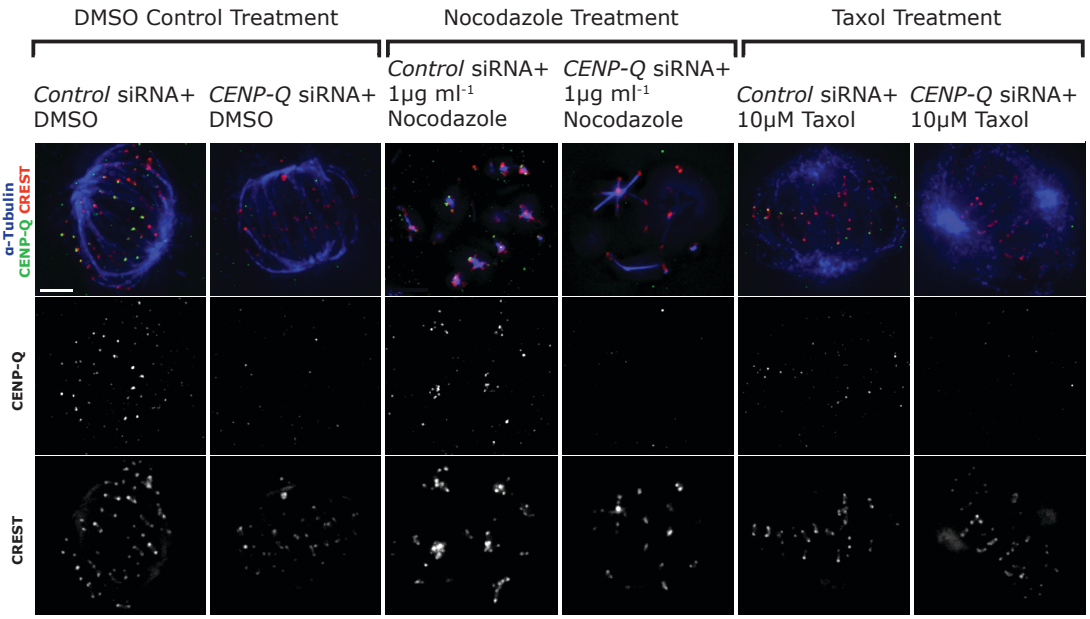

Figure 3.12 CENP-Q levels are not affected by MT depolymerisation **(a)** Immunofluorescence images of cells stained with CENP-Q (green), CREST (red) and α-tubulin (blue) antibodies. Images are a z-projection (10 focal planes at 0.2 µm spacing). Cells are treated with *Control* or *CENP-Q* siRNA and either DMSO (14 h), nocodazole (1 µM, 14 h) or taxol (10 µM, 1 h) before fixation. Scale bar = 3 µm.

staining of CENP-E and found levels of CENP-E were increased in CENP-Q and CENP-H double depleted cells compared to CENP-Q only depleted cells (Figure 3.13). This double depletion also reduced the polar chromosome phenotype normally associated with CENP-Q depletion. As a whole this indicates that although CENP-E loading is dependent upon CENP-Q, the dependency is almost certainly not due to a physical interaction. It is likely that the dependency results from modulation of K-fibre dynamics by CENP-Q, with rescue of CENP-E loading and chromosome alignment by CENP-H depletion supporting this idea.

Previous work has also shown that CENP-E is dependent upon Kif18a for kinetochore loading, possibly due to a direct or indirect physical interaction between Kif18a and CENP-E (Huang et al., 2009). To confirm this report and as a further control for our CENP-E kinetochore loading experiments, we proceeded to assay the effect of Kif18a depletion on levels of kinetochore bound CENP-E. In line with these previous findings immunofluorescence showed that siRNA mediated depletion of Kif18a greatly reduced the levels of kinetochore bound CENP-E (Figure 3.13a),

3.10 Fates of unaligned kinetochore pairs in CENP-Q and CENP-E depleted cells

Our characterisation of the CENP-Q/CENP-E loading dependency raised a key question; was the polar chromosome phenotype in CENP-Q depleted cells simply reflective of the unbinding of CENP-E from kinetochores? To ascertain whether this was the case we wanted to determine if the unaligned kinetochores in CENP-Q and CENP-E depleted cells behaved differently. We also wanted to determine if there was a difference between the behaviours of unaligned chromosomes with the same attachment status in the two depletions. To answer this question we first had to develop a system for denoting whether kinetochore pairs were biorientated or non-biorientated. To observe the behaviour of unaligned kinetochores we screened unperturbed HeLa K cells stably expressing eGFP-CENP-A (kinetochore marker) and eGFP-Centrin1 (spindle pole marker). Multiple examples of unaligned and polar kinetochores could be found in these cells, suggesting

Figure 3.13

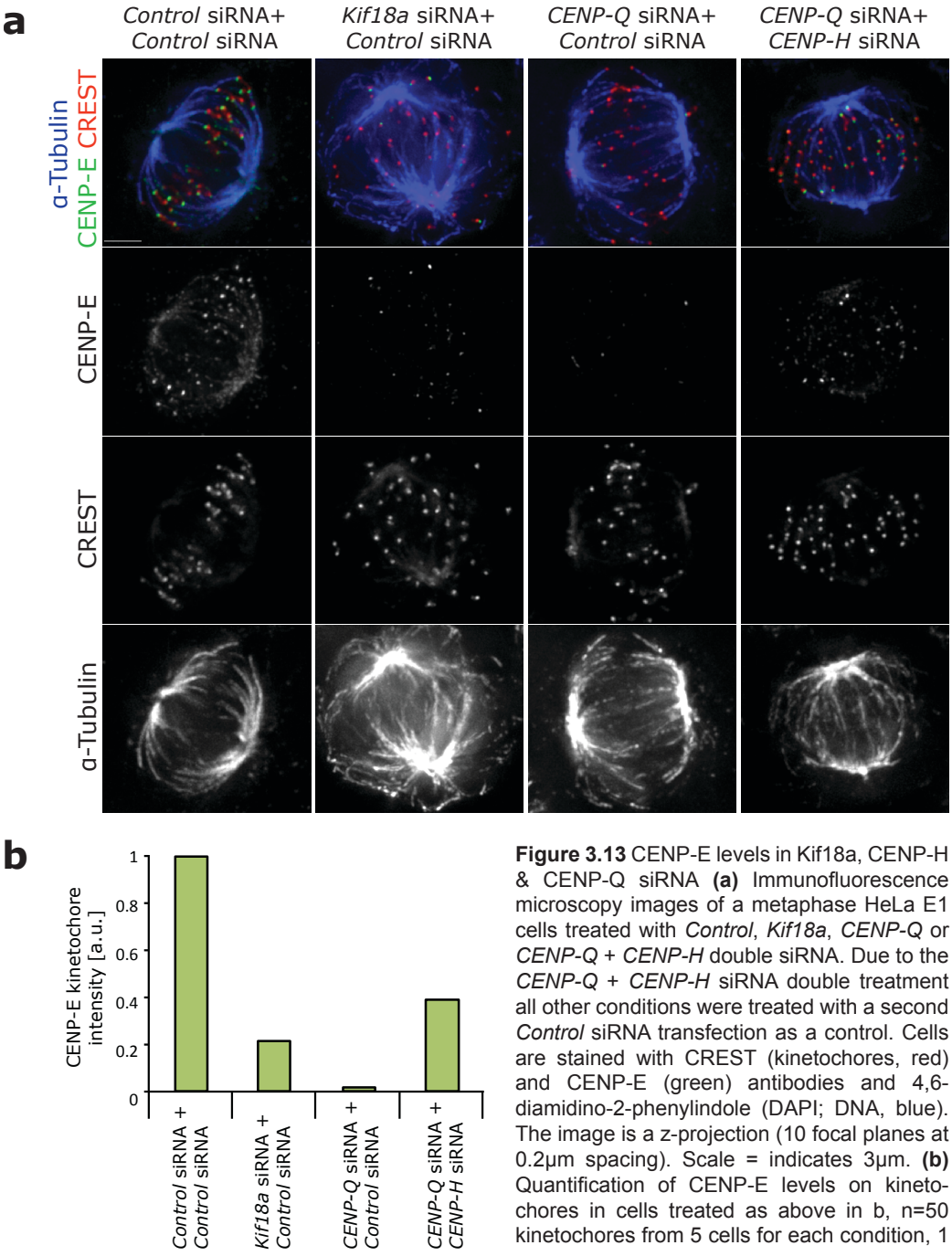

Figure 3.13 CENP-E levels in Kif18a, CENP-H & CENP-Q siRNA **(a)** Immunofluorescence microscopy images of a metaphase HeLa E1 cells treated with *Control*, *Kif18a*, *CENP-Q* or *CENP-Q* + *CENP-H* double siRNA. Due to the *CENP-Q* + *CENP-H* siRNA double treatment all other conditions were treated with a second *Control* siRNA transfection as a control. Cells are stained with CREST (kinetochores, red) and CENP-E (green) antibodies and 4,6-diamidino-2-phenylindole (DAPI; DNA, blue). The image is a z-projection (10 focal planes at 0.2µm spacing). Scale = indicates 3µm. **(b)** Quantification of CENP-E levels on kinetochores in cells treated as above in b, n=50 kinetochores from 5 cells for each condition, 1

that errant chromosomes may be a relatively common feature of prometaphase (Figure 3.14a,b,c). We next followed the fate of the unaligned kinetochores by imaging these cells every 7.5 sec for 10 min. We could observe sister pairs that were non-biorientated, because they were positioned behind the spindle pole where biorientation is geometrically impossible (Figure 3.14a). Sister pairs between the pole and plate, in which the sister-sister axis was at ~90º to the pole-pole axis, were also scored as non-biorientated (Figure 3.14b, first panel, red and yellow lines respectively). Biorientation would be highly unlikely with this geometry because kinetochores could not make end-on attachments with microtubules coming from opposite spindle pole. Sister pairs between pole and plate, in which the sister-sister axis was ≤ 45º from the pole-pole axis, were scored as orientated (Figure 3.14b, second panel, red and yellow lines respectively). These sister kinetochore pairs were scored as orientated because we cannot discriminate between biorientated kinetochore pairs and non-biorientated kinetochore pairs which are aligned with the spindle axis. Therefore in addition to biorientated kinetochores, this orientated state likely also contains sister pairs in which one sister is mono-orientated and the second laterally attached (see Kapoor et al., 2006; and schematic in Figure 3.15a chromosome 5).

During our 10 min movies we observed orientated kinetochore pairs move to the metaphase plate, presumably by depolymerisation-coupled end-on pulling or lateral sliding. Non-biorientated sister pairs could also be observed moving towards the metaphase plate, by lateral sliding (Figure 3.14c). Non-biorientated sisters could also move to orientate themselves with the spindle so that the sister-sister axis was in-line with the path of the K-fibre. This change could reflect either biorientation, or the lateral attachment of monoorientated kinetochores as previously described (Kapoor et al., 2006; Skibbens et al., 1993). This class of kinetochore sister-pairs thus congresses to the metaphase plate by either lateral sliding or end-on pulling (Figure 3.14c).

We next tracked the fates of uncongressed kinetochore pairs in CENP-Q and CENP-E depleted cells. Our earlier experiments suggested that imaging for 5 min would be sufficient to observe congression events, and we imaged cells for 5 min every 7.5 sec. Using the criteria developed

Figure 3.14

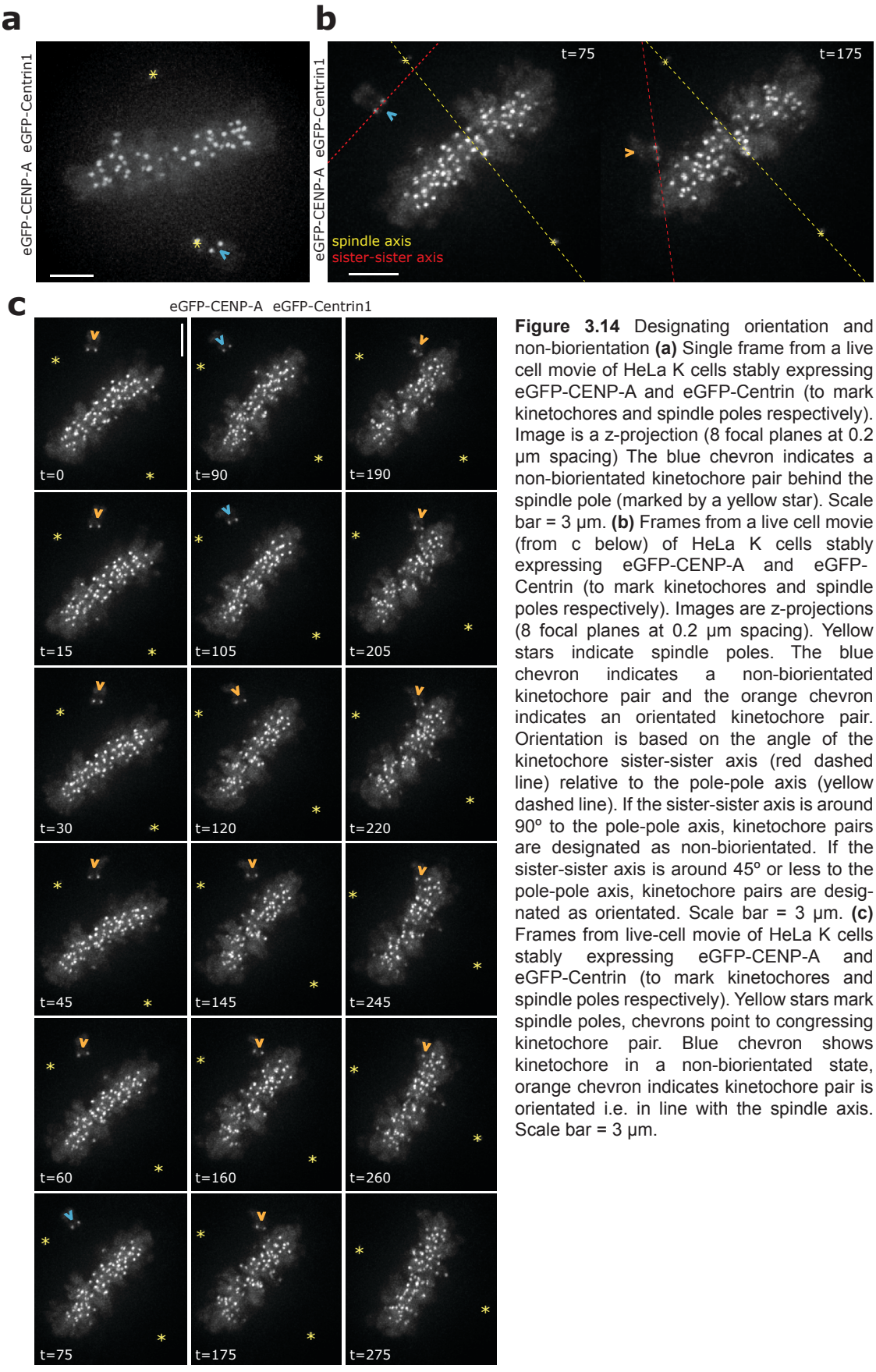

Figure 3.14 Designating orientation and non-biorientation **(a)** Single frame from a live cell movie of HeLa K cells stably expressing eGFP-CENP-A and eGFP-Centrin (to mark kinetochores and spindle poles respectively). Image is a z-projection (8 focal planes at 0.2 µm spacing) The blue chevron indicates a non-biorientated kinetochore pair behind the spindle pole (marked by a yellow star). Scale bar = 3 µm. **(b)** Frames from a live cell movie (from c below) of HeLa K cells stably expressing eGFP-CENP-A and eGFP-Centrin (to mark kinetochores and spindle poles respectively). Images are z-projections (8 focal planes at 0.2 µm spacing). Yellow stars indicate spindle poles. The blue chevron indicates a non-biorientated kinetochore pair and the orange chevron indicates an orientated kinetochore pair. Orientation is based on the angle of the kinetochore sister-sister axis (red dashed line) relative to the pole-pole axis (yellow dashed line). If the sister-sister axis is around 90° to the pole-pole axis, kinetochore pairs are designated as non-biorientated. If the sister-sister axis is around 45° or less to the pole-pole axis, kinetochore pairs are designated as orientated. Scale bar = 3 µm. **(c)** Frames from live-cell movie of HeLa K cells stably expressing eGFP-CENP-A and eGFP-Centrin (to mark kinetochores and spindle poles respectively). Yellow stars mark spindle poles, chevrons point to congressing kinetochore pair. Blue chevron shows kinetochore in a non-biorientated state, orange chevron indicates kinetochore pair is orientated i.e. in line with the spindle axis. Scale bar = 3 µm.

above we designated kinetochore pairs as non-biorientated or biorientated. The relative proportion of biorientated and non-biorientated uncongressed kinetochores was very similar in CENP-Q and CENP-E depleted cells, with ~80% occupying a non-biorientated state (Figure 3.15b). The fates of these non-biorientated unaligned kinetochore pairs were also very similar, with the majority in both cases (>90%) remaining stalled and unable to progress towards the spindle equator (Figure 3.15c, images in Figure 3.16). In CENP-Q depleted cells the orientated kinetochore pairs were also unable to congress and remained stalled (Figure 3.15d, images in Figure 3.16). However, in CENP-E depleted cells (where CENP-Q remains kinetochore-bound) 80% of orientated sister pairs were able to congress to the metaphase plate (Figure 3.15d, images in Figure 3.16). Because CENP-E is essential for lateral sliding these congression events are almost certainly due to biorientated kinetochores utilising depolymerisation-coupled pulling. In principle, this difference in the ability of biorientated kinetochores to congress could be due to a greater reduction of kinetochore bound CENP-E in *CENP-Q* siRNA treated cells compared to *CENP-E* siRNA treated cells. However, the levels of CENP-E protein bound at kinetochores are in fact significantly lower, being reduced by a further 15% following direct depletion of CENP-E with *CENP-E* siRNA compared to *CENP-Q* siRNA treatment (t-test p=0.0148; Figure 3.9b, d).

To confirm the result that biorientated kinetochores are able to congress in the absence of functional CENP-E we treated cells with the highly specific CENP-E inhibitor GSK923295 (Wood et al., 2010). GSK923295 is an allosteric inhibitor of CENP-E kinesin ATPase activity and is therefore able to inactivate CENP-E without the need to deplete the protein. This inhibition results from the binding of GSK923295 to the loop-5 domin of CENP-E, which inturn prevents CENP-E from releasing the inorganic phosphate generated by ATP hydrolysis. This causes CENP-E to become tightly bound to microtubules in a rigor state, no longer able to walk along the microtubule lattice (Wood et al., 2010). Previous studies have shown that 300 nM doses of GSK923295 added to cells in culture are effective at inhibiting CENP-E (Wood et al., 2010). We found that such doses gave similar results to siRNA mediated depletion of CENP-E, with almost 100% of non-biorientated kinetochores remaining stalled (Figure 3.15e) and over 50% of orientated kinetochores able to

Figure 3.15

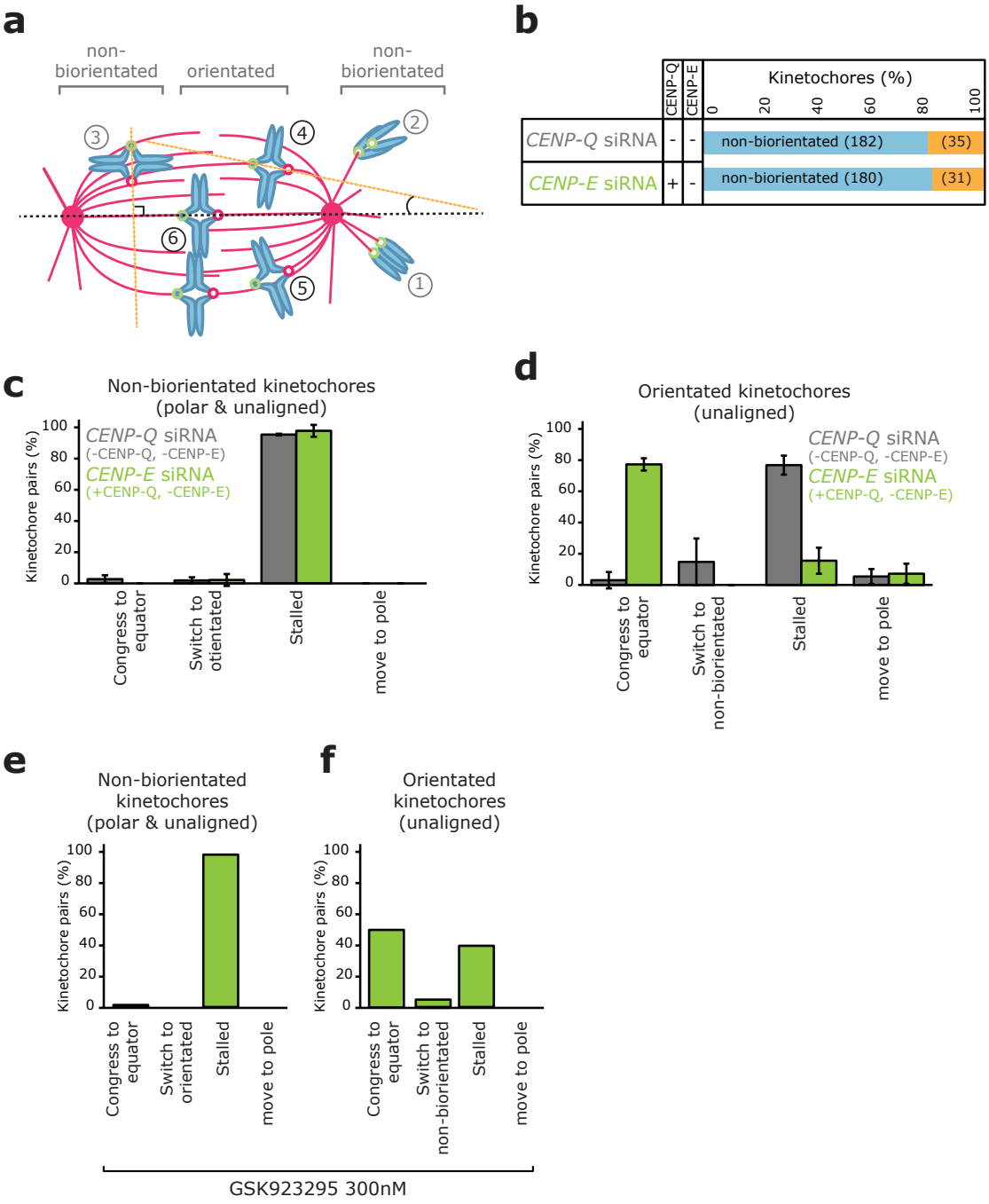

Figure 3.15 (a) Schematic representing the orientation of unaligned kinetochore pairs within the mitotic spindle. Black dotted line represents pole-to-pole axis, dotted orange lines represent sister-sister axis, the ~90° angle between the sister-sister axis and the spindle pole-to-pole axis (Chromosome 3) indicates non-biorientation. The reduced angle (≤45°) of chromosome 4 indicates biorientation. Chromosomes 1 and 2 are behind the pole and therefore non-biorientated. Chromosome 5 is mono-orientated by the pole proximal kinetochore and laterally attached to an adjacent k-fibre by the pole distal kinetochore. **(b)** Percentage of unaligned kinetochore pairs occupying an orientated or non-biorientated state in HeLa cells (stably expressing eGFP-CENP-A/eGFP-Centrin1) after treatment with *CENP-Q* or *CENP-E* siRNA. Numbers within the bars indicate number of kinetochore pairs, n≥3 independent experiments. **(c,d)** Fates of non-biorientated (c) or biorientated (d) kinetochore pairs in HeLa cells (stably expressing eGFP-CENP-A/eGFP-Centrin1) during a 5 min movies after treatment with CENP-Q or CENP-E siRNA. **(e,f)** Fates of non-biorientated (e) or biorientated (f) kinetochore pairs in HeLa cells (stably expressing eGFP-CENP-A/eGFP-Centrin1) during a 5 min movies after treatment with the CENP-E inhibitor GSK 923295 at 300 nM after 14 hours.

Figure 3.16

a

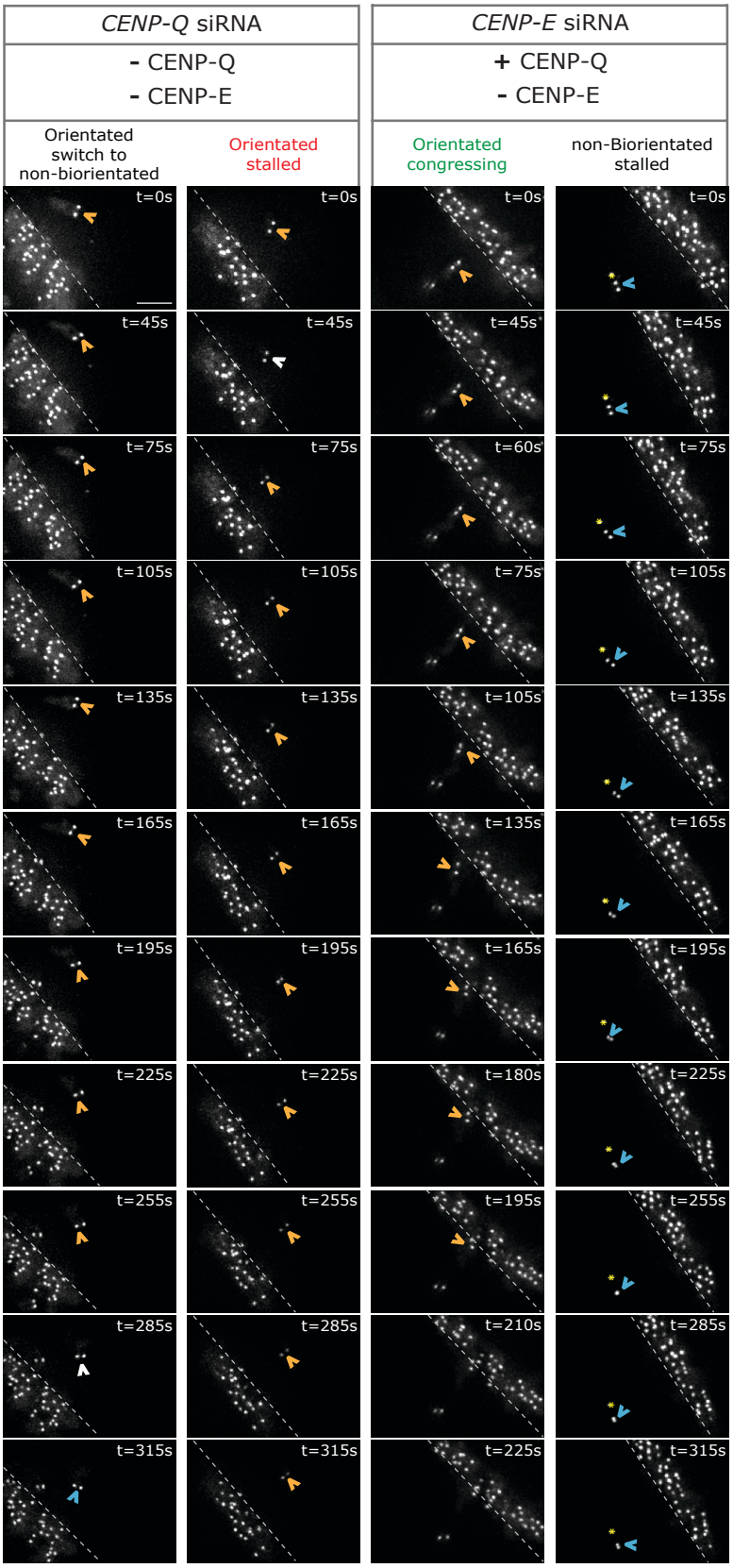

Figure 3.16 Example kinetochore fates in CENP-Q/E siRNA **(a)** Example frames from movies of kinetochore fates after treatment with CENP-Q or CENP-E siRNA. Orange chevrons indicate pairs that are orientated with the spindle axis, blue chevrons indicate pairs that are non-biorientated and white chevrons indicate where designation of state is unclear. Yellow stars indicate spindle pole when visible. First column shows an example of a biorientated kinetochore pair in a CENP-Q depleted cell, the pair does not congress, but switches to a non-biorientated state. Second column shows example of an orientated kinetochore pair that fails to congress in CENP-Q depleted cells. In contrast, third column shows an example of an orientated sister pair in CENP-E-depleted cells that are still able to congress to the metaphase plate. The forth column shows an aligned non-biorientated sister pair that cannot move to the metaphase plate in CENP-E-depleted cells. Scale bar = 3 μm, dashed grey line indicates metaphase plate boundary.

congress (Figure 3.15f). One prediction from these data is that CENP-E depleted cells should have a higher proportion of their uncongressed kinetochores trapped behind spindle poles, because many biorientated pairs are able to congress and therefore would form a smaller proportion of the uncongressed chromosome population. Indeed, 69.7% of uncongressed kinetochores reside behind the pole in CENP-E depleted cells, compared to 50.4% in CENP-Q depleted cells. These data suggest that a CENP-Q dependent (CENP-E independent) mechanism is required to move biorientated kinetochore pairs to metaphase plate by depolymerisation-coupled pulling.

3.11 CENP-Q and CENP-E generate counter-forces on polar chromosomes

Both CENP-Q and CENP-E function to align chromosomes that are unaligned but reside within the region between the spindle pole and equator. However, behind the spindle pole the geometry of microtubules is reversed, i.e. the plus-ends of astral microtubules are proximal to the cell cortex, in contrast to K-fibres that have plus-ends proximal to the metaphase plate. If CENP-Q directs depolymerisation-coupled pulling, it would move chromosomes behind the pole towards the pole, while plus-end directed lateral sliding by CENP-E would move chromosomes anti-poleward. We would thus predict that depletion of each protein would alter the positions of the kinetochore population relative to the spindle pole. To test this hypothesis we treated cells with siRNA against CENP-Q and CENP-E. These cells were then fixed and stained with antibodies against alpha-tubulin to mark the spindle and CREST antisera to indicate the positions of kinetochore pairs as well as DAPI to stain chromatin. These cells were imaged and kinetochore pairs were scored as proximal to the pole if they were located on the central mass of microtubules surrounding the pole, or distal if they were clearly separated from the spindle and attached to astral-microtubules (see pink and blue circles in Figure 3.17a). In CENP-E depleted cells the vast majority of kinetochore pairs occupied a position proximal to the spindle pole, the same being true of kinetochores in cells treated with the CENP-E inhibitor GSK 923295 (Figure 3.17b). In contrast, kinetochore pairs in CENP-Q depleted cells were found in similar quantities proximal to and distal from the pole (Figure

3.17b). This suggested that in the absence of CENP-E, polar kinetochores could be brought proximal to the pole, however, presumably due to the loss of CENP-E lateral sliding these pairs could not then be transported to the metaphase plate. In CENP-Q depleted cells the greatly increased number of distal polar kinetochores attached to astral microtubules suggests that CENP-Q is required to bring distal kinetochore pairs towards the spindle pole, most probably by end-on pulling mechanisms. Double siRNA treatment against CENP-Q and CENP-E gave the same result as CENP-Q depletion, with both proximal and distal polar kinetochores present. This result is consistent with the finding that CENP-Q depletion removes both CENP-Q and CENP-E from kinetochores.

In order to gain a more quantitative read-out of kinetochore distance from the pole we developed a quantitative semi-automated assay, in which the Euclidian distance of every kinetochore was measured from the centre of a monopole in CENP-Q and CENP-E depleted cells. Monopolar spindles were used as the geometry of the monopole recreates the microtubule geometry behind the pole. The centre of the monopole also provides a single point of reference. To generate monopolar spindles, cells were treated with the Eg5 inhibitor monastrol to prevent centrosome separation in prophase (Mayer et al., 1999). These cells were fixed and stained with antibodies against CENP-A to mark kinetochores and gamma-tubulin to mark spindle poles as well as DAPI to mark DNA. After imaging we used a macro created in Volocity 3D (PerkinElmer) to automatically measure the Euclidian distance of each kinetochore to the monopole centre (Figure 3.17c). The cumulative frequency plots of kinetochore-to-pole distances were calculated for each experiment. The averages are shown in Figure 3.17d, e. These plots show that depletion of CENP-E resulted in kinetochores being closer to the monopole compared to control cells (Figure 3.17d). We confirmed this result by treating cells for 14 hrs with 300nM GSK925293, which inhibits CENP-E motor activity by allosteric inhibition of ADP release, causing the kinesin to adopt a rigor bound state (Figure 3.17d). Conversely, kinetochores in CENP-Q depleted cells (which also lack the anti-poleward CENP-E force) occupied a similar mean distance from the monopole to kinetochores in control-depleted cells, albeit with a much narrower standard deviation (Figure 3.17e). This suggested that

Figure 3.17

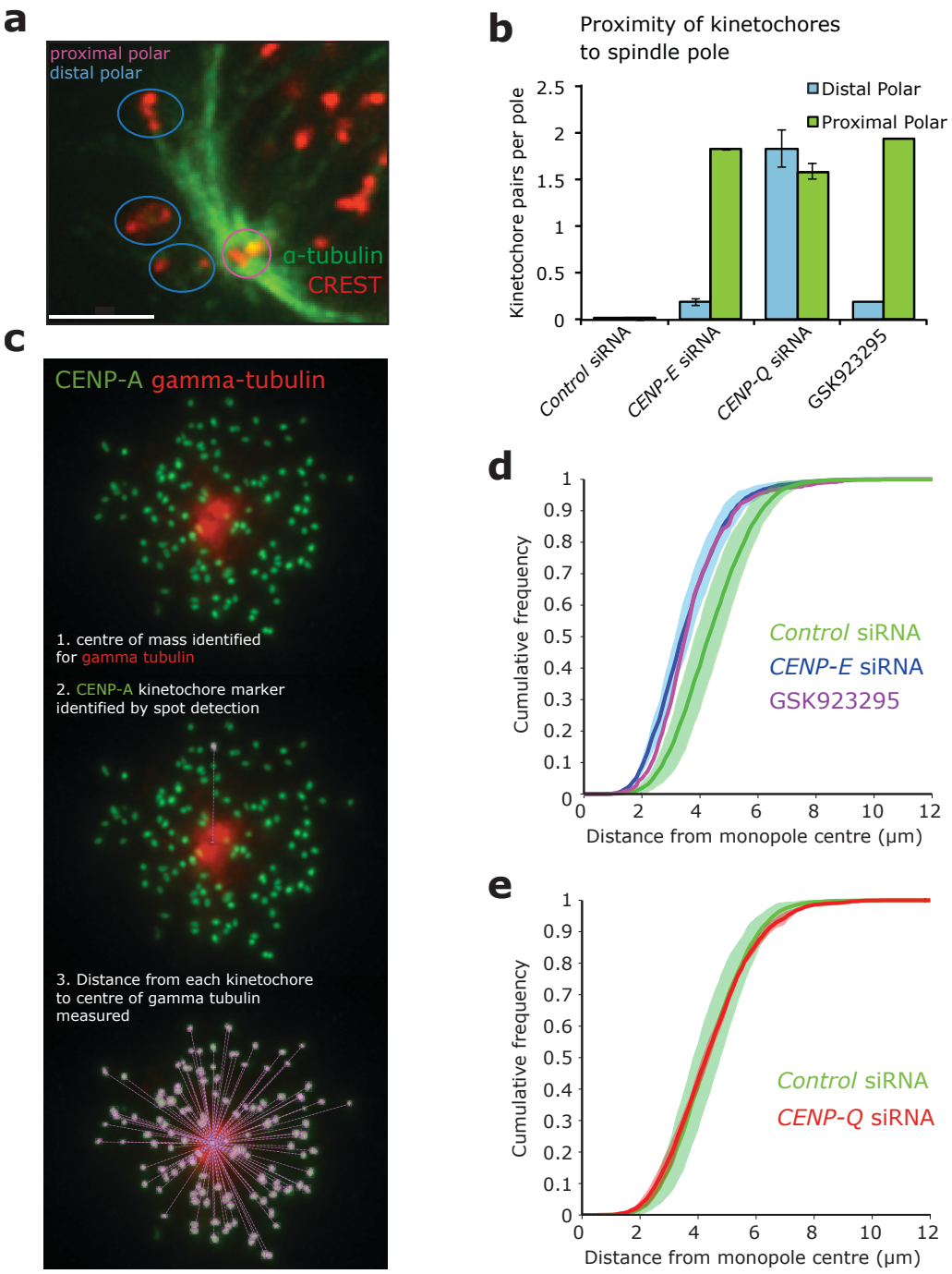

Figure 3.17 Kinetochore positions in CENP-Q/E siRNA **(a)** Immunofluorescence z-projection (10 focal planes at 0.2 μm spacing) of the spindle pole region of a cell stained with CREST (red) and α-tubulin (green) antibodies showing proximal (Blue) and distal (pink) kinetochore pairs. Scale bar = 3μm. **(b)** Quantification of proximal and distal kinetochore pairs per spindle pole. Error bars indicate standard deviation. n= ≥30 cells from at least three independent experiments. n=8 cells from one experiment in GSK923295 treatment and n=19 cells from one experiment in *CENP-Q/CENP-E* double siRNA experiment. **(c)** Image of a cell stained with CENP-A (green) and Y-tubulin (red) antibodies following treatment with control, *CENP-Q* or *CENP-E* siRNA followed by 90 min treatment with 1 μM monastrol to induce monopolarity. Lower panels outline the automated process of pole identification and kinetochore identification followed by distance measurement from each kinetochore to the pole. **(d)** Cumulative distribution of kinetochore distances from the monopole center in cells treated with Control siRNA (red lines, n=5 experiments with ≥ 8 cells), *CENP-E* siRNA (red lines, n=4 experiments with ≥ 8 cells) and GSK923295 (purple line, n=1 experiment with 10 cells). Shaded areas represent standard deviation. **(e)** Cumulative distribution of kinetochore distances from the monopole center in cells treated with Control siRNA (green lines, n=5 experiments with ≥ 8 cells) and *CENP-Q* siRNA (red lines, n=3 experiments with ≥ 8 cells). Shaded areas represent standard deviation.

after treatment with *CENP-Q* siRNA the absence of CENP-Q and CENP-E resulted in a net balance of forces acting on the population of kinetochores. The removal of both CENP-Q dependent depolymerisation coupled pulling and CENP-E dependent plus end motor activity resulting in an average distance from the monopole simerlar to that seen in control cells. Taken together, these data suggest that that CENP-E slides kinetochores towards microtubule plus-ends regardless of microtubule geometry. Our data also suggests that CENP-Q dependent mechanisms drive depolymerisation-coupled pulling that moves chromosomes towards or away from the pole depending on the microtubule geometry. In both cases CENP-Q acts to move chromosomes closer to the metaphase plate and thus facilitates chromosome congression.

3.12 Conclusion

Based on the results in this chapter we see that CENP-Q is essential to chromosome congression. CENP-Q is also essential for the loading of CENP-E, a dependency that most likely derives from the effects that kinetochore bound CENP-Q has on K-MT dynamics. The defects observed in chromosome congression after depletion of CENP-Q are a composite, resulting from the loss of CENP-Q and CENP-E from kinetochores. However, we find that although both proteins are important for chromosome congression they each have distinct roles in the process. Perhaps most importantly we find that CENP-Q is required for depolymerisation-coupled pulling of biorientated kinetochore pairs whilst CENP-E is dispensable for this process, although essential for lateral sliding. We also find that the two proteins have distinct effects on chromosomes around spindle poles, with CENP-E being essential for transport away from the pole and CENP-Q being required for transport towards the spindle pole, most likely by depolymerisation-coupled pulling. Both activities are likely to be important for the rescue of chromosomes that become trapped around the spindle pole.

CHAPTER 4: Control of Metaphase Kinetochore Dynamics by CENP-Q and CENP-E Dependent Mechanisms

4.1 Introduction

For several decades it has been known that, following chromosome congression, sister kinetochores oscillate at the spindle equator for several minutes prior to anaphase. This is the metaphase stage of mitosis (Skibbens, 1993; Hughes & Swann, 1949). In human cells, chromosomes oscillate for ~15 min prior to anaphase with an oscillatory half period of ~35 sec and a full period of ~70 sec (Jaqaman et al., 2010). It is believed that these oscillations arise predominantly as a result of K-MTs switching between growth and shrinkage and are required to maintain chromosomes at the metaphase plate (Skibbens et al., 1993). However, other factors such as plus-end directed chromokinesins present on chromosome arms, which interact with spindle microtubules, also have a role in the generation of oscillations (Levesque & Compton, 2001). Furthermore, experiments using drug treatments, single miniature chromosomes and laser ablation have shown that the kinetochore is the main factor powering alignment to the metaphase plate and kinetochore/chromosome oscillations (Khodjakov et al., 1997; Skibbens et al., 1995; Wise & Brinkley, 1997; Khodjakov & Rieder, 1996).

As cells approach anaphase, the amplitude of these oscillations decreases, as does the plus-end turnover of K-MT, providing further evidence that the two are linked. Indeed, “freezing” microtubule dynamics in established mitotic spindles by addition of the microtubule stabilising agent taxol has previously been shown to abolish these oscillations (Jaqaman et al., 2010). Work in our laboratory has closely examined these oscillations using high spatial and temporal resolution kinetochore

imaging coupled with bespoke analysis software. By calculating the autocorrelation over the time-series of displacements kinetochores make through the plane of the metaphase plate, it was shown that the half-period of oscillations in human cells during metaphase was ~35 sec (Jaqaman et al., 2010; see also Figure 4.1). Using this approach it was found that proteins which modulate K-MT dynamics influence these oscillations, a key example being depletion of the plus-end directed motor and depolymerase Kif18a, which results in an increase in the speed of sister kinetochore centre position during oscillatory movements (Jaqaman et al., 2010), as also observed by Stumpff and colleagues (Stumpff et al., 2008). Additionally the Jaqaman study found that depletion of the non-motile depolymerase MCAK reduced the speed of sister kinetochore centre position movements during oscillation at the metaphase plate, an effect also seen by Wordeman and colleagues (Wordeman et al., 2007). Auto-correlation analysis reveals that depletion of either MCAK or Kif18a increases the size of the first negative lobe of the autocorrelation and resulted in a small shift in sister kinetochore-breathing autocorrelation, suggesting that both depletions have an effect on kinetochore oscillations, albeit a modest one (Jaqaman et al., 2010).

Previous work has shown that CCAN is a major regulator of K-MT dynamics and kinetochore oscillations. For example, depletion of the CENP-H CCAN subunit results in rapid plus-end turn-over of K-MTs and a complete loss of kinetochore oscillations (Amaro et al., 2010); a similar effect can be observed in cells depleted of the CENP-L protein (Mchedlishvili et al., 2012). Depletion of the CENP-H subunit unbinds a number of other CCAN proteins including the CENP-O/P/Q/U sub-complex. These results are consistent with our findings in chapter 3, where we show that CENP-Q has a key role in end-on pulling of unaligned biorientated kinetochore pairs. However, we do not yet know whether depletion of CENP-Q alone is sufficient to abolish these oscillations. Given that previous studies have shown that CENP-Q is able to directly bind to microtubules *in vitro* (Amaro et al., 2010), and modulate MT dynamics *in vitro* and *in vivo* (Samora C.P., PhD thesis, 2012), we hypothesised that the protein would be likely to play a key role in K-MT dependent aligned kinetochore dynamics.

Figure 4.1

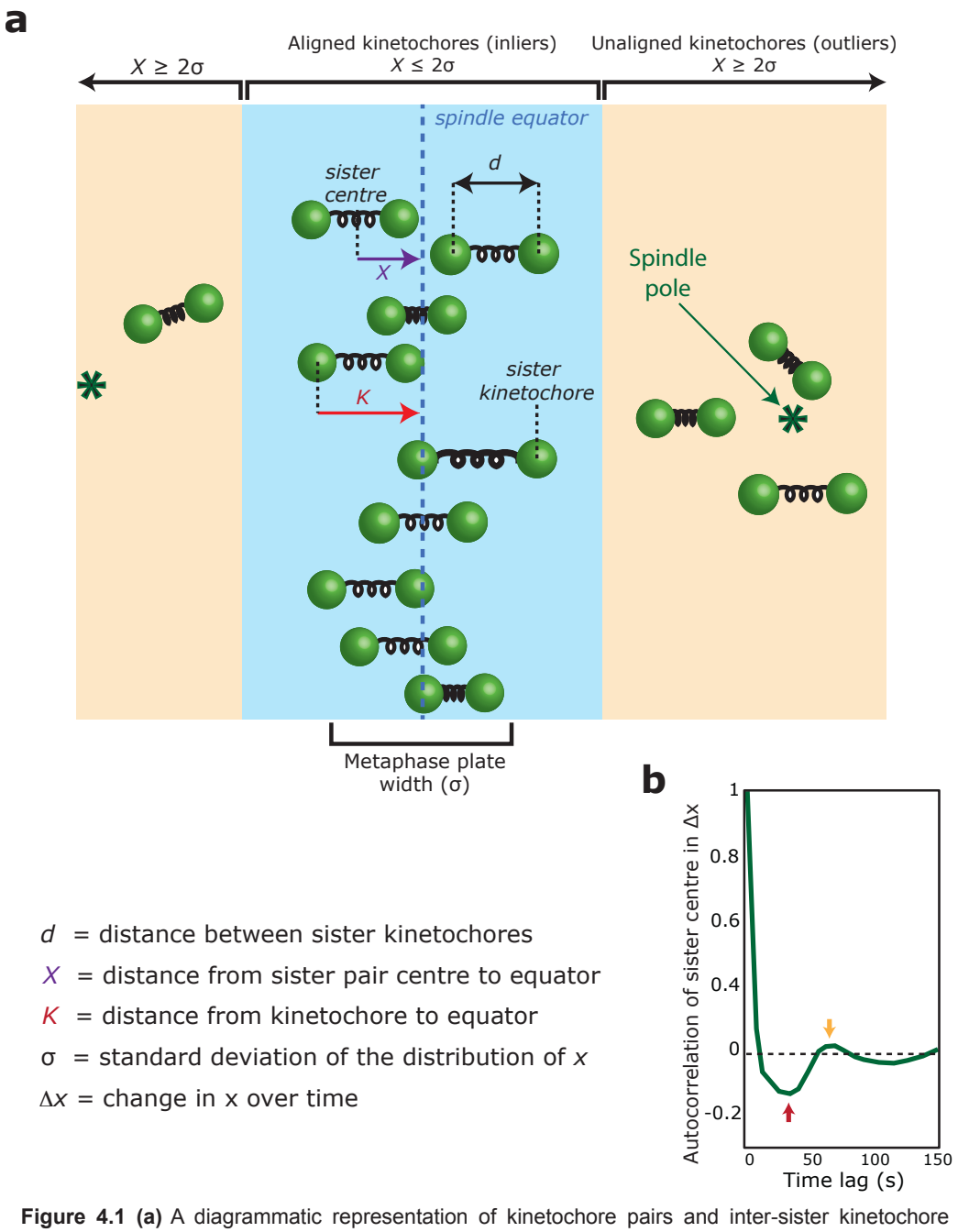

d = distance between sister kinetochores

X = distance from sister pair centre to equator

K = distance from kinetochore to equator

σ = standard deviation of the distribution of x

Δx = change in x over time

Figure 4.1 (a) A diagrammatic representation of kinetochore pairs and inter-sister kinetochore linkage (green spheres and black springs respectively) in our kinetochore tracking assay (based on Jaqaman et al., 2010). Kinetochores are detected and tracked over time using maximum intensity 3D spot tracking to detect the eGFP-CENP-A signal. Kinetochores are tracked for 5 mins every 7.5 seconds (30 x 0.5 μm z-planes). The metaphase plate is defined by fitting a plane through the the distribution of kinetochores, with the minimum distance from the maximum possible number of kinetochores (blue dotted line). Pairing of sister kinetochores (green spheres) is based on proximity and coupled motion. Multiple tracking parameters are then automatically calculated, those of relavence in this thesis are labeled and described below. The metaphase plate width is determined as the standard deviation (σ) of the distribution of X. Any kinetochore pairs with X position > 2σ are considered outliers (unaligned). Definition of tracking parameters as labeled above. **(b)** Schematic of the autocorrelation of change in sister centre position (ΔX) over time. Applying the autocorrelation function reveals the underlying periodicity and memory in change of X over time by comparing the change in position at each time point to previous time points. In unperturbed cells the underlying quasi-periodic motion of X manifests as a negative lobe at ~35 seconds (red arrow head) and a positive lobe at ~70 seconds (orange arrow head), representing the half and full period of sister-centre position (X) oscillations respectively.

In chapter 3, I reported that CENP-Q plays a key role in the recruitment of the CENP-E protein to kinetochores. However, it seemed unlikely that the loss of CENP-E would affect aligned kinetochore dynamics as previous work from our lab has demonstrated that depletion of CENP-E did not affect metaphase oscillations, although it did result in a number of chromosomes becoming trapped around the spindle poles (Jaqaman et al., 2010). This is consistent with the finding in chapter 3 that CENP-E is dispensable for end-on pulling mediated alignment of biorientated kinetochores to the metaphase plate. In contrast, recent work has shown that inhibition of CENP-E with the small molecule inhibitor GSK923295 results in a sub-population of aligned kinetochores "falling off" the metaphase plate (Gudimchuk et al., 2013). This led the authors to suggest that CENP-E might have a role in the maintenance of metaphase kinetochore alignment. However, we did not observe this phenotype in our earlier CENP-E depletion experiments (>25 movies observed each at 5 min duration), nor was such a phenotype described in the Jaqaman study (Jaqaman et al., 2010). The Gudimchuk study also showed that CENP-E was able to track depolymerising microtubules *in vitro* and that inhibition of CENP-E *in vivo* prevented kinetochores from tracking microtubules depolymerised by nocodazole treatment (Gudimchuk et al., 2013).

The results of the Gudimchuk study would suggest that CENP-E might play a role in maintenance of kinetochore alignment at the cellular equator and in end-on pulling. However, it seems unlikely that CENP-E preforms a role in the maintainiance of stable end-on attachemnts as the majority of chromosomes align normally to the mentaphase plate where they remain in both CENP-E depleted and inhibited cells (Jaqaman et al., 2010; Gudimchuk et al., 2013; this study Chapter 3). Furthermore, the Jaqaman study also showed aligned kinetochores in CENP-E depleted cells exhibit a normal inter-sister distance, suggesting normal tension across sister pairs, as would be exerted by stable K-MT attachments (Jaqaman et al., 2010). The most likely explanation is that differences between the Jaqaman and Gudimchuk studies could be a reflection of differences between siRNA mediated depletion of CENP-E (Jaqaman et al., 2010) and the CENP-E rigor state induced by addition of the GSK923295 CENP-E inhibitor (Gudimchuk et al., 2013). It is also possible that the chromosomes observed "falling off" the metaphase plate in the Gudimchuk study

could represent kinetochores that were yet to from stable end-on attachments. At the time of inhibitor addition these kinetochores may have still been laterally attached by CENP-E. In this chapter we set out to examine the role of CENP-Q and CENP-E in the maintenance of aligned kinetochore dynamics using a combination of siRNA mediated depletion and a small molecule inhibitor of CENP-E.

4.2 CENP-Q is required for oscillations of congressed kinetochores

To assess the dynamics of congressed sister kinetochores in CENP-Q depleted cells (Figure 4.2a, yellow bracket), we used our established kinetochore-tracking software, which tracks the 3D position of sister kinetochores in high spatial and temporal resolution (Jaqaman et al., 2010; see Figure 4.1 for summary of tracked parameters). This assay uses cells expressing eGFP-CENP-A as a kinetochore marker (see Figure 4.1), as well as eGFP-Centrin1 to serve as a spindle pole marker. To ascertain the effect of CENP-Q depletion on kinetochore dynamics, cells were treated with siRNA against CENP-Q or a control for 48 hrs and then imaged every 7.5 sec during metaphase. Imaging allowed clear visualisation of kinetochores at the metaphase plate in both conditions. In CENP-Q depleted cells the characteristic population of unaligned kinetochores was also present (Figure 4.2a, bottom panel). Initial attempts to track aligned kinetochores in CENP-Q depleted cells with the tracking software version used in the Jaqaman study failed to accurately define the plane of the metaphase plate. This failure resulted from the high number of unaligned kinetochores in CENP-Q depleted cells, which prevented the automated identification of the metaphase plate, even though the plate was clearly visible by eye. Plate identification is crucial as the plane of the metaphase plate provides a reference frame for kinetochore motion (see Figure 4.1). Therefore our kinetochore-tracking software had to be adapted to allow correct fitting of a plane through the metaphase distribution of kinetochores (see section 2.2.2).

We applied our modified tracking software to cells treated with *control* siRNA (example movie frame in Figure 4.2a, top panel) and found that kinetochores in these cells underwent quasi-

Figure 4.2

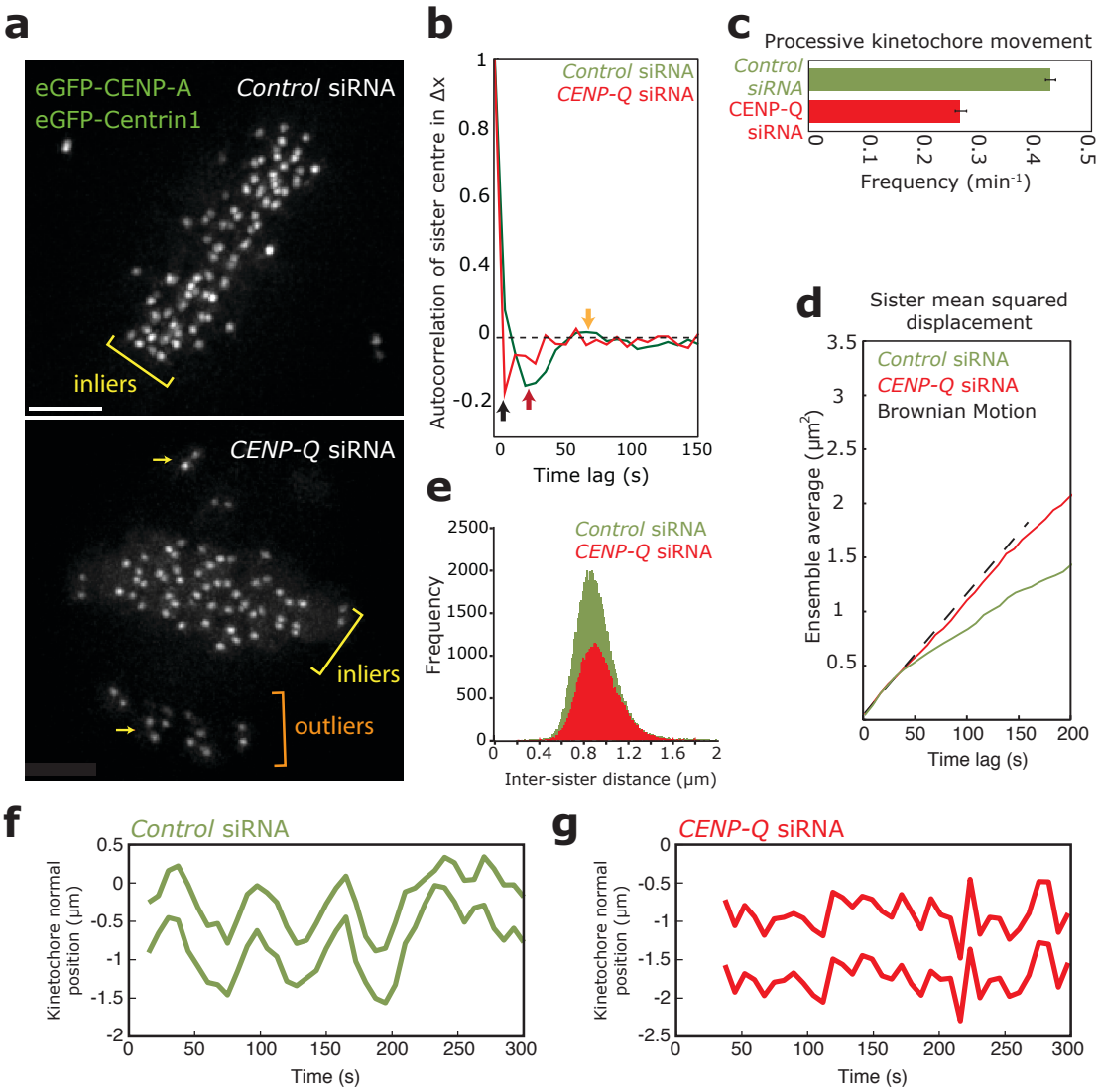

Figure 4.2 Dynamics of kinetochores in CENP-Q siRNA **(a)** Representative images from 5 min live-cell movies of HeLa K cells stably expressing eGFP-CENP-A/eGFP-Centrin1 (to mark kinetochores/spindle poles). Yellow arrows indicate unaligned kinetochores. The image is a z-projection (10 focal planes at 0.5 μm spacing). Cell in top panel has been treated with *Control* siRNA, cell in lower panel has been treated with *CENP-Q* siRNA. Scale bar = 3μm. Yellow and orange brackets represent inlying kinetochores and outlying kinetochores respectively **(b)** Autocorrelation of aligned tracked kinetochore pair sister centre positions after treatment with *Control* siRNA and *CENP-Q* siRNA. In the Control siRNA autocorrelation negative lobe at around 25-35 seconds (red arrow) and the positive lobe at around 60-70 seconds (orange arrow) indicate the half and full period of oscillations respectively. Oscillations are not present in *CENP-Q* siRNA treated cells, with the negative value at the first time step being indicative of random motion (black arrow). **(c)** Bar chart of the frequency of processive aligned kinetochore pair movements (defined as 4 or more movements in a single direction) from tracked kinetochores in cells treated with *Control* siRNA and *CENP-Q* siRNA. **(d)** Mean square displacement of aligned tracked kinetochore pairs, relative to Brownian motion in *Control* siRNA and *CENP-Q* siRNA treated cells. **(e)** Histogram of aligned tracked kinetochore sister pair separation distances after treatment with *Control* siRNA and *CENP-Q* siRNA. **(f-g)** Example aligned tracked kinetochore pair trajectories from *Control* siRNA (f) and *CENP-Q* siRNA (g) treated cells.

periodic oscillations back and forth about the metaphase plate as previously characterised (Jaqaman et al., 2010). Autocorrelation analysis showed that these oscillations had half and full periods similar to the half and full oscillatory periods identified in the Jaqaman study, which were ~35 and ~70 sec respectively (Figure 4.2b, green line; explanation of autocorrelation in 4.1b). We then applied our modified tracking to CENP-Q depleted cells, where kinetochores were tracked successfully now that the plane defining the metaphase plate was correctly positioned. Autocorrelation analysis revealed that kinetochores in CENP-Q depleted cells failed to undergo normal quasi-periodic oscillations, with the negative autocorrelation value at the first time lag being indicative of random motion (see Jaqaman et al., 2010; Figure 4.2b, red line). Although these autocorrelation plots are representative of thousands of kinetochores in multiple cells (see Table 9 below for *n* values of all tracking experiments), this behaviour can be clearly seen on the level of a single kinetochore pair (Figure 4.2f, g).

Table 9 – *n* values for all tracking experiments

Condition	Number of cells	Number of sister kinetochore pairs	Number of experiments
Control siRNA – 48 hrs	50	2187	4
CENP-Q siRNA – 48 hrs	31	1062	3
CENP-E siRNA – 48 hrs	82	3235	6
CENP-E siRNA – 20 hrs	29	1257	2
GSK923295 300 nM – 14 hrs	26	938	3
GSK923295 25 nM – 14 hrs	28	1424	1
GSK923295 300 nM – 1 hr	22	831	1

To oscillate normally, kinetochores must make sustained movements in a single direction before making a directional switch. As kinetochores in CENP-Q depleted cells do not oscillate, we suspected that these sustained or processive movements would be disrupted. To assess whether this was the case we used our kinetochore tracking data to measure the frequency of processive kinetochore pair movements. We defined a processive movement as the motion of the kinetochore pair sister centre position in the same direction for 4 time points or more (7.5 sec per time point). We found that the frequency of processive movements was decreased by over 1/3 in CENP-Q depleted cells when compared to control cells (Figure 4.2c). In accordance with the reduction in processive movements we also found that the mean squared displacement (MSD) of kinetochore sister centre positions was similar to that of Brownian motion, whereas kinetochores in control cells

were more constrained (Figure 4.2d). This Brownian like MSD provides further evidence that kinetochores in CENP-Q depleted cells are unable to make directed motion. This conclusion is supported by the examination of single kinetochore pair tracks in CENP-Q depleted cells (Figure 4.2g), which appear to "jitter" rather than making the smoother oscillatory motions observed in control kinetochore tracks (Figure 4.2f).

Further examination of kinetochore tracking data revealed that the metaphase plate thickness was slightly increased in CENP-Q depleted cells (*CENP-Q* siRNA = 1.26 μm, *control* siRNA = 1.14 μm, discussed below in 4.6), but inter-sister distance was normal (Figure 4.2e); the latter suggests that kinetochores could still generate pulling forces. The presence of these pulling forces suggests that kinetochores in CENP-Q depleted cells could still form normal end-on attachments with K-MTs. However, the lack of periodic oscillations indicated that the coordination of K-MT dynamics was likely to be perturbed. This is in agreement with recent work within our laboratory, which demonstrated that depletion of CENP-Q caused the K-MT population to turn over 3-fold slower compared to control cells (Samora C.P., PhD thesis, 2012). This disruption of K-MT dynamics is likely the same reason that biorientated kinetochores cannot make processive movements to the metaphase plate in CENP-Q depleted cells (chapter 3, Figure 3.15 & 3.16), and could lead to the observed defects in aligned kinetochore motion.

4.3 CENP-E contributes to force generation by end-on attached kinetochores

Our previous work has shown that depletion of CENP-E did not affect metaphase oscillations, suggesting that in human cells CENP-E was only required for lateral sliding during chromosome congression (Jaqaman et al., 2010). However, it was recently reported that inhibition of CENP-E with GSK923295 leads to a subset of chromosomes moving away from the metaphase plate in ~50% of cells. This was interpreted as CENP-E having a role in maintaining biorientated attachments (Gudimchuk et al., 2013). It is possible that this phenotype simply reflects a subset of

aligned kinetochores that are still laterally attached and sensitive to perturbation of CENP-E. Indeed, there is evidence that up to 11% of congressed kinetochores may remain laterally attached within the metaphase plate for some time after initial congression (Shrestha & Draviam, 2013). Gudimchuk and colleagues also showed that CENP-E inhibition prevented kinetochores from tracking depolymerising microtubules, as well as demonstrating that CENP-E could track depolymerising microtubules *in vitro* (Gudimchuk et al., 2013). This was interpreted as CENP-E motors being required for depolymerisation-coupled pulling movements, in contrast to our finding in chapter 3 that CENP-E was dispensable for this process.

To further investigate, we imaged and tracked kinetochores following depletion (by siRNA) or inhibition of CENP-E with GSK923295 (see Figure 4.3a for example frames; see Table 9 for *n* values). In contrast to our previous report (Jaqaman et al., 2010), we observed that kinetochores no longer underwent periodic oscillations following depletion of CENP-E motors (Figure 4.3b, example kinetochore pair tracks in f & g). We additionally found that compared to control cells, both CENP-E depletion or inhibition resulted in a MSD closer to Brownian motion than that seen in control cells (Figure 4.3c). This effect was most pronounced in cells treated with 300nM GSK923295, however, neither treatment affected MSD to the same degree as *CENP-Q* siRNA. Both the effects on oscillations and on MSD are consistent with the idea that CENP-E contributes to force-generation at end-on attached kinetochores. However, in CENP-E depleted cells we saw that the inter-sister kinetochore distance was not greatly effected, indicating that the disrupted dynamics of aligned kinetochores was not due to a defect in K-MT attachment (Figure 4.3d). In contrast we observed that kinetochore pairs in cells treated with 300 nM of the CENP-E inhibitor GSK923295 for 14 h were hyper-stretched (mean = 1.15 ± 0.29 μm in GSK923295 compared to 0.90 ± 0.18 μm in control cells; Figure 13a,c). This difference may reflect the fact that while siRNA mediated depletion removes CENP-E protein from cells by preventing translation, GSK923295 functions through allosteric inhibition of ADP release. GSK923295 therefore causes CENP-E motor domain to become locked in a rigor microtubule-bound state (Wood et al., 2010). The observed increase in sister-kinetochore separation suggests that kinetochore pairs are under increased

Figure 4.3

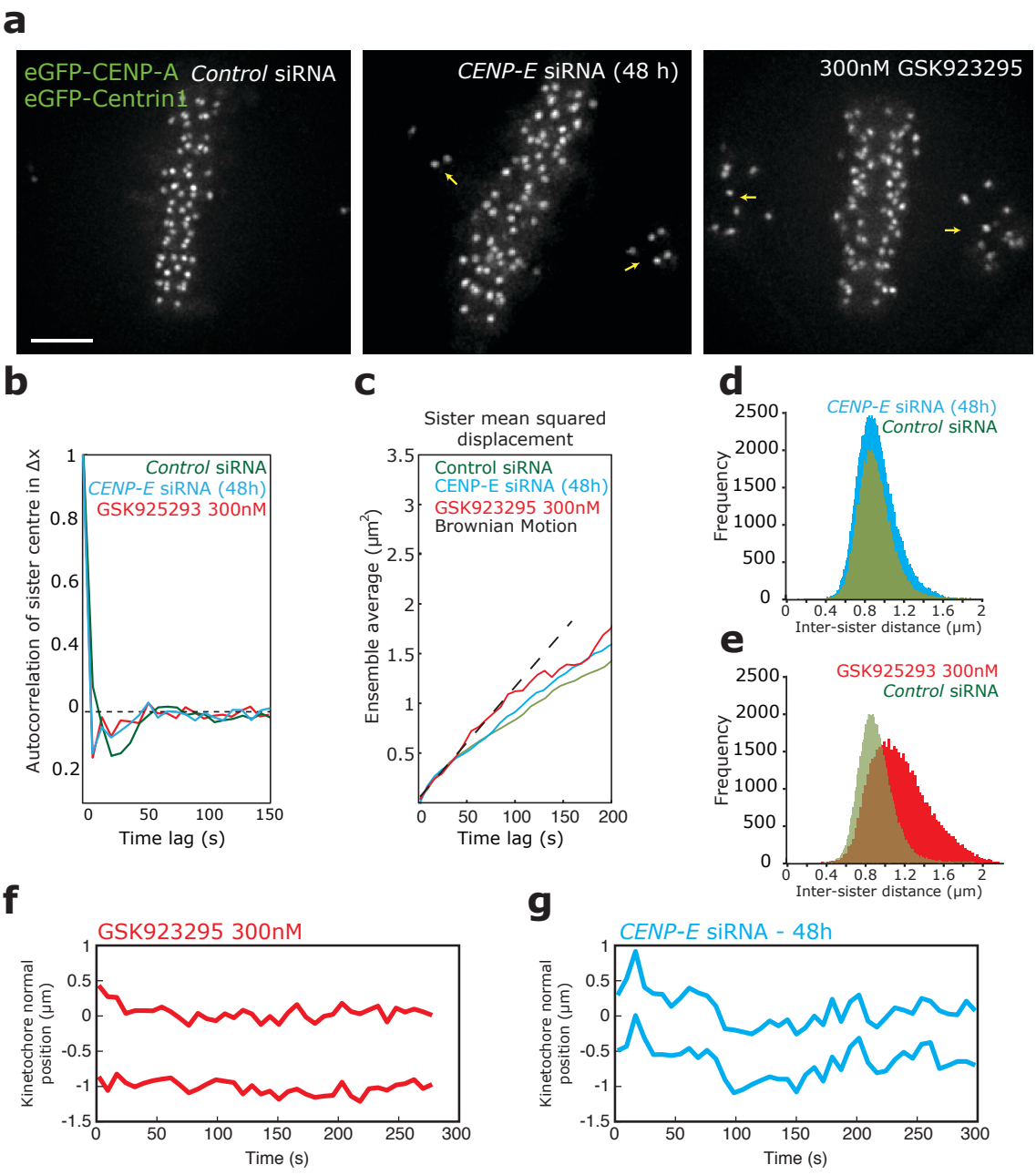

Figure 4.3 Dynamics of kinetochores in CENP-E siRNA & inhibitor **(a)** Representative images from 5 min live-cell movies of HeLa K cells stably expressing eGFP-CENP-A/eGFP-Centrin1 (to mark kinetochores/spindle poles). Yellow arrows indicate unaligned kinetochores. The image is a z-projection (10 focal planes at 0.5 μm spacing). Left cell has been treated with *Control* siRNA, middle cell with *CENP-E* siRNA and right cell with 300 nM of the CENP-E inhibitor GSK923295. Scale bar = 3μm. **(b)** Autocorrelation of aligned tracked kinetochore pair sister centre positions after treatment with *Control* siRNA, *CENP-E* siRNA or 300mM of the CENP-E inhibitor GSK923295. In the *Control* siRNA autocorrelation negative lobe at around 25-35 seconds and the positive lobe at around 60-70 seconds indicate the half and full period of oscillations respectively. Oscillations are not present in cells treated with *CENP-E* siRNA or 300 nM GSK923295. **(c)** Mean square displacement of aligned tracked kinetochore pairs relative to Browian motion after treatment with the above conditions. **(d-e)** Histograms of aligned tracked kinetochore sister pair separation distances after treatment with (d) *Control* siRNA and *CENP-E* siRNA and (e) *Control* siRNA and 300 nM GSK923295. **(f-g)** Example aligned tracked kinetochore pair trajectories from cells treated with (f) *CENP-E* siRNA or (g) 300nM GSK923295.

tension after inhibition of CENP-E, providing evidence that K-MT attachments are stable. However, the reason for the increased tension is unclear. It is possible that this phenotype is the result of off-target effects of GSK923295 on other kinesisns. This seems unlikely, as GSK923295 has been shown to be highly specific to CENP-E. Indeed, *in vitro* assays have shown that GSK923295 has little effect on the kinesins KSP, Kif1A, MKLP1, RabK6, HSET and MCAK at 40 nM concentrations whilst almost completely inhibiting CENP-E. In line with this high level of specific inhibition the GSK923295 has been shown to inhibit CENP-E with a K_i of 3.2 ± 0.2 nM (Wood et al., 2010).

4.4 Kinetochores are sensitive to small variations in CENP-E

Although our data indicates some clear differences between CENP-E depletion and CENP-E inhibition, in both conditions kinetochore oscillations were disrupted. This was in contrast to previous work by our group that showed that depletion of CENP-E did not disrupt normal kinetochore oscillations (Jaqaman et al., 2010). One possibility was previous tracking in CENP-E depleted cells represented incomplete siRNA mediated depletion. We therefore repeated our tracking experiments using a reduced *CENP-E* siRNA treatment time (from 48 h down to 20 h) in order to partially deplete CENP-E protein. We confirmed partial depletion by immunofluorescence, staining with antibodies against CENP-E and CENP-A, and found that 13.8% of kinetochore bound CENP-E protein remained following partial siRNA treatment, compared to 3.5% following the full siRNA treatment (t-test, p = 0.0001; Figure 4.4a). However, polar chromosomes were still abundant in partially CENP-E depleted cells. Following confirmation of partial depletion by immunofluorescence, cells stably expressing eGFP-CENP-A (kinetochore marker) and eGFP-Centrin1 (pole marker) were treated with partial *CENP-E* siRNA and then tracked as before (example frame in Figure 4.4b, bottom left panel; see Table 9 for *n* values). Following partial depletion, our tracking data demonstrated that kinetochores continued to oscillate, whilst still having polar chromosomes. Autocorrelation analysis revealed a negative lobe at ~35 sec denoting the oscillatory half period and a positive lobe at ~70 sec denoting the oscillatory full period as previously described in Jaqaman et al., 2010 (Figure 4.4a, b, c). Thus the data in the Jaqaman

Figure 4.4

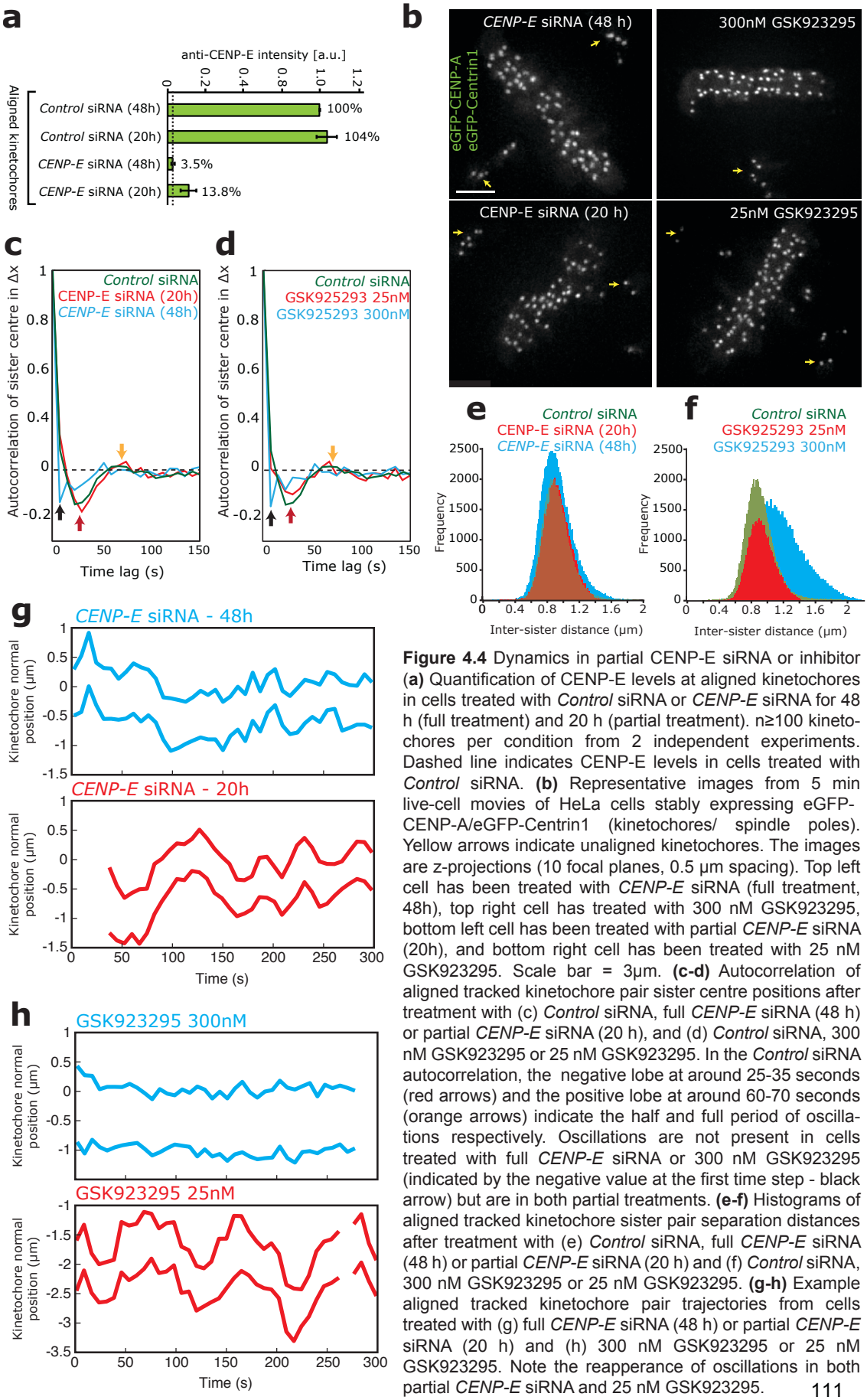

Figure 4.4 Dynamics in partial CENP-E siRNA or inhibitor (**a**) Quantification of CENP-E levels at aligned kinetochores in cells treated with *Control* siRNA or *CENP-E* siRNA for 48 h (full treatment) and 20 h (partial treatment). n≥100 kinetochores per condition from 2 independent experiments. Dashed line indicates CENP-E levels in cells treated with *Control* siRNA. **(b)** Representative images from 5 min live-cell movies of HeLa cells stably expressing eGFP-CENP-A/eGFP-Centrin1 (kinetochores/ spindle poles). Yellow arrows indicate unaligned kinetochores. The images are z-projections (10 focal planes, 0.5 μm spacing). Top left cell has been treated with *CENP-E* siRNA (full treatment, 48h), top right cell has treated with 300 nM GSK923295, bottom left cell has been treated with partial *CENP-E* siRNA (20h), and bottom right cell has been treated with 25 nM GSK923295. Scale bar = 3μm. **(c-d)** Autocorrelation of aligned tracked kinetochore pair sister centre positions after treatment with (c) *Control* siRNA, full *CENP-E* siRNA (48 h) or partial *CENP-E* siRNA (20 h), and (d) *Control* siRNA, 300 nM GSK923295 or 25 nM GSK923295. In the *Control* siRNA autocorrelation, the negative lobe at around 25-35 seconds (red arrows) and the positive lobe at around 60-70 seconds (orange arrows) indicate the half and full period of oscillations respectively. Oscillations are not present in cells treated with full *CENP-E* siRNA or 300 nM GSK923295 (indicated by the negative value at the first time step - black arrow) but are in both partial treatments. **(e-f)** Histograms of aligned tracked kinetochore sister pair separation distances after treatment with (e) *Control* siRNA, full *CENP-E* siRNA (48 h) or partial *CENP-E* siRNA (20 h) and (f) *Control* siRNA, 300 nM GSK923295 or 25 nM GSK923295. **(g-h)** Example aligned tracked kinetochore pair trajectories from cells treated with (g) full *CENP-E* siRNA (48 h) or partial *CENP-E* siRNA (20 h) and (h) 300 nM GSK923295 or 25 nM GSK923295. Note the reapperance of oscillations in both partial *CENP-E* siRNA and 25 nM GSK923295.

study almost certainly represented a partial depletion. Consistent with autocorrelation analysis, based on the entire aligned kinetochore population, we also observed that tracks of single kinetochore pairs' oscillations were visible after partial depletion but not after full depletion (Figure 4.4g).

Our partial depletion experiments suggested that kinetochores were sensitive to relatively small variations in the number of CENP-E motors. To confirm this, we treated cells with a high (300 nM) or low (25 nM) concentration of the CENP-E inhibitor GSK923295 for 14 hrs. We imaged and tracked these cells as described above. Consistent with our siRNA experiments we found that both concentrations of inhibitor resulted in the formation of polar chromosomes (Figure 4.4b), but only the high (300 nM) concentration abolished oscillations as detected by autocorrelation analysis (Figure 4.4d). Consistent with these results we were also able to visualise single kinetochore pairs undergoing oscillations after partial CENP-E inhibition with 25 nM GSK923295, but not after full inhibition with 300 nM GSK923295 (Figure 4.4h). Thus, a small number of CENP-E molecules aresufficient to sustain kinetochore oscillations in human cells, whereas much higher levels of CENP-E protein are required to facilitate congression by lateral sliding. We also observed that neither partial depletion nor partial inhibition of CENP-E affected kinetochore sister pair separation (Figure 4.4e, f).

4.5 Inhibition of CENP-E perturbs normal CENP-E loading to aligned kinetochores

Given the difference between partial and full doses of the CENP-E inhibitor GSK923295 and the unexpected increase in sister kinetochore distance we next examined the effect of 300 nM GSK923295 treatment on CENP-E levels and localisation in an effort to better understand the observed phenotype. Interestingly, immunofluorescence with anti-CENP-E antibodies showed that following treatment with GSK923295, the CENP-E protein accumulated on polar kinetochores (Figure 4.5a, quantification in b), as previously characterised (Hoffman et al., 2001). These polar

Figure 4.5

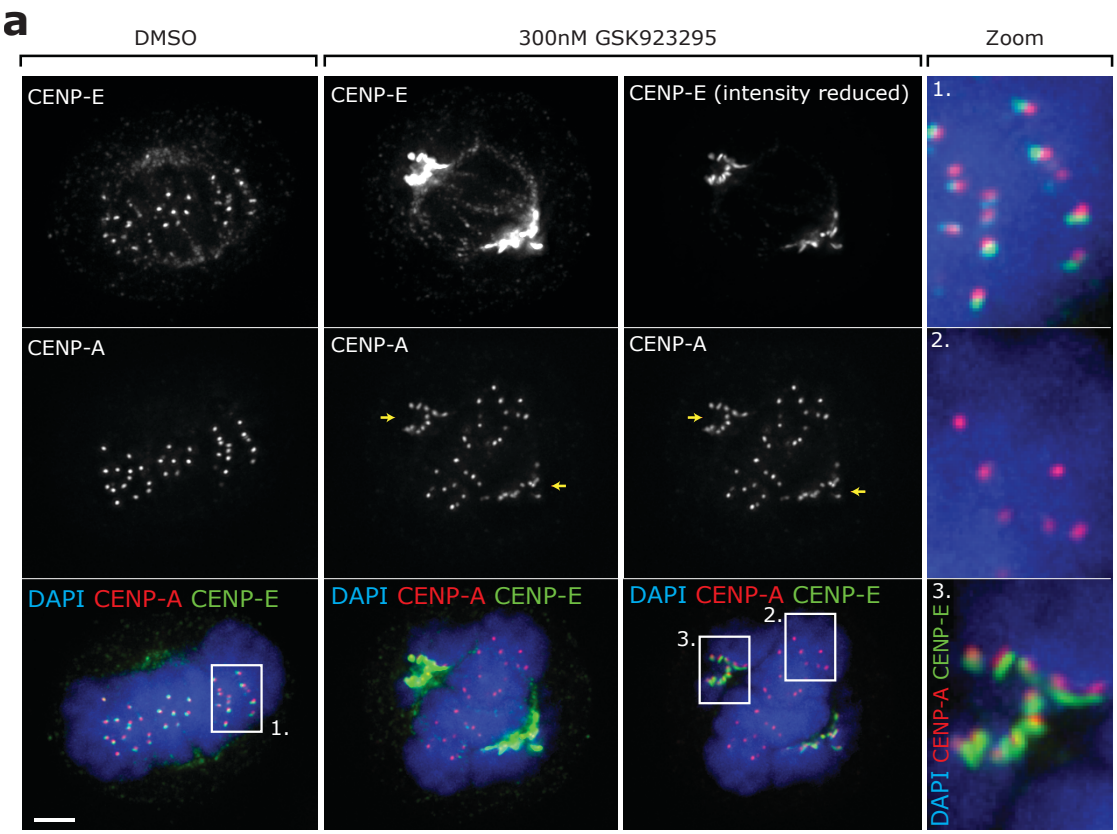

Figure 4.5 CENP-E levels after inhibitor treatment **(a)** Images of a metaphase cell stained with CENP-E (green) and CENP-A (red) antibodies and DAPI (blue). The image is a z-projection (10 focal planes at 0.2µm spacing). Cells are treated with DMSO or 300 nM GSK923295 for 14 h before fixation. Yellow arrows point to polar kinetochores, scale bar = 3 µm. Boxes 1, 2 and 3 are shown as zoom images around kinetochores to the right of the main panel. Box 1 shows CENP-E levels at aligned kinetochores treated with DMSO. Box 2 and 3 shows CENP-E levels at aligned and polar kinetochores respectively in cells treated with 300 nM GSK923295. **(b)** Quantification of CENP-E levels in cells treated with DMSO or 300 nM GSK923295 for 14 h. n≥50 kinetochores per condition from ≥5 cells. Dashed line indicates CENP-E levels at aligned kinetochores in DMSO

chromosomes result from the inactivation of the CENP-E motors and therefore represent a population of chromosomes that are dependent upon CENP-E for congression. However, the levels of CENP-E on aligned kinetochores were greatly reduced on congressed kinetochores following GSK923295 treatment (Figure 4.5a, quantification in b; low CENP-E levels on aligned kinetochores also reported in Gudimchuk et al., 2013). These data suggest an active motor domain is necessary for the normal recruitment of CENP-E to aligned kinetochores. However, the reason for the requirement of an active motor domain to facilitate aligned kinetochore CENP-E loading is unclear. One possibility is the rigor state of the CENP-E motor results in the molecule being stripped from the kinetochore by poleward microtubule flux. Another possibility is the active motor domain facilitates K-MT plus-end localisation, rather than kinetochore localisation per se (see discussion for details). In either case, the increased aligned inter-sister kinetochore distance in GSK923295 treated cells shows that a few remaining motors, in a rigor state, are sufficient to increase inter-sister kinetochore tension and disrupt normal aligned kinetochore dynamics.

4.6 Depletions of CENP-Q and CENP-E and inhibition of CENP-E each result in distinct aligned kinetochore phenotypes

Although the inhibition of CENP-E results in an increased inter-sister kinetochore distance; on first inspection the aligned kinetochore phenotype arising from depletion of CENP-E seems similar to that observed following CENP-Q depletion. However our kinetochore tracking data revealed several key differences between the CENP-Q and CENP-E depletion phenotypes. Cells depleted of CENP-E or treated with 300nM GSK923295 exhibit a decreased metaphase plate width of 0.82 μm and 0.88 μm respectively, compared to 1.14 μm in control cells (Figure 4.6a, right and middle panels). In contrast CENP-Q depleted cells exhibit an increased metaphase plate width of 1.26 μm (Figure 4.6b, left panel). This plate width is calculated by taking the standard deviation of sister kinetochore centre positions relative to the plane of the metaphase plate; the value obtained is then multiplied by 2 to represent the distribution on both sides of plane of the metaphase plate. The increase in metaphase plate width observed in CENP-Q depleted cells suggests that that CENP-Q depletion reduces the alignment of kinetochores at the metaphase plate, whereas depletion or inhibition of CENP-E has the opposite effect.

Thus, plate width yields a well-defined difference between the CENP-Q depletion and CENP-E depletion or inhibition phenotypes. This difference in phenotype is more significant when one considers that cells lacking CENP-Q also lack CENP-E. It is likely that the increase in metaphase plate width reflects the disruption of both end-on pulling and lateral sliding alignment mechanisms in CENP-Q depleted cells. This would prevent kinetochores from aligning to the plate by lateral sliding as well as maintenance of normal metaphase organisation by the tightly depolymerase-coupled pulling, which would normally give rise to metaphase oscillations. However, in CENP-E depleted or inhibited cells, end-on pulling mechanisms remain functional (see chapter 3) facilitating alignment of biorientated kinetochore pairs. This is supported by MSD data which shows that aligned kinetochores in CENP-Q depleted cells move randomly (similar to Brownian motion) whereas kinetochores in CENP-E depleted or inhibited cells are more constrained, indicating more

Figure 4.6

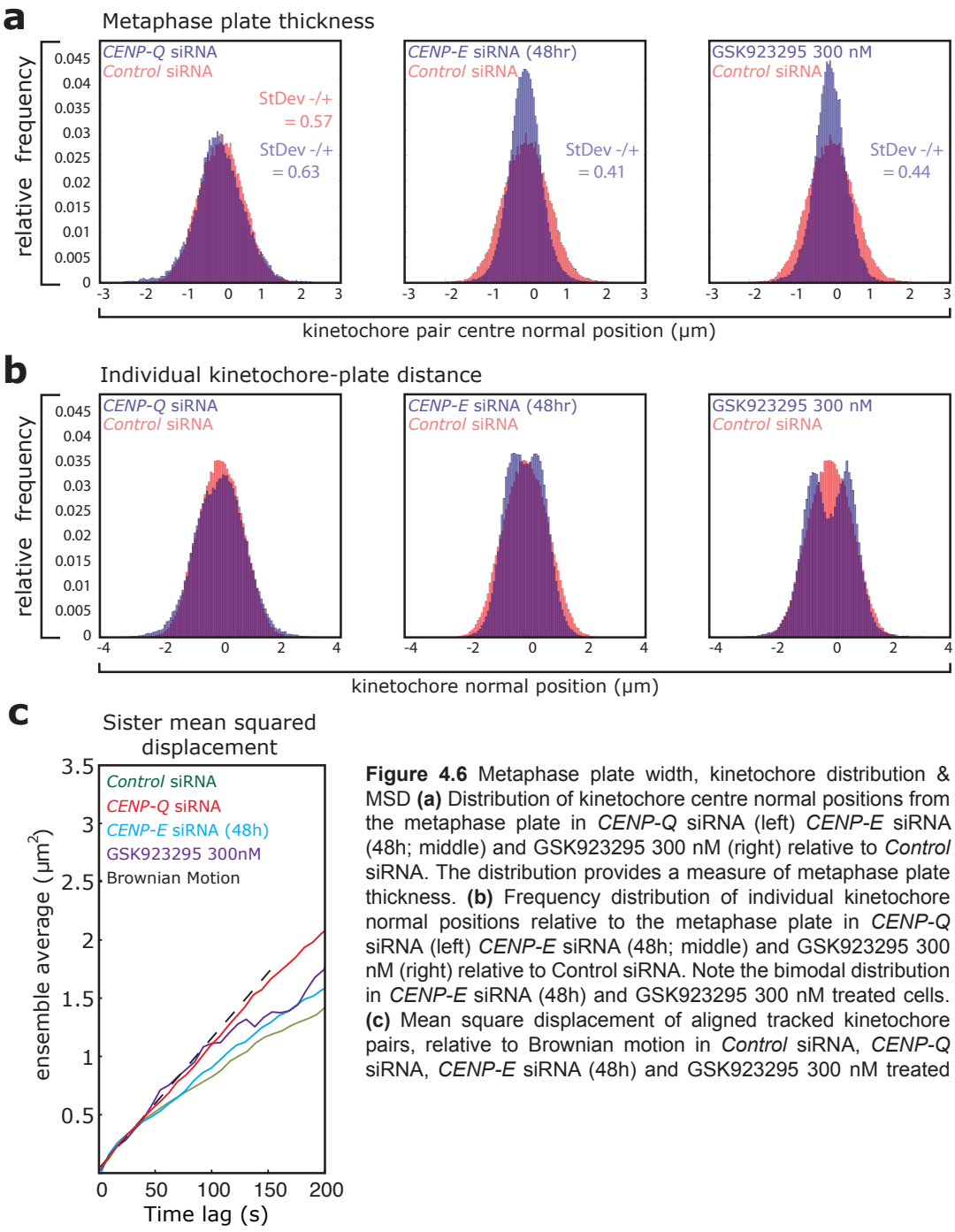

Figure 4.6 Metaphase plate width, kinetochore distribution & MSD **(a)** Distribution of kinetochore centre normal positions from the metaphase plate in *CENP-Q* siRNA (left) *CENP-E* siRNA (48h; middle) and GSK923295 300 nM (right) relative to *Control* siRNA. The distribution provides a measure of metaphase plate thickness. **(b)** Frequency distribution of individual kinetochore normal positions relative to the metaphase plate in *CENP-Q* siRNA (left) *CENP-E* siRNA (48h; middle) and GSK923295 300 nM (right) relative to Control siRNA. Note the bimodal distribution in *CENP-E* siRNA (48h) and GSK923295 300 nM treated cells. **(c)** Mean square displacement of aligned tracked kinetochore pairs, relative to Brownian motion in *Control* siRNA, *CENP-Q* siRNA, *CENP-E* siRNA (48h) and GSK923295 300 nM treated

directed motion (Figure 4.6c). The decrease in metaphase plate width in CENP-E depleted or inhibited cells compared to control cells is therefore likely to result from the prolonged mitotic arrest experienced by CENP-E depleted cells. This arrest may allow hyper alignment of biorientated kinetochores still capable of directed motion by end-on pulling due to the extra time allowed, owing to the prevention of anaphase onset by the population of polar chromosomes.

Given that our data shows clear differences in the distribution of sister centre position between CENP-Q depletion and CENP-E depletion or inhibition, we next examined our data to ascertain if this was the case for the distribution of individual kinetochores to the metaphase plate. Surprisingly we found that depletion of CENP-E resulted in a bimodal normal distribution of kinetochores at the metaphase plate (Figure 4.6b, middle panel), an effect that is even greater in cells treated with the CENP-E inhibitor GSK923295 at 300 nM (Figure 4.6b, right panel). This bimodal distribution of kinetochores is not observed in control or CENP-Q depleted cells (Figure 4.6b, left panel), and likely reflects the tight organisation of kinetochores aligned at the metaphase plate due to a prolonged mitotic arrest resulting from the presence of polar chromosomes. Additionally, kinetochores in CENP-E depleted or inhibited cells do not undergo oscillatory movement. It is likely that this bimodal distribution is not seen in control-depleted cells because of the presence of kinetochore oscillations, which may abolish this bimodal distribution due to continued back and forth motion of kinetochores about the plate. The larger plate width observed in control cells, would also make any bimodality that was present less pronounced. Taken together this data shows key differences in CENP-Q and CENP-E depletion or inhibition phenotypes. Despite the lack of metaphase oscillations, biorientated kinetochores in CENP-E depleted or inhibited cells are capable of tight alignment to the metaphase plate, likely because end-on pulling mechanisms remain functional (as shown in chapter 3). The mitotic arrest caused by polar chromosomes would give the biorientated kinetochores capable of alignment by end-on pulling extra time to align, resulting in a tightly organised metaphase plate.

4.7 Acute inhibition of CENP-E perturbs chromosome oscillations

Our earlier experiments show that CENP-E is important in the oscillation of chromosomes aligned at the metaphase plate. However, both the CENP-E depletion (48 hrs) and the inhibition of CENP-E with 300 nM GSK923295 (14 hrs) represent chronic treatments. We therefore investigated the effect of acute (1 hr) inhibition of CENP-E with 300 nM GSK923295 to ascertain whether this had the same effect as chronic treatments. After 1 hr treatment with the inhibitor cells expressing eGFP-CENP-A eGFP-Centrin1 were imaged as described in section 4.2. Visual inspection of these movies showed that polar chromosomes indicative of CENP-E inhibition or depletion were clearly visible (Figure 4.7a, right panel). Aligned kinetochores in these cells were tracked using our tracking software. Autocorrelation analysis of kinetochore-sister centre position revealed that kinetochores in cells treated with 300 nM GSK923295 for 1 hr no longer undergo the normal quasi-periodic oscillations seen in control cells (Figure 4.7b, red line), as indicated by the negative autocorrelation value at the first time step was (Figure 4.7b, black arrow). Thus, the lack of oscillations in cells treated with the inhibitor for 14 hours is not as a result of chronic treatment. However, the autocorrelation analysis of kinetochores in cells treated with GSK923295 for 1 hr did show the remnants of a negative lobe at ~30 sec suggesting that some number of kinetochores may still be oscillating after a 1 hr treatment.

We next examined the distribution of sister-kinetochore pair centre positions relative to the plain of the metaphase plate, the standard deviation of this value providing a measure of metaphase plate thickness. This analysis revealed that cells treated with 300 nM GSK923295 for 1 hour had a reduced metaphase plate width compared to control cells (0.98 μm and 1.14 μm respectively; Figure 4.7c). This decrease in metaphase plate width is less than observed in the 14 hour inhibitor treatments and depletion experiments (0.88 and 0.82 respectively; Figure 4.6a). The most striking aspect of the 14 hr 300 nM GSK923295 treatment was the hyper-stretched inter-sister kinetochore phenotype. However, we found that in 1 hour treated cells kinetochore-pairs were not hyper-stretched (Figure 4.7d), with a mean inter-kinetochore distance of 0.889 μm compared to 0.876 μm

Figure 4.7

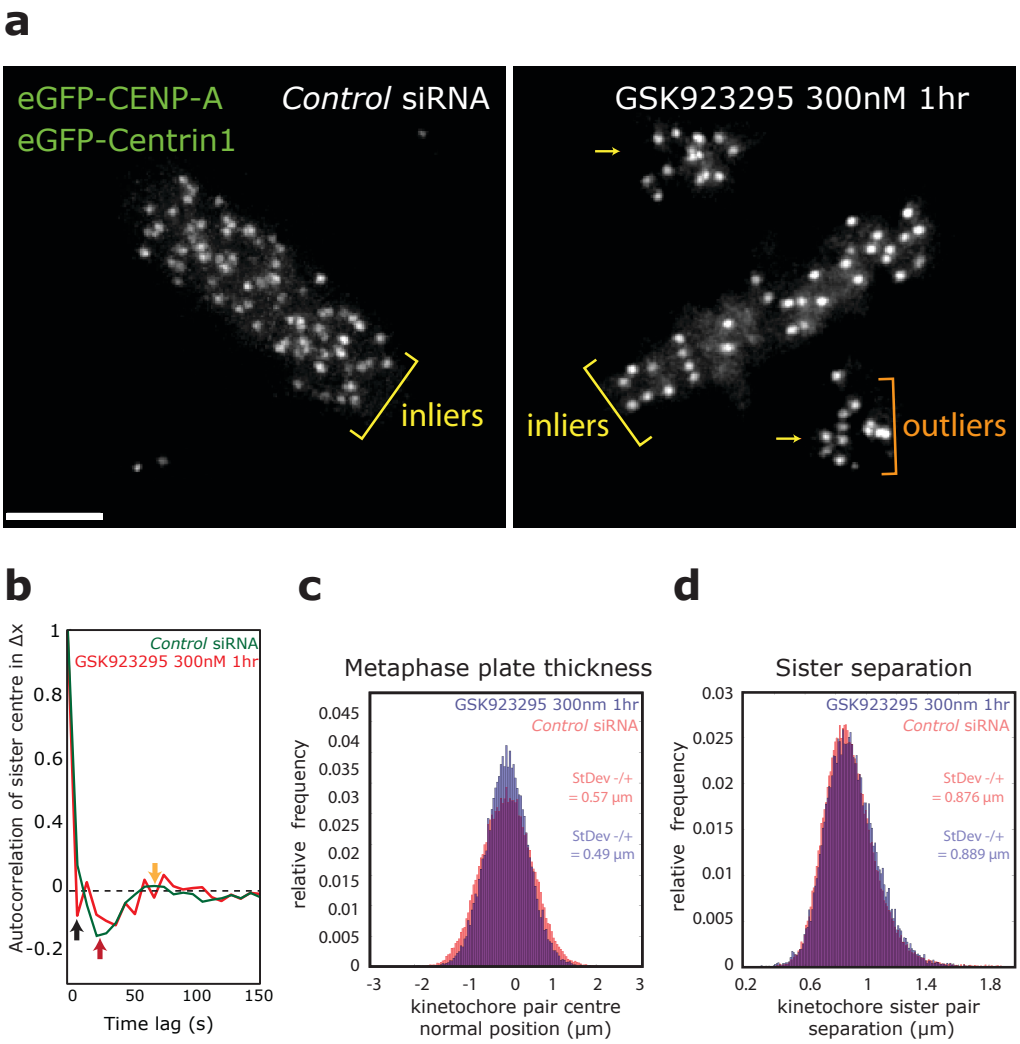

Figure 4.7 Acute inhibition of CENP-E. One hour treatments with GSK923295 at 300 nM perturbe kinetochore oscillations. **(a)** Representative images from 5 min live-cell movies of HeLa cells stably expressing eGFP-CENP-A/eGFP-Centrin1 (kinetochores/ spindle poles). Yellow arrows indicate unaligned kinetochores. The images are z-projections (10 focal planes, 0.5 μm spacing). Left cell has been treated with *Control* siRNA (for 48 hrs), right cell has been treated with the CENP-E inhibitor GSK923295 at 300 nM for 1 hr. Yellow brackets indicate inlying kinetochores included in tracking and orange brackets indicate outliers not included in tracking. **(b)** Autocorrelation of aligned tracked kinetochore pair sister centre positions after treatment with *Control* siRNA or CENP-E inhibitor GSK923295 at 300 nM for 1 hr. In the *Control* siRNA autocorrelation, the negative lobe at around 25-35 seconds (red arrow) and the positive lobe at around 60-70 seconds (orange arrow) indicate the half and full period of oscillations respectively. Oscillations are perturbed in cells treated with full GSK923295 at 300 nM for 1 hr, negative value at the first time step is indicative of random motion (black arrow). **(c)** Distribution of kinetochore centre normal positions from the metaphase plate in cells treated with GSK923295 at 300 nM for 1 hr compared to cells treated with *Control* siRNA for 48 hrs. The distribution provides a measure of meta- phase plate thickness. **(d)** Histograms of aligned tracked kinetochore sister pair separation distances after treatment with GSK923295 at 300 nM for 1 hr compared to cells treated with *Control* siRNA for 48 hrs.

in control cells. This represents, at most, a slight increase in inter-kinetochore distance and suggests that the hyper-stretching phenotype only arises after longer treatments with GSK923295, unlike the loss of normal oscillations and metaphase plate tightening, which arise rapidly.

4.8 Conclusions

In this chapter we have shown that CENP-Q is required for normal aligned kinetochore dynamics, as depletion of the protein results in a loss of kinetochore oscillations and processive movements. This effect could be seen both on the population level and on the level of individual kinetochore pair trajectories. However, depletion of CENP-Q does not affect normal K-MT attachment as sister kinetochore separation in CENP-Q depleted cells is normal. In contrast to previous work from our laboratory (Jaqaman et al., 2010), we find that depletion of CENP-E also abolished aligned kinetochore oscillations. We confirmed this result by treating cells with the CENP-E inhibitor GSK923295 (300 nM), which also abolished oscillations. This difference in phenotype from the previous study is almost certainly due to the data in the Jaqaman study representing a partial CENP-E depletion, as partial depletion or inhibition of CENP-E still causes polar chromosomes but aligned kinetochores continue to oscillate. Thus, small levels of active CENP-E are required to drive oscillations whilst larger levels are necessary to drive congression by lateral sliding. We also find that chronic treatments (14 hrs) with the CENP-E inhibitor GSK923295, which locks CENP-E in a rigor state, results in increased inter-sister kinetochore distance, suggesting that rigor CENP-E increases inter-sister kinetochore tension. However, 1 hr treatments with GSK923295 do not result in this phenotype. Despite causing polar chromosomes we find that treatments with 300 nM GSK923295 or depletion of CENP-E does not prevent organisation of kinetochores at the metaphase plate, as plate width is actually decreased in comparison to control cells.

CHAPTER 5: Discussion

5.1 Summary of findings

It is essential that chromosomes congress to the metaphase plate to enable accurate segregation in anaphase. The majority of chromosomes are able to biorientate at the metaphase plate and align by the almost “instantaneous” mechanisms described by Magdison and colleagues (Magdison et al., 2011). However, it is essential that chromosomes that do not become biorientated in this initial wave of attachment are able to congress to the metaphase plate. Thus at least two rescue mechanisms exist to facilitate the alignment of such chromosomes; (1) the well characterised lateral sliding of chromosomes to the metaphase plate by the kinesin 7, CENP-E as described by Kapoor and colleagues (Kapoor et al., 2006), (2) depolymerisation-coupled pulling of biorientated chromosomes (Skibbens et al., 1993). In chapters 3 and 4 we show that the CENP-Q protein is essential for chromosome congression by both depolymerisation-coupled pulling and lateral sliding. Moreover, we demonstrate that the recruitment of the lateral sliding kinesin CENP-E to kinetochores requires CENP-Q. In chapter 4 we show how both CENP-Q and CENP-E dependent mechanisms are important for the normal movement of end-on attached kinetochores. However, despite causing polar chromosomes and disrupting oscillations we find that treatments with 300 nM GSK923295 or depletion of CENP-E does not prevent organisation of kinetochores at the metaphase plate. Based on these results, and the existing literature, we propose an updated model of how kinetochores are captured and then congressed to the metaphase plate (see sections 5.2 to 5.6 below). Our data also inform a modified view of how aligned biorientated kinetochores make directed movements during metaphase, which give rise to oscillations.

5.2 Multi mechanism model for chromosome congression

Our data support a model in which there are at least two distinct mechanisms that drive the congression of polar chromosomes (Figure 5.1). The first mechanism is the sliding of

chromosomes along the lattice of existing K-fibres towards their plus-ends (plateward; see chromosome 1 in Figure 5.1). These movements require CENP-E (Kapoor et al., 2006), and are thought to increase the probability that mono-orientated kinetochore pairs engage microtubules from the opposite pole, thus becoming biorientated. During this process mono-orientated kinetochore pairs form lateral attachments with existing adjacent K-fibres through the unattached kinetochore. CENP-E motors bound on this kinetochore then make processive plus-end directed motion along the adjacent K-MTs, resulting in “towing” of the non-biorientated pair to the spindle equator. Once kinetochores reach the equator they are then more likely to become biorientated due to the increased number of MTs emanating from the opposite spindle pole (Kapoor et al., 2006). Importantly we find that this lateral sliding is also dependent upon the CENP-Q subunit of the CCAN, as CENP-Q facilitates kinetochore binding of CENP-E (see section 5.7).

In addition to its role in CENP-E recruitment, we also find a CENP-E independent role for CENP-Q in a second chromosome congression mechanism. Unlike CENP-E, we find that CENP-Q is required for the movement of orientated sisters to the metaphase plate (this study; Figure 5.1, Chromosome 2). Importantly, it is the dependency relationship between CENP-E and CENP-Q that allowed us to uncover the CENP-Q specific role in this process. In CENP-E depleted cells, where lateral sliding can no longer occur, kinetochore pairs that are orientated with the spindle axis are able to congress to the cellular equator. As this process occurs in the absence of CENP-E it cannot be as a result of lateral sliding and therefore must represent biorientated attached chromosomes that undergo depolymerisation-coupled pulling. However, in CENP-Q depleted cells, where both CENP-Q and CENP-E are absent from kinetochores, this process no longer occurs. As this process is unperturbed in CENP-E depleted cells it must represent a CENP-Q specific role in chromosome congression.

In principle one could argue that this difference could be due a greater loss of CENP-E from kinetochores in *CENP-Q* siRNA, compared to *CENP-E* siRNA treatments. However, the level of CENP-E protein bound at kinetochores is in fact significantly less (15%) following depletion of

Figure 5.1

a

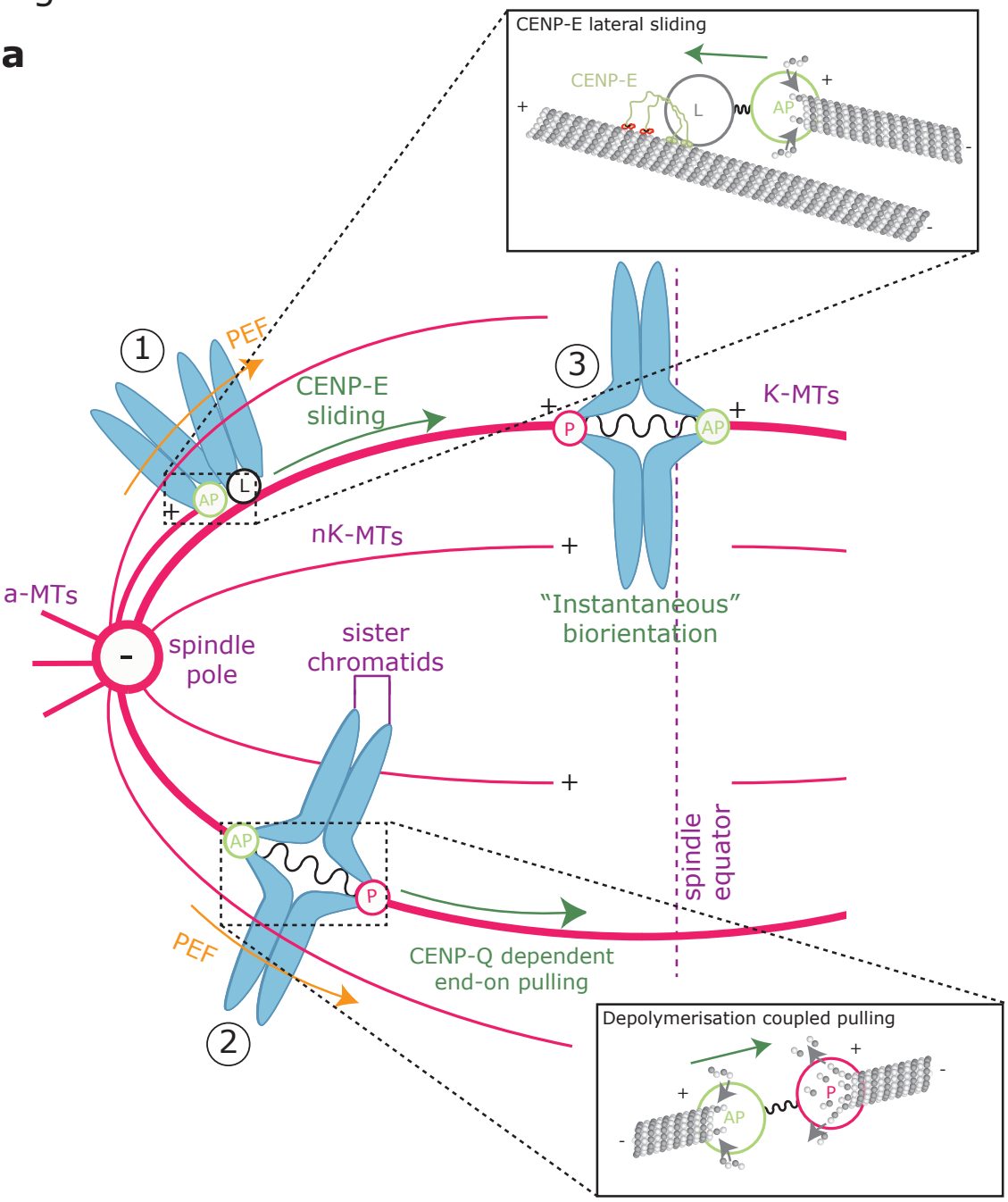

Figure 5.1 (a) Multiple mechanisms of chromosome congression. **Chromosome 1** is end-on attached to K-fibre microtubules (red lines) at the anti-poleward (AP) sister kinetochore (green circle), and laterally attached (L) to an adjacent K-fibre by the opposite kinetochore (black circle). CENP-E bound at the laterally attached kinetochore walks towards the plus end of the laterally attached K-fibre; this plus end directed walking has the effect of transporting the chromosome to the metaphase plate. The zoom panel of chromosome 1 (top right) shows a detailed view of this process with CENP-E motors marked in green at the laterally attached sister, white and grey spheres represent tubulin heterodimers assembled to form microtubules. Green arrow represents the directio of chromosome movement. **Chromosome 2** is end-on attached at both sister kinetochores (biorientated) and is congressing to the plate by CENP-Q dependent depolymerisation-coupled pulling. This process is powered by depolymerisation at the poleward (P) sister kinetochore (red), whilst the K-fibre attached to the AP sister (green) remains in a net polymerising state. The zoom panel of chromosome 2 (bottom right) shows a detailed view of this process with microtubules polymerising at the AP sister and depolymerising at the P sister. Green arrow represents the direction of chromosome movement. **Chromosome 3** has been captured in the initial wave of "instantaneous" biorientation due to its position close to the spindle equator. Blue represents chromosome arms. Orange arrow represents the polar ejection force (PEF) which acts on chromosome arms to push them away from the spindle pole.

CENP-E compared to CENP-Q (t-test p=0.0148; Figure 3.9). Moreover, inhibition of CENP-E with 300 nM GSK925293 gave a similar result, with almost 100% of non-biorientated kinetochores remaining stalled and over 50% of orientated kinetochores able to congress (Figure 3.15). Therefore these biorientated movements are clearly CENP-E independent and CENP-Q dependent.

These CENP-Q-dependent movements are analogous to those described by Skibbens and colleagues 20 years ago. In the Skibbens study, enhanced video-DIC microscopy was used to show that biorientated kinetochores could undergo long duration motion to the spindle equator (Skibbens et al, 1993). This motion is a consequence of one sister (facing the metaphase plate) remaining in a poleward (P) moving state, while the other sister maintains an away-from-the-pole (AP) state. It is now know that these movements are largely powered by the depolymerisation of K-MTs attached to the P moving sister kinetochore (Khodjakov & Rieder, 1996; Dumont et al., 2012). As sister kinetochores lacking CENP-Q are unable to sustain their P or AP state this results in the observed stalling behavior and failure to congress. How CENP-Q contributes to P/AP movements is discussed fully below (see section 5.5).

5.3 How do cells initially move chromosomes to spindle poles?

Existing models state that movement to the pole is necessary to increase the probability of forming microtubule attachments due to the higher density of microtubules at the spindle poles (Skibbens et al., 1993). This poleward transport may be powered by end-on pulling in the case of mono-orientated kinetochore pairs (Khodjakov & Rieder, 1996; Skibbens et al., 1993; Hayden et al., 1990), or dynein motor dependent minus end directed sliding in the case of laterally attached kinetochores (Yang et al, 2007; Li et al., 2007). Once at the pole, kinetochore pairs can then become mono-orientated or biorientated and congress by lateral sliding or depolymerisation-coupled end-on pulling respectively (Kapoor et al., 2006; Skibbens et al., 1993; see Figure 5.1a chromosomes 1 and 2).

However, the unique geometry behind the spindle pole presents kinetochores that become trapped there with a unique challenge. The plus ends of astral microtubules terminate at the cellular cortex, and as a result plus end directed transport of kinetochores moves them towards the cell cortex in the opposite direction from the spindle equator (Figure 5.2a chromosomes 3). As predicted our data shows that CENP-E-dependent sliding of kinetochores moves chromosomes that are behind the pole further away from the pole and towards the plus-end of astral-microtubules (Figure 5.2a chromosomes 3). If this activity were uncontrolled it would result in chromosomes becoming trapped at the cell cortex, unable to congress. Therefore CENP-E activity must be tightly regulated, this regulation could be mediated by the kinase Aurora A (Kim et al., 2010). The kinase is located at the spindle pole, therefore CENP-E bound to kinetochores which are proximal to the spindle pole becomes phosphorylated by Aurora A (Figure 5.2a, b). This phosphorylation of CENP-E has the effect of decreasing the processivity of the kinesin along single microtubules. Thus, it is proposed that CENP-E driven kinetochore movements along astral microtubules, which consist only of single microtubules, are reduced (Kim et al., 2010). In addition to the CENP-E motor activity at the kinetochore, chromosome arms are also pushed away from the pole by the polar ejection force (Levesque & Compton, 2001; Rieder et al., 1986). This force is generated by the chromokinesin Kid (kinesin-10 family), which localises to chromosome arms (Levesque & Compton, 2001). As the kinesin walks towards microtubule plus ends it has the effect of generating anti-poleward force (Stumpff et al., 2012).

Mechanisms must exist that counter these anti-poleward forces and bring chromosomes closer to the spindle poles. Minus end-directed dynein motors can slide laterally attached kinetochores towards the pole (Yang et al, 2007, Li et al., 2007). Based on our observations in mono-polar and bipolar spindles we propose that there is a second CENP-Q-dependent process moving chromosomes poleward (Figure 5.2a chromosome 4). Based on evidence in bipolar spindles, which shows that CENP-Q is required for depolymerisation-coupled pulling and suggest that this process is likely to reflect the effect of CENP-Q on mono-orientated kinetochores. It follows that the failure of biorientated sister pairs to congress to the spindle equator is most likely due to defective

Figure 5.2

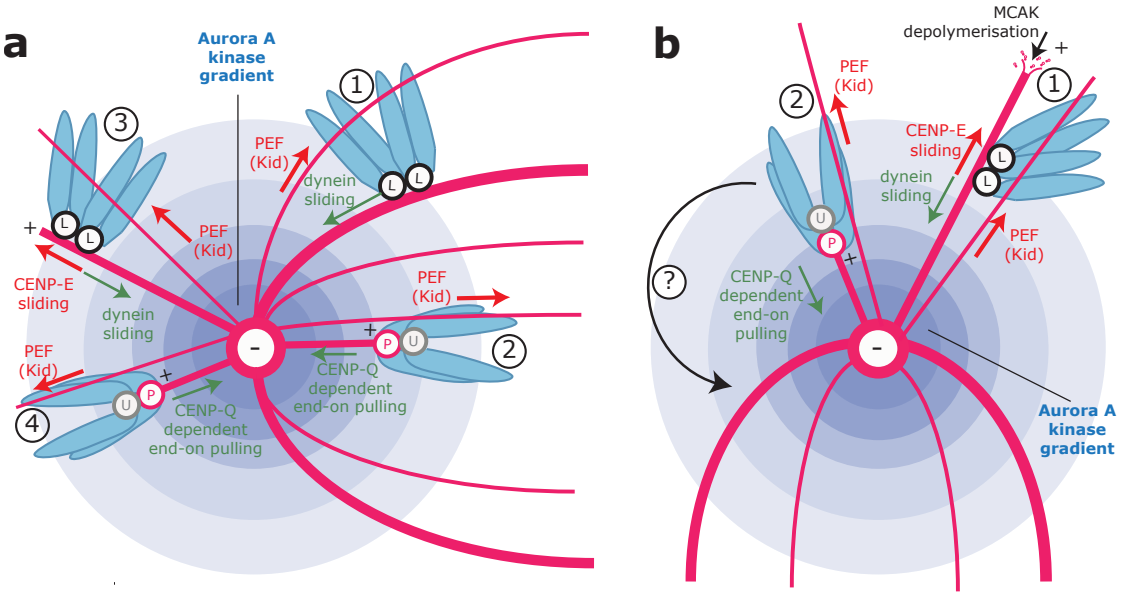

Figure 5.2 Model for chromosome transport to the spindle pole. Long red lines terminating at the red circle represent spindle microtubules terminating at the spindle pole. Red arrows labelled PEF (Kid) represent the polar ejection force (PEF) acting upon chromosome arms to push chromosomes away from the spindle pole. Red arrows labelled "CENP-E sliding" represents CENP-E plus-end directed motor activity. Green arrows represent poleward forces imparted by dynein motor activity or CENP-Q dependent end-on pulling. **(a) Chromosome 1** has no-end on attachments but is laterally attached (L) to an adjacent K-fibre by both kinetochores (shown as black circles). The chromosome is sliding to the spindle pole due to the minus-end directed motor dynein bound at the kinetochore walking along the lattice of the K-fibre to which the kinetochores are attached. **Chromosomes 2** has formed end on attachments at the poleward sister (P, shown in red) and is unattached at the other sister (U, shown in grey). This chromosome is therefore mono-orientated. The chromosome is being transported to the spindle pole by CENP-Q dependent depolymerisation-coupled pulling at the P sister. **Chromosomes 3** has no end on attachments but is laterally attached (L) to an adjacent K-fibre by both kinetochores (shown as black circles). The chromosome is sliding to the spindle pole due to the minus-end directed motor dynein bound at the kinetochore walking along the lattice of the K-fibre to which the kinetochores are attached. If CENP-E were also active at this kinetochore it would act in opposition to the minus-end directed dynein, as would the PEF. **Chromosome 4** is in the same state as Chromosome 2 but is behind the spindle pole and is being transported towards the spindle pole by CENP-Q dependent depolymerisation-coupled end-on pulling. **(b)** Model of chromosome transition between lateral and end-on attachment. **Chromosome 1** is behind the spindle pole and is laterally attached (L) to a microtubule at both kinetochores (black circles). The chromosome is being carried away from the spindle pole by CENP-E motor activity. PEF also acts to push the chromosome arms away from the pole whist dynein activity acts to bring chromosomes closer to the spindle pole. The Aurora A kinase activity gradient at the pole prevents processive CENP-E motor activity along single astral microtubules, thus reducing the distance that the chromosome is carried towards the astral microtubule plus-ends (Kim et al., 2010). MCAK-mediated depolymerisation activity acts to shorten the astral microtubule to the point of lateral attachment (Shrestha & Draviam, 2013). Chromosomes can then switch to end-on attachment due to the proximity of the microtubule end to the kinetochore. **Chromosome 2** has made the transition to end-on attachment at the P sister kinetochore (red circle) but remains unattached at the other sister (U, grey circle). The chromosome is being brought proximal to the pole by CENP-Q dependent depolymerisation coupled pulling. The '?' and arrow denotes the unknown mechanism by which the chromosome becomes laterally attached or biorientated, both presumably requiring rotation about the spindle pole.

P-kinetochore movement (depolymerisation-coupled pulling), rather than AP-kinetochore (pushing) movement. This model is consistent with the current view that the force to drive kinetochore/chromosome movement is generated at the poleward moving kinetochore (Khodjakov & Rieder, 1996; Dumont et al., 2012).

5.4 Converting between attachment states

For CENP-Q dependent end-on pulling of chromosomes at the spindle pole they must first form end-on attachments. For this reason it will be important to determine how kinetochores are converted between lateral and end-on attached states. In this regard, recent work has revealed that the transition from lateral attachment to an end-on configuration requires the microtubule depolymerase MCAK and CENP-E (Shrestha & Draviam, 2013). MCAK is proposed to depolymerise the microtubules back to the kinetochore, which is held in a laterally attached state by CENP-E (Figure 5.2b chromosome 1). Lateral attachments rarely release, therefore this depolymerisation is essential as it promotes mono-orientation of the kinetochore by bringing the plus end of the microtubule proximal to the kinetochore (Figure 5.2b chromosome 2). This work, along with our own findings, could explain why the polar kinetochores in CENP-E depleted cells are unable to biorientate. Our data shows that polar kinetochores (and those around a monopole) are positioned closer to the spindle pole in CENP-E depleted cells, this is further from the plus-ends of microtubules due to the absence of CENP-E plus end directed motor activity. Thus the probability of the astral-microtubule shrinking back far enough to reach the kinetochore is reduced. However, Shrestha and Draviam suggest that the primary role of CENP-E may be the maintenance of stable lateral attachments to allow efficient release of wall contacts and end-on attachment formation (Shrestha & Draviam, 2013). It is also speculated in this study that the conversion from lateral to end-on attachment may be a gradual process and that MCAK may also be important for promoting end-on attachments by removing curved protofilaments that may otherwise prevent this process. Indeed, other studies have shown that the absence of MCAK prevents the formation of normal end-

on attachments, with its depletion leading to perturbed chromosome congression due to improper kinetochore attachments (Kline-Smith et al., 2004).

Overall, current data suggests that kinetochores utilise poleward and anti-poleward mechanisms to position themselves at the optimum distance from the spindle pole to promote biorientation. However, much remains unknown about how polar chromosomes achieve biorientation after forming end-on attachments behind the pole (Figure 5.2b – step denoted by "?"). Previous work in *D. melanogaster* has shown that the polar ejection force generated by the chromokinesin Nod (kinesisn-10) is able maintain stable monotelic end-on attachments (Cane et al., 2013). These attachments are maintained because the anti-poleward force generated by the Nod kinesin on chromosome arms generates sufficient tension upon the monotelic attachments to prevent error correction by Aurora B kinase. Such a stabilisation mechanism may explain why monotelic attachments, through depolymerisation-coupled pulling, are able to move poleward without being released by Aurora B. If this is the case, then the question remains; how do these kinetochores switch into a biorientated state?

One potential mechanism would be that chromosomes reaching the pole were able to form additional lateral attachments to nearby K-fibres via the unattached sister. These kinetochores could then effectively "walk out" from behind the pole driven by CENP-E lateral sliding (Kapoor et al., 2006). The high Aurora A kinase activity around the pole may also ensure that this CENP-E driven sliding was directed along K-fibres rather than along astral microtubules (Kim et al., 2010; see chapter 1, section 1.4.2). Alternatively, biorientation could be achieved by releasing monotelic attachments once chromosomes have reached close proximity to the spindle pole. Once unattached, the sister kinetochores would be able to form new, potentially biorientated, attachments. However, this mechanism would require the tight control of the position at which the chromosome was released. There is little known about how monotelic attachment release could be tightly controlled based on position relative to the pole. One idea is that as the chromosome approaches the pole the tension generated by the polar ejection force could be reduced, possibly

mediated by Aurora A phosphorylation. This would reduce inter-kinetochore tension and allow attachment destabilisation by the well characterised Aurora B mediated error correction pathway (Welburn et al., 2010; Akiyosh et al., 2010; reviewed in Lampson & Cheeseman, 2011). However, there is presently no evidence that the kinesin-10 family proteins responsible for generating the PEF are phosphorylated by Aurora A. An alternative possibility is that as chromosomes approach the spindle pole the stability of monotelic attachments are reduced directly by the high levels Aurora A kinase activity rather than by Aurora B. Indeed there is evidence of overlapping roles of Aurora A and Aurora B as these kinases have many phosphorylation targets in common (Hochegger et al., 2013), and both kinases have very similar consensus target sequences (Alexander et al., 2011).

5.5 How could CENP-Q contribute to depolymerisation-coupled pulling?

Once an end-on attached state has been reached our data suggest that CENP-Q is required for normal depolymerisation-coupled pulling. However, the reason for the requirement of CENP-Q is unknown. One idea is that the CENP-Q protein directly regulates or coordinates the dynamics of microtubule plus-ends within the K-fibre (see schematic in Figure 5.3a, b). This idea is supported by evidence, which shows that CENP-Q is able to bind to microtubules *in vitro* (Amaro et al., 2010). Furthermore, recent work in our lab also shows that CENP-Q is able to directly modulate microtubule dynamics *in vitro* (Samora C.P., PhD thesis, 2012). Total internal reflection microscopy (TIRF) assays show that addition of purified CENP-Q to dynamic microtubules increases the transition frequency between catastrophe and rescue events. This is consistent with a model in which CENP-Q increases the off-rate or exchange rate of tubulin heterodimers at K-fibre microtubule plus-ends (Figure 5.3a).

However, *in vitro* TIRF assays also show that purified CENP-Q decreases the speed of microtubule growth and shrinkage and that CENP-Q is able to track depolymerising microtubule plus-ends

Figure 5.3

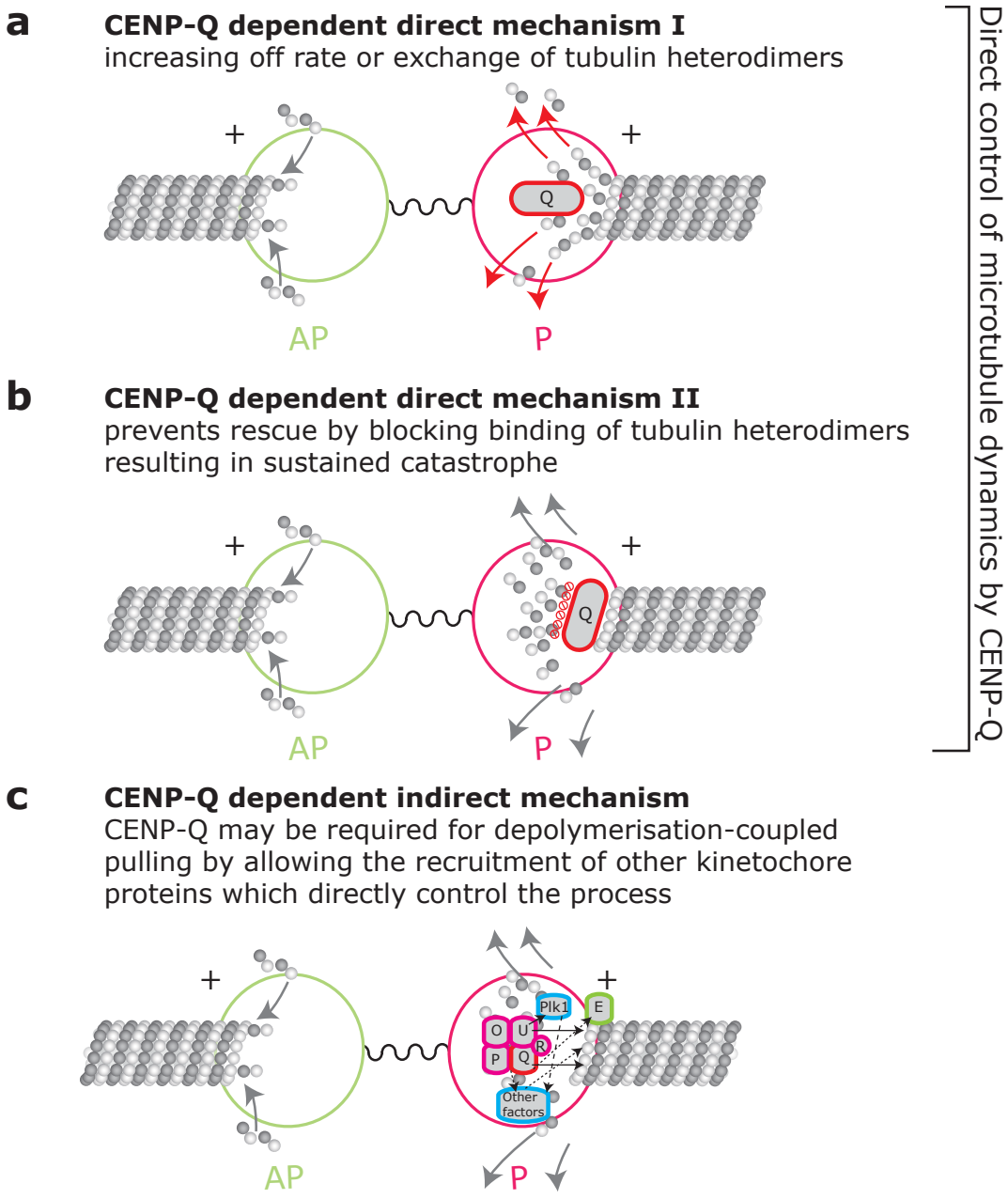

Figure 5.3 Model mechanisms for regulation of depolymerisation-coupled pulling by CENP-Q. Circles represent kinetochores, spring represents inter-sister kinetochore linkage. Grey and white spheres represent tubulin heterodimers forming microtubules. **(a)** One possible model for CENP-Q activity is that CENP-Q may increase the off rate or exchange rate of tubulin heterodimers facilitating sustained catastrophe of the K-fibre attached to the P kinetochore. **(b)** Alternatively CENP-Q may sustain depolymerisation by preventing addition of new tubulin heterodimers, and thus could help sustain depolymerisation events required for depolymerisation-coupled pulling by preventing rescue events requiring reformation of microtubule GTP-caps. **(C)** The role of CENP-Q in the process of depolymerisation-coupled pulling may be an indirect one. CENP-Q may be required to recruit additional factors which directly or indirectly regulate depolymerisation-coupled pulling.

(Samora C.P., PhD thesis, 2012). This data may be consistent with an alternative mechanism; CENP-Q could directly regulate microtubule dynamics by “capping” microtubule plus-ends and block the addition of new tubulin heterodimers (Figure 5.3b). It is possible this activity could have the effect of preventing rescue events during microtubule depolymerisation, ensuring that the K-fibre at the P sister was kept in a depolymerising state. Such sustained depolymerisation events would be required to power sustained or “persistent” kinetochore movements in a single direction powered by depolymerisation-coupled pulling.

These models, in which CENP-Q directly regulates K-MT dynamics are supported by live cell assays, which show that depletion of CENP-Q reduces the turnover of K-MTs in live cells (Samora C.P., PhD thesis, 2012). However, it has previously been shown that CENP-E depletion also lowers the turnover of the K-MT population in a similar manner to the CENP-Q depletion (Maffini et al., 2009). As CENP-E is also absent from kinetochores in CENP-Q depleted cells we are presently unable to attribute the reduced K-fibre plus-end turnover specifically to the loss of CENP-Q. However, depletion of CENP-Q does not affect the poleward flux of tubulin through the spindle where as depletion of CENP-E results in a loss of poleward flux (Maffini et al., 2009), suggesting that the effect of CENP-Q depletion on spindle dynamics is distinct from the CENP-E depletion phenotype.

The alternative possibility is that CENP-Q indirectly affects depolymerisation-coupled pulling by modulating the binding of other factors to kinetochores (Figure 5.3c). Loss of CENP-Q destabilises the binding of four CCAN proteins (CENP-O/P/U/R) with which it forms the CENP-O sub-complex (Hori et al., 2008b; Figure 5.4a, b). Of these proteins, CENP-U can also bind microtubules *in vitro* (Hua et al., 2011), and could conceivably contribute to the observed phenotypes, although at present there is no evidence that CENP-U modulates microtubule dynamics. Based on our finding that CENP-E is absent from the kinetochores, it is also most likely that the same is true of the Clasp proteins; CLASP1 and CLASP2, as they are dependent upon CENP-E for kinetochore binding (Maffini et al., 2009; Figure 5.4a, b). It has also been shown that the effect of losing

Figure 5.4

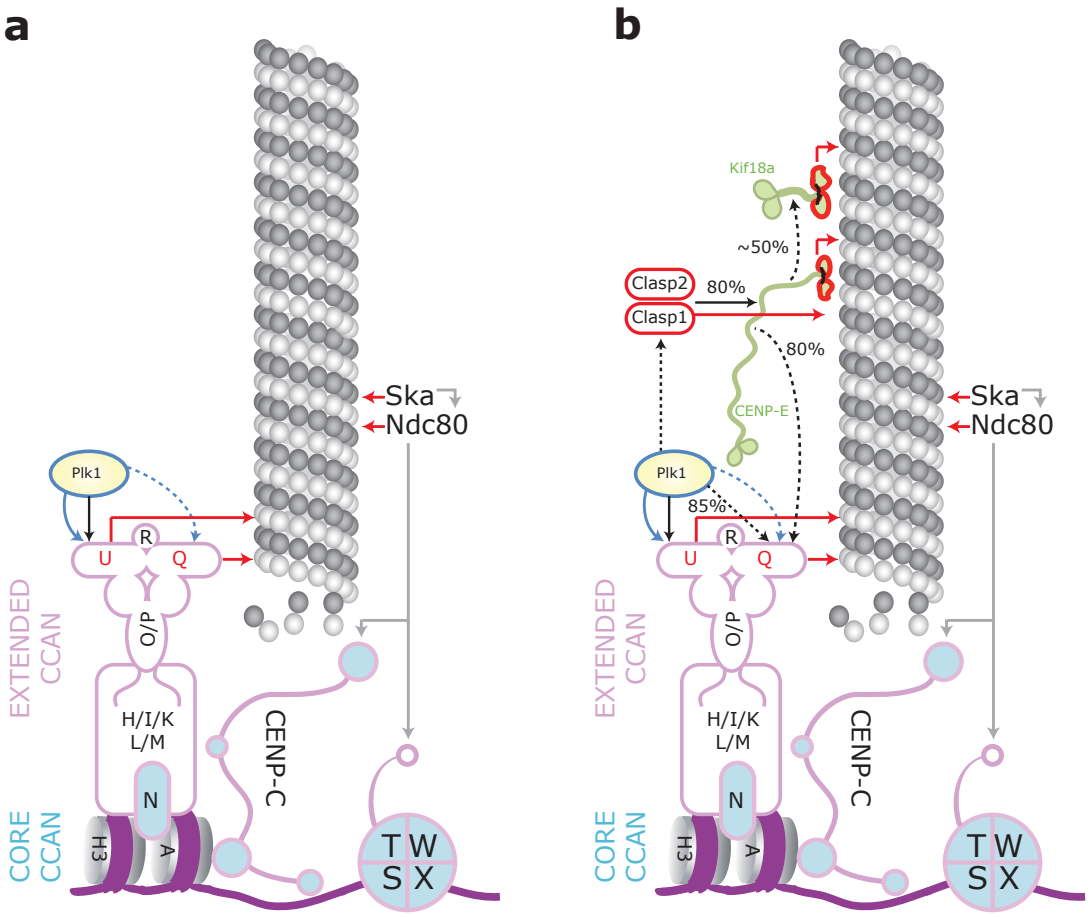

Figure 5.4 Further insight into CCAN interactions and loading dependencies. **(a)** Represents CCAN interactions with kinetochore proteins and loading dependencies prior to this thesis. **(b)** Represents dependencies and interactions discovered during this thesis or now known to be linked to, or relevant to, the CCAN as a result of the findings of this thesis. **Key**- Blue arrows represent phosphorylation events. CCAN proteins are represented by pink outlines, blue infilling denotes core CCAN proteins. Direct interactions are represented by solid grey and black lines. Loading dependencies which are not direct or not known to be direct are shown by black dashed lines. Red lines represent microtubule binding. Blue solid lines represent direct phosphorylation events, dashed blue lines represent phosphorylation events which are not known to be direct. Purple lines represent DNA, CENP-A and H3-containing histones are represented by grey cylinders. Grey spheres represent tubulin heterodimers associating to form a K-fibre microtubule.

CLASP1 from kinetochores has the effect of perturbing both K-MT plus-end turnover and poleward flux (Maffini et al., 2009). Furthermore, loss of CLASP1 is partially required for kinetochore loading of polo like kinase (Plk) 1 (Maia et al., 2012; Figure 5.4 b).

5.6 Potential regulation by phosphorylation

The situation is further complicated as CENP-U (CENP-50/PBIP1) represents the major kinetochore-loading platform for Plk1 to kinetochores (Kang et al., 2011). This interaction is essential for facilitating the phosphorylation of both CENP-U and CENP-Q by Plk1 (Kang et al., 2011). We found that Plk1 does not bind kinetochores in CENP-Q depleted cells (Figure 5.4b and Figure 3.4c). This dependency likely reflects the interdependency of the CENP-O/P/Q/U proteins for kinetochore loading (Hori et al., 2008b), i.e. depletion of CENP-Q causes loss of CENP-U, which is the primary kinetochore-binding site of Plk1.

Loss of Plk1 does not, however, explain the loss of CENP-E from kinetochores since CENP-E remains present at kinetochores following inhibition of Plk1 (Sumara et al., 2004). However, the loss of kinetochore bound Plk1 could still contribute to the observed chromosome congression defects in CENP-Q depleted cells. Previous studies have shown that loss of Plk1 from cells or inhibiting the kinase with the small molecule inhibitor BI2536 results in failed centrosome maturation and separation, resulting in monopolar spindles (Sumara et al., 2004; Lenart et al., 2007; reviewed in Petronczki et al., 2008). However, in CENP-Q depleted cells Plk1 is lost specifically from kinetochores and can still localise to the spindle poles (Figure 3.4c). Studies have shown that loss of Plk1 specifically from kinetochores does not prevent centrosome separation and bipolar spindle formation, although it does lead to congression defects (Hanisch et al., 2005). Visual inspection of these images suggests that mis-aligned kinetochores are polar, similar to those observed in CENP-Q depleted cells. Thus, we cannot exclude the possibility that loss of Plk1 from kinetochores contributes to the chromosome congression phenotype observed in CENP-Q depleted cells. Interestingly, CENP-Q is phosphorylated *in vivo* on serine 50 (Rigbolt et al., 2011),

and serine 249 (Olsen et al., 2010). The former site (DLSSE) being a possible match for the polo kinase consensus sequence ([D/N/E]-x-[T/S]-[I/L/M/V/F/W/Y]; Alexander et al., 2011), although it is known that the Plk1 consensus is also simerlar to that of Mps1 (Dou et al., 2011). I have conducted some preliminary work to investigate the possibility that phosphorylation of these sites (potentially by Plk1) is required for normal CENP-Q function. Expression of a CENP-Q-eGFP transgene, in which these sites, along with their immediate neighbour serine residues, were mutated to alanine, failed to rescue the polar chromosome phenotype of *CENP-Q* siRNA (Figure 5.5 for full details). Visual inspection of CENP-E immuno-staining in these cells also suggested that this construct was unable to restore kinetochore localisation of the kinesin (Figure 5.5b). Moreover, expression of a phosphomimetic version of CENP-Q in which these serine residues were mutated to aspartic acid was able to rescue the phenotype (see Figure 5.5 for full details). Visual inspection of CENP-E immuno-staining in these cells suggested that CENP-E kinetochore binding was partly restored (Figure 5.5b). This suggests that phosphorylation is important for CENP-Q function and that constitutive phosphorylation is sufficient to maintain activity. Clearly, future work will involve identifying whether this is through Plk1 activity and how these phosphorylation events alter the function of CENP-Q. Because CENP-U must be kinetochore bound (CENP-Q would not bind kinetochores in its absence) we predict that Plk1 is bound to kinetochores in the CENP-Q mutant in which the potentially phosphoralated serine residues were substituted with alanine. This would rule out Plk1-dependent phosphorylation of other kinetochore proteins being the cause of the chromosome congression defects in CENP-Q depleted cells. In this regard, tethering Plk1 at kinetochores slows the turnover of K-MT dynamics, whereas the opposite is true of CENP-Q as loss of the protein from kinetochores slows K-MT plus-end dynamics (Samora C.P., PhD thesis, 2012; Liu et al, 2012). Thus, at least some aspects of the CENP-Q depletion phenotype are independent of Plk1 activity.

5.7 Molecular mechanism required for CENP-E/Q recruitment

As described above, CENP-E requires CENP-Q for kinetochore binding; however, it seems unlikely that CENP-Q recruits CENP-E via (direct or indirect) protein-protein interactions. This reasoning is

based on two lines of evidence: (1) CENP-E remains bound to kinetochores in CENP-H or CENP-L depleted cells, both of which being CCAN proteins required for CENP-Q binding to kinetochores (McClelland et al., 2007; Amaro et al., 2010; Mchedlishvili et al., 2012). (2) The binding of CENP-E to kinetochores in CENP-Q-depleted cells is partially restored on treatment with nocodazole or co-depletion of CENP-H (this study; Figure 3.11 & Figure 3.13). Thus, CENP-E only requires CENP-Q when K-MTs are present. One possibility is that the slower turnover of K-MTs in the absence of CENP-Q has a negative effect on CENP-E binding, an effect that is suppressed by depolymerising K-MTs with nocodazole. This mechanism is consistent with the observation that there is a reduction in CENP-E kinetochore-binding as cells move from metaphase to anaphase, which is correlated with a reduction in K-MT turnover (Zhai et al, 1995). Our ability to partially rescue CENP-E levels in CENP-Q depleted cells by co-depleting CENP-H, which increases K-fibre plus-end turnover (Amaro et al., 2010), further supports this idea (Figure 3.13). However, the relationship between K-MT stabilisation and CENP-E kinetochore binding is not as simple as it may first appear, as CENP-E still binds kinetochores in taxol-treated cells (this study Figure 3.11 and Hoffman et al., 2001). One possibility is that that the rescue of CENP-E levels by nocodazole reflects the generation of additional CENP-E binding sites at the kinetochore that are independent of CENP-Q.

Work by Huang and colleagues show that CENP-E kinetochore loading is also dependent upon Kif18a, a report that is confirmed by our findings in chapter 3 (Figure 3.13; Huang et al., 2009). It is therefore possible that CENP-Q depletion prevents CENP-E kinetochore binding by preventing the binding of Kif18a to kinetochores. However, this seems unlikely as CENP-Q is also absent in CENP-H depleted cells but CENP-E remains kinetochore bound (Amaro et al., 2010). The CENP-Q depletion phenotype is also less severe than the Kif18a depletion phenotype; CENP-Q depleted cells are able to form a metaphase plate whereas many Kif18a depleted cells do not (Figure 3.13; Mayr et al., 2007; Huang et al., 2009; Mayr et al., 2011; Stumpff & Wordeman, 2007). CENP-Q depletion also has the opposite effect on K-MT turnover to that observed after Kif18a depletion, with Kif18a depletion increasing K-MT plus-end turnover and CENP-Q depletion reducing it

Figure 5.5

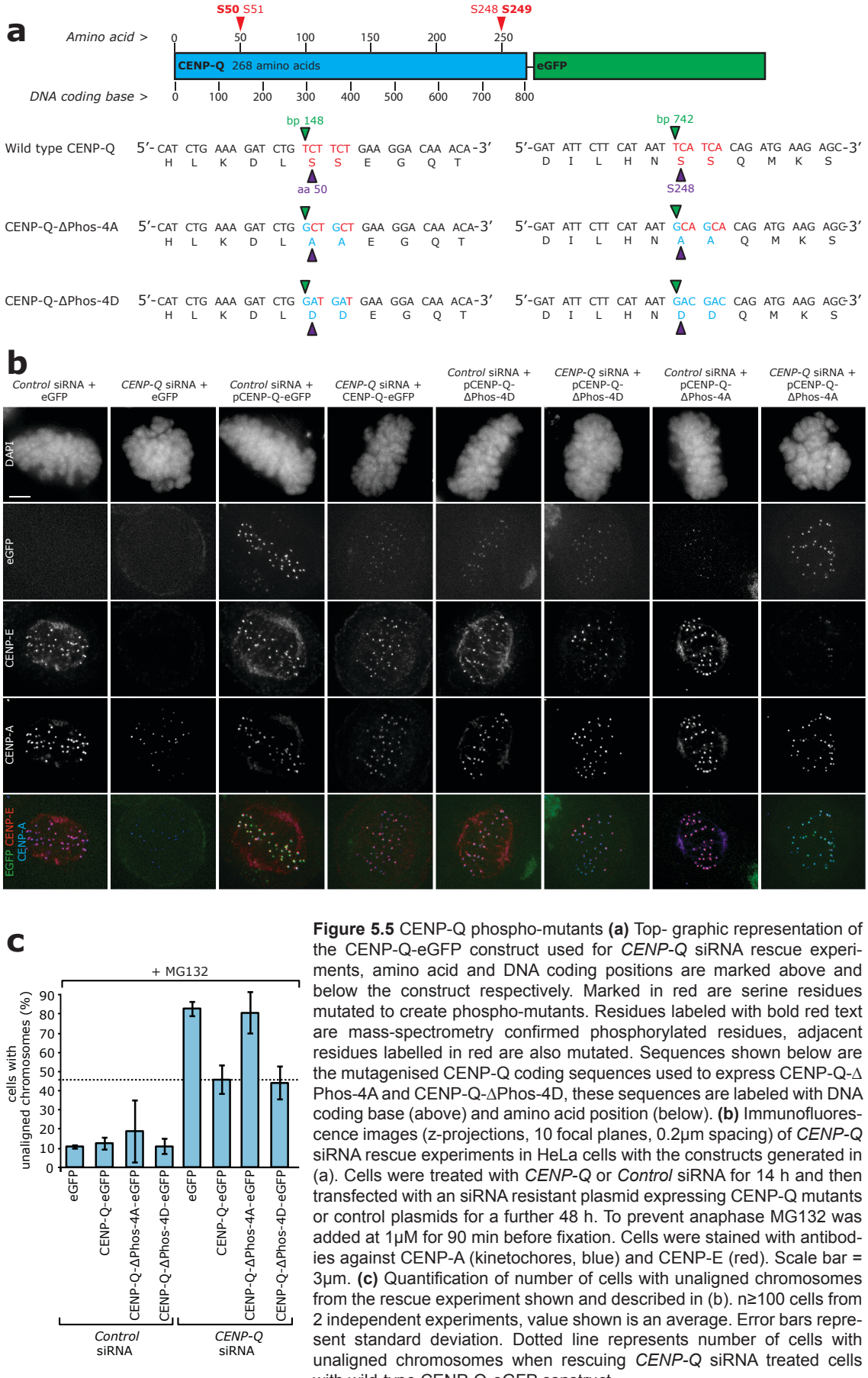

Figure 5.5 CENP-Q phospho-mutants **(a)** Top- graphic representation of the CENP-Q-eGFP construct used for *CENP-Q* siRNA rescue experiments, amino acid and DNA coding positions are marked above and below the construct respectively. Marked in red are serine residues mutated to create phospho-mutants. Residues labeled with bold red text are mass-spectrometry confirmed phosphorylated residues, adjacent residues labelled in red are also mutated. Sequences shown below are the mutagenised CENP-Q coding sequences used to express CENP-Q-ΔPhos-4A and CENP-Q-ΔPhos-4D, these sequences are labeled with DNA coding base (above) and amino acid position (below). **(b)** Immunofluorescence images (z-projections, 10 focal planes, 0.2µm spacing) of *CENP-Q* siRNA rescue experiments in HeLa cells with the constructs generated in (a). Cells were treated with *CENP-Q* or *Control* siRNA for 14 h and then transfected with an siRNA resistant plasmid expressing CENP-Q mutants or control plasmids for a further 48 h. To prevent anaphase MG132 was added at 1µM for 90 min before fixation. Cells were stained with antibodies against CENP-A (kinetochores, blue) and CENP-E (red). Scale bar = 3µm. **(c)** Quantification of number of cells with unaligned chromosomes from the rescue experiment shown and described in (b). n≥100 cells from 2 independent experiments, value shown is an average. Error bars represent standard deviation. Dotted line represents number of cells with unaligned chromosomes when rescuing *CENP-Q* siRNA treated cells with wild-type CENP-Q-eGFP construct.

(Manning et al., 2010; Samora C.P., PhD thesis, 2012). This finding, along with those discussed above, show that there are clearly a series of complex positive and negative feedbacks between the CCAN, microtubule dynamics and MAP/motor binding to kinetochores (summarised in Figure 5.4).

5.8 CENP-E is not simply a congression motor.

Our data show that kinetochores in CENP-E depleted cells are still able to congress by end-on pulling (Figure 3.15 & 3.16) but are not able to undergo the oscillatory movements normally present at metaphase (Figure 4.3). Unlike depletion of CENP-Q the depletion or inhibition of CENP-E does not disrupt the organisation of chromosomes at the metaphase plate, instead resulting in a decrease in metaphase plate width. This key difference from CENP-Q depleted cells likely reflect our observation that in CENP-Q depleted cells both lateral sliding and end-on pulling mechanisms are perturbed, whilst end-on pulling mechanisms are still functional in CENP-E depleted cells. It is possible that this end-on pulling activity is sufficient to drive the tight alignment of biorientated chromosomes at the metaphase plate. Indeed, mean squared displacement (MSD) analysis of kinetochore movement in CENP-E depleted cells shows that kinetochores move less randomly than those in CENP-Q depleted cells, despite lacking oscillations (Figure 4.6c). Thus, kinetochores in CENP-E depleted or inhibited are capable of sufficient directed motion in the absence of oscillations to align at the metaphase. It is possible that the extreme alignment of kinetochores at the metaphase plate in these cells results from the extra time kinetochores have to align due to the mitotic arrest resulting from the polar chromosomes caused by the absence of CENP-E activity. This hyper-alignment in the absence of oscillations almost certainly gives rise to the biomodal distribution observed in kinetochore normal position relative to the metaphase plate. This distribution is not seen in control depleted cells because the kinetochores are not as tightly aligned at the plate, additionally kinetochores in control depleted cells oscillate and it is likely that these oscillations would disrupt any bimodality in kinetochore position.

Our data also indicate that much lower levels of CENP-E are needed to maintain oscillations than to facilitate congression by lateral sliding, as partial depletions of CENP-E did not perturb oscillations but did result in the accumulation of polar chromosomes (Figure 4.4). Taken together, these results suggest that CENP-E is required for force-generation when kinetochores are biorientated at the spindle equator, whilst the protein is dispensable for the generation of force during congression of unaligned biorientated sister kinetochores by depolymerisation-coupled pulling. This finding is in contrast to recent work, which showed that CENP-E was required for kinetochores to track depolymerising microtubules (Gudimchuk et al., 2013). However, in the Gudimchuk study these depolymerisation events were observed in mono-polar spindles and were induced by the addition of nocodazole, it is therefore possible that the gross nature of these drug induced depolymerisation events are the cause of this difference. It would also be interesting to ascertain whether the depletion of CENP-Q could also prevent kinetochores tracking depolymerising microtubules under these conditions.

Previous work has shown that CENP-E levels decrease at kinetochores as they congress (Hoffman et al., 2001) and this may go someway to explaining our observation that aligned sister kinetochores are very robust to changes in motor number compared to those that are uncongressed. Thus, a limited number of CENP-E motors are sufficient for aligned biorientated kinetochores to generate normal force. This is in contrast to kinetochores lacking the CENP-Q subunit of CCAN, which are unable to generate depolymerisation-coupled forces at both congressed and uncongressed sister-kinetochore pairs.

The key remaining question is: why would depletion of the motor affect the oscillation of biorientated kinetochores in the metaphase plate? We suggest that biorientated kinetochores may undergo a switch during congression into a mode that requires CENP-E motor activity. This would explain why CENP-E is not required for congression by end-on pulling but is required for metaphase oscillations. Understanding the nature of the role of CENP-E in facilitating these oscillations will be an important future direction. One potential mechanism is that the protein is

required to modulate the tightly controlled microtubule dynamics that give rise to oscillations, perhaps by ensuring sustained polymerisation at the AP sister kinetochore. This could reduce the frequency of directional switch events by preventing the K-fibre attached to the AP kinetochore from switching into a depolymerising state (Figure 5.6a). This idea is supported by *in vitro* evidence, which shows that CENP-E has a stabilizing effect on dynamic microtubules increasing plus-end elongation (Sardar et al., 2010). *In vivo* it has been shown that depletion of CENP-E reduces mitotic spindle length, suggesting reduced spindle microtubule polymerisation (Maffini et al., 2009). Although *in vitro* evidence suggests that this role may be a direct one, it is also possible that such a function could be a result of CENP-E dependent recruitment of other factors *in vivo* (represented by black box in Figure 5.6a). An alternative possibility is that CENP-E acts to increase or control K-fibre plus-end turnover to allow modulation of growth and catastrophe events by other factors (Figure 5.6b). In support of this idea it is known that depletion of CENP-E results in decreased K-MT plus-end turnover (Maffini et al., 2009). However, depletion of CLASP proteins, which are also dependent upon CENP-E for kinetochore binding also have the same effect on K-MT plus-end turnover. Therefore this model should also consider an indirect role for CENP-E (Figure 5.6b, represented by black box).

5.9 Chronic inhibition of CENP-E results in high tension between kinetochore pairs

Locking CENP-E into a rigor state with the inhibitor GSK923295 also disrupted oscillations after both acute (1 hr) and chronic (14 hr) treatments. Chronic treatments with 300 nM GSK923295 also led to hyper-stretching of the inter-sister linkage, where as acute treatments resulted in only a minimal increase in inter-kinetochore distance. The reason for this dramatic shift in force generation upon chronic treatment with GSK923295 is unclear. We also see a large reduction in the kinetochore bound levels of the motor after 14 hr treatment with the inhibitor (Figure 4.5). This reduction was also observed after treatment of cells with the GSK923295 after only 15 min (Gudimchuk et al., 2013). The levels of the motor are however greatly enriched on the polar

Figure 5.6

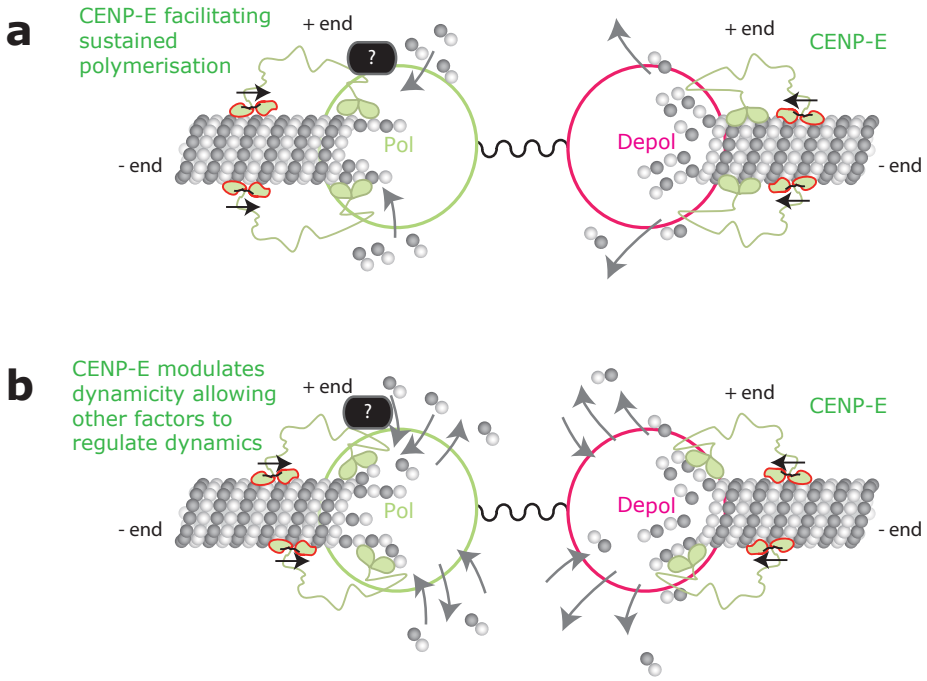

Figure 5.6 Potential model for the role of CENP-E in kinetochore oscillations at the metaphase plate. Circles represent kinetochores, springs represent inter-sister kinetochore linkage. Grey and white sphere represent tubulin heterodimers forming microtubules. CENP-E motor dimers are represented as cartoons in green, with the red outline representing the motor domain. **(a)** CENP-E may be required for sustained polymerisation of the AP sister kinetochore, perhaps by stabilising newly formed protofilaments within the growing K-fibre microtubules. If this process were disrupted it may result in the K-fibre on the AP sister switching into a depolymerising state frequently, thus disrupting the normal K-fibre dynamics that would give rise to coherent movement, and therefore oscillations. This mechanism could also be indirect, with CENP-E recruiting other factors (represented by the black box). **(b)** CENP-E may be required to modulate dynamics at both kinetochores, e.g. increasing both on and off rates of tubulin heterodimers. This increase in dynamics may be required for other regulatory factors to modulate K-fibre dynamics giving rise to oscillations. This mechanism could also be indirect, with CENP-E recruiting other factors such as CLASP proteins (represented by the black box). This model is consistent with the observations that CENP-E and CLASP depletion reduce K-fibre microtubule plus-end turnover (Maffini et al., 2009).

chromosomes, which result from inhibition of CENP-E (Figure 4.5).

The reason for the reduction of CENP-E at aligned kinetochores is currently unknown, one possibility is that the motor is stripped from the kinetochore by K-fibre poleward flux, as the rigor bound motor would no longer be able to walk against the direction of the flux. An alternative possibility is that the motor loads to the kinetochores by walking to the plus-end of K-fibres, which are coincident with the kinetochore and therefore allows for efficient kinetochore loading. *In vitro* experiments demonstrate that CENP-E motors are able to autonomously track polymerising/depolymerising microtubule tips (Gudimchuk et al., 2013), a property which would be independent of kinetochore binding. However, this end tracking behavior requires both an active motor domain and the C-terminal MT binding domain. It is therefore possible that at least part of the decrease in CENP-E levels at kinetochores detected by immunofluorescence in the presence of GSK923295, results from loss of a kinetochore proximal population of CENP-E at K-fibre ends rather than kinetochore bound CENP-E. As CENP-E requires an active motor domain to track microtubule plus ends the addition of the inhibitor would mean that any CENP-E molecules that were not kinetochore bound but where instead tracking the plus-ends of microtubules proximal to the kinetochore would be lost.

The surprising hyper-stretching of sister kinetochores after 14 hr treatment with the CENP-E inhibitor GSK923295 likely represents increased tension between sisters (Figure 4.4). However, at present we do not know the cause of this increased tension and why the effect is only seen after 14 hr treatment with GSK923295. Perhaps the simplest explanation for this phenotype is that the rigor CENP-E motors form fixed links between kinetochore microtubules and the kinetochore (Figure 5.7b, representation of DMSO control in a). As these microtubules treadmill through minus-end depolymerisation, excess pulling force would be exerted on the sister kinetochores by the C-terminal kinetochore-binding domain as the CENP-E motor domain is pulled towards the pole. However, the low remaining levels of CENP-E at kinetochores after GSK923295 treatment makes this idea seem less likely as each remaining motor would have to transfer a large amount of force

Figure 5.7

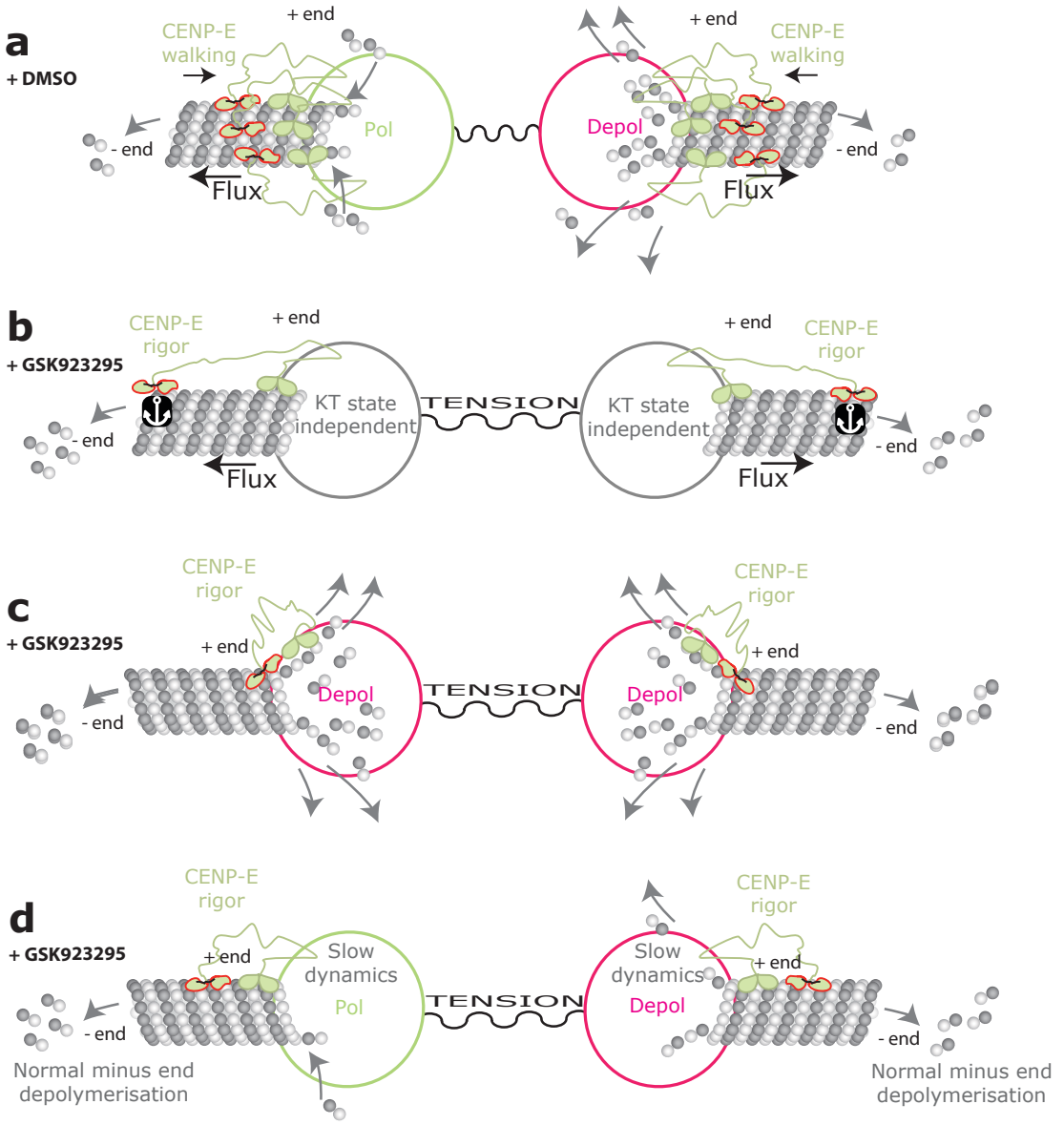

Figure 5.7 Potential models for hyper-tension resulting from GSK923295 treatment. Circles represent kinetochores, springs represent inter-sister kinetochore linkage. Grey and white sphere represent tubulin heterodimers forming microtubules. CENP-E motor dimers are represented as cartoons in green, with the red outline representing the motor domain. **(a)** Represents kinetochores in control cells. CENP-E is bound at the kinetochore where its kinesin motor activity allows it to walk towards the microtubule plus-ends, this has been propsed to operate as a dynamic coupler (Kim et al., 2008). CENP-E is therefore is not displaced or pulled by the poleward flux of K-fibre microtubules. **(b-d)** Possible models for the observed effects of GSK923295 which locks CENP-E into a rigor state (Wood et al., 2010). **(b)** Rigor-bound CENP-E motor is pulled towards the spindle poles by the treadmilling within the K-fibre thus generating excess poleward force amd hyper-stretching of the sister-sister linkage. This could also result in the stripping of the motor and therefore the observed low kinetochore-bound levels of CENP-E. **(c)** Rigor microtubule-bound CENP-E motor could switch K-fibres into a depolymerisating state at both sisters, causing both sisters to move in their respective poleward directions. This would result in a build up of tension between the two sisters. **(d)** The loss of CENP-E from kinetochores results in decreased plus end K-fibre polymerisation whilst depolymerisation at the pole proceeds at a normal rate. The net effect would be to shorten K-fibres and impart pulling across sister-kinetochores.

to the kinetochore. Furthermore, one would also expect this process would occur quickly if flux pulling CENP-E motors were the cause, and after 1 hr treatment kinetochores only exhibit a minor increase in inter-sister distance.

An alternative possibility is that treatment with GSK923295 switches K-fibres attached to both kinetochores into a net depolymerising state (Figure 5.7c). If this were the case, switching both K-fibres into a depolymerisng state would have the effect of pulling both sisters towards their respective poles, resulting in increased inter-sister kinetochore tension. This switch to depolymerisation at the K-fibres could conceivably result from the rigor CENP-E motors inducing depolymerisation. However, such an effect would be unlikely to result from loss of CENP-E from kinetochores as depletion of CENP-E does not result in increased inter-sister kinetochore stretching. A further potential mechanism for the hyper stretching phenotype is that the CENP-E motors remaining at the kinetochore, in a rigor state, have the effect of slowing plus-end polymerisation whilst leaving depolymerisation at the pole unperturbed (Figure 5.7d). This would have the effect of shrinking the K-fibres and thus causing the attached kinetochores to be pulled towards their respective poles, generating tension. Other work has shown that a prolonged mitotic arrest can result in cohesin ring fatigue, eventually resulting in sister chromatid separation (Daum et al., 2011). However, this is unlikely to be the cause of increased inter-kinetochore distance after 14 hr GSK923295 treatment, as we do not see kinetochore pairs part, additionally DNA staining in immunofluorescence experiments shows that chromosomes are intact. Further more, CENP-E and CENP-Q depleted cells are also subject to similar mitotic arrests but do not exhibit such increased inter-kinetochore distances.

5.10 Future directions

In this thesis I have shown that CENP-Q is required for depolymerisation-coupled pulling to drive congression of biorientated chromosomes. I have also shown that kinetochore bound CENP-Q is required to recruit CENP-E to kinetochores to facilitate congression by lateral sliding. Both CENP-

Q and CENP-E are required to drive normal kinetochore metaphase oscillations, although the levels of CENP-E required to drive oscillation are lower than those required to power congression by lateral sliding. Despite these findings there are many interesting questions remaining to form the basis of future work. One of the most important areas on which to focus will be to understand which aspects of the CENP-Q phenotype result directly from depletion of CENP-Q and those that may be the result of losing other protein components that are dependent on CENP-Q for kinetochore-binding (e.g. CENP-O/U/P, CENP-E, PLK1, CLASP1). Whether binding these factors is through physical interaction or indirectly through changes in K-MT dynamcis will also need investigating. A second key area is the potential phospho-regulation of CENP-Q (and other members of the CENP-O sub-complex). This will involve determining how such modifications affect the function of the protein *in vitro* and *in vivo* and identifiying which kinases are involved. Finally, our data points to kinetochores being in different states when congressing: i.e. CENP-E activity is only required for depolymerisation-coupled pulling when chromosomes are aligned. It will be important to determine whether this reflects differences in kinetochore composition or is a consequence of posttranslational modification. In this regard, it remains unknown how biorientated kinetochores “know” that they have reached the spindle equator, and in this way, allow the efficient congression of all chromosomes during mitosis. Determining how kinetochores make the transitions from a monorientated state behind the pole to a biorientated state also remains a poorly understood process. Elucidating the mechanisms kinetochores employ to make this transition will be important in furthering our knowledge of chromosome congression.

Bibliography

Akhmanova A, Hoogenraad CC, Drabek K, Stepanova T, Dortland B, Verkerk T, Vermeulen W, Burgering BM, De Zeeuw CI, Grosveld F, Galjart N. (2001) Clasps are CLIP-115 and -170 associating proteins involved in the regional regulation of microtubule dynamics in motile fibroblasts. *Cell*, Vol. 104, pp. 923-935.

Akiyoshi B, Sarangapani KK, Powers AF, Nelson CR, Reichow SL, Arellano-Santoyo H, Gonen T, Ranish JA, Asbury CL, Biggins S. (2010) Tension directly stabilizes reconstituted kinetochore-microtubule attachments. *Nature*, Vol. 468, pp. 576-579.

Al-Bassam J, Chang F. (2011) Regulation of microtubule dynamics by TOG-domain proteins XMAP215/Dis1 and CLASP. *Trends Cell Biol*, Vol. 21, pp. 604-614.

Al-Bassam J, Kim H, Brouhard G, van Oijen A, Harrison SC, Chang F. (2010) CLASP promotes microtubule rescue by recruiting tubulin dimers to the microtubule. *Dev Cell*, Vol. 19, pp. 245-258.

Alexander J, Lim D, Joughin B, Hegemann B, Hutchins J, Ehrenberger T. (2011) Spatial exclusivity combined with positive and negative selection of phosphorylation motifs is the basis for context-dependent mitotic signaling. *Sci sig*, Vol. 4, pp. ra42.

Alushin GM, Ramey VH, Pasqualato S, Ball DA, Grigorieff N, Musacchio A, Nogales E. (2010) The Ndc80 kinetochore complex forms oligomeric arrays along microtubules. *Nature*, Vol. 467, pp. 805-810.

Amano M, Suzuki A, Hori T, Backer C, Okawa K, Cheeseman IM, Fukagawa T. (2009) The CENP-S complex is essential for the stable assembly of outer kinetochore structure. *J Cell Biol*, Vol. 186,

pp. 173-182.

Amaro AC, Samora CP, Holtackers R, Wang E, Kingston IJ, Alonso M, Lampson M, McAinsh AD, Meraldi P. (2010) Molecular control of kinetochore-microtubule dynamics and chromosome oscillations. *Nat Cell Biol*, Vol. 12, pp. 319-329.

Ando S, Yang H, Nozaki N, Okazaki T, Yoda K. (2002) CENP-A, -B, and -C chromatin complex that contains the I-type alpha-satellite array constitutes the prekinetochore in HeLa cells. *Mol Cell Biol*, Vol. 22, pp. 2229-2241.

Andrews PD, Ovechkina Y, Morrice N, Wagenbach M, Duncan K, Wordeman L, Swedlow JR. (2004) Aurora B regulates MCAK at the mitotic centromere. *Dev Cell*, Vol. 6, pp. 253-268.

Antonio C, Ferby I, Wilhelm H, Jones M, Karsenti E, Nebreda AR, Vernos I. (2000) Xkid, a chromokinesin required for chromosome alignment on the metaphase plate. Cell, Vol. 102, pp. 425-35.

Bader JR, Vaughan KT. (2010) Dynein at the kinetochore: Timing, Interactions and Functions. *Semin Cell Dev Biol*, Vol. 21, pp. 269-275.

Bahmanyar S, Nelson WJ, Barth AIM. (2009) Role of APC and its binding partners in regulating microtubules in mitosis. *Adv Exp Med Biol*, Vol. 656, pp. 65-74.

Bajer A. (1958) Ciné-micrographic studies on mitosis in endosperm. V. Formation of the metaphase plate. *Experimental Cell Research*, Vol. 15, pp. 370-383.

Bieling P, Laan L, Schek H, Munteanu EL, Sandblad L, Dogterom M, Brunner D, Surrey T. (2007) Reconstitution of a microtubule plus-end tracking system in vitro. *Nature*, Vol. 450, pp. 1100-1105.

Black BE, Jansen LET, Maddox PS, Foltz DR, Desai AB, Shah JV, Cleveland DW. (2007) Centromere identity maintained by nucleosomes assembled with histone H3 containing the CENP-A targeting domain. *Mol Cell*, Vol. 25, pp. 309-322.

Blower MD, Sullivan BA, Karpen GH. (2002) Conserved organization of centromertic chromatin in flies and humans. *Dev Cell*, Vol. 3, pp. 319-330.

Bock LJ, Pagliuca C, Kobayashi N, Grove RA, Oku Y, Shrestha K, Alfieri C, Golfieri C, Oldani A, Dal Maschio M, Bermejo R, Hazbun TR, Tanaka TU, De Wulf P. (2012) Cnn1 inhibits the interactions between the KMN complexes of the yeast kinetochore. *Nat Cell Biol*, Vol. 14, pp. 614-624.

Brinkley B, Stubblefield E. (1966) The fine structure of the kinetochore of a mammalian cell in vitro. *Chromosoma*, Vol. 19, pp. 28-43.

Brouhard G, Hunt A. (2005) Microtubule movements on the arms of mitotic chromosomes: polar ejection forces quantified in vitro. *PNAS*, Vol, 102 pp. 13903-13908.

Brust-Mascher I, Scholey JM. (2011) Mitotic motors and chromosome segregation: the mechanisms of anaphase B. *Biochem Soc trans*, Vol. 39, pp. 1149-1153.

Buffin E, Lefebvre C, Huang J, Gagou ME, Karess RE. (2005) Recruitment of Mad2 to the kinetochore requires the Rod/Zw10 complex. *Curr Biol*, Vol. 15, pp. 856-861.

Burns N, Grimwade B, Ross-Macdonald PB, Choi EY, Finberg K, Roeder GS, Snyder M. (1994) Large-scale analysis of gene expression, protein localization, and gene disruption in

Saccharomyces cerevisiae. *Genes Dev*, Vol. 8, pp. 1087-1105.

Cane S, Ye AA, Luks-Morgan SJ, Maresca TJ. (2013) Elevated polar ejection forces stabilize kinetochore-microtubule attachments. *J Cell Biol*, Vol. 21, pp. 203-218.

Carroll CW, Milks KJ, Straight AF. (2010) Dual recognition of CENP-A nucleosomes is required for centromere assembly. *J Cell Biol*, Vol. 189, pp. 1143-1155.

Carroll CW, Silva MCC, Godek KM, Jansen LET, Straight AF. (2009) Centromere assembly requires the direct recognition of CENP-A nucleosomes by CENP-N. *Nat Cell Biol*, Vol. 11, pp. 896-902.

Cassimeris L, Rieder C, Rupp G, Salmon E. (1990) Stability of microtubule attachment to metaphase kinetochores in PtK1 cells. *J Cell Sci*, Vol. 96, pp. 9-15.

Cassimeris LU, Walker RA, Pryer NK, Salmon ED. (1987) Dynamic instability of microtubules. *Bioessays*, Vol. 7, pp. 149-54.

Chan YW, Fava LL, Uldschmid A, Schmitz MHA, Gerlich DW, Nigg EA, Santamaria A. (2009) Mitotic control of kinetochore-associated dynein and spindle orientation by human Spindly. *J Cell Biol*, Vol. 185, pp. 859-874.

Chan YW, Jeyaprakash AA, Nigg EA, Santamaria A. (2012) Aurora B controls kinetochore-microtubule attachments by inhibiting Ska complex-KMN network interaction. *J Cell Biol*, Vol. 196, pp. 563-571.

Cheeseman IM, Chappie JS, Wilson-Kubalek EM, Desai A. (2006) The conserved KMN network constitutes the core microtubule-binding site of the kinetochore. *Cell*, Vol. 127, pp. 983-997.

Cheeseman IM, Desai A. (2008) Molecular architecture of the kinetochore-microtubule interface. *Nat Rev Mol Cell Biol*, Vol. 9, pp. 33-46.

Cheeseman IM, Hori T, Fukagawa T, Desai A. (2008) KNL1 and the CENP-H/I/K complex coordinately direct kinetochore assembly in vertebrates. *Mol Biol Cell*, Vol. 19, pp. 587-594.

Cheeseman IM, Niessen S, Anderson S, Hyndman F, Yates JR 3rd, Oegema K, Desai A. (2004) A conserved protein network controls assembly of the outer kinetochore and its ability to sustain tension. *Genes Dev,* Vol. 18, pp. 2255-2268.

Chen Y, Riley D, Zheng L, Chen P, Lee W. (2002) Phosphorylation of the mitotic regulator protein Hec1 by Nek2 kinase is essential for faithful chromosome segregation. *J Biol Chem*, Vol. 277, pp. 49408-49416.

Ciferri C, Pasqualato S, Screpanti E, Varetti G, Santaguida S, Dos Reis G, Maiolica A, Polka J, De Luca JG, De Wulf P, Salek M, Rappsilber J, Moores CA, Salmon ED, Musacchio A. (2008) Implications for kinetochore-microtubule attachment from the structure of an engineered Ndc80 complex. *Cell*, Vol. 133, pp. 427-439.

Cimini D, Wan X, Hirel CB, Salmon ED. (2006) Aurora kinase promotes turnover of kinetochore microtubules to reduce chromosome segregation errors. *Curr Biol*, Vol. 16, pp.1711-1718.

Cleveland DW, Mao Y, Sullivan KF. (2003) Centromeres and kinetochores: from epigenetics to mitotic checkpoint signaling. *Cell*, Vol. 112, pp. 407-421.

Coue M, Lombillo VA, McIntosh JR. (1991) Microtubule depolymerization promotes particle and chromosome movement in vitro. *J Cell Biol*, Vol. 112, pp. 1165-1175.

Daum J, Potapova T, Sivakumar S, Daniel J, Flynn J, Rankin S. (2011) Cohesion fatigue induces chromatid separation in cells delayed at metaphase. *Curr Biol*, Vol, 21, pp. 1018-1024.

Daum JR, Wren JD, Daniel JJ, Sivakumar S, McAvoy JN, Potapova TA, Gorbsky GJ (2009) Ska3 is required for spindle checkpoint silencing and the maintenance of chromosome cohesion in mitosis. *Current Biology*, Vol. 19, pp. 1467-1472.

DeLuca JG, Dong Y, Hergert P, Strauss J, Hickey JM, Salmon ED, McEwen BF. (2005) Hec1 and nuf2 are core components of the kinetochore outer plate essential for organizing microtubule attachment sites. *Mol Biol Cell*, Vol. 16, pp. 519-531.

DeLuca JG, Gall WE, Ciferri C, Cimini D, Musacchio A, Salmon ED. (2006) Kinetochore microtubule dynamics and attachment stability are regulated by Hec1. *Cell*, Vol. 127, pp.969-982.

Diamantopoulos GS, Perez F, Goodson HV, Batelier G, Melki R, Kreis TE, Rickard JE. (1999) Dynamic localization of CLIP-170 to microtubule plus ends is coupled to microtubule assembly. *J Cell Biol*, Vol. 144, pp. 99-112.

Dikovskaya D, Schiffmann D, Newton IP, Oakley A, Kroboth K, Sansom O, Jamieson TJ, Meniel V, Clarke A, Näthke IS. (2007) Loss of APC induces polyploidy as a result of a combination of defects in mitosis and apoptosis. *J Cell Biol*, Vol. 176, pp. 183-195.

Domnitz SB, Wagenbach M, Decarreau J, Wordeman L. (2012) MCAK activity at microtubule tips regulates spindle microtubule length to promote robust kinetochore attachment. *J Cell Biol*, Vol. 197, pp. 231-237.

Dong Y, Vanden Beldt KJ, Meng X, Khodjakov A, McEwen BF. (2007) The outer plate in vertebrate

kinetochores is a flexible network with multiple microtuble interactions. *Nat Cell Biol*, Vol. 9, pp. 516-522.

Dou Z, von Schubert C, Körner R, Santamaria A, Elowe S, Nigg EA. (2011) Quantitative mass spectrometry analysis reveals similar substrate consensus motif for human Mps1 kinase and Plk1. *PLoS ONE*, Vol. 6, pp. e18793

Draviam VM, Shapiro I, Aldridge B, Sorger PK. (2006) Misorientation and reduced stretching of aligned sister kinetochores promote chromosome missegregation in EB1- or APC-depleted cells. *The EMBO Journal*, Vol. 25, pp. 2814-2827.

Du Y, English CA, Ohi R. (2010) The kinesin-8 Kif18A dampens microtubule plus-end dynamics. *Curr Biol*, Vol. 20, pp. 374-380.

Dujardin D, Wacker UI, Moreau A, Schroer TA, Rickard JE, De Mey JR. (1998) Evidence for a role of CLIP-170 in the establishment of metaphase chromosome alignment. *J Cell Biol*, Vol. 141, pp. 849-862.

Dumont S, Salmon ED, Mitchison TJ. (2012) Deformations within moving kinetochores reveal different sites of active and passive force generation. *Science*, Vol. 337, pp. 355-358.

Elbashir SM, Harborth J, Lendeckel W, Yalcin A, Weber K, Tuschl T. (2001) Duplexes of 21-nucleotide RNAs mediate RNA interference in cultured mammalian cells. *Nature*, Vol. 411, pp. 494-498.

Ems-McClung SC, Hainline SG, Devare J, Zong H, Cai S, Carnes SK, Shaw SL, Walczak CE. (2013) Aurora B Inhibits MCAK Activity through a Phosphoconformational Switch that Reduces Microtubule Association. *Curr Biol*, Vol. 23, pp. 2491-2499.

Eskat A, Deng W, Hofmeister A, Rudolphi S, Emmerth S, Hellwig D, Ulbricht T, Döring V, Bancroft JM, McAinsh AD, Cardoso MC, Meraldi P, Hoischen C, Leonhardt H, Diekmann S. (2012) Step-wise assembly, maturation and dynamic behavior of the human CENP-P/O/R/Q/U kinetochore sub-complex. *PLoS ONE*, Vol. 7, p. e44717.

Espeut J, Cheerambathur DK, Krenning L, Oegema K, Desai A. (2012) Microtubule binding by KNL-1 contributes to spindle checkpoint silencing at the kinetochore. *J Cell Biol*, Vol. 196, pp. 469-482.

Fernius J, Marston A. (2009) Establishment of cohesion at the pericentromere by the Ctf19 kinetochore subcomplex and the replication fork-associated factor, Csm3. *PLoS genetics*, Vol. 5, e1000629.

Fodde R, Kuipers J, Rosenberg C, Smits R, Kielman M, Gaspar C, van Es JH, Breukel C, Wiegant J, Giles RH, Clevers H. (2001) Mutations in the APC tumour suppressor gene cause chromosomal instability. *Nat Cell Biol*, Vol. 3, pp. 433-438.

Foltz DR, Jansen LET, Black BE, Bailey AO, Yates JR, Cleveland DW. (2006) The human CENP-A centromeric nucleosome-associated complex. *Nat Cell Biol*, Vol. 8, pp. 458-469.

Fukagawa T, Regnier V, Ikemura T. (2001) Creation and characterization of temperaure-sensitive CENP-C mutants in vertibrate cells. *Nucleic Acids Res*, Vol. 29, pp. 796-803.

Funabiki H, Murray A. (2000) The Xenopus chromokinesin Xkid is essential for metaphase chromosome alignment and must be degraded to allow anaphase chromosome movement. *Cell*, Vol. 102, pp. 411-24.

Gadde S, Heald R. (2004) Mechanisms and molecules of the mitotic spindle. *Curr Biol*, Vol. 14, pp. 797-805.

Gaitanos TN, Santamaria A, Jeyaprakash AA, Wang B, Conti E, Nigg EA. (2009) Stable kinetochore-microtubule interactions depend on the Ska complex and its new component Ska3/C13Orf3. *EMBO J*, Vol. 28, pp. 1442-1452.

Ganguly A, Yang H, Pedroza M, Bhattacharya R, Cabral F. (2011) Mitotic centromere-associated kinesin (MCAK) mediates paclitaxel resistance. *J Biol Chem*, Vol. 286, pp. 36378-36384.

Gascoigne K, Cheeseman I. (2013) CDK-dependent phosphorylation and nuclear exclusion coordinately control kinetochore assembly state. *J Cell Biol*, Vol. 201, pp. 23-32.

Gascoigne KE, Takeuchi K, Suzuki A, Hori T, Fukagawa T, Cheeseman IM. (2011) Induced Ectopic Kinetochore Assembly Bypasses the Requirement for CENP-A Nucleosomes. *Cell*, Vol. 145, pp. 410-422.

Gassmann R, Holland AJ, Varma D, Wan X, Civril F, Cleveland DW, Oegema K, Salmon ED, Desai A. (2010) Removal of Spindly from microtubule-attached kinetochores controls spindle checkpoint silencing in human cells. *Genes Dev*, Vol. 24, pp. 957-971.

Goldstone S, Reyes C, Gay G, Courthéoux T, Dubarry M, Tournier S, Gachet Y. (2010) Tip1/CLIP-170 protein is required for correct chromosome poleward movement in fission yeast. *PLoS ONE*, Vol. 5, p. e10634.

Gonen S, Akiyoshi B, Iadanza MG, Shi D, Duggan N, Biggins S, Gonen T. (2012) The structure of purified kinetochores reveals multiple microtubule-attachment sites. *Nat Struct Mol Biol*, Vol. 19, pp. 925-929.

Griffis ER, Stuurman N, Vale RD. (2007) Spindly, a novel protein essential for silencing the spindle assembly checkpoint, recruits dynein to the kinetochore. *J Cell Biol*, Vol. 177, pp. 1005-1015.

Gudimchuk N, Vitre B, Kim Y, Kiyatkin A, Cleveland DW, Ataullakhanov FI, Grishchuk EL. (2013) Kinetochore kinesin CENP-E is a processive bi-directional tracker of dynamic microtubule tips. *Nat Cell Biol*, Vol. 15, pp. 1-13.

Guimaraes GJ, Dong Y, McEwen BF, Deluca JG. (2008) Kinetochore-microtubule attachment relies on the disordered N-terminal tail domain of Hec1. *Curr Biol*, Vol. 18, pp. 1778-1784.

Hanisch A, Silljé HH, Nigg EA. (2006a) Timely anaphase onset requires a novel spindle and kinetochore complex comprising Ska1 and Ska2. *EMBO J*, Vol. 25, pp. 5504-5515.

Hanisch A, Wehner A, Nigg E, Silljé H. (2006b) Different Plk1 functions show distinct dependencies on Polo-Box domain-mediated targeting. *Mol Biol Cell*, Vol. 17, pp. 448-459.

Hardwick K, Shah J. (2010) Spindle checkpoint silencing: ensuring rapid and concerted anaphase onset. *F1000 Biol Rep*, Vol. 2, pp. 55.

Hayden J, Bowser S, Rieder C. (1990) Kinetochores capture astral microtubules during chromosome attachment to the mitotic spindle: direct visualization in live newt lung cells. *J Cell Biol*, Vol. 111, pp. 1039-1045.

Hertzer KM, Ems-McClung SC, Kline-Smith SL, Lipkin TG, Gilbert SP, Walczak CE. (2006) Full-length dimeric MCAK is a more efficient microtubule depolymerase than minimal domain monomeric MCAK. *Mol Biol Cell*, Vol. 17, pp. 700-710.

Hewitt L, Tighe A, Santaguida S, White AM, Jones CD, Musacchio A, Green S, Taylor SS. (2010) Sustained Mps1 activity is required in mitosis to recruit O-Mad2 to the Mad1-C-Mad2 core complex. *J Cell Biol*, Vol. 190, pp. 25-34.

Hinshaw SM, Harrison SC. (2013) An iml3-chl4 heterodimer links the core centromere to factors required for accurate chromosome segregation. *Cell Rep*, Vol. 5, pp. 29-36.

Hochegger H. Hégarat N, Pereira-Leal J. (2013) Aurora at the pole and equator: overlapping functions of Aurora kinases in the mitotic spindle. *Open Biol*, Vol. 3, pp. 120185.

Hoffman DB, Pearson CG, Yen TJ, Howell BJ, Salmon ED. (2001) Microtubule-dependent changes in assembly of microtubule motor proteins and mitotic spindle checkpoint proteins at PtK1 kinetochores. *Mol Biol Cell*, Vol. 12, pp. 1995-2009.

Holzbaur EL, Vallee RB. (1994) DYNEINS: molecular structure and cellular function. *Annu Rev Cell Biol*, Vol. 10, pp. 339-372.

Honnappa S, Gouveia SM, Weisbrich A, Damberger FF, Bhavesh NS, Jawhari H, Grigoriev I, van Rijssel FJA, Buey RM, Lawera A, Jelesarov I, Winkler FK, Wüthrich K, Akhmanova A, Steinmetz MO. (2009) An EB1-binding motif acts as a microtubule tip localization signal. *Cell*, Vol. 138, pp. 366-376.

Hori T, Amano M, Suzuki A, Backer CB, Welburn JP, Dong Y, McEwen BF, Shang W-H, Suzuki E, Okawa K, Cheeseman IM, Fukagawa T. (2008a) CCAN makes multiple contacts with centromeric DNA to provide distinct pathways to the outer kinetochore. *Cell*, Vol. 135, pp. 1039-1052.

Hori T, Okada M, Maenaka K, Fukagawa T. (2008b) CENP-O class proteins form a stable complex and are required for proper kinetochore function. *Mol Biol Cell*, Vol. 19, pp. 843-854.

Hori T, Shang W-H, Takeuchi K, Fukagawa T. (2013) The CCAN recruits CENP-A to the centromere and forms the structural core for kinetochore assembly. *J Cell Biol*, Vol. 200, pp. 45-60.

Howell BJ, McEwen BF, Canman JC, Hoffman DB, Farrar EM, Rieder CL, Salmon ED. (2001) Cytoplasmic dynein/dynactin drives kinetochore protein transport to the spindle poles and has a role in mitotic spindle checkpoint inactivation. *J Cell Biol*, Vol. 155, pp. 1159-72.

Hua S, Wang Z, Jiang K, Huang Y, Ward T, Zhao L, Dou Z, Yao X. (2011) CENP-U cooperates with Hec1 to orchestrate kinetochore-microtubule attachment. *J Biol Chem*, Vol. 286, pp. 1627-1638.

Huang H, Feng J, Famulski J, Rattner JB, Liu ST, Kao GD, Muschel R, Chan GKT, Yen TJ. (2007) Tripin/hSgo2 recruits MCAK to the inner centromere to correct defective kinetochore attachments. *J Cell Biol*, Vol. 177, pp. 413-424.

Huang Y, Yao Y, Xu H-Z, Wang Z-G, Lu L, Dai W. (2009) Defects in chromosome congression and mitotic progression in KIF18A-deficient cells are partly mediated through impaired functions of CENP-E. *Cell Cycle*, Vol. 8, pp. 2643-2649.

Hughes A, Swann MM. (1949) Cell Division. *Nature*, Vol. 164, pp. 131-133.

Hunter AW, Caplow M, Coy DL, Hancock WO, Diez S, Wordeman L, Howard J. (2003) The kinesin-related protein MCAK is a microtubule depolymerase that forms an ATP-hydrolyzing complex at microtubule ends. *Mol Cell*, Vol. 11, pp. 445-457.

Inoue Y, do Carmo Avides M, Shiraki M, Deak P, Yamaguch M, Nishimoto Y. (2000) Orbit, a novel microtubule-associated protein essential for mitosis in Drosophila melanogaster. *J Cell Biol*, Vol.

149, pp. 153-166.

Izuta H, Ikeno M, Suzuki N, Tomonaga T, Nozaki N, Obuse C, Kisu Y, Goshima N, Nomura F, Nomura N, Yoda K. (2006) Comprehensive analysis of the ICEN (Interphase Centromere Complex) components enriched in the CENP-A chromatin of human cells. *Genes Cells*, Vol. 11, pp. 673-684.

Jackson J, Patrick D, Dar M, Huang P. (2007) Targeted anti-mitotic therapies: can we improve on tubulin agents. *Nat Rev Canc*, Vol. 7, pp. 107-117.

Jaqaman K, King EM, Amaro AC, Winter JR, Dorn JF, Elliott HL, McHedlishvili N, McClelland SE, Porter IM, Posch M, Toso A, Danuser G, McAinsh AD, Meraldi P, Swedlow JR. (2010) Kinetochore alignment within the metaphase plate is regulated by centromere stiffness and microtubule depolymerases. *J Cell Biol*, Vol. 188, pp. 665-679.

Jeyaprakash AA, Santamaria A, Jayachandran U, Chan YW, Benda C, Nigg EA, Conti E (2012) Structural and functional organization of the Ska complex, a key component of the kinetochore-microtubule interface. *Mol Cell*, Vol. 46, pp. 274-286.

Jokelainen P. (1967) The ultrastructure and spatial organization of the metaphase kinetochore in mitotic rat cells. *J Ultrastruct Res*, Vol. 19, pp. 19-44.

Kang YH, Park CH, Kim T-S, Soung N-K, Bang JK, Kim BY, Park J-E, Lee KS. (2011) Mammalian polo-like kinase 1-dependent regulation of the PBIP1-CENP-Q complex at kinetochores. *J Biol Chem*.

Kapoor TM, Lampson MA, Hergert P, Cameron L, Cimini D, Salmon ED, McEwen BF, Khodjakov A. (2006) Chromosomes can congress to the metaphase plate before biorientation. *Science*, Vol.

311, pp. 388-391.

Karess R. (2005) Rod-Zw10-Zwilch: a key player in the spindle checkpoint. *Trends Cell Biol*, Vol. 15, pp. 386-392.

Kasuboski JM, Bader JR, Vaughan PS, Tauhata SBF, Winding M, Morrissey MA, Joyce MV, Boggess W, Vos L, Chan GK, Hinchcliffe EH, Vaughan KT. (2011) Zwint-1 is a novel Aurora B substrate required for the assembly of a dynein-binding platform on kinetochores. *Mol Biol Cell*, Vol. 22, pp. 3318-3330.

Khodjakov A, Cole RW, McEwen BF, Buttle KF, Rieder CL. (1997) Chromosome fragments possessing only one kinetochore can congress to the spindle equator. *J Cell Biol*, Vol. 136, pp. 229-240.

Khodjakov A, Rieder CL. (1996) Kinetochores moving away from their associated pole do not exert a significant pushing force on the chromosome. *J Cell Biol*, Vol. 135, pp. 315-327.

Kim Y, Heuser JE, Waterman CM, Cleveland DW. (2008) CENP-E combines a slow, processive motor and a flexible coiled coil to produce an essential motile kinetochore tether. *J Cell Biol*, Vol. 181, pp. 411-419.

Kim Y, Holland AJ, Lan W, Cleveland DW. (2010) Aurora kinases and protein phosphatase 1 mediate chromosome congression through regulation of CENP-E. *Cell*, Vol. 142, pp. 444-455.

Kinzler KW, Vogelstein B. (1996) Lessons from hereditary colorectal cancer. *Cell*, Vol. 87, pp. 159-170.

Kirschner M, Mitchison T. (1986) Beyond self-assembly: from microtubules to morphogenesis. *Cell*,

Vol. 45, pp. 329-342.

Kitajima TS, Ohsugi M, Ellenberg J. (2011) Complete kinetochore tracking reveals error-prone homologous chromosome biorientation in mammalian oocytes. *Cell*, Vol. 146, pp. 568-581.

Kiyomitsu T, Cheeseman IM. (2013) Cortical dynein and asymmetric membrane elongation coordinately position the spindle in anaphase. *Cell*, Vol. 154, pp. 391-402.

Kiyomitsu T, Obuse C, Yanagida M. (2007) Human Blinkin/AF15q14 is required for chromosome alignment and the mitotic checkpoint through direct interaction with Bub1 and BubR1. *Dev Cell*, Vol. 13, pp. 663-676.

Kline SL, Cheeseman IM, Hori T, Fukagawa T, Desai A. (2006) The human Mis12 complex is required for kinetochore assembly and proper chromosome segregation. *J Cell Biol*, Vol. 173, pp. 9-17.

Kline-Smith SL, Khodjakov A, Hergert P, Walczak CE. (2004) Depletion of centromeric MCAK leads to chromosome congression and segregation defects due to improper kinetochore attachments. *Mol Biol Cell*, Vol. 15, pp. 1146-59.

Knowlton AL, Lan W, Stukenberg PT. (2006) Aurora B is enriched at merotelic attachment sites, where it regulates MCAK. *Curr Biol*, Vol. 16, pp. 1705-1710.

Komarova Y, Lansbergen G, Galjart N, Grosveld F, Borisy GG, Akhmanova A. (2005) EB1 and EB3 control CLIP dissociation from the ends of growing microtubules. *Mol Biol Cell*, Vol. 16, pp. 5334-5345.

Kops GJ, Kim Y, Weaver BA, Mao Y, McLeod, Yates JR 3rd, Tagaya M, Cleveland DW. (2005)

ZW10 links mitotic checkpoint signaling to the structural kinetochore. *J Cell Biol*, Vol. 169, pp. 49-60.

Kops GJPL, Saurin AT, Meraldi P. (2010) Finding the middle ground: how kinetochores power chromosome congression. *Cell Mol Life Sci*, Vol. 67, pp. 2145-2161.

Koshland DE, Mitchison TJ, Kirschner MW. (1988) Polewards chromosome movement driven by microtubule depolymerization in vitro. *Nature*, Vol. 331, pp. 499-504.

Krenn V, Wehenkel A, Li X, Santaguida S, Musacchio A. (2012) Structural analysis reveals features of the spindle checkpoint kinase Bub1-kinetochore subunit Knl1 interaction. *J Cell Biol*, Vol. 196, pp. 451-467.

Kwon M-S, Hori T, Okada M, Fukagawa T. (2007) CENP-C is involved in chromosome segregation, mitotic checkpoint function, and kinetochore assembly. *Mol Biol Cell*, Vol. 18, pp. 2155-2168.

Lampson MA, Cheeseman IM. (2011) Sensing centromere tension: Aurora B and the regulation of kinetochore function. *Trends Cell Biol*, Vol. 21, pp. 133-140.

Lemos C, Sampaio P, Maiato H, Costa M, Omel'yanchuk L, Liberal V. (2000) Mast, a conserved microtubule-associated protein required for bipolar mitotic spindle organization. *EMBO J*, Vol. 19, pp. 3668-3682.

Lénárt P, Petronczki M, Steegmaier M, Di Fiore B, Lipp J, Hoffmann M. (2007) The small-molecule inhibitor BI 2536 reveals novel insights into mitotic roles of polo-like kinase 1. *Curr Biol*, Vol. 17, pp. 304-315.

Levesque A, Compton D. (2001) The chromokinesin Kid is necessary for chromosome arm orientation and oscillation, but not congression, on mitotic spindles. *J Cell Biol*, Vol. 154, pp. 1135-1146.

Lewis WH. (1939) Changes of viscosity and cell activity. *Science*, 89:400.

Li Y, Yu W, Liang Y, Zhu X. (2007) Kinetochore dynein generates a poleward pulling force to facilitate congression and full chromosome alignment. *Cell Res*, Vol. 17, pp. 701-712.

Ligon LA, Shelly SS, Tokito MK, Holzbaur EL. (2006) Microtubule binding proteins CLIP-170, EB1, and p150Glued form distinct plus-end complexes. *FEBS Lett*, Vol. 580, pp. 1327-32.

Lin Y-T, Chen Y, Wu G, Lee W-H. (2006) Hec1 sequentially recruits Zwint-1 and ZW10 to kinetochores for faithful chromosome segregation and spindle checkpoint control. *Oncogene*, Vol. 25, pp. 6901-6914.

Liu D, Davydenko O, Lampson MA. (2012) Polo-like kinase-1 regulates kinetochore-microtubule dynamics and spindle checkpoint silencing. *J Cell Biol*, Vol. 198, pp. 491-499.

Liu D, Vleugel M, Backer C, Hori T, Fukagawa T, Cheeseman I. (2010) Regulated targeting of protein phosphatase 1 to the outer kinetochore by KNL1 opposes Aurora B kinase. *J Cell Biol*, Vol. 188, pp. 809-820.

Liu ST, Hittle JC, Jablonski SA, Campbell MS, Yoda K, Yen TJ. (2003) Human CENP-I specifies localization of CENP-F, MAD1 and MAD2 to kinetochore and is essential for mitosis. *Nat Cell Biol*, Vol. 5, pp. 341-345.

London N, Ceto S, Ranish JA, Biggins S. (2012) Phosphoregulation of Spc105 by Mps1 and PP1

regulates Bub1 localization to kinetochores. *Curr Biol*, Vol. 22, pp. 900-906.

Lopus M, Manatschal C, Buey RM, Bjelić S, Miller HP, Steinmetz MO, Wilson L. (2012) Cooperative stabilization of microtubule dynamics by EB1 and CLIP-170 involves displacement of stably bound P(i) at microtubule ends. *Biochemistry*, Vol. 51, pp. 3021-3030.

Maciejowski J, George KA, Terret ME, Zhang C, Shokat KM, Jallepalli PV. (2010) Mps1 directs the assembly of Cdc20 inhibitory complexes during interphase and mitosis to control M phase timing and spindle checkpoint signaling. *J Cell Biol*, Vol. 190, pp. 89-100.

Maffini S, Maia ARR, Manning AL, Maliga Z, Pereira AL, Junqueira M, Shevchenko A, Hyman A, Yates JR, Galjart N, Compton DA, Maiato H. (2009) Motor-independent targeting of CLASPs to kinetochores by CENP-E promotes microtubule turnover and poleward flux. *Curr Biol*, Vol. 19, pp. 1566-1572.

Magidson V, O'Connell CB, Lončarek J, Paul R, Mogilner A, Khodjakov A. (2011) The spatial arrangement of chromosomes during prometaphase facilitates spindle assembly. *Cell*, Vol. 146, pp. 555-567.

Maia ARR, Garcia Z, Kabeche L, Barisic M, Maffini S, Macedo-Ribeiro S, Cheeseman IM, Compton DA, Kaverina I, Maiato H. (2012) Cdk1 and Plk1 mediate a CLASP2 phospho-switch that stabilizes kinetochore-microtubule attachments. *J Cell Biol*, Vol. 199, pp. 285-301.

Maiato H, Fairley EAL, Rieder CL, Swedlow JR, Sunkel CE, Earnshaw WC. (2003a) Human CLASP1 is an outer kinetochore component that regulates spindle microtubule dynamics. *Cell*, Vol. 113, pp. 891-904.

Maiato H, Khodjakov A, Rieder CL. (2005) Drosophila CLASP is required for the incorporation of

microtubule subunits into fluxing kinetochore fibres. *Nat Cell Biol*, Vol. 7, pp. 42-47.

Maiato H, Rieder C, Earnshaw W, Sunkel C. (2003b) How do kinetochores CLASP dynamic microtubules? *Cell cycle*, Vol. 2, pp. 511-514.

Maney T, Hunter AW, Wagenbach M, Wordeman L. (1998) Mitotic centromere-associated kinesin is important for anaphase chromosome segregation. *J Cell Biol*, Vol. 142, pp. 787-801.

Manna T, Honnappa S, Steinmetz MO, Wilson L. (2008) Suppression of microtubule dynamic instability by the +TIP protein EB1 and its modulation by the CAP-Gly domain of p150glued. *Biochemistry*, Vol. 47, pp. 779-786.

Manning A, Bakhoum S, Maffini S, Correia-Melo C, Maiato H, Compton D. (2010) CLASP1, astrin and Kif2b form a molecular switch that regulates kinetochore-microtubule dynamics to promote mitotic progression and fidelity. *EMBO J*, Vol. 29, pp. 3531-3543.

Martin-Lluesma S, Stucke VM, Nigg EA. (2002) Role of Hec1 in spindle checkpoint signaling and kinetochore recruitment of Mad1/Mad2. *Science*, Vol. 297, pp. 2267-2270.

Masumoto H, Masukata H, Muro Y, Nozaki N, Okazaki T. (1989) A human centromere antigen (CENP-B) interacts with a short specific sequence in alphoid DNA, a human centromeric satellite. *J Cell Biol*. Vol. 109, pp. 1963-1973.

Matson DR, Demirel PB, Stukenberg PT, Burke DJ. (2012) A conserved role for COMA/CENP-H/I/N kinetochore proteins in the spindle checkpoint. *Genes Dev*, Vol. 26, pp. 542-547.

Mayer TU, Kapoor TM, Haggarty SJ, King RW, Schreiber SL, Mitchison TJ. (1999) Small molecule inhibitor of mitotic spindle bipolarity identified in a phenotype-based screen. *Science*, Vol. 286, pp.

971-974.

Mayr MI, Hümmer S, Bormann J, Grüner T, Adio S, Woehlke G, Mayer TU. (2007) The human kinesin Kif18A is a motile microtubule depolymerase essential for chromosome congression. *Curr Biol*, Vol. 17, pp. 488-498.

Mayr M, Storch M, Howard J, Mayer T. (2011) A non-motor microtubule binding site is essential for the high processivity and mitotic function of kinesin-8 Kif18A. *PloS One*, Vol. 6, e27471.

McAinsh AD, Meraldi P. (2011) The CCAN complex: linking centromere specification to control of kinetochore-microtubule dynamics. *Semin Cell Dev Biol*, Vol. 22, pp. 946-952.

McAinsh AD, Meraldi P, Draviam VM, Toso A, Sorger PK. (2006) The human kinetochore proteins Nnf1R and Mcm21R are required for accurate chromosome segregation. *EMBO J*, Vol. 25, pp. 4033-4049.

McClelland SE, Borusu S, Amaro AC, Winter JR, Belwal M, McAinsh AD, Meraldi P. (2007) The CENP-A NAC/CAD kinetochore complex controls chromosome congression and spindle bipolarity. *EMBO J*, Vol. 26, pp. 5033-5047.

McEwen BF, Hsieh CE, Mattheyses AL, Rieder CL. (1998) A new look at kinetochore structure in vertebrate somatic cells using high-pressure freezing and freeze substitution. *Chromosoma*, Vol. 107, pp. 366-375.

Mchedlishvili N, Wieser S, Holtackers R, Mouysset J, Belwal M, Amaro AC, Meraldi P. (2012) Kinetochores accelerate centrosome separation to ensure faithful chromosome segregation. *J Cell Sci*, Vol. 125, pp. 906-918.

McIntosh JR, Grishchuk EL, Morphew MK, Efremov AK, Zhudenkov K, Volkov VA, Cheeseman IM, Desai A, Mastronarde DN, Ataullakhanov FI. (2008) Fibrils connect microtubule tips with kinetochores: a mechanism to couple tubulin dynamics to chromosome motion. *Cell*, Vol. 135, pp. 322-333.

Melters DP, Pauliulis LV, Korf IF, Chan SW. (2012) Holocentric chromosomes: convergent evolution, meiotic adaptations, and genomic analysis. *Chromosome Res*, Vol. 20, pp. 579-593.

Meraldi P, Draviam VM, Sorger PK. (2004) Timing and checkpoints in the regulation of mitotic progression. *Dev Cell*, Vol. 7, pp. 45-60.

Meraldi P, McAinsh AD, Rheinbay E, Sorger PK. (2006) Phylogenetic and structural analysis of centromeric DNA and kinetochore proteins. *Genome Biol*, Vol. 7, pp. R23.

Meunier S, Vernos I. (2012) Microtubule assembly during mitosis - from distinct origins to distinct functions? *J Cell Sci*, Vol. 125, pp. 2805-2814.

Mikami Y, Hori T, Kimura H, Fukagawa T. (2005) The functional region of CENP-H interacts with the Nuf2 complex that localizes to centromere during mitosis. *Mol Cell Biol*, Vol. 25, pp. 1958-1970.

Miller SA, Johnson ML, Stukenberg PT. (2008) Kinetochore attachments require an interaction between unstructured tails on microtubules and Ndc80(Hec1). *Curr Biol*, Vol. 18, pp. 1785-1791.

Mitchison TJ, Salmon ED. (1992) Poleward kinetochore fiber movement occurs during both metaphase and anaphase-A in newt lung cell mitosis. *J Cell Biol*, Vol. 119, pp. 569-582.

Moores CA, Milligan RA. (2006) Lucky 13-microtubule depolymerisation by kinesin-13 motors. *J Cell Sci*, Vol. 119, pp. 3905-3913.

Meunier S, Vernos I. (2012) Microtubule assembly during mitosis - from distinct origins to distinct functions?. *J Cell Sci*, Vol. 125, pp. 2805-14.

Musinipally V, Howes S, Alushin GM, Nogales E. (2013) The Microtubule Binding Properties of CENP-E's C-Terminus and CENP-F. *J Mol Biol*

Nishihashi A, Haraguchi T, Hiraoka Y, Ikemura T, Regnier V, Dodson H, Earnshaw WC, Fukagawa T. (2002) CENP-I is essential for centromere function in vertebrate cells. *Dev Cell*, Vol. 2, pp. 463-476.

Nishino T, Rago F, Hori T, Tomii K, Cheeseman IM, Fukagawa T. (2013) CENP-T provides a structural platform for outer kinetochore assembly. *EMBO J*, Vol. 32, pp. 424-436.

Nishino T, Takeuchi K, Gascoigne Karen E, Suzuki A, Hori T, Oyama T, Morikawa K, Cheeseman Iain M, Fukagawa T. (2012) CENP-T-W-S-X Forms a Unique Centromeric Chromatin Structure with a Histone-like Fold. *Cell*, Vol. 148, pp. 487-501.

Obuse C, Yang H, Nozaki N, Goto S, Okazaki T, Yoda K. (2004) Proteomics analysis of the centromere complex from HeLa interphase cells: UV-damaged DNA binding protein 1 (DDB-1) is a component of the CEN-complex, while BMI-1 is transiently co-localized with the centromeric region in interphase. *Genes Cells*, Vol. 9, pp. 105-120.

O'Connell CB, Wang YL. (2000) Mammalian spindle orientation and position respond to changes in cell shape in a dynein-dependent fashion. *Mol Biol Cell*, Vol. 11, pp. 1765-1774.

Okada M, Cheeseman IM, Hori T, Okawa K, McLeod IX, Yates JR, Desai A, Fukagawa T. (2006) The CENP-H-I complex is required for the efficient incorporation of newly synthesized CENP-A into

centromeres. *Nat Cell Biol*, Vol. 8, pp. 446-457.

Olsen JV, Vermeulen M, Santamaria A, Kumar C, Miller ML, Jensen LJ, Gnad F, Cox J, Jensen TS, Nigg EA, Brunak S, Mann M. (2010) Quantitative phosphoproteomics reveals widespread full phosphorylation site occupancy during mitosis. *Sci Signal*, Vol. 3, p. ra3.

Park J-E, Erikson RL, Lee KS. (2011) Feed-forward mechanism of converting biochemical cooperativity to mitotic processes at the kinetochore plate. *Proc Natl Acad Sci USA*

Paul R, Wollman R, Silkworth WT, Nardi IK, Cimini D, Mogilner A. (2009) Computer simulations predict that chromosome movements and rotations accelerate mitotic spindle assembly without compromising accuracy. *Proc Natl Acad Sci USA*, Vol. 106, pp. 15708-15713.

Pereira AJ, Maiato H. (2012) Maturation of the kinetochore-microtubule interface and the meaning of metaphase. *Chromosome Res*, Vol. 20, pp. 563-577.

Perpelescu M, Fukagawa T. (2011) The ABCs of CENPs. *Chromosoma*, Vol. 120, pp. 425-446.

Petronczki M, Lénárt P, Peters J. (2008) Polo on the Rise-from Mitotic Entry to Cytokinesis with Plk1. *Dev Cell*, Vol. 14, pp. 646-659.

Petrovic A, Pasqualato S, Dube P, Krenn V, Santaguida S, Cittaro D, Monzani S, Massimiliano L, Keller J, Tarricone A, Maiolica A, Stark H, Musacchio A. (2010) The MIS12 complex is a protein interaction hub for outer kinetochore assembly. *J Cell Biol*, Vol. 190, pp. 835-852.

Pot I, Knockleby J, Aneliunas V, Nguyen T, Ah-Kye S, Liszt G, Snyder M, Hieter P, Vogel J. (2005) Spindle checkpoint maintenance requires Ame1 and Okp1. *Cell Cycle*, Vol. 4, pp. 1448-1456.

Przewloka MR, Venkei Z, Bolanos-Garcia VM, Debski J, Dadlez M, Glover DM. (2011) CENP-C is a structural platform for kinetochore assembly. *Curr Biol*, Vol. 21, pp. 399-405.

Putkey FR, Cramer T, Morphew MK, Silk AD, Johnson RS, McIntosh JR, Cleveland DW. (2002) Unstable kinetochore-microtubule capture and chromosomal instability following deletion of CENP-E. *Dev Cell*, Vol. 3, pp. 351-365.

Raaijmakers JA, Tanenbaum ME, Maia AF, Medema RH. (2009) RAMA1 is a novel kinetochore protein involved in kinetochore-microtubule attachment. *J Cell Sci*, Vol. 122, pp. 2436-2445.

Rieder C. (1982) The formation, structure, and composition of the mammalian kinetochore and kinetochore fiber. *Int Rev Cytol*, Vol. 79, pp. 1-58.

Rieder CL, Davison EA, Jensen LC, Cassimeris L, Salmon ED. (1986) Oscillatory movements of monooriented chromosomes and their position relative to the spindle pole result from the ejection properties of the aster and half-spindle. *J Cell Biol*, Vol. 103, pp. 581-591.

Rigbolt KTG, Prokhorova TA, Akimov V, Henningsen J, Johansen PT, Kratchmarova I, Kassem M, Mann M, Olsen JV, Blagoev B. (2011) System-wide temporal characterization of the proteome and phosphoproteome of human embryonic stem cell differentiation. *Sci Signal*, Vol. 4, p. rs3.

Rogers G, Rogers S, Schwimmer T, Ems-McClung S, Walczak C, Vale R. (2004) Two mitotic kinesins cooperate to drive sister chromatid separation during anaphase. *Nature*, Vol. 427, pp. 364-370.

Rusan NM, Peifer M. (2008) Original CIN: reviewing roles for APC in chromosome instability. *J Cell Biol*, Vol. 181, pp. 719-726.

Samora CP, Mogessie B, Conway L, Ross JL, Straube A, McAinsh AD. (2011) MAP4 and CLASP1 operate as a safety mechanism to maintain a stable spindle position in mitosis. *Nat Cell Biol*, Vol. 13, pp. 1040-1050.

Sandall S, Severin F, McLeod IX, Yates JR 3rd, Oegema K, Hyman A, Desai A. (2006) A Bir1-Sli15 complex connects centromeres to microtubules and is required to sense kinetochore tension. *Cell*, Vol. 127, pp. 1179-1191.

Santaguida S, Musacchio A. (2009) The life and miracles of kinetochores. *EMBO J*, Vol. 28, pp. 2511-2531.

Santaguida S, Tighe A, D'Alise AM, Taylor SS, Musacchio A. (2010) Dissecting the role of MPS1 in chromosome biorientation and the spindle checkpoint through the small molecule inhibitor reversine. *J Cell Biol*, Vol. 190, pp. 73-87.

Sardar HS, Luczak VG, Lopez MM, Lister BC, Gilbert SP. (2010) Mitotic kinesin CENP-E promotes microtubule plus-end elongation. *Curr Biol*, Vol. 20, pp. 1648-1653.

Schaar BT, Chan GK, Maddox P, Salmon ED, Yen TJ. (1997) CENP-E function at kinetochores is essential for chromosome alignment. *J Cell Biol*, Vol. 139, pp. 1373-1382.

Schittenhelm RB, Chaleckis R, Lehner CF. (2009) Intrakinetochore localization and essential functional domains of Drosophila Spc105. *EMBO*, Vol. 28, pp. 2374-2386.

Schleiffer A, Maier M, Litos G, Lampert F, Hornung P, Mechtler K, Westermann S. (2012) CENP-T proteins are conserved centromere receptors of the Ndc80 complex. *Nat Cell Biol*, Vol. 14, pp. 604-613.

Schmidt JC, Arthanari H, Boeszoermenyi A, Dashkevich NM, Wilson-Kubalek EM, Monnier N, Markus M, Oberer M, Milligan RA, Bathe M, Wagner G, Grishchuk EL, Cheeseman IM. (2012) The kinetochore-bound Ska1 complex tracks depolymerizing microtubules and binds to curved protofilaments. *Dev Cell*, Vol. 23, pp. 968-980.

Schmitzberger F, Harrison SC. (2012) RWD domain: a recurring module in kinetochore architecture shown by a Ctf19-Mcm21 complex structure. *EMBO Rep*, Vol. 13, pp. 216-222.

Screpanti E, De Antoni A, Alushin GM, Petrovic A, Melis T, Nogales E, Musacchio A. (2011) Direct binding of Cenp-C to the Mis12 complex joins the inner and outer kinetochore. *Curr Biol*, Vol. 21, pp. 391-398.

Sczaniecka M, Hardwick K. (2008) The spindle checkpoint: how do cells delay anaphase onset? *SEB Exp Biol Ser*, Vol. 59, pp. 243-256.

Sekulic N, Bassett EA, Rogers DJ, Black BE. (2010) The structure of (CENP-A-H4)(2) reveals physical features that mark centromeres. *Nature*, Vol. 467, pp. 347-351.

Sekulic N, Black BE. (2009) A reader for centromeric chromatin. *Nat Cell Biol*, Vol. 11, pp. 793-795.

Sheltzer JM, Amon A. (2011) The aneuploidy paradox: costs and benefits of an incorrect karyotype. *Trends Genet*, Vol. 27, pp. 446-453.

Shepperd LA, Meadows JC, Sochaj AM, Lancaster TC, Zou J, Buttrick GJ, Rappsilber J, Hardwick KG, Millar JB. (2012) Phosphodependent recruitment of Bub1 and Bub3 to Spc7/KNL1 by Mph1 kinase maintains the spindle checkpoint. *Curr Biol*, Vol. 22, pp. 891-899.

Shrestha RL, Draviam VM. (2013) Lateral to End-on Conversion of Chromosome-Microtubule Attachment Requires Kinesins CENP-E and MCAK. *Current Biology*, pp. 1-13.

Singh TR, Saro D, Ali AM, Zheng XF, Du CH, Killen MW, Sachpatzidis A, Wahengbam K, Pierce AJ, Xiong Y, Sung P, Meetei AR. (2010) *Mol Cell*, Vol. 37, pp. 879-886.

Skibbens RV, Rieder CL, Salmon ED. (1995) Kinetochore motility after severing between sister centromeres using laser microsurgery: evidence that kinetochore directional instability and position is regulated by tension. *J Cell Sci*, Vol. 108 (Pt 7), pp. 2537-2548.

Skibbens RV, Skeen VP, Salmon ED. (1993) Directional instability of kinetochore motility during chromosome congression and segregation in mitotic newt lung cells: a push-pull mechanism. *J Cell Biol*, Vol. 122, pp. 859-875.

Starr DA, Saffery R, Li Z, Simpson AE, Choo KH, Yen TJ, Goldberg ML. (2000) HZwint-1, a novel human kinetochore component that interacts with HZW10. *J Cell Sci*, Vol. 113 (Pt 11), pp. 1939-1950.

Stepanova T, Slemmer J, Hoogenraad CC, Lansbergen G, Dortland B, De Zeeuw CI, Grosveld F, van Cappellen G, Akhmanova A, Galjart N. (2003) Visualization of microtubule growth in cultured neurons via the use of EB3-GFP (end-binding protein 3-green fluorescent protein). *J Neurosci*, Vol. 23, pp. 2655-2664.

Stumpff J, Du Y, English CA, Maliga Z, Wagenbach M, Asbury CL, Wordeman L, Ohi R. (2011) A tethering mechanism controls the processivity and kinetochore-microtubule plus-end enrichment of the kinesin-8 Kif18A. *Mol Cell*, Vol. 43, pp. 764-775.

Stumpff J, von Dassow G, Wagenbach M, Asbury C, Wordeman L. (2008) The kinesin-8 motor

Kif18A suppresses kinetochore movements to control mitotic chromosome alignment. *Dev Cell,* Vol. 14, pp. 252-262.

Stumpff J, Wagenbach M, Franck A, Asbury CL, Wordeman L. (2012) Kif18A and chromokinesins confine centromere movements via microtubule growth suppression and spatial control of kinetochore tension. *Dev Cell*, Vol. 22, pp. 1017-1029.

Stumpff J, Wordeman L. (2007) Chromosome congression: the kinesin-8-step path to alignment. *Curr Biol*, Vol. 17, R326-328.

Su LK, Burrell M, Hill DE, Gyuris J, Brent R, Wiltshire R, Trent J, Vogelstein B, Kinzler KW. (1995) APC binds to the novel protein EB1. *Cancer Res*, Vol. 55, pp. 2972-2977.

Sumara I, Giménez-Abián JF, Gerlich D, Hirota T, Kraft C, de la Torre C, Ellenberg J, Peters J-M. (2004) Roles of polo-like kinase 1 in the assembly of functional mitotic spindles. *Curr Biol*, Vol. 14, pp. 1712-1722.

Sundin LJR, Guimaraes GJ, DeLuca JG. (2011) The NDC80 complex proteins Nuf2 and Hec1 make distinct contributions to kinetochore-microtubule attachment in mitosis. *Mol Biol Cell*, Vol. 22, pp. 759-768.

Suzuki A, Hori T, Nishino T, Usukura J, Miyagi A, Morikawa K, Fukagawa T. (2011) Spindle microtubules generate tension-dependent changes in the distribution of inner kinetochore proteins. *J Cell Biol*, Vol. 193, pp. 125-140.

Takeuchi K, Nishino T, Mayanagi K, Horikoshi N, Osakabe A, Tachiwana H. (2013, Nov 14) The centromeric nucleosome-like CENP-T-W-S-X complex induces positive supercoils into DNA. *Nucleic Acids Res*.

Tanaka K, Chang HL, Kagami A, Watanabe Y. (2009) CENP-C functions as a scaffold for effectors with essential kinetochore functions in mitosis and meiosis. *Dev Cell*, Vol. 17, pp. 334-343.

Tanenbaum ME, Galjart N, van Vugt MATM, Medema RH. (2006) CLIP-170 facilitates the formation of kinetochore-microtubule attachments. *EMBO J*, Vol. 25, pp. 45-57.

Tirnauer JS, Canman JC, Salmon ED, Mitchison TJ. (2002) EB1 targets to kinetochores with attached, polymerizing microtubules. *Mol Biol Cell*, Vol. 13, pp. 4308-4316.

Tokai N, Fujimoto-Nishiyama A, Toyoshima Y, Yonemura S, Tsukita S, Inoue J, Yamamota T. (1996). Kid, a novel kinesin-like DNA binding protein, is localized to chromosomes and the mitotic spindle. *EMBO J*, Vol. 15, pp. 457-467.

Tooley JG, Miller SA, Stukenberg PT. (2011) The Ndc80 complex uses a tripartite attachment point to couple microtubule depolymerization to chromosome movement. *Mol Biol Cell*, Vol. 22, pp. 1217-1226.

Tooley J, Stukenberg PT. (2011) The Ndc80 complex: integrating the kinetochore's many movements. *Chromosome Res*, Vol. 19, pp. 377-391.

Toso A, Winter JR, Garrod AJ, Amaro AC, Meraldi P, McAinsh AD. (2009) Kinetochore-generated pushing forces separate centrosomes during bipolar spindle assembly. *J Cell Biol*, Vol. 184, pp. 365-372.

Tsvetkov AS, Samsonov A, Akhmanova A, Galjart N, Popov SV. (2007) Microtubule-binding proteins CLASP1 and CLASP2 interact with actin filaments. *Cell Motil Cytoskeleton*, Vol. 64, pp. 519-530.

van Vugt, M, Medema R. (2005) Getting in and out of mitosis with Polo-like kinase-1. *Oncogene*, Vol. 24, pp. 2844-2859.

Varga et al. (2009) Kinesin-8 motors act cooperatively to mediate length-dependent microtubule depolymerization. *Cell*, Vol. 138, pp. 1174-1183.

Varma D, Monzo P, Stehman SA, Vallee RB. (2008) Direct role of dynein motor in stable kinetochore-microtubule attachment, orientation, and alignment. *J Cell Biol*, Vol. 182, pp. 1045-1054.

Varma D, Salmon ED. (2012) The KMN protein network--chief conductors of the kinetochore orchestra. *J Cell Sci*, Vol. 125, pp. 5927-5936.

Vaughan KT, Vallee RB. (1995) Cytoplasmic dynein binds dynactin through a direct interaction between the intermediate chains and p150Glued. *J Cell Biol*, Vol. 131, pp. 1507-16.

Vázquez-Novelle MD, Mirchenko L, Uhlmann F, Petronczki M. (2010) The 'anaphase problem': how to disable the mitotic checkpoint when sisters split. *Biochem Soc Trans*, Vol.38, pp.1660-1666.

Venkei Z, Przewloka M, Glover D. (2011) Drosophila Mis12 complex acts as a single functional unit essential for anaphase chromosome movement and a robust spindle assembly checkpoint. *Genetics*, Vol. 187, pp. 131-140.

Vigneron S, Prieto S, Bernis C, Labbé JC, Castro A, Lorca T. (2004) Kinetochore localization of spindle checkpoint proteins: who controls whom? *Mol Biol Cell*, Vol. 15, pp. 4584-4596.

Vitre B, Coquelle FM, Heichette C, Garnier C, Chrétien D, Arnal I. (2008) EB1 regulates

microtubule dynamics and tubulin sheet closure in vitro. *Nat Cell Biol*, Vol. 10, pp. 415-421.

Vogel PD. (2005) Nature's design of nanomotors. *Eur J Pharm Biopharm*, Vol. 60, pp. 267-277.

Von Delius M, Leigh D. (2011) Walking molecules, *Chem Soc Rev*, Vol. 40, pp. 3656-3676.

Walczak CE, Cai S, Khodjakov A. (2010) Mechanisms of chromosome behaviour during mitosis. *Nat Rev Mol Cell Biol*, Vol. 11, pp. 1-24.

Walczak CE, Heald R. (2008) Mechanisms of mitotic spindle assembly and function. *Int Rev Cytol*, Vol. 265, pp. 111-158.

Wan X, O'Quinn RP, Pierce HL, Joglekar AP, Gall WE, DeLuca JG, Carroll CW, Liu S-T, Yen TJ, McEwen BF, Stukenberg PT, Desai A, Salmon ED. (2009) Protein architecture of the human kinetochore microtubule attachment site. *Cell*, Vol. 137, pp. 672-684.

Weaver BAA, Bonday ZQ, Putkey FR, Kops GJPL, Silk AD, Cleveland DW. (2003) Centromere-associated protein-E is essential for the mammalian mitotic checkpoint to prevent aneuploidy due to single chromosome loss. *J Cell Biol*, Vol. 162, pp. 551-563.

Weaver B, Silk A, Montagna C, Verdier-Pinard P, Cleveland D. (2007) Aneuploidy acts both oncogenically and as a tumor suppressor. *Cancer Cell*, Vol. 11, pp. 25-36.

Weaver LN, Ems-McClung SC, Stout JR, LeBlanc C, Shaw SL, Gardner MK, Walczak CE. (2011) Kif18A uses a microtubule binding site in the tail for plus-end localization and spindle length regulation. *Curr Biol*, Vol. 21, pp. 1500-1506.

Wei RR, Al-Bassam J, Harrison SC. (2007) The Ndc80/HEC1 complex is a contact point for

kinetochore-microtubule attachment. *Nat Struct Mol Biol*, Vol. 14, pp. 54-59.

Wei R, Ngo B, Wu G, Lee WH. (2011) Phosphorylation of the Ndc80 complex protein, HEC1, by Nek2 kinase modulates chromosome alignment and signaling of the spindle assembly checkpoint. *Mol Biol Cell*, Vol. 22, pp. 3584-3594.

Welburn JP, Grishchuk EL, Backer CB, Wilson-Kubalek EM, Yates JR 3rd, Cheeseman IM. (2009) The human kinetochore Ska1 complex facilitates microtubule depolymerization-coupled motility. *Dev Cell*, Vol. 16, pp. 374-385.

Welburn JPI, Vleugel M, Liu D, Yates JR, Lampson MA, Fukagawa T, Cheeseman IM. (2010) Aurora B phosphorylates spatially distinct targets to differentially regulate the kinetochore-microtubule interface. *Mol Cell*, Vol. 38, pp. 383-392.

Westermann S, Drubin DG, Barnes G. (2007) Structures and functions of yeast kinetochore complexes. *Annu Rev Biochem*, Vol. 76, pp. 563-591.

Westhorpe FG, Straight AF. (2013) Functions of the centromere and kinetochore in chromosome segregation. *Curr Opin Cell Biol*, Vol. 25, pp. 1-7.

Wise DA, Brinkley BR. (1997) Mitosis in cells with unreplicated genomes (MUGs): spindle assembly and behavior of centromere fragments. *Cell Motil Cytoskeleton*, Vol. 36, pp. 291-302.

Wojcik E, Basto R, Serr M, Scaërou F, Karess R, Hays T. (2001) Kinetochore dynein: its dynamics and role in the transport of the Rough deal checkpoint protein. *Nat Cell Biol*, Vol. 3, pp. 1001-7.

Wood KW, Lad L, Luo L, Qian X, Knight SD, Nevins N, Brejc K, Sutton D, Gilmartin AG, Chua PR, Desai R, Schauer SP, McNulty DE, Annan RS, Belmont LD, Garcia C, Lee Y, Diamond MA,

Faucette LF, Giardiniere M, Zhang S, Sun C-M, Vidal JD, Lichtsteiner S, Cornwell WD, Greshock JD, Wooster RF, Finer JT, Copeland RA, Huang PS, Morgans DJ, Dhanak D, Bergnes G, Sakowicz R, Jackson JR. (2010) Antitumor activity of an allosteric inhibitor of centromere-associated protein-E. *Proc Natl Acad Sci USA*, Vol. 107, pp. 5839-5844.

Wood KW, Sakowicz R, Goldstein LS, Cleveland DW. (1997) CENP-E is a plus end-directed kinetochore motor required for metaphase chromosome alignment. *Cell*, Vol. 91, pp. 357-366.

Wordeman L, Mitchison TJ. (1995) Identification and partial characterization of mitotic centromere-associated kinesin, a kinesin-related protein that associates with centromeres during mitosis. *J Cell Biol*, Vol. 128, pp. 95-104.

Wordeman L, Wagenbach M, von Dassow G. (2007) MCAK facilitates chromosome movement by promoting kinetochore microtubule turnover. *J Cell Biol,* Vol. 179, pp. 869-879.

Wu X, Xiang X, Hammer J. (2006) Motor proteins at the microtubule plus-end. *Trends Cell Biol*, Vol. 16, pp. 135-143.

Yajima J, Edamatsu M, Watai-Nishii J, Tokai-Nishizumi N, Yamamoto T, Toyoshima Y. (2003) The human chromokinesin Kid is a plus end-directed microtubule-based motor. *EMBO J*, Vol. 22, pp. 1067-1074.

Yamagishi Y, Yang CH, Tanno Y, Watanabe Y. (2012) MPS1/Mph1 phosphorylates the kinetochore protein KNL1/Spc7 to recruit SAC components. *Nat Cell Biol*, Vol. 14, pp. 746-752.

Yan Z, Delannoy M, Ling C, Daee D, Osman F, Muniandy PA, Shen X, Oostra AB, Du H, Steltenpool J, Lin T, Schuster B, Décaillet C, Stasiak AZ, Stone S, Hoatlin ME, Schindler D, Woodcock CL, Joenje H, Sen R, de WinterJP, Li L, Seidman MM, Whitby MC, Myung K,

Constantinou A, Wang W. (2010) A histone-fold complex and FANCM form a conserved DNA-remodeling complex to maintain genome stability. *Mol Cell*, Vol. 37, pp. 865-878.

Yang Z, Tulu US, Wadsworth P, Rieder CL. (2007) Kinetochore dynein is required for chromosome motion and congression independent of the spindle checkpoint. *Curr Biol*, Vol. 17, pp. 973-980.

Yardimci H, van Duffelen M, Mao Y, Rosenfeld SS, Selvin PR. (2008) The mitotic kinesin CENP-E is a processive transport motor. *Proc Natl Acad Sci U S A*, Vol. 105, pp. 6016-6021.

Zhai Y, Kronebusch P, Borisy G. (1995) Kinetochore Microtubule dynamics and the metaphase-anaphase transition. *J Cell Biol*, Vol. 131, pp. 721-734.

Zhang G, Kelstrup CD, Hu X-W, Kaas Hansen MJ, Singleton MR, Olsen JV, Nilsson J. (2012) The Ndc80 internal loop is required for recruitment of the Ska complex to establish end-on microtubule attachment to kinetochores. *J Cell Sci*, Vol. 125, pp. 3243-3253.

Appendix 1

OPEN ACCESS Freely available online

PLOS ONE

Step-Wise Assembly, Maturation and Dynamic Behavior of the Human CENP-P/O/R/Q/U Kinetochore Sub-Complex

Anja Eskat[1☯¤a], Wen Deng[2☯], Antje Hofmeister[1], Sven Rudolphi[1], Stephan Emmerth[3¤b], Daniela Hellwig[1¤c], Tobias Ulbricht[1], Volker Döring[1], James M. Bancroft[5], Andrew D. McAinsh[5], M. Cristina Cardoso[4], Patrick Meraldi[3], Christian Hoischen[1], Heinrich Leonhardt[2], Stephan Diekmann[1]*

1 Molecular Biology, FLI, Jena, Germany, **2** Department of Biology II, Center for Integrated Protein Science, Ludwig Maximilians University Munich, Planegg-Martinsried, Munich, Germany, **3** Institute of Biochemistry, ETH Zurich, Zurich, Switzerland, **4** Department of Biology,Technische Universität Darmstadt, Darmstadt, Germany, **5** Centre for Mechanochemical Cell Biology, Warwick Medical School, University of Warwick, Coventry, United Kingdom

Abstract

Kinetochores are multi-protein megadalton assemblies that are required for attachment of microtubules to centromeres and, in turn, the segregation of chromosomes in mitosis. Kinetochore assembly is a cell cycle regulated multi-step process. The initial step occurs during interphase and involves loading of the 15-subunit constitutive centromere associated complex (CCAN), which contains a 5-subunit (CENP-P/O/R/Q/U) sub-complex. Here we show using a fluorescent three-hybrid (F3H) assay and fluorescence resonance energy transfer (FRET) in living mammalian cells that CENP-P/O/R/Q/U subunits exist in a tightly packed arrangement that involves multifold protein-protein interactions. This sub-complex is, however, not pre-assembled in the cytoplasm, but rather assembled on kinetochores through the step-wise recruitment of CENP-O/P heterodimers and the CENP-P, -O, -R, -Q and -U single protein units. SNAP-tag experiments and immuno-staining indicate that these loading events occur during S-phase in a manner similar to the nucleosome binding components of the CCAN, CENP-T/W/N. Furthermore, CENP-P/O/R/Q/U binding to the CCAN is largely mediated through interactions with the CENP-N binding protein CENP-L as well as CENP-K. Once assembled, CENP-P/O/R/Q/U exchanges slowly with the free nucleoplasmic pool indicating a low off-rate for individual CENP-P/O/R/Q/U subunits. Surprisingly, we then find that during late S-phase, following the kinetochore-binding step, both CENP-Q and -U but not -R undergo oligomerization. We propose that CENP-P/O/R/Q/U self-assembles on kinetochores with varying stoichiometry and undergoes a pre-mitotic maturation step that could be important for kinetochores switching into the correct conformation necessary for microtubule-attachment.

Citation: Eskat A, Deng W, Hofmeister A, Rudolphi S, Emmerth S, et al. (2012) Step-Wise Assembly, Maturation and Dynamic Behavior of the Human CENP-P/O/R/Q/U Kinetochore Sub-Complex. PLoS ONE 7(9): e44717. doi:10.1371/journal.pone.0044717

Editor: Barbara Mellone, University of Connecticut, Storrs, United States of America

Received April 23, 2012; **Accepted** August 6, 2012; **Published** September 18, 2012

Funding: This work was supported by Deutsche Forschungsgemeinschaft (DFG DI 258/17-1, SPP1128, SPP1395), and Thüringer Aufbaubank (2007 FE 9011). The funders had no role in study design, data collection and analysis, decision to publish, or preparation of the manuscript.

Competing Interests: The authors have declared that no competing interests exist.

* E-mail: diekmann@fli-leibniz.de

☯ These authors contributed equally to this work.

¤a Current address: Institute of Biochemistry, ETH Zurich, Zurich, Switzerland
¤b Current address: Friedrich Miescher Institute for Biomedical Research, Basel, Switzerland
¤c Current address: HKI, Jena, Germany

Introduction

During mitosis, accurate chromosome segregation is essential for the correct transmission of the genetic material to the daughter cells. A multi-protein complex, the kinetochore, assembles at the centromere of each chromatid in order to mediate this function. Kinetochores contain an inner core that is present throughout the cell cycle [1,2], and a set of outer kinetochore proteins that stably associate with the inner core during mitosis [3,4]. The kinetochore is built from two major conserved protein networks, (1) the CCAN (constituitive centromere associated network) complex [5–13] which is associated to centromeric nucleosomes [5,14–16] that consist of repetitive α-satellite DNA containing the histone H3 variant CENP-A [17,18], and (2) the KMN network [7,19–27] which directly connects the kinetochore to microtubules [3,28,29]. Functionally, the CCAN is required for the efficient recruitment of CENP-A into centromeric nucleosomes at the end of mitosis [6,14,30,31] and the maintenance of centromeric chromatin, but is also involved in chromosome alignment, kinetochore fiber stability and bipolar spindle assembly [1,2,5,6,8,32–34]. The CCAN was suggested to establish, in interphase, an inner kinetochore structure which functions as an assembly platform for KMN network proteins in mitosis, and only the KMN proteins then connect the inner kinetochore to microtubules [3]. However, ectopical CENP-T and -C alone are able to establish a functional outer kinetochore [16,35] indicating that instead of being only a structural platform, the CCAN seems to be a regulator of the mitotic kinetochore-microtubule attachment [36].

The CCAN proteins CENP-U, -O, -P, -Q, and -R were identified as a CCAN subclass (named CENP-O class proteins)

[3,5,6,10,37]. CENP-PORQU proteins are non-essential showing, when depleted, common mitotic defects and slower proliferation rates [6,10,33,38]. Kinetochore localization of CENP-PORQU is interdependent [5,10,36]. In chicken DT40 cells, and when these genes are expressed in *E. coli*, CENP-O, -P, -U and -Q form a stable complex to which CENP-R can associate [10]. These data describe the CENP-PORQU complex as a stable unit which might function as a structural element in the CCAN. However, CENP-PORQU proteins have different protein specific functions: CENP-U [39] as well as CENP-Q [36] are able to bind to microtubules, only depletion of CENP-O seems to destabilise microtubule bundles at kinetochores influencing bipolar spindle assembly [34,39], and CENP-U interacts with Hec1, an interaction negatively regulated by Aurora-B kinase [39]. In the complex, CENP-P is closely associated with CENP-O, and CENP-U binds to CENP-Q [10,40–42]. In order to resolve these different views, we analysed protein binding, complex architecture and dynamics of the human kinetochore CENP-PORQU sub-complex by various *in vivo* techniques.

Materials and Methods

Plasmids

Plasmids pIC133, pIC190, pIC141, pIC140, and pIC235 encoding LAP-CENP-K, -Q, -P, -O, respectively -R fusion proteins were a kind gift of Dan Foltz and Iain Cheeseman. The full length cDNA clone of CENP-L, IRAUp969 EO882D, was from RZPD, Berlin, Germany). They were used for amplification of full length CENP-K, -L, -Q, -P, -O, and -R by PCR (Expand high fidelity^{PLUS} PCR System, Roche, Penzberg, Germany) applying forward primer 5′-GGGGACAAGTTTGTACAAAAA-AGCAGGCTTCGAAAACCTGTATTTTCAGGGC*GCCACCA-TGG*GCATGAATCAGGAGGATTTAGATCC -3′ and reverse primer 5′- GGGGACCACTTTGTACAAGAAAGCTGGGTC-TGATGGAAAGCTTCTAATCTTATT -3′ for CENP-K, forward primer 5′- GGGGACAAGTTTGTACAAAAAAGCAGG-CTTCGAAAACCTGTATTTTCAGGGC*GCCACC*ATGGATT-CTTACAGTGCACCAG -3′ and reverse primer 5′- GGGGAC-CACTTTGTACAAGAAAGCTGGGTCTCAATTTGAAAAAT-TGCCAGTTCTG for CENP-L, forward primer 5′- GGGGA-CAAGTTTGTACAAAAAAGCAGGCTTCGAAAACCTGTAT-TTTCAGGGCGCCACCATGGGCATGTCTGGTAAAGCAAA-TGCTTC -3′ and reverse primer 5′- GGGGACCACTTTGTA-CAAGAAAGCTGGGTAGATGCATCCAGTTTCTTATAGG -3′ for CENP-Q, forward primer 5′- GGGGACAAGTTTGTA-CAAAAAAGCAGGCTTCGAAAACCTGTATTTTCAGGGC-GCCACCATGGACGCAGAGCTGGCAGA -3′ and reverse primer 5′- GGGGACCACTTTGTACAAGAAAGCTGGGTG-TTGTTCTCCTCTGCACAAAGC -3′ for CENP-P, forward primer 5′- GGGGACAAGTTTGTACAAAAAAGCAGGCTT-CGAAAACCTGTATTTTCAGGGCGCCACCATGGAGCAG-GCGAACCCTTT -3′ and reverse primer 5′- GGGGACCAC-TTTGTACAAGAAAGCTGGGTGGAGACCAGACTCATAT-CCAAC -3′ for CENP-O, and forward primer 5′- GGGGAC-AAGTTTGTACAAAAAAGCAGGCTTCGAAAACCTGTATT-TTCAGGGCGCCACCATGGGCATGCCTGTTAAAAGATCA-CTGAA -3′ and reverse primer 5- GGGGACCACTTTGTA-CAAGAAAGCTGGGTGTTTAAAATGGCTTTAAGGAATT-CA -3′ for CENP-R. The CENP-Q, -P, -O, and -R harbouring linear PCR fragments were transferred into vector pDONR221 by BP recombination reaction (Invitrogen, Carlsbad, CA, USA). After verification by sequencing (MWG Biotech, Ebersberg, Munich, Germany), the genes were cloned by LR recombination reactions into various modified pFP-C and pFP-N (BD Biosciences, Clontech, Palo Alto, CA, USA) based Destination vectors. As the result we obtained expression vectors carrying the genes coding for CENP-Q, -P, -O, and -R fused to the C-termini as well as to the N-termini of EGFP and mCherry. In the constructed fluorescent proteins (FP)-CENP-Q, -P, -O, and -R, the amino acid (aa) linker between the fused proteins is SGTSLYKKAGFENLYFQGAT. Due to the cloning protocol, the aa sequence TQLSCTKW is added to the C-terminal ends of FP-CENP-Q, -P, -O, and -R. In the constructs where CENP-Q, -P, -O, and -R are fused to the N-termini of EGFP respectively mCherry, the (aa) linker is TQLSCTKWLDPPVAT. The cloning of CENP-U and -C [43] and CENP-N [44] have been described previously. Vector pIRES2 used for the simultaneous expression of EGFP and mRFP, was a friendly gift of J. Langowski (Heidelberg). For expression of a mRFP-EGFP fusion protein, we digested vector pmRFP-C1 with SnaBI and XmaI and ligated the resulting 1012 bps DNA fragment containing mRFP into a 7106 bp DNA obtained from a SnabI-XmaI digest of vector pH-G-C. In the resulting Gateway expression vector pH-mR-G-C, the amino acid linker between mRFP and EGFP is SGLRSRAQASNSAVDG-TAGPVAT. Full length protein expression of the fusion constructs was confirmed by Western Blots.

Live cell FRET measurements

FRET was measured by applying the acceptor photo-bleaching method using the FRET pair EGFP-mCherry. Co-transfected HEp-2 cells grown on coverslips were analyzed using a confocal laser scanning microscope (LSM 510 Meta) and a C-Apochromat 63×/1.2NA oil immersion objective (Carl Zeiss, Jena, Germany). EGFP fluorescence was excited with the Argon 488 nm laser line and analyzed using the Meta detector (ChS1+ChS2: 505–550 nm). mCherry fluorescence was excited with the 561 nm laser line (DPSS 561-10) and detected in one of the confocal channels using a 575–615 nm band-pass filter. To minimize cross talk between the channels, each image was collected separately in the multi-track-mode, i.e. both fluorophores were exited and recorded specifically and separately. Cells moderately expressing both fusion proteins with comparable expression levels were selected for analysis. Acceptor photo-bleaching was achieved by scanning a region of interest (ROI) including up to five centromeres of a nucleus 50 times (scans at 1.6 µsec pixel time) using the 561 nm laser line at 100% intensity. Bleaching times per pixel were identical for each experiment, however, total bleaching times varied depending on the size of the bleached ROIs. 4 donor and acceptor fluorescence images were taken before and up to 4 images after the acceptor photo-bleaching procedure to assess changes in donor and acceptor fluorescence. To minimize the effect of photo-bleaching of the donor during the imaging process, the image acquisition was performed at low laser intensities. To compare the time course of different experiments, donor intensities in the ROI were averaged and normalized to the intensity measured at the first time point after photo-bleaching, and acceptor intensities in the ROI were averaged and normalized to the mean intensity measured at time points 2–4 before photo-bleaching. The FRET efficiency was calculated by comparing the fluorescence intensity (I_{DA}) before bleaching (in presence of the acceptor) with the intensity (I_D) measured after bleaching (in the absence of the acceptor) according to $E = 1 - I_{DA}/I_D$. The FRET efficiencies of numerous bleached and unbleached locations were compared by a paired t-test ($\alpha = 0.05$). The difference between the means is a measure for the FRET-value, which was interpreted to have occurred when the paired t-test revealed a statistically significant difference between the two input groups with a p-value below 0.001. A p-value >0.001 was interpreted as an indication for insignificant FRET.

In two cases, the acceptor-bleaching FRET data were confirmed by additional fluorescence lifetime FLIM experiments. In FLIM experiments, the donor fluorescence lifetime was determined by time-correlated single photon counting (TCSPC) in living human HEp-2 cells. For donor fluorescence excitation, a pulsed picosecond diode laser (LDH Series, PicoQuant, Berlin, Germany) with a frequency of 20 MHz along with a dedicated driver (PDL Series, PicoQuant) was used. Via a fiber coupling unit, the excitation light was guided into a confocal laser scanning microscope (LSM 510 Meta). Laser power was adjusted to give average photon counting rates of 10^4–10^5 photons/sec (0.0001–0.001 photon counts per excitation event) or less to avoid pulse pile-up. Images of 256×256 pixels were acquired with a 63× C-Apochromat water immersion objective (NA 1.20, Carl Zeiss). Photons emitted by the sample were collected by the water immersion objective and detected by a single photon avalanche diode (PDM series, PicoQuant). The data were acquired by the PicoHarp 300 TCSPC module (PicoQuant) working in the TTTR mode (time-tagged time-resolved). To calculate the fluorescence lifetime, the SymPhoTime software package (v4.7, PicoQuant) was used. Selected areas of the images corresponding to single centromeres (resulting in the fluorescence lifetime histograms) or the sum of all centromeric regions were fitted by maximum likelihood estimation (MLE). Depending on the quality of a fit indicated by the value of χ^2, a mono- or bi-exponential fitting model including background was applied. A model was rejected when χ^2 exceeded a value of 1.5. In this way, the presence of scattered light in few measurements could be identified and separated. However, due to low photon numbers and too close time constants, the simultaneous presence of two different donor fluorescence lifetimes for complexes with donor-only and donor plus acceptor in one centromere could not be separated by a bi-exponential fit. A donor fluorescence lifetime obtained from a centromere in a cell co-expressing donor and acceptor molecules was considered to be significantly different from the control measurement, when the lifetime differed from the mean of the control values by >3 standard deviations. The FRET efficiency was calculated by comparing the donor fluorescence lifetime (τ_{DA}) in the presence of the acceptor with the respective fluorescence lifetimes (τ_D) of control measurements obtained in absence of an acceptor following $E = 1-\tau_{DA}/\tau_D$.

F3H

BHK cells containing a *lac* operator repeat array [45] were cultured in DMEM medium with 10% FCS and seeded on coverslips in 6-well plates for microscopy. After attachment, cells were co-transfected with expression vectors for the indicated fluorescent fusion proteins and a LacI-GBP fusion [46,47] using polyethylenimine (Sigma, St. Louis, USA). After about 16 hrs cells were fixed with 3.7% formaldehyde in PBS for 10 minutes, washed with PBST (PBS with 0.02% Tween), stained with DAPI and mounted in Vectashield medium (Vector Laboratories, Servison, Switzerland).

Samples were analyzed with a confocal fluorescence microscope (TCS SP5, Leica, Wetzlar, Germany) equipped with a 63×/1.4 numerical aperture Plan-Apochromat oil immersion objective as described [47]. DAPI, EGFP and mCherry were excited by 405 nm diode laser, 488 nm argon laser and 561 nm diode-pumped solid-state laser, respectively. Images were recorded with a frame size of 512×512 pixels.

Cell culture, transfection and Western Blots

HeLa, HEp-2 and U2OS cells (ATCC, Manassas, USA) were cultured and Western blots were carried out as described [44,48]. In order to determine cell cycle dependent CENP-O/Q/P levels, HEp-2 or HeLa cells were synchronised by double-thymidine block. Aliquots of equal cell numbers were taken after 2, 4, 6, 8 and 10 hrs after release and lysed. In the Western blot, CENP-O [33], CENP-P [36] and CENP-Q (Rockland, Gilbertsville, USA) are identified by specific primary antibodies which are then detected by fluorescently labelled secondary antibody (Molecular Probes, Eugene, USA). CENP-O/P/Q amounts are quantified by the ODYSSEY Infrared Imaging System (LiCor, Lincoln, USA) following the protocol of the manufacturer.

Fluorescence Cross-Correlation Spectroscopy (FCCS)

FCCS analyses [49,50] were performed at 37°C on an LSM 710 Confocor3 microscope (Carl Zeiss, Jena, Germany) using a C-Apochromat infinity-corrected 40×/1.2 NA water objective. U2OS cells were double transfected with vectors for the simultaneous expression of EGFP and mCherry fusion proteins and analysed. On cells expressing both fusion proteins at relatively low and comparable levels, we selected spots for the FCCS measurements in areas of the nucleoplasm which were free of kinetochores. For illumination of the EGFP-fusion proteins, we used the 488 nm laser line of a 25 mW Argon/2-laser (Carl Zeiss) and for simultaneous illumination of the mCherry fusion proteins a DPSS 561-10-laser (Carl Zeiss), both at moderate intensities between 0.2 and 0.5%. The detection pinhole was set to a relatively small diameter of 40 µm (corresponding to about 0.8 airy units). After passing a dichroic beam splitter for APDs (avalange photodiode detector; NTF 565), the emission of mCherry was recorded in channel 1 through a BP-IR 615–680 nm bandpath filter by an APD (Carl Zeiss), whereas the emission of EGFP was simultaneously recorded in channel 2 through a BP-IR 505–540 nm bandpath filter by a second APD. Before each measurement, we analysed possible crosstalk between the channels and used only cells without or with very little crosstalk. In addition, measurements with autocorrelation values below 1.06 for both, the mRFP channel as well as the EGFP channel, were not further analysed. For the measurements, 10×10 time series of 10 sec each were simultaneously recorded for mCherry and for EGFP. After averaging, the data were superimposed for fitting with the Fit-3Dfree-1C-1Tnw model of the ZEN-software (Carl Zeiss), a diffusion model in three dimensions with triplet function. Applying this procedure, we obtained autocorrelations of channels 1 and 2 as well as the cross-correlation of channels 1 versus channel 2. Before starting a set of experiments, the pinhole was adjusted. As negative control, U2OS cells were transfected with vector pIRES2, separately expressing EGFP and mRFP as single molecules with fluorescence intensities comparable to those in the FCCS analysis with CENP fusion proteins. As a positive control, U2OS cells were transfected with pH-mR-G-C expressing a mRFP-EGFP fusion protein, again with fluorescence intensities comparable to those in the FCCS analysis with CENP fusion proteins.

Cellular imaging

In vivo and *in situ* cellular imaging including immuno-fluorescence, SNAP-tag analysis, FRAP, RICS and cell cycle sychronisation were conducted as described in Orthaus et al. [48,51], Hellwig et al. [43,44] and McClelland et al [8]. For immuno-flourescence, primary antibodies were used at 1:250 (PCNA), 1:300 (anti-CENP-Q), 1:250 (CREST) with DAPI at 1:2000.

Results

CENP-O class proteins form a tightly packed complex

In chicken DT40 cells, the CENP-O class proteins form a tight kinetochore sub-complex [10]. Here we analysed the CENP-O class protein packaging at kinetochores in living human cells by measuring which proteins are in close proximity. We tagged all five CENP-O class proteins with fluorescent proteins, either EGFP or mCherry, at either termini, and confirmed by live cell imaging in human U2OS cells that all tagged CENP-O class proteins localise to kinetochores during interphase and mitosis, consistent with published results [5,6,10,33,36,39]. This kinetochore localisation was independent of which terminus of the CENP proteins was tagged.

Then, by FRET we measured the proximity between chromophores tagged to CENP-O class proteins. FRET between the donor fluorophore (here: EGFP) and the acceptor fluorophore (here: mCherry) can only generate a positive result when the distance between donor and acceptor is less than ~10 nm. When FRET occurs, both the intensity and lifetime of the donor fluorescence decrease while the intensity of the acceptor emission increases. We measured the FRET donor fluorescence intensity with or without photo-inactivation of the acceptor (acceptor-photo-bleaching FRET, AB-FRET) and, in order to confirm our AB-FRET results, in two cases also the donor fluorescence lifetime (FLIM). In AB-FRET, the acceptor chromophore is destroyed by photo-bleaching, thereby preventing FRET from the donor to the acceptor. Thus, when the donor is in close proximity to the acceptor (sufficient for FRET, <10 nm), photo-bleaching of the acceptor results in an observable increase in donor fluorescence. In our experiments, two separate kinetochore locations were identified in each image (marked "1" and "2"; Fig. 1A and 1D). In spot "2" the acceptor (CENP-R-mCherry (Fig. 1A), CENP-P-mCherry (Fig. 1D)) was photo-bleached, while spot "1" was not photo-bleached, serving as an internal control for any non-FRET effects. During bleaching of the acceptor (CENP-R-mCherry) in spot 2, the donor (EGFP-CENP-U) fluorescence intensity significantly increased indicating that FRET occurred between EGFP-CENP-U and CENP-R-mCherry (Fig. 1B). Careful quantification indicated that such FRET transfer occurred in 60% of the cases, yielding a FRET efficiency E_{FRET} between 6 and 18% (40 bleached spots in 18 cells, black bars in Fig. 1C). The unbleached control spots show a narrow fluorescence variation E_{var} around zero (39 bleached spots in 18 cells, grey bars in Fig. 1C). The E_{FRET} distribution is significantly different from the E_{var} control distribution ($p<0.001$). Such experiments demonstrated that the majority of pairs gave a positive FRET signal suggesting that the CENP-PORQU subunits are closely associated (see Table 1). Importantly, a number of pairs did not show FRET: We detected no FRET between EGFP-CENP-Q/CENP-P-mCherry (Fig. 1D–F). Here, after acceptor-bleaching, the donor fluorescence did not increase (Fig. 1E) and the distribution of the E_{FRET} values (black bars, Fig. 1F) superimposes with the distribution of the E_{var} control values (grey bars). Furthermore, we did not observe FRET between EGFP-CENP-P/CENP-O-mCherry and between EGFP-CENP-U/CENP-O-mCherry (see Table 1). For CENP-Q-EGFP and mCherry-CENP-P and for CENP-P-EGFP and mCherry-CENP-O, we confirmed these results by measuring FRET at kinetochores in the lifetime domain (FLIM) by time-correlated single photon counting (TCSPC) using the same fluorescent protein FRET pair EGFP-mCherry. This approach is less error prone compared to acceptor-bleaching FRET in the intensity domain, however, it is considerably more elaborate and time-consuming. We determined the CENP-Q-EGFP donor lifetime in the absence of an acceptor as $\tau = 2.45 \pm 0.10$ nsec. When the acceptor is close, the donor life time decreases due to energy transfer to the acceptor: for CENP-Q-EGFP/mCherry-CENP-P we measured $\tau = 2.08 \pm 0.04$ nsec and for CENP-P-EGFP/mCherry-CENP-O we measured $\tau = 2.16 \pm 0.05$ nsec. The FLIM results (marked by "F" in Table 1) indicate the proximity between CENP-Q and -P as well as between CENP-P and -O and confirm our acceptor-bleaching FRET data. We conclude that in human cells at kinetochores, CENP-O class proteins are in close proximity to one another. In earlier studies we had detected FRET between the CENP-U N-terminal region and the N-termini of CENP-B and CENP-I, but not to the N-termini of CENP-A and CENP-C [43].

If the orientation of the fluorophore dipole moment of the acceptor relative to that of the donor were known, or at least one of them would rotate freely faster than nanoseconds, a more detailed distance between donor and acceptor could be deduced from the measured E_{FRET} values. In our live cell experiments however, this information is not available to us. We therefore do not deduce defined distance values but interpret the appearance of FRET as an indication that donor and acceptor chromophores are close to one another within 10 nm. Our FRET data depend on which protein terminus is tagged: if the two protein termini are clearly separated in space, a fluorophore fused to one terminus might show FRET to another protein while the fluorophore fused to the other terminus might not. In a number of cases, we could not detect FRET between two fusion proteins. Measuring no FRET signal might either be due to donor and acceptor fluorophores being distal (>10 nm) or, alternatively, that donor and acceptor dipole moments are oriented relative to one another in an unfavorable way so that FRET cannot occur although donor and acceptor are close. Therefore, observing no FRET signal cannot be used for structural information.

PORQU undergoes a post-loading oligomerisation step

Recombinant CENP-Q that is expressed and purified form *E. coli* lysates, exists as a soluble homo-octameric complex [36]. We therefore asked if CENP-Q oligomerises at kinetochores in living human cells. Indeed, we observed FRET at kinetochores between the N-termini of CENP-Q and between its C-termini in interphase cells, suggesting that CENP-Q oligomerises when kinetochore-bound. In order to find out when in the cell cycle CENP-Q oligomerizes, we carried out cell cycle dependent FRET measurements between C- and N-termini of CENP-Q (see Table 1, Fig. 2). U2OS cells were synchronised by double thymidine block and released into S-phase. Subsequent cell cycle phases were identified by CENP-F and PCNA staining. We found no FRET in G1, early and mid S-phase, however, we detected a significant FRET signal in late S-phase for both, the CENP-Q N- and C-termini, and in G2 for the CENP-Q N-termini (Fig. 2). Consistent with this, quantitative immuno-flourescence demonstrates that CENP-Q protein levels increase at kinetochores during S-phase and become maximal in late S-phase (see below). We also detected a FRET proximity between two CENP-U N-termini at kinetochores in late but not in early or middle S-phase (data not shown).

PORQU proteins show multiple pair-wise interactions

Then we asked which of the CENP-O class proteins is able to interact with other protein members of this class. In the mammalian three-hybrid (F3H) assay applied here [46,47], EGFP tagged CENP-O class proteins (bait) were recruited to the *lac* operator repeat array by the GFP-binding protein fused to the Lac repressor (GBP-LacI) forming a green spot in the nucleus (Fig. 3).

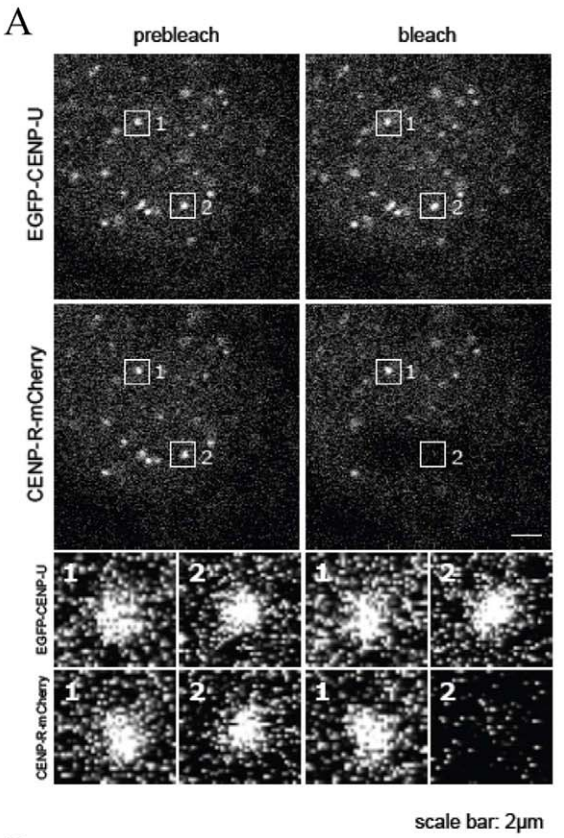

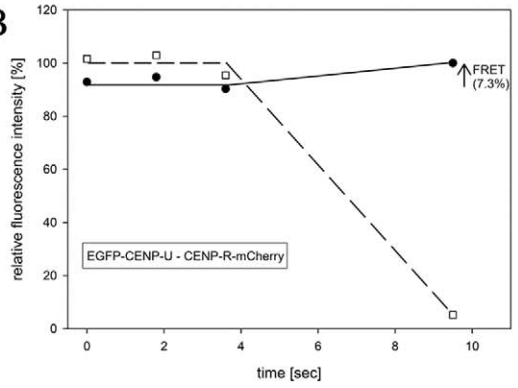

C
EGFP-CENP-U + CENP-R-mCherry

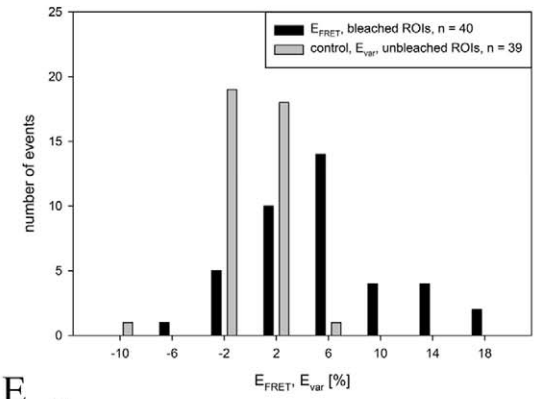

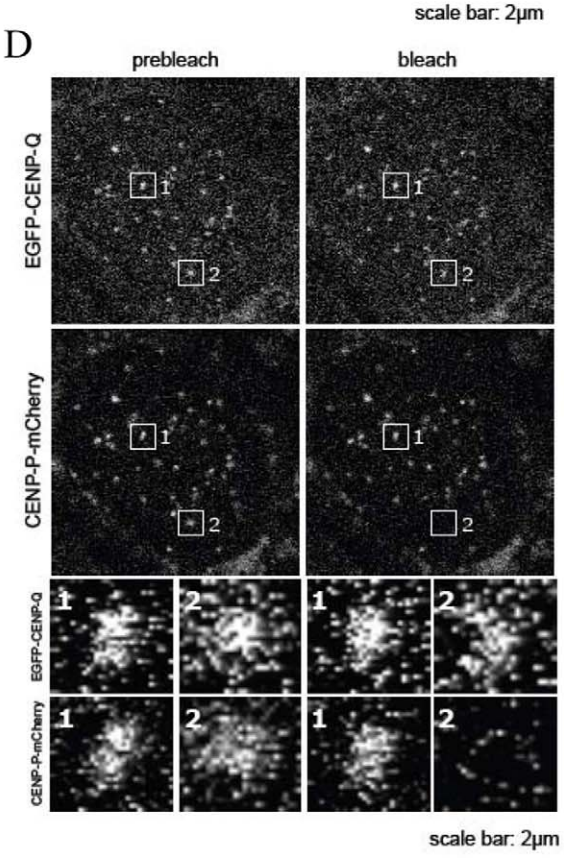

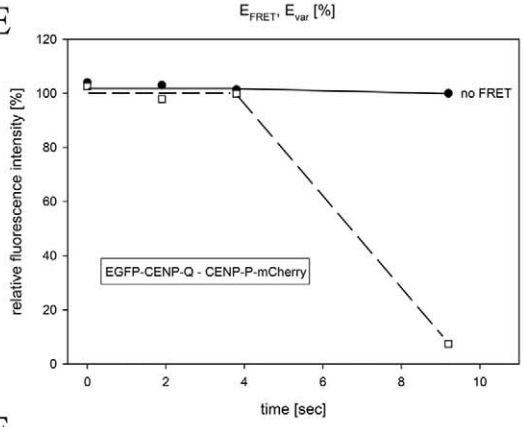

F
EGFP-CENP-Q + CENP-P-mCherry

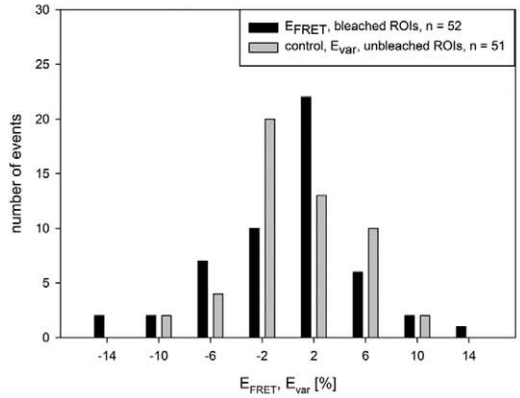

Figure 1. Acceptor-bleaching FRET of the protein pairs EGFP-CENP-U/CENP-R-mCherry (FRET signal) and EGFP-CENP-Q/CENP-P-mCherry (no FRET signal). Typical HEp-2 cell nuclei are displayed in (A) and (D) showing centromere location of all four CEN proteins. Two of these locations, spot 1 and spot 2 in each of the two graphs, were selected for fluorescence intensity analysis before and after acceptor bleaching (see enlargements below). Spot 1 served as control and showed no detectable intensity change. At spot 2, the acceptor fluorophore mCherry was bleached (compare pre-bleach and post-bleach in (A) and (D)). In (B) and (E), the time course of the fluorescence intensity of the donor and the acceptor of both FRET pairs are shown. The acceptor intensities in the ROI (''region of interest''; open squares) were averaged and normalized to the mean intensity measured at the three time points before bleaching. The donor intensities in the ROI were averaged and normalized to the intensity measured at the time point after bleaching. Bleaching of the acceptor resulted in a fluorescence intensity increase of the donor (black dots) for EGFP-CENP-U (B) indicating the presence of FRET (see arrow), but no fluorescence intensity increase for EGFP-CENP-Q (E) indicating the absence of FRET. (C) and (F): Donor fluorescence intensity variation observed during acceptor bleaching normalized to the intensity measured at the first time point after bleaching. Control: spot 1 (acceptor not bleached) yielding E_{var} (grey bars), FRET measurement: spot 2 (acceptor bleached) yielding E_{FRET} (black bars). For protein pairs indicated, number of observed single cases (grouped into E_{var} or E_{FRET} value ranges of 4%) displayed versus values of E_{var} or E_{FRET}. (C) EGFP-CENP-U (donor) and CENP-R-mCherry (acceptor): distribution of E_{FRET} (40 bleached kinetochores) is clearly distinct from the distribution of E_{var} (39 non-bleached kinetochores) indicating FRET. (F): EGFP-CENP-Q (donor) and CENP-P-mCherry (acceptor): distribution of E_{FRET} (52 bleached kinetochores) superimposes the distribution of E_{var} (51 non-bleached kinetochores) indicating no FRET.
doi:10.1371/journal.pone.0044717.g001

Co-expressed mCherry-tagged CENP-O class proteins (prey) may either interact with the EGFP-tagged protein at the *lac* operator array (visible as red spot and yellow in the overlay) or may not interact resulting in a disperse distribution. For each mCherry fusion, EGFP was used to control for unspecific interactions. In the upper two rows of Fig. 3A, the clear interaction between EGFP-CENP-O and mCherry-CENP-P as well as EGFP-CENP-P and mCherry-CENP-O are shown. The lower two rows show the corresponding results for CENP-O and CENP-Q. While EGFP-CENP-Q did not interact with and recruit mCherry-CENP-O to the *lac* spot, we found a very weak interaction in the reverse combination. Such differences for reverse combinations might be explained by sterical hindrance at the interaction site due to the attachment to GBP-LacI for one but not the other tagged terminal region. All results of this F3H interaction assay are listed in Table 2. The results of this CENP-O class protein interaction analysis indicate strong interactions between particular members of this class (Fig. 3B). CENP-O, -P and -Q each are able to strongly recruit and thus specifically bind two, while CENP-U and -R are able to recruit three of the remaining four proteins. In addition, CENP-U and CENP-R are able to bind to themselves. We detected homo-interaction of CENP-R also by a Yeast-two-Hybrid (Y2H) assay. CENP-U binding to itself is supported by our FRET data indicating close proximity between CENP-U N-termini in late S-phase (see above). Our data that CENP-P is closely associated with CENP-O, and CENP-U with CENP-Q, agree well with published results [10,41,42]; here we detected an additional weaker interaction between CENP-Q and CENP-R. However, none of the CENP-O class proteins is able to recruit all four other proteins of this class which would be expected when the

Table 1. FRET interactions between CENP-O class proteins.

EGFP fusion	mCherry fusion	p	FRET
EGFP-CENP-P	mCherry-CENP-O	<0.001	++
EGFP-CENP-P	CENP-O-mCherry	0.093	−
CENP-P-EGFP	mCherry-CENP-O	<0.001	++F
CENP-P-EGFP	CENP-O-mCherry	<0.001	++
EGFP-CENP-Q	mCherry-CENP-O	<0.001	++
EGFP-CENP-Q	CENP-O-mCherry	<0.001	++
EGFP-CENP-Q	mCherry-CENP-P	<0.001	++
EGFP-CENP-Q	CENP-P-mCherry	0.724	−
EGFP-CENP-Q	mCherry-CENP-Q	<0.001	++
CENP-Q-EGFP	CENP-Q-mCherry	<0.001	++
CENP-Q-EGFP	mCherry-CENP-P	<0.001	++F
EGFP-CENP-U	mCherry-CENP-O	<0.001	++
EGFP-CENP-U	CENP-O-mCherry	0.655	−
EGFP-CENP-U	mCherry-CENP-P	0.003	+
EGFP-CENP-U	CENP-P-mCherry	<0.001	++
EGFP-CENP-U	mCherry-CENP-Q	<0.001	++
EGFP-CENP-U	mCherry-CENP-R	<0.001	++
EGFP-CENP-U	CENP-R-mCherry	<0.001	++
CENP-U-EGFP	mCherry-CENP-P	<0.001	++
EGFP-CENP-B	CENP-Q-mCherry	<0.001	++
EGFP-CENP-O	mCherry-CENP-K	<0.001	++
CENP-O-EGFP	mCherry-CENP-K	0.004	+
EGFP-CENP-R	mCherry-CENP-K	<0.001	++
CENP-R-EGFP	mCherry-CENP-K	<0.001	++
EGFP-CENP-U	mCherry-CENP-K	<0.001	++
CENP-U-EGFP	mCherry-CENP-K	0.167	−
EGFP-CENP-U	mCherry-CENP-U	<0.001	++
CENP-N-EGFP	mCherry-CENP-K	<0.001	++

The FRET pair EGFP-mCherry is used. ''F'' indicates that for these fusions FRET was detected also by FLIM. ++: strong FRET, +: weak FRET, −: no FRET.
doi:10.1371/journal.pone.0044717.t001

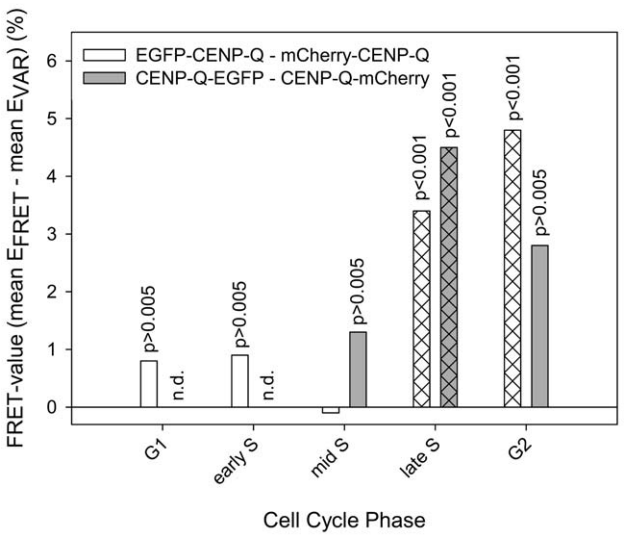

Figure 2. Cell cycle-dependent FRET between CENP-Q C- (grey bars) and N-termini (white bars). In late S-phase and G2, significant FRET is observed ($p<0.001$). In G1, early and mid S-phase, no FRET is observed ($p>0.005$).
doi:10.1371/journal.pone.0044717.g002

complex pre-forms in the nucleoplasm. Furthermore, ectopic recruitment to the *lac* operator repeat array obviously is not strong enough to enable indirect binding: e.g. CENP-L recruits CENP-R, and CENP-R recruits CENP-Q, but CENP-L is not able to attrack CENP-Q to this site. Thus, this F3H assay is, to a large extent, specific for direct interactions.

CENP-PORQU subcomplex contacts other CCAN proteins

Kinetochore localization is determined by CENP-A which is recognized by CENP-N and CENP-C [14–16]. CENP-L binds to the C-terminal region of CENP-N *in vitro* [14] and CENP-K kinetochore localisation depends on the presence of CENP-N and -C [5,8,14,52]. We therefore asked, if these kinetochore proteins, being directly or closely linked to CENP-A, are able to recruit single CENP-PORQU proteins or the whole complex to an ectopic chromatin site in human cell nuclei *in vivo*. We studied the interaction of CENP-C, -L, -K and -N with CENP-PORQU proteins by F3H; the results are listed in Table 2 and displayed in Fig. 3B. CENP-N shows binding to CENP-R and some weak binding to CENP-U, however, only for mCherry-tagged CENP-N (prey) while EGFP-tagged CENP-N (bait) does not show any interaction with CENP-PORQU proteins. CENP-L shows strong binding to CENP-R and moderate binding to CENP-U (strong in one, weak in the other version; see Table 2) and very weak binding to CENP-C (only in one orientation). Furthermore, RFP-tagged CENP-L also shows weak interactions with CENP-Q and CENP-K. Next to CENP-L, also CENP-K shows strong interactions with CENP-PORQU proteins: CENP-K strongly interacts with CENP-O and -U, moderately with CENP-R (strong in one, weak in the other version; see Table 2), and in one version weakly with CENP-Q. CENP-K also weakly binds to itself. By Y2H we detected an interaction between CENP-K and CENP-O, consistent with results of McClelland et al. [8], and an interaction between CENP-K and CENP-H, supporting data of Qui et al. [53], however no interaction had been detected by Y2H between CENP-O and either CENP-H or CENP-N [8]. We thus conclude that to some extend CENP-N, but more efficiently CENP-L and even more so CENP-K mainly recruit CENP-O, -U and -R to kinetochores but much less so CENP-Q, and not CENP-P. This finding agrees with results of Okada et al. [6] who observed in human and DT40 cells that the localization of CENP-O, -P, -Q and -H was disrupted in CENP-K and CENP-L depleted cells. Our results extend their observations by identifying the pairwise interactions responsible for the observed data: Potentially CENP-P and CENP-Q are disrupted from CENP-K and -L depleted cells due to being members of the CENP-PORQU complex and not due to specific protein-protein interactions. Similarly, the dependence of CENP-U kinetochore localization on the presence of CENP-H and -I [38] might be explained by CENP-H and -I being required for CENP-K binding which then recruits the CENP-PORQU complex. F3H yields more direct data on protein-protein interactions than depletion experiments which by their very nature also influence the presence of proteins down-stream of the depleted protein.

We observed no recruitment to the ectopic chromatin site of any CENP-PORQU protein by CENP-C. Furthermore, CENP-L and -N do not recruit all five CENP-PORQU proteins, again indicating that the CENP-PORQU complex does not pre-form in the nucleoplasm.

We confirmed these F3H results by FRET studies. We measured the close neighbourhood of CENP-K to several CENP-PORQU proteins and to CENP-N, and found proximities between the N-terminus of CENP-K with both termini of CENP-R, the N-termini of CENP-O and -U and to the C-terminus of CENP-N (see Table 1). These results place CENP-K inbetween CENP-N and the CENP-PORQU proteins.

PORQU does not preassemble in the cytoplasm

In order to analyse CENP-PORQU complex pre-assembly, in interphase we measured the mobility of the five CENP-O class proteins in the nucleoplasm of human U2OS cells by Raster Image Correlation Spectroscopy (RICS) [54] and found fast mobility between 4.7 and 5.9 ($\pm$15%) μm^2/sec. The proteins are thus more mobile than other inner kinetochore proteins [44,55]. The experimental variation of the measured mobilities, however, does not allow for a conclusion on multimerisation. We therefore performed Fluorescence Cross-Correlation Spectrometry (FCCS) studies to determine if CENP-O class proteins form hetero-dimers in the nucleoplasm. In double-transfected U2OS cells we analysed various protein pairs: EGFP-CENP-O/mCherry-CENP-P, EGFP-CENP-P/mCherry-CENP-Q, EGFP-CENP-R/mCherry-CENP-Q, EGFP-CENP-Q/mCherry-CENP-Q, CENP-O-EGFP/mCherry-CENP-Q, EGFP-CENP-U/mCherry-CENP-Q, EGFP-CENP-R/mCherry-CENP-R, EGFP-CENP-R/CENP-R-mCherry, CENP-U-EGFP/CENP-U-mCherry, CENP-U-EGFP/mCherry-CENP-U and EGFP-CENP-U/mCherry-CENP-O. For these protein pairs we found unequivocal cross-correlation only between CENP-O and CENP-P. From 12 cells, all 12 showed cross-correlation indicating that CENP-O and CENP-P move together, i.e. they are part of one and the same complex in the nucleoplasm outside kinetochores. The cross-correlation analysis (Fig. 4A) resulted in a correlation of 1.020 (Fig. 4A, insert b) indicating that 29% of the molecules are co-migrating in the nucleoplasm. As negative control, U2OS cells were analysed separately expressing EGFP and mRFP as single molecules. The cross-correlation curve (Fig. 4B) resulted in a value of 1.001 (Fig. 4B, insert b) indicating the absence of any complexation between EGFP and mRFP. As a positive control, U2OS cells were transfected with pH-mR-G-C expressing a mRFP-EGFP fusion protein. Cross-correlating the two channels against each other, we obtained a value of 1.029 indicating that about 50% of the molecules are detected as a complex (Fig. 4C). We obtained similar cross-correlation values for the fusion EGFP-mCherry, in agreement with results of Kohl et al. [56]. For such fusion proteins, 100% cross correlation should be observed. The lower value of 50% could be explained by a much slower maturation and lower stability of mRFP compared to EGFP: EGFP molecules bound to an immature mRFP are interpreted by FCCS as free molecules. Thus, cross-correlation values seem to underestimate the percentage of co-migrating molecules. Consequently, hetero-dimerisation of EGFP-CENP-O and mCherry-CENP-P probably is higher than the calculated 20–30%, we estimate 40–60%.

In 2 out of 12 analyzed cells, a weak cross-correlation ($\sim$10%) was observed for CENP-Q and CENP-R indicating that in a few cases CENP-Q and CENP-R co-migrate in the nucleoplasm outside kinetochores. The other analyzed protein pairs showed no cross-correlation demonstrating that the CENP-PORQU complex does not pre-form in the nucleoplasm outside kinetochores. CENP-R and CENP-U are able to bind to themselves at an ectopic chromatin site (see above). However, by FCCS we did not detect any cross correlation, clearly indicating that these proteins do not stably aggregate in the nucleoplasm. Recombinant CENP-Q can oligomerise to octamers [36] and, when kinetochore-bound, oligomerises in late S-phase, as detected by FRET (see above). In the nucleoplasm, however, CENP-Q does not form di- or multimers, as shown here by FCCS. This FCCS result is confirmed by the absence of a FRET signal between two tagged

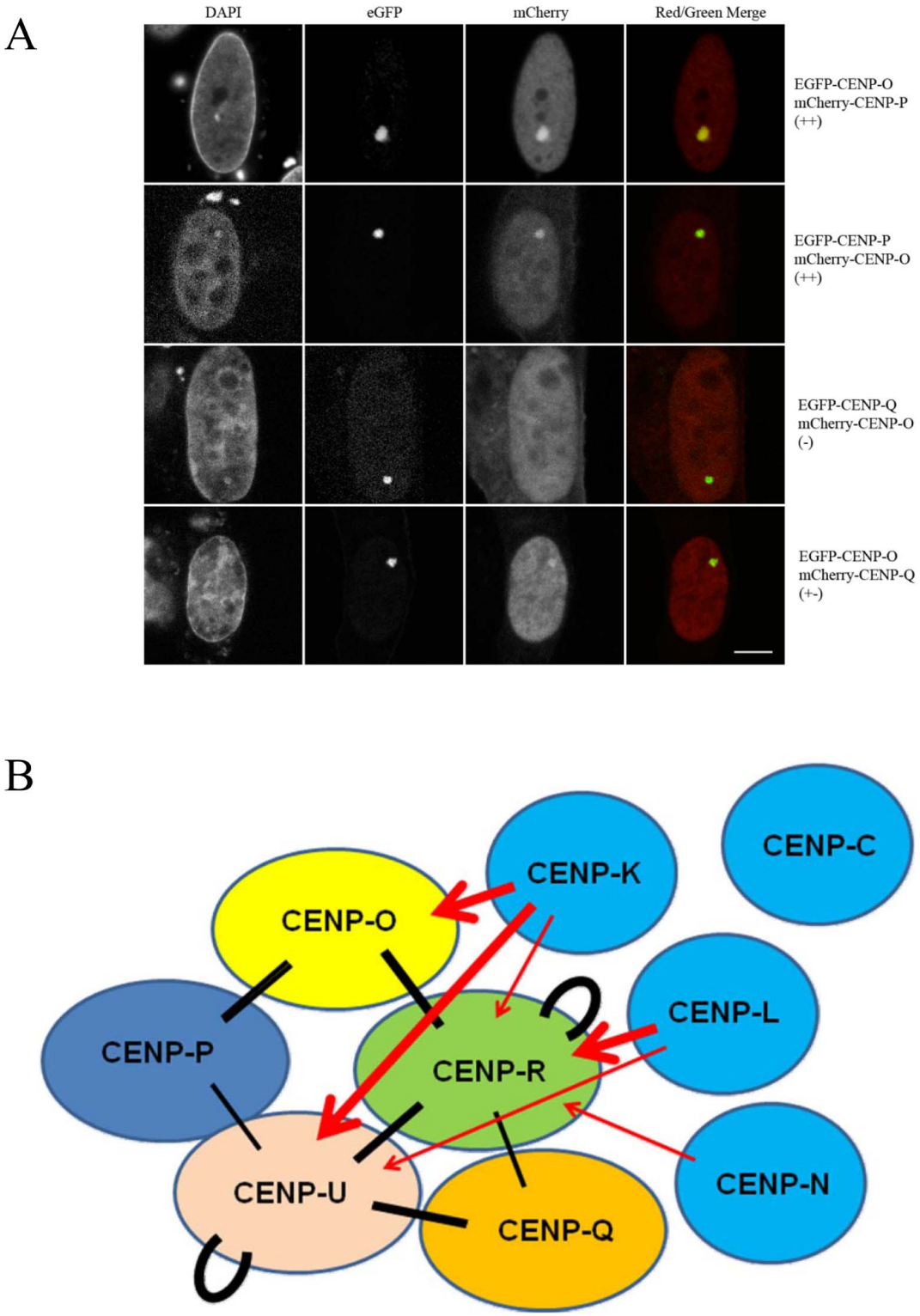

Figure 3. Centromere protein interactions analyzed by F3H assay. (A) EGFP tagged centromere proteins (bait, green) were recruited to the *lac* operator repeat array by the GFP-binding protein fused to the Lac repressor (LacI-GBP). Co-expressed mCherry tagged centromere proteins (prey, red) may either interact with the GFP-tagged protein (yellow in the overlay) or may not interact resulting in a disperse distribution. Upper two rows: interaction between EGFP-CENP-O and mCherry-CENP-P, EGFP-CENP-P and mCherry-CENP-O. Lower two rows: EGFP-CENP-Q did not interact with and recruit mCherry-CENP-O to the *lac* spot, but shows a weak interaction in the reverse combination. For all results see Table 1. Bar: 5 μm. (B): Strong F3H interactions are displayed (++: thick lines, +: thin lines). Black bars: interactions between CENP-PORQU proteins, red arrows: recruitment of CENP-PORQU proteins by CENP-K, -L, and -N. CENP-C is not able to recruit any of the CENP-PORQU proteins (data see Table 2).
doi:10.1371/journal.pone.0044717.g003

Table 2. F3H analysis of CENP-O class protein interactions.

mCherry\EGFP	CENP-O	CENP-P	CENP-Q	CENP-R	CENP-U	CENP-K	CENP-L	CENP-N	CENP-C
CENP-O	−	++	−	++	−	+	−	−	−
CENP-P	+	−	+−	+−	+	−	−	−	−
CENP-Q	+−	−	−	+	+	−	−	−	−
CENP-R	++	+−	+	++	++	+−	++	−	−
CENP-U	−	+	++	++	++	++	+−	−	−
CENP-K	++	−	+−	+	++	+−	−	−	−
CENP-L	−	−	+−	+	+	+−	−	−	+−
CENP-N	−	−	−	+	+−	−	−	−	−
CENP-C	−	−	−	−	−	−	−	−	−

GFP-tagged CENP-O class proteins, CENP-K, -L, -N and -C (rows) were bound to ectopic chromosomes sites. When RFP-tagged CENP-O class proteins, CENP-K, -L, -N and -C (lines) were recruited to these proteins, this was visible by a yellow dot. Signal intensity at the nuclear spot was used an indicator for interaction strength. ++, +: strong interaction; +−: weak interaction; −: no interaction.

doi:10.1371/journal.pone.0044717.t002

CENP-Q in the nucleoplasm outside kinetochores (data not shown).

These data show that, with the two exceptions CENP-O/-P and CENP-Q/-R, the pairwise CENP-O class protein interactions detected by F3H do not result in a homo- or hetero-dimerisation of these proteins stable enough for FCCS detection. Since these proteins do not pre-aggregate, they must enter the nucleoplasm as single proteins. CENP-O, -P, -Q and -R are small enough (molecular weights $<$34 kDa) for not needing a nuclear localisation domain (NLS) for entering the nucleus. Only CENP-U is larger (47.5 kDa) and indeed contains two NLS [57,58].

PORQU loads onto kinetochores in S-phase and form a stable subcomplex

We next asked when during the cell cycle the CENP-PORQU complex assembles. By applying SNAP-tag technology, we determined at which cell cycle phase CENP-O is loaded to the kinetochore. The SNAP protein tag can catalyze the formation of a covalent bond to a benzyl-guanine moiety coupled to different fluorescent or non-fluorescent membrane-permeable reagents [59]. This tag allows pulse-chase experiments at a single protein level. Consistent with previous data [60], we detected TMR-star fluorescence on SNAP-CENP-A only in G1 cells, confirming that CENP-A is specifically loaded in G1, while we observed a time window of mid G1 to G2 for CENP-N binding and loading to kinetochores [44]. Here we transfected a SNAP-CENP-O construct. After double-thymidine and aphidicolin block release and applying the same protocol, we found SNAP-CENP-O present at kinetochores of G2 cells (Fig. 5A), indicating that CENP-O is loaded onto kinetochores in or before G2. To extend our temporal analysis to further phases of the cell cycle, we repeated these experiments in U2OS cells since these cells have a longer cell cycle: 12 hrs after release and following the same experimental procedure, U2OS cells can be analysed in late-S-phase. Here, TMR-star fluorescence for SNAP-CENP-O was already detected in late S-phase as judged by PCNA-GFP fluorescence (Fig. 5B). Thus, CENP-O assembles at kinetochores already in late S-phase or earlier. Finally, to measure the earliest time point at which CENP-O can assemble into kinetochores, SNAP-CENP-O transfected HeLa cells were arrested in mitosis for 12 hrs by a nocodazole block and quenched with BTP for 30 min. 4 hrs after quenching, the cells were released from nocodazole arrest. Further 5 hrs later, SNAP-tagged CENP-O was fluorescently labelled with TMR-star for 30 min and fixed for examination. No TMR-star fluorescence was detected indicating that SNAP-CENP-O is not loaded in G1 (Fig. 5C). Overall these experiments suggest a time window of S-phase to G2 for CENP-O loading to kinetochores. Also for CENP-T and -W [61], CENP-N [44] and CENP-U [62] loading to kinetochores in S-phase was observed.

Our recent work showed that CENP-T and -W [61] as well as CENP-N [44] are loaded to human kinetochores by slow loading dynamics, mainly during the second half of S-phase. This is in contrast to CENP-A which is loaded at the end of mitosis and G1 [55,60]. We speculated that the CENP-O class proteins might also be loaded slowly, mainly in S-phase. We thus studied the dynamic binding of these EGFP-tagged CENPs by Fluorescence Recovery After Photobleaching (FRAP) in living human U2OS cells. For none of the five CENP-O class proteins, at any cell cycle phase, we could detect fluorescence recovery within 150 sec after bleaching, indicating rather stable kinetochore binding of all five proteins, consistent with observations of Minoshima et al. [38] for CENP-U. We then studied fluorescence recovery of these five proteins during the cell cycle in a longer time frame, now over 4 hours. Different cell cycle phases were identified by staining with CENP-F and by co-expressing mRFP-PCNA for identifying S-phase and its sub-phases [63,64], as recently described [44,55,65]. In G1, all five CENP-O class proteins show complete recovery; four proteins have an exchange rate ($t_{1/2}$) of about one hour while only CENP-R exchanges slower with $t_{1/2} = 2$ hrs. In S-phase and G2, CENP-O, -P and -Q show partial recovery values of 40 to 80% with a slower exchange rate compared to G1 of about 2 hrs (see Table 3 and Fig. 6; in same cases for CENP-O and -P, the recovery only allows to estimate the final recovery level (values in brackets)). These recovery amplitudes are in the same range of values as for those of CENP-T and -W (70±8%) [61] and CENP-N (45±6%, see Table 3) [44]. The slow recovery times during the second half of S-phase coincide with the slow recovery times of CENP-T and -W ($t_{1/2} = 70 \pm 10$ min) [61], but are slower than the exchange of CENP-N ($t_{1/2} = 38 \pm 7$ min) [44]. In G2, CENP-P and -Q seem to show slightly faster recovery times compared to S-phase. The FRAP dynamics of CENP-U and -R are distinct from that of CENP-O, -Q and -P. CENP-U shows 100% recovery throughout the cell cycle with the exception of late S-phase when most of CENP-U (71±2%) is immobile (the remaining 29% of CENP-U exchange with $t_{1/2} = 50 \pm 8$ min). Our FRET data indicate that CENP-U di- or multimerises in late S-phase. This CENP-U self-

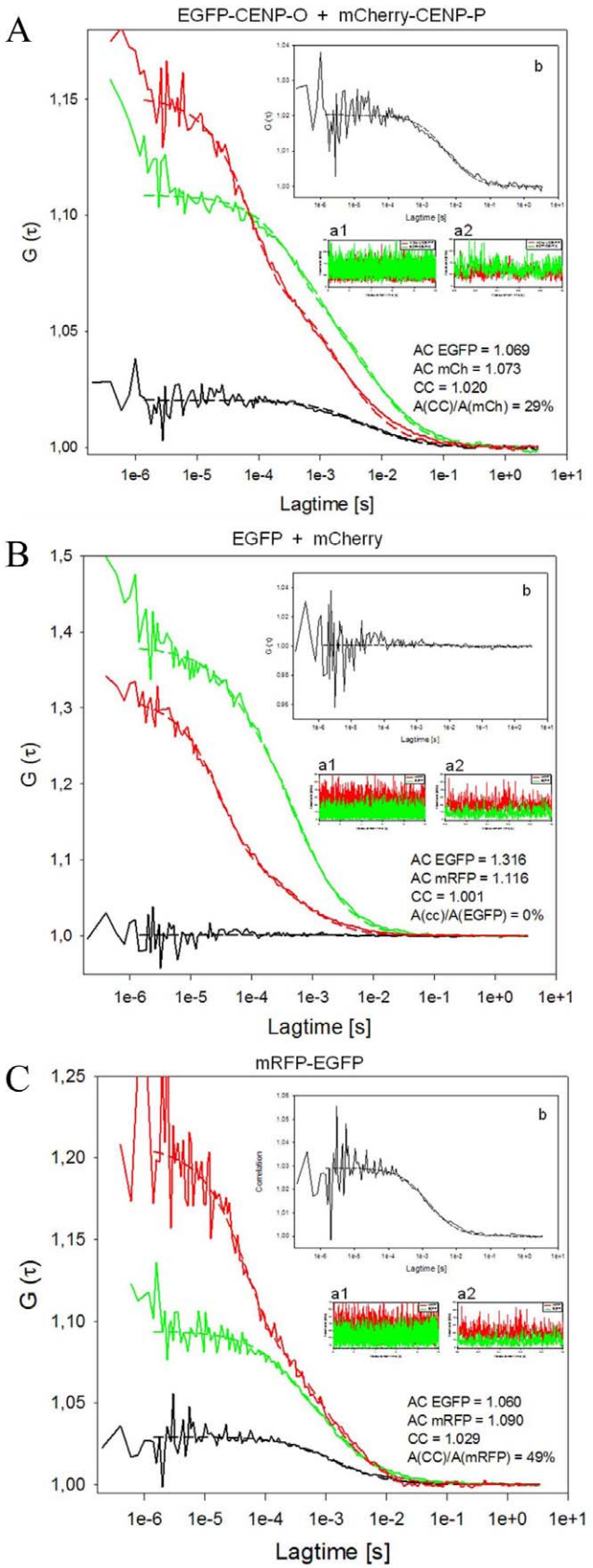

Figure 4. FCCS measurements displaying G versus lag time. Red: mCherry (A, B) or mRFP (C), green: EGFP, black: auto-correlation. Count rates are displayed over 10 sec (inserts a1) indicating the absence of photobleaching, and 1 sec (inserts a2) indicating the absence of larger protein aggregates. The cross-correlation analyses are amplified in inserts b. (A) EGFP-CENP-O and mCherry-CENP-P indicate complex formation in the nucleoplasm (amplitude of cross-correlation/amplitude of mCherry signal: 29%). The amplitude of the cross-correlation curve A(CC), relative to the diffusion-related amplitude of one of the autocorrelation curves A(AC) of EGFP or mCherry, is a measure of binding or dynamic colocalization [49,50]. According to this ratio of amplitudes A(CC)/A(AC), up to 20–30% of nucleoplasmic CENP-O and -P are hetero-dimers. Count rates were recorded simultaneously for both fluorophores. The count rate detected in a 10 sec measurement (insert a1) demonstrates the absence of photobleaching, while the count rate in a 1 sec resolution time scale (insert a2) indicates the absence of larger protein aggregates. The autocorrelations yielded 1.069 and 1.073 for EGFP-CENP-O and mCherry-CENP-P, respectively. The cross-correlation analysis (with a magnified scale of G(τ); insert b) resulted in a correlation of 1.02 indicating that 29% of the molecules are co-migrating in the nucleoplasm. (B) EGFP and mCherry expressed as single non-fused proteins (negative control) do not show any cross-correlation (A(CC)/A(EGFP) = 0%). The count rates (inserts a1 and a2) indicate the absence of photobleaching and larger proteins. The autocorrelations yielded 1.316 and 1.116 for EGFP and mRFP, respectively. The cross-correlation curve (with a magnified scale of G(τ), insert b) resulted in a value of 1.001 indicating the absence of any complexation between EGFP and mRFP. (C) mRFP-EGFP fusion protein (positive control) shows cross-correlation (A(CC)/A(mRFP) = 49%). The count rates indicate that photobleaching and the presence of larger protein aggregates can be excluded (inserts a1, a2) and that the autocorrelations of EGFP (1.06) and mRFP (1.09) were comparable to the values obtained for EGFP-CENP-O and mCherry-CENP-P. Cross-correlating the two channels against each other, we obtained a value of 1.029 indicating that about 50% of the molecules are detected as a complex (with a magnified scale of G(τ) in insert b).
doi:10.1371/journal.pone.0044717.g004

assembly could reduce CENP-U exchange at the kinetochore in late S-phase, explaining the high immobile fraction detected by FRAP. This CENP-U/-U interaction seems not be mediated by Plk1 since Plk1 binding to kinetochores occurs during late G2 [41]. Our data indicate that CENP-Q and CENP-U form di- or oligomers after kinetochore binding before the onset of mitosis, potentially denoting a conformational change.

Different from the behaviour of the other four proteins, for all cell cycle phases CENP-R shows recovery values of 100% with slow loading times of 2 to 3 hrs (Table 3). Thus, CENP-R recovery is considerably slower than that of the other four CENP-O class proteins. The observed distinct dynamical behaviour of the CENP-O class proteins indicates that the complex does not bind to the kinetochore as a pre-formed complex in the nucleoplasm and that these proteins retain distinct dynamic behaviour also when bound to the kinetochore.

Cell-cycle dependent protein abundance

The CCAN protein CENP-N shows varying abundance in the cell with a maximal protein level at kinetochores in late S-phase [8,44]. Furthermore, the presence of CENP-U at HeLa kinetochores increases during late G1 and early S-phase, remains high through late S and G2 and decreases strongly during M-phase [40]. For human CENP-O, a decrease in kinetochore presence down to about 60% from interphase to mitosis was detected by immuno-fluorescence [33]. Here we extended these CENP-O data and measured the cell cycle dependent amount of CENP-O relative to tubulin in HEp-2 cells by Western blot 2, 4, 6 (S-phase), 8 (G2), and 10 hours (M-phase) after release from a double thymidine block (Fig. 7A). The cellular amount of CENP-O remains rather stable from G1/S over the entire S-phase, is reduced already in G2 and reduces further in M-phase, consistent with findings of McAinsh et al. [33]. A corresponding Western blot

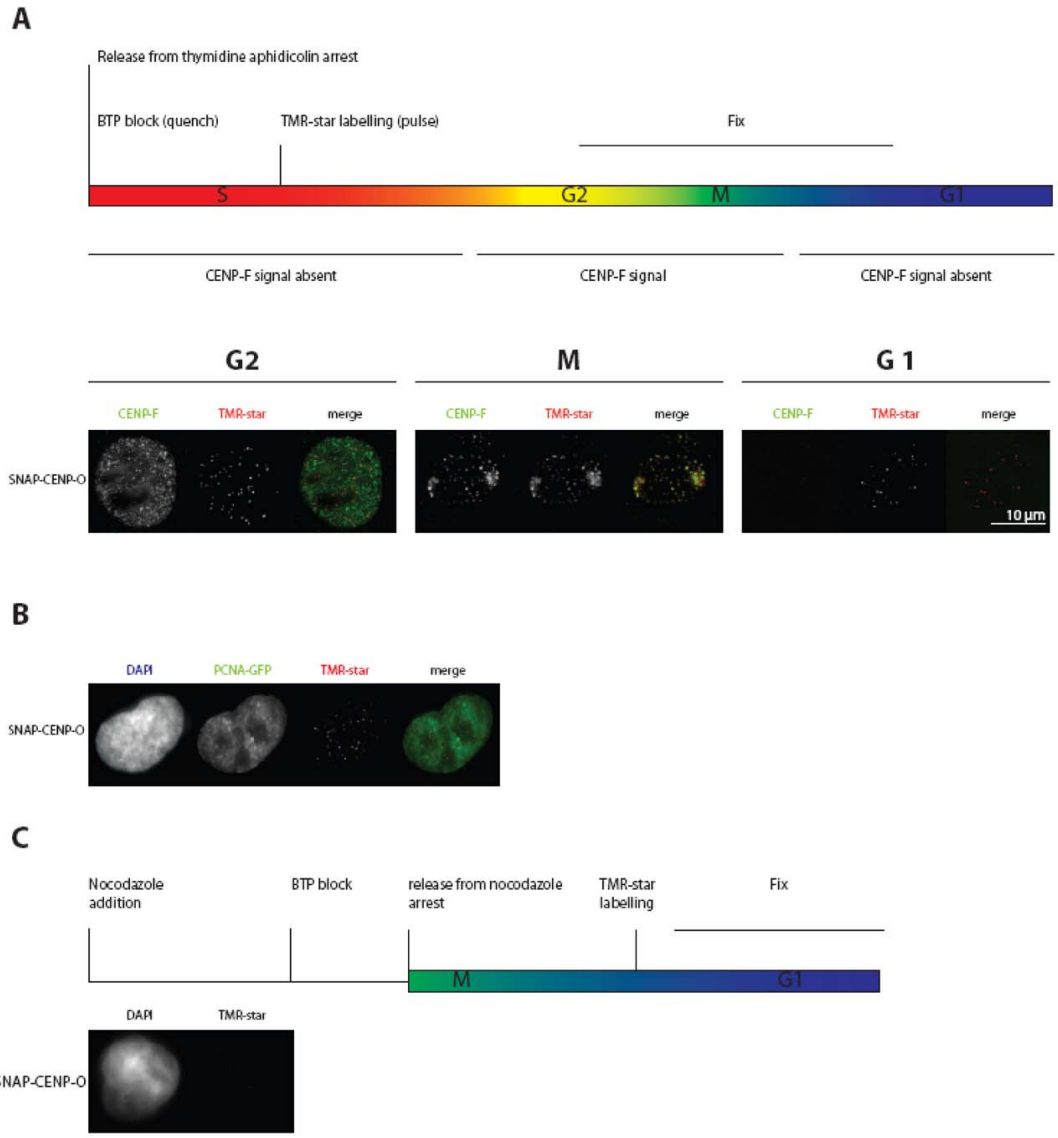

Figure 5. CENP-O loading to kinetochores measured by the SNAP-tag technology. (A) Top: schematic representation of the performed experiment. Below: representative images of cells showing TMR-star fluorescence for SNAP-CENP-O in G2, M-phase and the following G1. Cell cycle phases G2 (CENP-F staining of the whole nucleus) and mitosis (specific kinetochore binding of CENP-F) are clearly identified. (B) The same experiment as in (A) was performed with U2OS cells stably expressing PCNA-GFP. SNAP-CENP-O fluorescence appears at kinetochores in late S-phase as judged from cellular PCNA distributions. (C) Top: schematic representation of the performed experiment. Below: representative images of cells expressing SNAP-CENP-O showing no fluorescence at kinetochores during G1. CENP-O is thus loaded to kinetochores in S-phase.
doi:10.1371/journal.pone.0044717.g005

analysis was conducted for CENP-P and CENP-Q: The level of CENP-P decreases from late S-phase through G2 to M-phase (Fig. 7B, D), whereas CENP-Q displayed stable protein levels from G1/S into mitosis (Fig. 7C, D). In contrast to the constant level of CENP-Q levels in the cell, immune-fluorescence detected an increase of the amounts of CENP-Q at kinetochores during S-phase, reaching a maximum in late S-phase and strongly decreasing in G2 (Fig. 7E, F).

Discussion

The centromeric histone H3 variant CENP-A is the central marker of centromere location and inherits this location to daughter cells [55]. The kinetochore recognizes this epigenetic mark, in part, through the CCAN network of proteins. The CENP-N subunit directly binds the CENP-A CATD region of the CENP-A containing nucleosome while the CENP-C subunit binds the C-terminal tail of CENP-A [14–16]. In addition to these CENP-A binding mechanisms, CENP-T/W/S/X form a unique centromeric chromatin structure next to histone H3 containing nucleosomes that supercoils DNA [9,12,61]. If we are to fully understand the pathways and mechanisms that allow a mature kinetochore to assemble, it will be crucial to define how these chromatin-interacting complexes recruit the other 11 CCAN subunits. Of these subunits the CENP-PORQU were reported to form a stable complex when being expressed in *E. coli* [10], whereas the CENP-H, -I, -K, -L and -M (CENP-H class) are not known to associate into any stable sub-complexes [8]. Dependency experiments show that CENP-PORQU requires the CENP-H class for kinetochore binding but not *vice versa* [5,6,8,14,52]. The

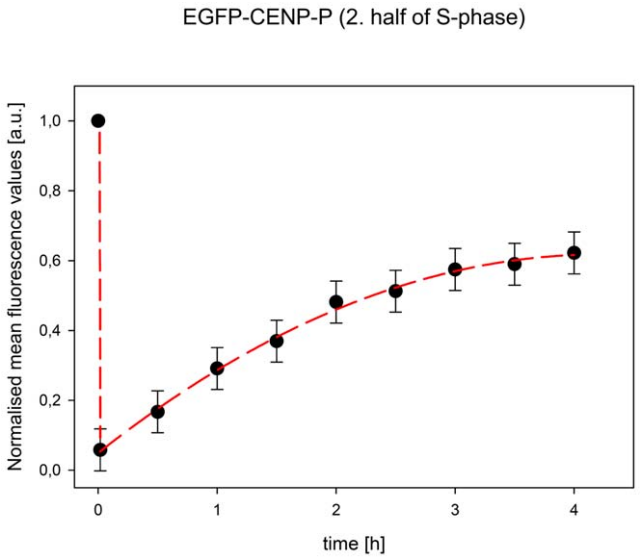

Figure 6. Fluorescence recovery after photobleaching of EGFP-CENP-P in mid S-phase. Normalised mean fluorescence values of 55 kinetochores taken in time steps of 30 min over 4 hours. Recovery levels off, indicative of an about 40% immobile fraction.
doi:10.1371/journal.pone.0044717.g006

working model thus involves the stepwise recruitment of CENP-N/CENP-TWSX≫CENP-HIKLM≫CENP-PORQU [2]. In line with this, CENP-L can bind directly to CENP-N *in vitro* [14] and may be involved in stabilising CENP-N binding to the CENP-A nucleosome [44]. We now show by F3H that CENP-N, CENP-K and CENP-L are all, to some extent, capable of recruiting CENP-O, -U and -R to an ectopic chromosomal site, whereas CENP-C is not directly involved in CENP-PORQU binding. The next step will be to identify the physical interactions that mediate this assembly reaction.

The CENP-PORQU proteins assemble at kinetochores during S-phase. For example, newly synthesized CENP-O is incorporated in S-phase and remains at the kinetochore during mitosis (although levels decrease, consistent with previous findings [33]) into the following G1 where they can exchange slowly and to near completion (however, without exchange with newly synthesized CENP-O). During the cell cycle, the CENP-PORQU proteins show different protein abundance in the cell: while CENP-Q protein levels do not change from G1/S to M-phase, the levels of CENP-O and -P decrease, CENP-P levels already during S-phase but those of CENP-O only after S-phase. The protein amount at kinetochores is maximal in late S-phase for CENP-Q, as shown here, and at late S-phase and G2 for CENP-U [40]. This variance of protein abundance in the cell and at kinetochores supports our conclusion that the CENP-PORQU complex assembles from proteins with individual behavior, and might indicate a varying stoichiometry of the CENP-PORQU proteins in the complex.

The reported stable interaction of CENP-PORQU in *E. coil* lysates [10] suggests that these proteins may form a pre-assembled complex in the nucleoplasm before loading onto kinetochores in S-phase. We show here, however, by FCCS that the CENP-PORQU subunits do not exist as a single preformed complex prior to kinetochore-binding. Instead, in the nucleoplasm, we can only detect a CENP-O/P (to an amount of about 50%), and, to a very minor extent, a CENP-Q/R heterodimer. However, by F3H we could show that each CENP-PORQU subunit can recruit two or three other proteins of this group to an ectopic chromosomal site. This confirms that these proteins specifically interact with each other in mammalian cells. One caveat of this experiment is that CCAN proteins might be specifically modified at centromere locations. These centromere specific modifications would be absent at the ectopic chromosomal site, potentially influencing protein interactions. Since pair-wise binding is weak in most cases, the strong kinetochore binding of the CENP-PORQU subunits (identified by slow FRAP recovery times) supports multi-fold CENP-PORQU interactions at the kinetochore. No single subunit of CENP-PORQU can recruit all other subunits, further supporting our finding that the complex does not pre-form in the nucleoplasm. Our FRAP experiments, consistent with previous studies [38], show that the cell cycle dependent turnover of CENP-P/O/Q is similar but distinct from the behavior of CENP-U and CENP-R. This indicates that the CENP-PORQU sub-complex does not behave as a single unit but instead is an ensemble of autonomously behaving proteins.

Our FRET measurements show that the CENP-PORQU proteins, once bound and incorporated into the inner kinetochore structure, are positioned in close proximity to one another. Previously, we reported that the amino-terminus of CENP-U was in close proximity to the amino-terminus of CENP-B and CENP-I, but not to the amino-terminus of CENP-A and CENP-C [43]. This indicates that, to some extent, CENP-PORQU is imbedded within the CCAN complex. Moreover, not all FRET connectivities should be thought of as occurring necessarily within a single CCAN inner kinetochore complex (intra-CCAN FRET). It is possible that some observed FRET proximities may reflect protein neighborhoods between two different adjacent CCAN complexes (inter-CCAN FRET). Such inter-CCAN interactions are likely, given super-resolution experiments that support models in which kinetochores are formed from multiple adjacent microtubule

Table 3. Long term FRAP results for the CENP-PORQU proteins.

Cell cycle	CENP-O		CENP-P		CENP-Q		CENP-U		CENP-R	
	rec/%	$t_{1/2}$/min	rec/%	$t_{1/2}$/min	rec/%	$t_{1/2}$/min	rec/%	$t_{1/2}$/min	rec/%	$t_{1/2}$/min
G1	100	71±15	100	77±15	90±10	57±10	100	72±15	100	125±15
early S	(45)	-	(70)	-	59±6	118±15	100	163±40	100	147±20
mid S	(40)	-	62±6	81±5	65±6	125±30	100	93±15	100	160±15
late S	75±15	131±30	49±10	103±10	75±8	136±15	29±2	50±8	100	180±20
G2	(80)	-	56±8	78±5	64±6	90±14	100	76±8	100	137±20

rec: fluorescence recovery relative to the initial fluorescence value before bleaching, $t_{1/2}$: time for half height recovery (in min). Recovery values in brackets: estimated recovery value; for these data, a $t_{1/2}$ value could not be determined.
doi:10.1371/journal.pone.0044717.t003

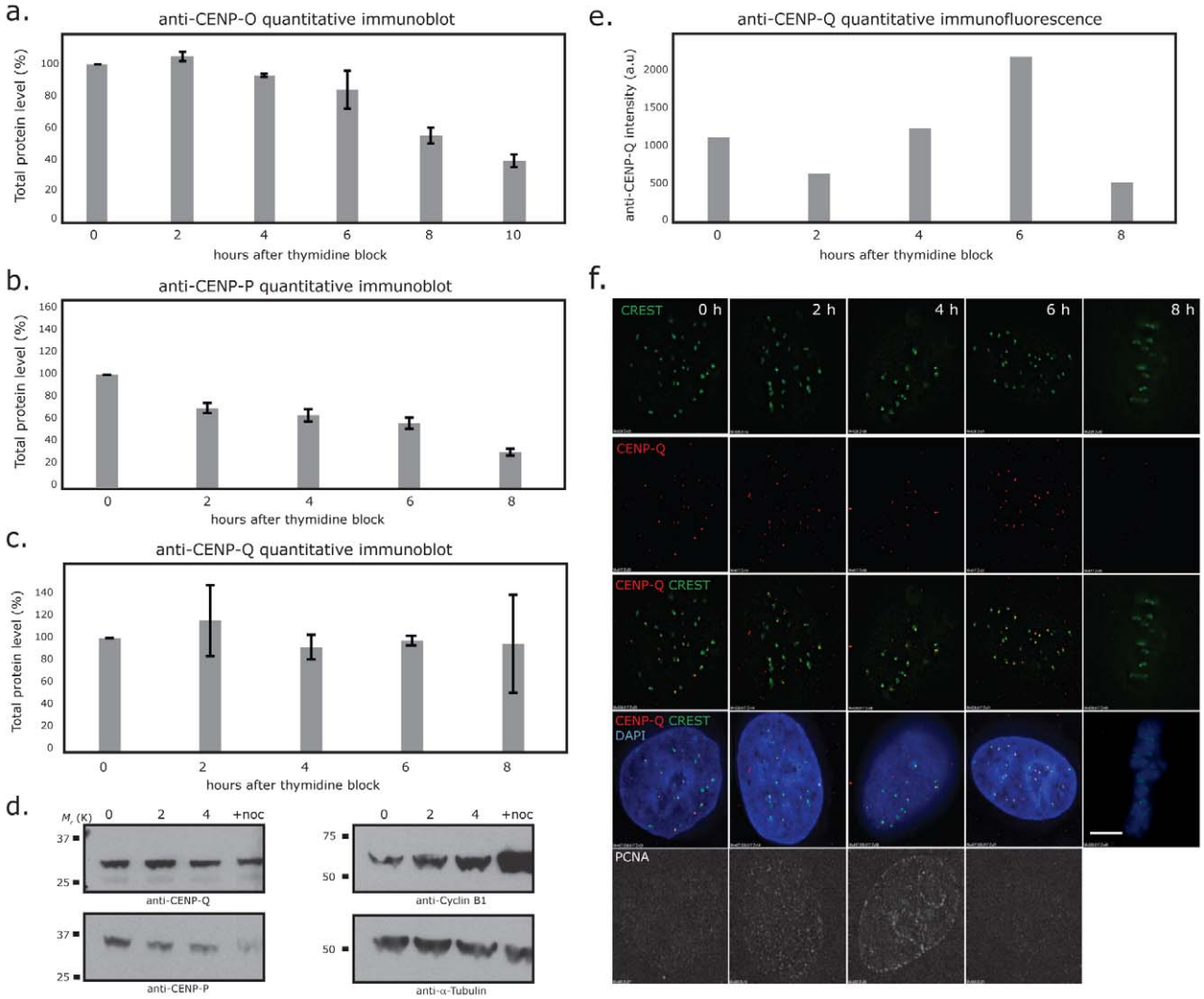

Figure 7. Levels of CENP-O/P/Q total protein during the cell cycle. (A) Quantitative immunoblot of CENP-O relative to α-Tubulin. Protein amounts are measured at G1/S (0 h), 2, 4, 6, 8 and 10 hrs after release from the double thymidine block in synchronised human HEp-2 cells. CENP-F and PCNA staining identify the time points 2, 4, and 6 hrs as S-phase, time point 8 hrs as G2 and 10 hrs as M-phase. The cellular amount of CENP-O reduces in G2 and further in M-phase. (B, C) Quantitative immuno-blots of CENP-P and CENP-Q protein levels relative to α-Tubulin at 0 (G1/S), 2 (early S), 4 (middle S), 6 (late S-phase), 8 (G2) hrs after release from double thymidine block in synchronized HeLa cells. Cycle stages were attributed from FACs analysis, PCNA staining and phase contrast microscopy (data not shown). (D) Representative immunoblots showing CENP-P, CENP-Q, Cyclin-B1 and α-Tubulin at the 0 (G1/S), 2 (early S), 4 (middle S) hrs time points and cells arrested in mitosis with nocodazole (16 hrs). (E) Quantitative four-colour immuno-flourence using anti-CENP-Q (red), CREST (green), DAPI (blue) and anti-PCNA (far red) antibodies in the same cells used in panel B. Pixel intensities of CENP-Q (signal – background) at kinetochores (n = 50 from 5 cells) are shown for each time point after release from double thymidine block (E) and representative images (F). CENP-Q loads onto kinetochores during S-phase reaching maximal binding in late S-phase (6 h). Scale bar = 5 μm.
doi:10.1371/journal.pone.0044717.g007

binding sites [66–68]. We expect that three-dimensional inner kinetochore model building will allow us to evaluate and explore these ideas.

The multifold interactions of the CENP-PORQU proteins result in stable binding of these proteins to kinetochores, suggesting a self-assembly mechanism [69]. In this regard, CENP-U and CENP-R are able to homo-dimerise at an ectopic chromosomal site (see Table 2), although we could not detect homo-dimerisation from our FCCS measurements. Nevertheless, upon kinetochore binding and before mitosis, these proteins are proximal to themselves, as detected by FRET between CENP-U/-U. Human CENP-Q, when expressed in *E. coli*, oligomerises into octameric complexes [36]. In late S-phase, after kinetochore binding and before mitosis, we detected FRET between the CENP-Q carboxy- as well as amino-terminal regions, indicating homo-di- or oligomerisation. We could not detect such homo-dimerisation at an ectopic chromosomal site, and found by FCCS that CENP-Q migrates as a monomer in the nucleoplasm, showing that the oligomerization event occurs at kinetochores. This self-association of CENP-U and -Q might hint towards the presence of more than one of these proteins (CENP-U, -Q) in one CCAN complex, indicating a varying stoichiometry in the complex. Alternatively, these proteins might make inter-CCAN interactions with themselves. Such an interaction between different CCAN complexes might induce or stabilize centromere specific chromatin structures and/or microtubule binding sites

[70]. The latter hypothesis is attractive given that both CENP-Q and CENP-U bind directly to microtubules *in vitro* [36,39]. We speculate that this self-association of CENP-Q and -U after kinetochore binding is a pre-mitotic maturation process that might switch kinetochores into the correct conformation for microtubule attachment.

Acknowledgments

We thank N. Klöcker, D. Foltz, J. Langowski and I. Cheeseman for the kind gift of plasmids and S. Pfeifer and S. Ohndorf for expert technical support.

Author Contributions

Conceived and designed the experiments: AE WD SR SE DH TU VD JMB ADM PM CH HL SD. Performed the experiments: AE WD AH SR SE DH TU VD JMB MCC CH HL. Analyzed the data: AE WD AH SR SE DH TU VD JMB ADM PM CH HL SD. Contributed reagents/materials/analysis tools: WD JMB MCC. Wrote the paper: DH ADM HL CH SD.

References

1. Perpelescu M, Fukagawa T (2011) The ABCs of CENPs. Chromosoma 120: 425–446.
2. Takeuchi K, Fukagawa T (2012) Molecular architecture of vertebrate kinetochores. Exp Cell Res 318: 1367–1374.
3. Cheeseman IM, Desai A (2008) Molecular architecture of the kinetochore-microtubule interface. Nat Rev Mol Cell Biol 9: 33–46.
4. Przewloka M, Glover DM (2009) The kinetochore and the centromere: a working long distance relationship. Annu Rev Genet 43: 439–465.
5. Foltz DR, Jansen LET, Black BE, Bailey AO, YatesIII JR, et al. (2006) The human CENP-A centromeric complex. Nat Cell Biol 8: 458–469.
6. Okada M, Cheeseman IM, Hori T, Okawa K, McLeod IX, et al. (2006) The CENP-H-I complex is required for the efficient incorporation of newly synthesized CENP-A into centromeres. Nature Cell Biol 8: 446–457.
7. Meraldi P, McAinsh AD, Rheinbay E, Sorger PK (2006) Phylogenetic and structural analysis of centromeric DNA and kinetochore proteins. Genome Biol 7: R23.
8. McClelland SE, Borusu S, Amaro AC, Winter JR, Belwal M, et al. (2007) The CENP-A NAC/CAD kinetochore complex controls chromosome congression and spindle bipolarity. EMBO J 26: 5033–5047.
9. Hori T, Amano M, Suzuki A, Backer CB, Welburn JP, et al. (2008) CCAN makes multiple contacts with centromeric DNA to provide distinct pathways to the outer kinetochore. Cell 135: 1039–1052.
10. Hori T, Okada M, Maenaka K, Fukagawa T (2008) CENP-O class proteins form a stable complex and are required for proper kinetochore function. Mol Biol Cell 19: 843–854.
11. Amano M, Suzuki A, Hori T, Backer C, Okawa K, et al. (2009) The CENP-S complex is essential for the stable assembly of outer kinetochore structure. J Cell Biol 186: 173–182.
12. Nishino T, Takeuchi K, Gascoigne KE, Suzuki A, Hori T, et al. (2012) CENP-T-W-S-X forms a unique centromeric chromatin structure with a histone-like fold. Cell 148: 487–501.
13. Santaguida S, Musacchio A (2009) The life and miracles of kinetochores. EMBO J 28: 2511–2531.
14. Carroll CW, Silva MCC, Godek KM, Jansen LET, Straight AF (2009) Centromere assembly requires the direct recognition of CENP-A nucleosomes by CENP-N. Nat Cell Biol 11: 896–902.
15. Carroll CW, Milks KJ, Straight AF (2010) Dual recognition of CENP-A nucleosomes is required for centromere assembly. J Cell Biol 189: 1143–1155.
16. Guse A, Carroll CW, Moree B, Fuller CJ, Straight AF (2011) In vitro centromere and kinetochore assembly on defined chromatin templates. Nature 477: 354–358.
17. Tachiwana H, Kagawa W, Shiga T, Osakabe A, Miya Y, et al. (2011) Crystal structure of the human centromeric nucleosome containing CENP-A. Nature 476: 232–235.
18. Bui M, Dimitriadis EK, Hoischen C, An E, Quenet D, et al. (2012) Cell cycle-dependent structural transitions in the human CENP-A nucleosome in vivo. Cell 150: 317–326.
19. De Wulf P, McAinsh AD, Sorger PK (2003) Hierarchical assembly of the budding yeast kinetochore from multiple subcomplexes. Genes Dev 17: 2902–2921.
20. Cheeseman IM, Niessen S, Anderson S, Hyndman F, Yates JR 3rd, et al. (2004) A conserved protein network controls assembly of the outer kinetochore and its ability to sustain tension. Genes Dev 18: 2255–2268.
21. Cheeseman IM, Chappie JS, Wilson-Kubalek EM, Desai A (2006) The conserved KMN network constitutes the core microtubule-binding site of the kinetochore. Cell 127: 983–997.
22. Obuse C, Yang H, Nozaki N, Goto S, Okazaki T, et al. (2004) Proteomics analysis of the centromere complex from HeLa interphase cells: UV-damaged DNA binding protein 1 (DDB-1) is a component of the CEN-complex, while BMI-1 is transiently co-localised with the centromeric region in interphase. Genes to Cells 9: 105–120.
23. Liu X, McLeod I, Anderson S, Yates JR 3rd, He X (2005) Molecular analysis of kinetochore architecture in fission yeast. EMBO J 24: 2919–2930.
24. Petrovic A, Pasqualato S, Dube P, Krenn V, Santaguida S, et al. (2010) The Mis12 complex is a protein interaction hub for outer kinetochore assembly. J Cell Biol 190: 835–852.
25. Kiyomitsu T, Iwasaki O, Obuse C, Yanagida M (2010) Inner centromere formation requires hMis14, a trident kinetochore protein that specifically recruits HP1 to human chromosomes. J Cell Biol 188: 791–807.
26. Liu D, Vleugel M, Backer CB, Hori T, Fukagawa T, et al. (2010) Regulated targeting of protein phosphatise 1 to the outer kinetochore by KNL1 opposes Aurora B kinase. J Cell Biol 188: 809–820.
27. Przewloka MR, Venkei Z, Bolanos-Garcia VM, Debski J, et al. (2011) CENP-C is a structural platform for kinetochore assembly. Curr Biol 21: 399–405.
28. Tanaka TU, Desai A (2008) Kinetochore-microtubule interactions: the means to the end. Curr Opin Cell Biol 20: 53–63.
29. Wan X, O'Quinn RP, Pierce HL, Joglekar AP, Gall WE, et al. (2009) Protein architecture of the human kinetochore microtubule attachment site. Cell 137: 672–684.
30. Moree B, Meyer CB, Fuller CJ, Straight AF (2011) CENP-C recruits M18BP1 to centromeres to promote CENP-A chromatin assembly. J Cell Biol 194: 855–871.
31. Barnhart MC, Kuich HJL, Stellfox ME, Ward JA, Bassett EA, et al. (2011) HJURP is a CENP-A chromatin assembly factor sufficient to form a functional de novo kinetochore. J Cell Biol 194: 229–243.
32. Fukagawa T, Mikami Y, Nishihashi A, Regnier V, Haraguchi T, et al. (2001) CENP-H, a constitutive centromere component, is required for centromere targeting of CENP-C in vertebrate cells. EMBO J 20: 4603–4617.
33. McAinsh AD, Meraldi P, Draviam VM, Toso A, Sorger PK (2006) The human kinetochore proteins Nnf1R and Mcm21R are required for accurate chromosome segregation. EMBO J 25: 4033–4049.
34. Toso A, Winter JR, Garrod AJ, Amaro AC, Meraldi P, et al. (2009) Kinetochore-generated pushing forces separate centrosomes during bipolar spindle assembly. J Cell Biol 184: 365–372.
35. Gascoigne KE, Takeuchi K, Suzuki A, Hori T, Fukagawa T, et al. (2011) Induced ectopic kinetochore assembly bypasses the requirement for CENP-A nucleosomes. Cell 145: 410–422.
36. Amaro AC, Samora CP, Holtackers R, Wang E, Kingston IJ, et al. (2010) Molecular control of kinetochore-microtubule dynamics and chromosome oscillations. Nature Cell Biol 12: 319–329.
37. Izuta H, Ikeno M, Suzuki N, Tomonaga T, Nozaki N, et al. (2006) Comprehensive analysis of the ICEN (Interphase Centromere Complex) components enriched in the CENP-A chromatin of human cells. Genes Cells 11: 673–684.
38. Minoshima Y, Hori T, Okada M, Kimura H, Haraguchi T, et al. (2005) The constitutive centromere component CENP-50 is required for recovery from spindle damage. Mol Cell Biol 25: 10315–10328.
39. Hua S, Wang Z, Jiang K, Huang Y, Ward T, et al. (2011) CENP-U cooperates with Hec1 to orchestrate kinetochore-microtubule attachment. J Biol Chem 286: 1627–1638.
40. Kang YH, Park JE, Yu LR, Soung NK, Yun SM, et al. (2006) Self-regulated Plk1 recruitment to kinetochores by the Plk1-PBIP1 interaction is critical for proper chromosome segregation. Mol Cell 24: 409–422.
41. Kang YH, Park C-H, Kim T-S, Soung N-K, Bang JK, et al. (2011) Mammalian Polo-like kinase 1-dependent regulation of the PBIP1-CENP-Q complex at kinetochores. J Biol Chem 286: 19744–19757.
42. Schmitzberger F, Harrison SC (2012) RWD domain: a recurring module in kinetochore architecture shown by Ctf19-Mcm21 complex structure. EMBO Rep 13: 216–222.
43. Hellwig D, Hoischen C, Ulbricht T, Diekmann S (2009) Acceptor-photobleaching FRET analysis of core kinetochore and NAC proteins in living human cells. Eur Biophys J 38: 781–791.
44. Hellwig D, Emmerth S, Ulbricht T, Doering V, Hoischen C, et al. (2011) Dynamics of CENP-N kinetochore binding during the cell cycle. J Cell Sci 124: 3871–3883.
45. Tsukamoto T, Hashiguchi N, Janicki SM, Tumbar T, Belmont AS, et al. (2000) Visualization of gene activity in living cells. Nat Cell Biol 2: 871–878.
46. Rothbauer U, Zolghadr K, Tillib S, Nowak D, Schermelleh L, et al. (2006) Targeting and tracing antigens in live cells with fluorescent nanobodies. Nat Methods 3: 887–889.
47. Zolghadr K, Mortusewicz O, Rothbauer U, Kleinhans R, Goehler H, et al. (2008) A fluorescent two-hybrid assay for direct visualization of protein interactions in living cells. Mol Cell Proteomics 7: 2279–2287.

48. Orthaus S, Biskup C, Hoffmann B, Hoischen C, Ohndorf S, et al. (2008) Assembly of the inner kinetochore proteins CENP-A and CENP-B in living human cells. Chem Bio Chem 9: 77–92.
49. Bacia K, Schwille P (2003) A dynamic view of cellular processes by *in vivo* fluorescence auto- and cross-correlation spectroscopy. Methods 29: 74–85.
50. Bacia K, Schwille P (2007) Practical guidelines for dual-color fluorescence cross-correlation spectroscopy. Nature Protocols 2.28422856.
51. Orthaus S, Klement K, Happel N, Hoischen C, Diekmann S (2009) Linker Histone H1 is present in centromeric chromatin of living human cells next to inner kinetochore proteins. Nucl Acids Res 37: 3391–3406.
52. Milks KJ, Moree B, Straight AF (2009) Dissection of CENP-C directed centromere and kinetochore assembly. Mol Biol Cell 20: 4246–4255.
53. Qui SL, Wang JN, Yu C, He DC (2009) CENP-K and CENP-H may form coiled-coils in the kinetochores. Sci China Ser C-Life Sci 52: 352–359.
54. Digman MA, Brown CM, Sengupta P, Wiseman PW, Horwitz AR, et al. (2005) Measuring fast dynamics in solutions and cells with a laser scanning microscope. Biophys J 89: 1317–1327.
55. Hemmerich P, Weidtkamp-Peters S, Hoischen C, Schmiedeberg L, Erliandri I, et al. (2008) Dynamics of inner kinetochore assembly and maintenance in living cells. J Cell Biol 180: 1101–1114.
56. Kohl T, Haustein E, Schwille P (2005) Determining protease activity *in vivo* by fluorescence cross-correlation analysis. Biophys J 89: 2770–2782.
57. Hanissian SH, Akbar U, Teng B, Janjetovic Z, Hoffmann A, et al. (2004) cDNA cloning and characterization of a novel gene encoding the MLF1-interacting protein MLF1IP. Oncogene 23: 3700–3707.
58. Suzuki H, Arakawa Y, Ito M, Saito S, Takeda N, et al. (2007) MLF1-interacting protein is mainly localized in nucleolus through N-terminal bipartite nuclear localization signal. Anticancer Res 27: 1423–1430.
59. Keppler A, Gendreizig S, Gronemeyer T, Pick H, Vogel H, et al. (2003) A general method for the covalent labelling of fusion proteins with small molecules *in vivo*. Nat Biotechnol 21: 86–89.
60. Jansen LET, Black BE, Foltz DR, Cleveland DW (2007) Propagation of centromeric chromatin requires exit from mitosis. J Cell Biol 176: 795–805.
61. Prendergast L, van Vuuren C, Kaczmarczyk A, Döring V, Hellwig D, et al. (2011) Premitotic assembly of human CENPs -T and -W switches centromeric chromatin to a mitotic state. PloS Biol 9: e1001082.
62. Lee KS, Oh DY, Kang YH, Park JE (2008) Self-regulated mechanism of Plk1 localisation to kinetochores: lessons from the Plk1-PBIP1 interaction. Cell Div 3: 4.
63. Leonhardt H, Rahn HP, Weinzierl P, Sporbert A, Cremer T, et al. (2000) Dynamics of DNA replication factories in living cells. J Cell Biol 149: 271–280.
64. Sporbert A, Domaing P, Leonhardt H, Cardoso MC (2005) PCNA acts as a stationary loading platform for transiently interacting Okazaki fragment maturation proteins. Nucleic Acids Res 33: 3521–3528.
65. Schmiedeberg L, Weisshart K, Diekmann S, Meyer zu Hoerste G, Hemmerich P (2004) High- and low-mobility populations of HP1 in heterochromatin of mammalian cells. Mol Biol Cell 15: 2819–2833.
66. Ribeiro SA, Vagnarelli P, Dong Y, Hori T, McEwen BF, et al. (2010) A super-resolution map of the vertebrate kinetochore. Proc Natl Acad Sci USA 107: 10484–10489.
67. Johnston K, Joglekar A, Hori T, Suzuki A, Fukagawa T, Salmon ED (2010) Vertebrate kinetochore protein architecture: protein copy number. J Cell Biol 189: 937–943.
68. Lawrimore J, Bloom KS, Salmon ED (2011) Point centromeres contain more than a single centromere-specific Cse4 (CENP-A) nucleosome. J Cell Biol 195: 573–582.
69. Hemmerich P, Schmiedeberg L, Diekmann S (2011) Dynamic as well as stable protein interactions contribute to genome function and maintenance. Chromosome Res 19: 131–151.
70. Dong Y, VandenBeldt KJ, Meng X, Khodjakov A, McEwen BF (2010) The outer plate in vertebrate kinetochores is a flexible network with multiple microtubule interactions. Nat Cell Biol 9: 516–522.